Institut de Géologie et d'Hydrogéologie
Université de Neuchâtel
Suisse

Géologie structurale de l'Anti-Atlas oriental, Maroc

Thèse de doctorat présentée à la Faculté des Sciences
Institut de Géologie et d'Hydrogéologie
Université de Neuchâtel

Pour l'obtention du grade de docteur ès sciences

par

Charles Robert-Charrue

- Soutenue le 19 septembre 2006 -

Acceptée sur proposition du jury :

Prof. Karl Föllmi, Université de Neuchâtel, Directeur de thèse remplaçant
Prof. Thierry Adatte, Université de Neuchâtel
Prof. Dominique Frizon de Lamotte, Université de Cergy-Pontoise, France
Prof. Abderrhamane Soulaïmani, Université Cadi-Ayyad, Marrakech, Maroc
Dr. Mahmoud Zizi, ONHYM, Maroc

Université de Neuchâtel

IMPRIMATUR POUR LA THESE

Géologie structurale de l'Anti-Atlas oriental, Maroc

Charles ROBERT-CHARRUE

UNIVERSITE DE NEUCHATEL

FACULTE DES SCIENCES

La Faculté des sciences de l'Université de Neuchâtel,
sur le rapport des membres du jury

MM. K. Föllmi (directeur de thèse),
T. Adatte,
D. Frizon de Lamotte (Cergy-Pontoise F)
A. Soulaimani (Cadi Ayyad, Maroc)
et M. Zizi (Rabat, Maroc)

autorise l'impression de la présente thèse.

Neuchâtel, le 23 octobre 2006

UNIVERSITE DE NEUCHATEL
FACULTE DES SCIENCES
Secrétariat-décanat de la faculté
Rue Emile-Argand 11 - CP 158
CH-2009 Neuchâtel

Le doyen :

J.-P Derendinger

Faculté des Sciences
■ Rue Emile-Argand 11 ■ CP 2 ■ CH-2007 Neuchâtel
■ Téléphone : +41 32 718 21 00 ■ Fax : +41 32 718 21 03 ■ E-mail : secretariat.sciences@unine.ch ■ www.unine.ch

CE TRAVAIL EST DÉDIÉ À LA MEMOIRE DE

MARTIN BURKHARD

QUI NOUS A QUITTÉ PRÉMATURÉMENT EN AOÛT 2006.

NOUS GARDERONS LE SOUVENIR

D'UN HOMME DE SCIENCE AU SERVICE DE LA SOCIÉTÉ
D'UN PÉDAGOGUE TOUJOURS DISPONIBLE
D'UN HOMME SOURIANT À LA VIE
D'UN AMBASSADEUR DE LA TERRE

RESUME

Mots-clés : Anti-Atlas, Maroc ; Tectonique d'inversion ; Orogène varisque ; Paléozoïque ; Interférence de plis ; Profondeur de détachement ; Déformation interne ; Plis associés aux failles extensives.

La chaîne de l'Anti-Atlas du Maroc est située sur la bordure nord du craton ouest africain. Sa forme générale est un vaste anticlinal d'orientation ENE-WSW, formé en son cœur de boutonnières de socle et sur ses flancs d'une couverture plissée. Le socle Précambrien recèle les traces des orogènes Eburnéen (2 Ga) et Pan Africain (600 Ma). Dès la fin du Néoprotérozoïque, un rift initie un nouveau cycle de Wilson. A l'issue de la sédimentation syn-rift, le rift est avorté, mais une subsidence régulière permet le dépôt d'une épaisse couverture Paléozoïque dans un environnement de mer peu profonde. Ce bassin intracontinental est inversé au Carbonifère moyen, créant ainsi la chaîne plissée de l'Anti-Atlas. La particularité de cette chaîne est l'absence de décollement majeur.

Les études géologiques menées dans l'Anti-Atlas oriental ont permis de décrire sa structure et de caractériser son style structural. Les deux paramètres qui contrôlent le type de la déformation sont (1) la pré-structuration du socle lors du rift Néoprotérozoïque – Cambrien et (2) la rhéologie particulièrement incompétente de la couverture. La compression varisque inverse les anciennes failles normales du socle. A grande échelle, la couverture accommode la déformation par drapage, mais elle est également affectée par un raccourcissement interne qui se traduit par la formation de petites structures compressives, visibles dans les quelques formations plus compétentes qui jalonnent la série Paléozoïque. L'analyse des structures a permis de discerner deux orientations distinctes de déformation. L'une correspond à l'orientation générale de l'Anti-Atlas, l'autre adopte l'orientation de la chaîne de l'Ougarta située au sud-est. La superposition de ces deux orientations provoque une figure d'interférence en dômes et bassins.

Dix coupes décrivent la structure générale de l'Anti-Atlas oriental. La restauration à différents stades de l'une d'entre elle, a permis de calculer une profondeur de détachement méso-crustal de -18 à -20 km. Une nouvelle méthode d'équilibration intégrant le raccourcissement interne a été développée et a permis de mettre en évidence un raccourcissement interne de 11 à 17%.

Une extension tardive attribuée à l'ouverture du bassin Mésozoïque du Haut Atlas (au nord de l'Anti-Atlas oriental) réactive les structures profondes et crée dans la couverture des failles normales raides et des plis associés.

Les relations avec les sédiments post-varisques montrent que l'inversion du Haut Atlas ne provoque pas de déformation mais une légère surrection dans l'Anti-Atlas oriental. Ce soulèvement combiné à celui induit par une anomalie thermique récente explique la haute topographie de l'Anti-Atlas oriental.

ABSTRACT

Keywords : Anti-Atlas, Morocco ; Inversion tectonics ; Variscan orogeny ; Paleozoic ; Folds interference ; Depth to detachment ; Bed-length shortening ; Extensional fault-related folding.

The Anti-Atlas belt of Morocco is situated on the northern edge of the West African Craton. The Anti-Atlas appears as a huge NE-SW anticlinorium. Locally, the basement is cropping out as inliers, but the main part is made of a gently folded Paleozoic cover. The Eburnean (2 Ga) and Pan African (600 Ma) orogenies left their imprints in the Precambrian basement. A new Wilson Cycle was initiated by the formation of a rift in Late Neoproterozoic. After syn-rift sediments, the rift is aborted, but the regular subsidence allowed for the deposition of a thick pile of Paleozoic sediments in a shallow-water environment. This intracontinental basin is inverted in mid-Carboniferous, forming the Anti-Atlas fold belt. The main feature of this chain is the lack of a major *décollement* or duplex structure.

Inspection of the structure was carried out during fieldwork to characterize its structural style. The two principal parameters which control the deformation type were (1) the pre-structuration of the basement during the Neoproterozoic – Cambrian rift and (2) the ultraweak mechanical propriety of the cover. Variscan compression led to the inversion of the basements former normal faulting. On a larger scale, the cover accommodates the bed-length shortening by the formation of small-scale compressive structures observable in the rigid members, which mark the Paleozoic series. The analysis of these structures shows two distinct orientations of deformation. One corresponding to the Anti-Atlas' major trend; the second to the Ougarta chain, situated to the southeast. The superimposition of these two orientations created an egg-box interference pattern.

Ten cross-sections describe the structure of the eastern Anti-Atlas. The restoration at different stages of one of these cross-sections, has allowed for the calculation of a mid-crustal depth to detachment of –18 to –20 km. A new balancing method, integrating bed-length shortening has been developed. This indicated an internal shortening of 11 to 17 %.

A later extension, attributed to the opening of the Mesozoic High Atlas basin, reactivated the deep structures, creating normal faults and extensional fault-related folds in the Paleozoic cover.

Relationship with post-Variscan sediments show that the High Atlas inversion did not deform the eastern Anti-Atlas. The influence was felt more in terms of a smooth uplift. This uplift combined with a recent thermal anomaly, are responsible for the high topography of the eastern Anti-Atlas.

SOMMAIRE

SOMMAIRE DES ANNEXES

NB : Les figures marquées d'un astérisque dans le texte, sont de taille réduite. Elles sont présentées dans l'annexe D dans un format plus grand.

1

INTRODUCTION

1.1. Le projet

L'étude structurale de l'Anti-Atlas oriental s'insère dans le projet du Professeur Martin Burkhard de l'Université de Neuchâtel. Le projet débute en 1997 avec Séverine Caritg et Urs Helg, deux doctorants qui concentreront leurs études sur la partie sud-occidentale de la chaîne. De ces études découlent deux articles principaux : Helg U., M. Burkhard, S. Caritg, C. Robert-Charrue (2004), Folding and inversion tectonics in the Anti-Atlas of Morocco, *Tectonics*, Vol. 23 et Caritg S., M. Burkhard, R. Ducommun, U. Helg, L. Kopp, C. Sue (2004), Fold interference patterns in the Late Palaeozoic Anti-Atlas belt of Morocco, *Terra Nova*, 16. En 1999, trois diplômants (Romain Ducommun, Lionel Kopp et moi-même) prennent part au projet. Tandis que Romain Ducommun et Lionel Kopp s'attaquent aux plis d'interférence de la région de Tata dans le sud-ouest, mes études me mènent dans le Tafilalt. Ce choix est influencé par la possession de trois lignes sismiques levées dans cette région par l'actuel ONHYM (Office National des Hydrocarbures et des Mines) et interprétées par A. Bally et M. Zizi. Une partie des données récoltées dans cette extrémité de la chaîne, servent à l'écriture de Robert-Charrue & Burkhard (2006), Variscan inversion tectonics and interference pattern in the Tafilalt, Anti-Atlas, Morocco soumis au *Journal of African Earth Sciences*. A l'issue de ce travail de diplôme, sur proposition de Martin Burkhard, mes recherches sont étendues à l'Anti-Atlas oriental dans le cadre d'un travail de doctorat. L'article : Tectonics of Anti-Atlas of Morocco

(2006) de M. Burkard, S. Caritg, U. Helg, Ch. Robert-Charrue et A. Soulaïmani traîte en particulier du bassin Paléozoïque et de la tectonique de l'inversion varisque. Il paraît dans un numéro des Comptes Rendus Geoscience consacré à la géologie de l'Afrique du Nord avec comme rédacteurs invités D. Frizon de Lamotte, A. Michard et O. Saddiqi.

1.2. Situation géographique et bases géologiques

Au Nord-ouest du continent africain, l'Anti-Atlas constitue le domaine austral du Royaume du Maroc. Comme le suggère l'image satellite (Figure 1 gauche), ces régions arides et semi-désertiques présentent une qualité d'affleurement exceptionnelle.

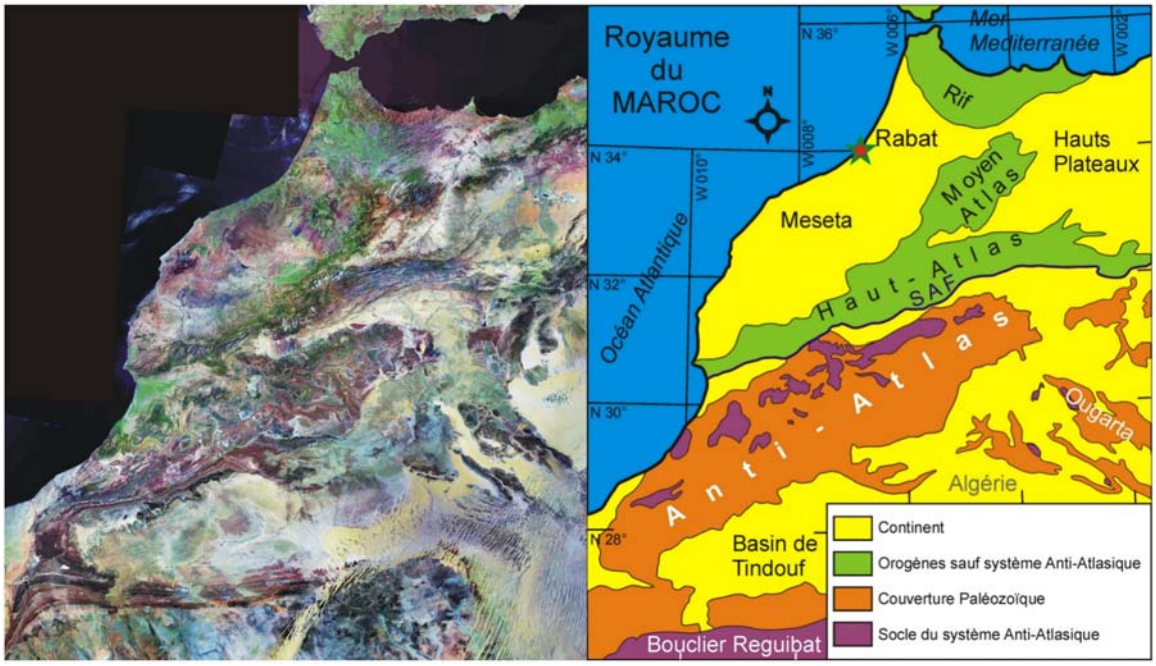

Figure 1. Situation de l'Anti-Atlas du Maroc. Gauche : mosaïque de vue satellite. Droite : carte géologique simplifiée.

La chaîne de l'Anti-Atlas se présente sous la forme d'un vaste bombement anticlinal comportant en son cœur des affleurements de socle appelés boutonnières, elles-même bordées par une couverture sédimentaire paléozoïque plissée (Figure 1 droite). L'axe de cet anticlinal suit une orientation ENE-WSW.

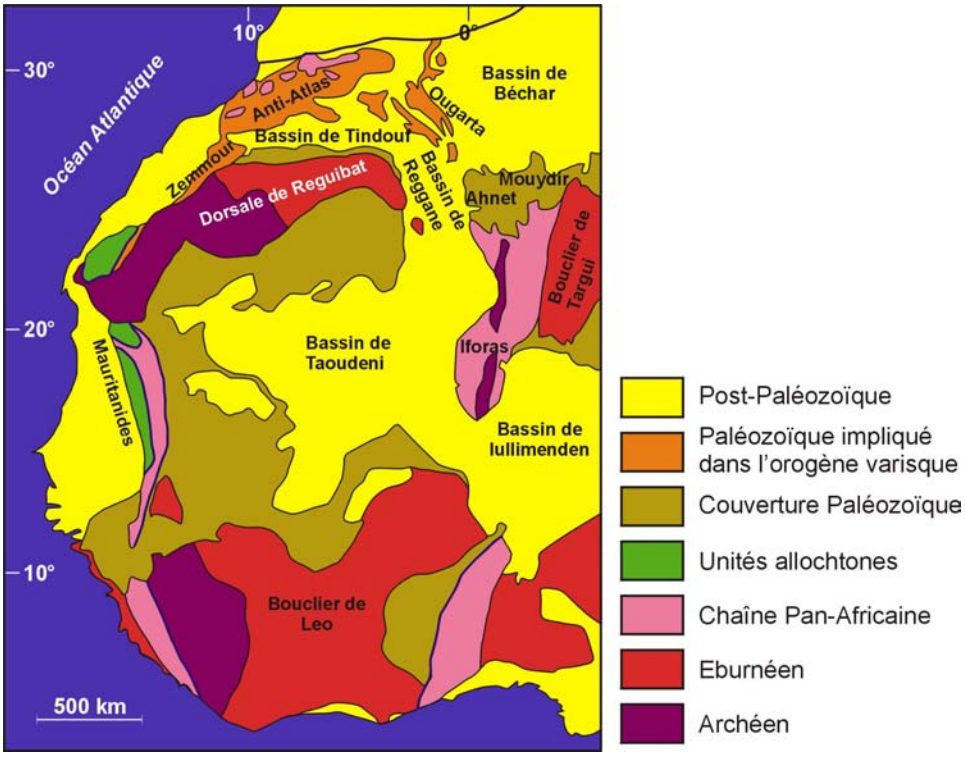

Figure 2. Carte générale du Craton Ouest Africain. D'après Dallmeyer et Lécorché (1991) cité dans Piqué (2001).

Au sud-ouest l'Anti-Atlas se prolonge par la chaîne du Zemmour et les Mauritanides avec une orientation NE-SW. A l'est, il est relayé par la chaîne de l'Ougarta d'orientation NW-SE. Ces différentes chaînes dessinent un arc qui constitue la bordure septentrionale du craton ouest africain (WAC, *West-African craton*) (Figure 2). Au sud le bassin de Tindouf est constitué de la même couverture paléozoïque que l'Anti-Atlas à la seule différence qu'elle n'est point déformée. Au nord, l'Anti-Atlas est limité aujourd'hui par le Haut-Atlas, un bassin mésozoïque inversé lors de l'orogène alpin. L'histoire de la Meseta (Figure1) est contemporaine de celle de l'Anti-Atlas, mais non identique. Sa déformation a eu lieu dans une situation beaucoup plus interne de l'orogène varisque.

1.3. Buts de l'étude

Les études publiées sur la déformation varisque de l'Anti-Atlas oriental sont rares (A. Piqué dans son ouvrage sur la géologie du nord-ouest de l'Afrique (2001)).

Le projet dans sa globalité vise à décrire la structure de cette chaîne plissée et plus particulièrement à caractériser les paramètres contrôlant la déformation varisque en terme de style tectonique. Une question fondamentale est celle de la relation entre le socle et la couverture. La déformation est-elle de type *thick-skin* ou *thin-skin* ? En d'autres termes, la déformation affecte-t-elle autant la couverture que le socle ou la couverture se désolidarise-t-elle du socle par un décollement basal comme on peut l'observer dans bien des chaînes d'avant-pays typiques ? A première vue, l'absence de front ou de chevauchement majeur font de cette chaîne un objet d'étude singulier.

Quelques critères de terrains fourniront quelques éléments de réponse à la question posée en début de projet, de la cause de la topographie étonnamment élevée et du relief extrêmement jeune de l'Anti-Atlas. Mais les travaux spécifiques à cette problématique de Frizon de Lamotte et de son équipe, sur la base de données géophysiques fourniront une réponse plus étayée (Missenard *et al.*, 2006 ; Saddiqi *et al.*, 2005).

Les premières études faites dans le sud-ouest se sont davantage focalisées sur les plis et les relations entre les longueurs d'onde différentes observées dans les bancs marqueurs de la couverture. Cette déformation de type flambage (*buckling*), où chaque banc se plisse indépendamment selon ces propres caractéristiques, n'est pas observée à grande échelle dans l'Anti-Atlas oriental où la déformation semble affecter l'ensemble de la couverture d'une manière homogène. Un des buts est donc de caractériser cette différence. L'Anti-Atlas oriental se poursuit au SE par la chaîne de l'Ougarta (Figures 1 et 2), il diffère également par la présence de structures extensives qui n'affectent pas la partie occidentale. L'interférence de ces différents traits géologiques constitue une clef dans la compréhension de l'édifice. Les objectifs pour cette étude sont de fournir une image de la géométrie globale de l'Anti-Atlas oriental, d'en définir le style structural et d'en quantifier la déformation. L'ambition ultime étant de proposer un modèle dynamique expliquant la chronologie et les paramètres contrôlants la mise en place de cette partie de la chaîne.

1.4. Méthodes, outils, données

Etant donnés la grande taille de l'objet et l'état des connaissances, limité en terme de structures, les méthodes visant à « dégrossir » la structure de l'Anti-Atlas oriental sont élémentaires.

L'outil principal est la cartographie. Pratiquement, la boussole permet la mesure de l'orientation des plans de stratification, des plans de failles et des stries. Ces mesures servent à dessiner les coupes, calculer l'orientation des axes de plis et déduire l'orientation des contraintes qui ont généré ces déformations (plis et failles). La boussole utilisée est une Brunton® GEO Transit. La déclinaison magnétique utilisée provient des cartes du *British Geological Survey* [1]. Le positionnement géographique se fait à l'aide des cartes topographiques au 1 :100'000 du Maroc et d'un GPS Garmin® III. Le système géodésique choisi est le WGS84. Les coordonnées sont sous la forme longitude/latitude en degré, minute, millième de minute (000° 00.000'). Un millième de minute pour cette région correspond environ à 0.9 m en latitude et 0.7 m en longitude. Les mesures d'épaisseur sont calculées cartographiquement par le dessin de coupes locales généralement au 1 :25'000. Malgré les lacunes de données structurales, les cartes géologiques au 1 :200'000 sont un outil précieux, elles fournissent d'excellentes descriptions stratigraphiques.

Les images satellites sont une source d'information inestimable vu la qualité d'affleurement de ces régions. Les images utilisées sont celles de la génération Landsat 7 ETM+ (*Enhanced Thematic Mapper*). Elles sont traitées à partir de 3 bandes de fréquence. Elles sont orthorectifées, géoréférencées et ont une résolution de 14.25 m. Ces vues sont téléchargeables gratuitement depuis internet [2] et peuvent être exportées en image (.tif) à l'aide du programme GeoViewer de Lizardtech™.

Les modèles numériques de terrain (MNT) proviennent du modèle GTOPO 30 (*Global 30 Arc Second Elevation Data*) qui a une maille d'approximativement 1

km^2. Ces données sont gratuites et disponibles sur internet [3]. Le programme Surfer 8.01 de *Golden Software, Inc.* permet la génération de cartes et la création de vues tridimensionnelles.

Trois lignes sismiques fournies par l'ONAREP (actuellement ONHYM) ont permis de mieux contraindre le modèle géométrique en profondeur. Une première interprétation de la ligne RS 8 a été réalisée dans le cadre du travail de diplôme. Cette interprétation a été revue et corrigée pour le premier article.

1.5. Logistique et approche

Cette étude a nécessité plusieurs voyages au Maroc :

Printemps 2002	-Terrain, Anti-Atlas oriental du 7 au 29.03.
	-Anti-Atlas central avec Martin Burkhard, 30.03 - 6.04.
	-Congrès « Marrakech International Oil & Gas », 7 - 10.04.
Automne 2002	-Terrain, Anti-Atlas oriental du 22.09 au 12.10.
Printemps 2003	-Terrain, Anti-Atlas oriental du 10.03 au 2.04.
Automne 2003	-Terrain, Anti-Atlas oriental du 5.10 au 4.11.
Hiver 2003-2004	-Anti-Atlas occidental avec M. Burkhard, S. Caritg et Zeshan Ismat (*Assistant Professor* au *Franklin & Marshall College*, Lancaster PA, USA) 30.12.2003-11.01.2004.
Printemps 2004	-Excursion de l'Institut de Géologie, UniNe, 5 - 21.04.
Printemps 2005	-Congrès 3Ma (Magmatisme, Métamorphisme et Minéralisations associés), Agadir, 5 - 7.05.
	-Excursion du congrès 3Ma dans l'Anti-Atlas occidental et central, 8 - 11.05.
	-Terrain, Anti-Atlas oriental du 12 au 18.05.

Les autorisations de mission de terrain ont été délivrées par la Division de la Géologie du ministère de l'Energie et des Mines à Rabat.

Le travail de terrain a été effectué seul. La carte d'accès (Figure 3) montre les endroits visités lors des différentes sessions de terrain dans l'Anti-Atlas oriental. A l'exception de la dernière session, les déplacements pour le travail de terrain se sont faits en Landrover® Defender aménagé, permettant une autonomie de plusieurs jours, afin d'éviter des trajets inutiles.

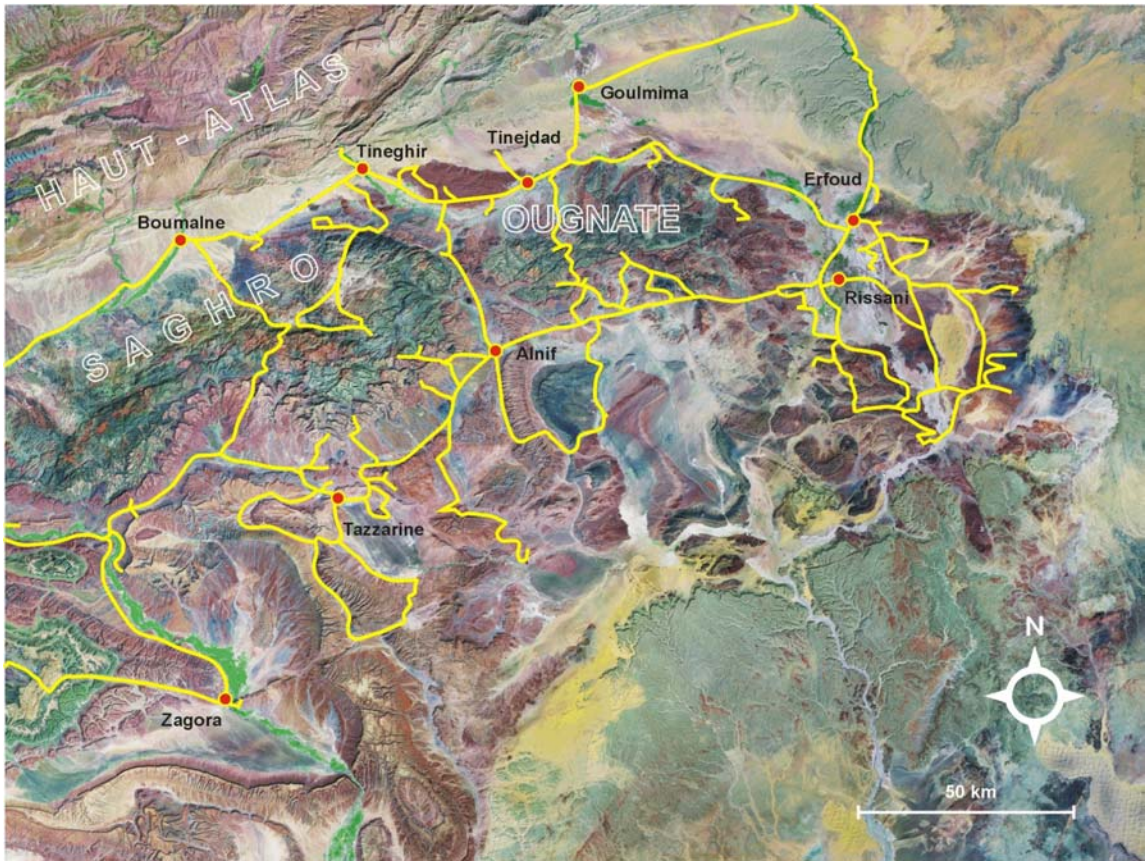

Figure 3. Carte d'accès des études menées dans l'Anti-Atlas oriental.

L'approche du terrain a été dictée par les recherches. Outre les mesures de la géométrie générale, on a, dans un premier temps, cherché plus particulièrement à observer le contact socle - couverture et à définir l'épaisseur des formations dans les différentes régions de l'Anti-Atlas oriental. Des profils de coupes ont été tracés perpendiculairement à l'axe des boutonnières, selon les variations de la structure générale et les possibilités d'accès. Le terrain est très facilement abordable par les routes nord (Erfoud-Tinejdad-Tineghir-Boumalne) et centrale

(Rissani-Alnif-Tazzarine) (Figure 3). Les possibilités de traversées des massifs du Saghro et de l'Ougnate ainsi que les explorations vers le sud sont limitées à de rares pistes parfois abandonnées. L'observation et la recherche de structures plus petites (invisibles sur les cartes et les images satellites) a été systématiques.

2

CADRE GEOLOGIQUE

Etat des connaissances

2.1. Tectonique globale

L'Anti-Atlas est situé sur la bordure nord du craton ouest africain (Figure 2, p. 3). Cette zone est particulière dans le sens que de nombreux événements tectoniques affectent cette région au cours des temps géologiques. Sur la base des compilations paléogéographiques de Stampfli et Borel (2002) (Figure 4), voici un aperçu des mouvements tectoniques globaux précédents et suivants l'épisode varisque.

A l'issue de l'orogenèse Pan-Africaine, la marge nord du Gondwana voit le détachement successif de plusieurs terrains et donc l'ouverture de différents océans. Après l'océan Prototéthys, les terrains Avaloniens quittent le Gondwana et font place à l'océan Rhéic (stade 490 Ma de la Figure 4). Durant le Silurien, de l'autre côté de l'océan, la collision des terrains Avaloniens, du continent Baltica et de Laurentia (craton nord américain) crée le continent Laurussia (440 Ma). Durant cette même période, le départ des terrains Huniques de la marge du Gondwana, font place à l'océan Paléotéthys (400 Ma). L'océan Rhéic se referme alors sur la marge du continent Laurussia (340 Ma), puis le Paléotéthys se referme à son tour (320 Ma). La collision des continents Gondwana et Laurussia forment le super-continent Pangée (280 Ma). Ces deux derniers stades correspondent à la déformation varisque étudiée dans l'Anti-Atlas. A la fin du

Trias et durant le Jurassique (200 Ma et 180 Ma), la Pangée est disloquée par l'ouverture de l'océan Atlantique.

Les événements décrits ci-dessus ne constituent qu'un seul cycle de Wilson (rift - ouverture océanique - fermeture du bassin - collision - rift). D'autres cycles ont précédé et suivent ce cycle varisque.

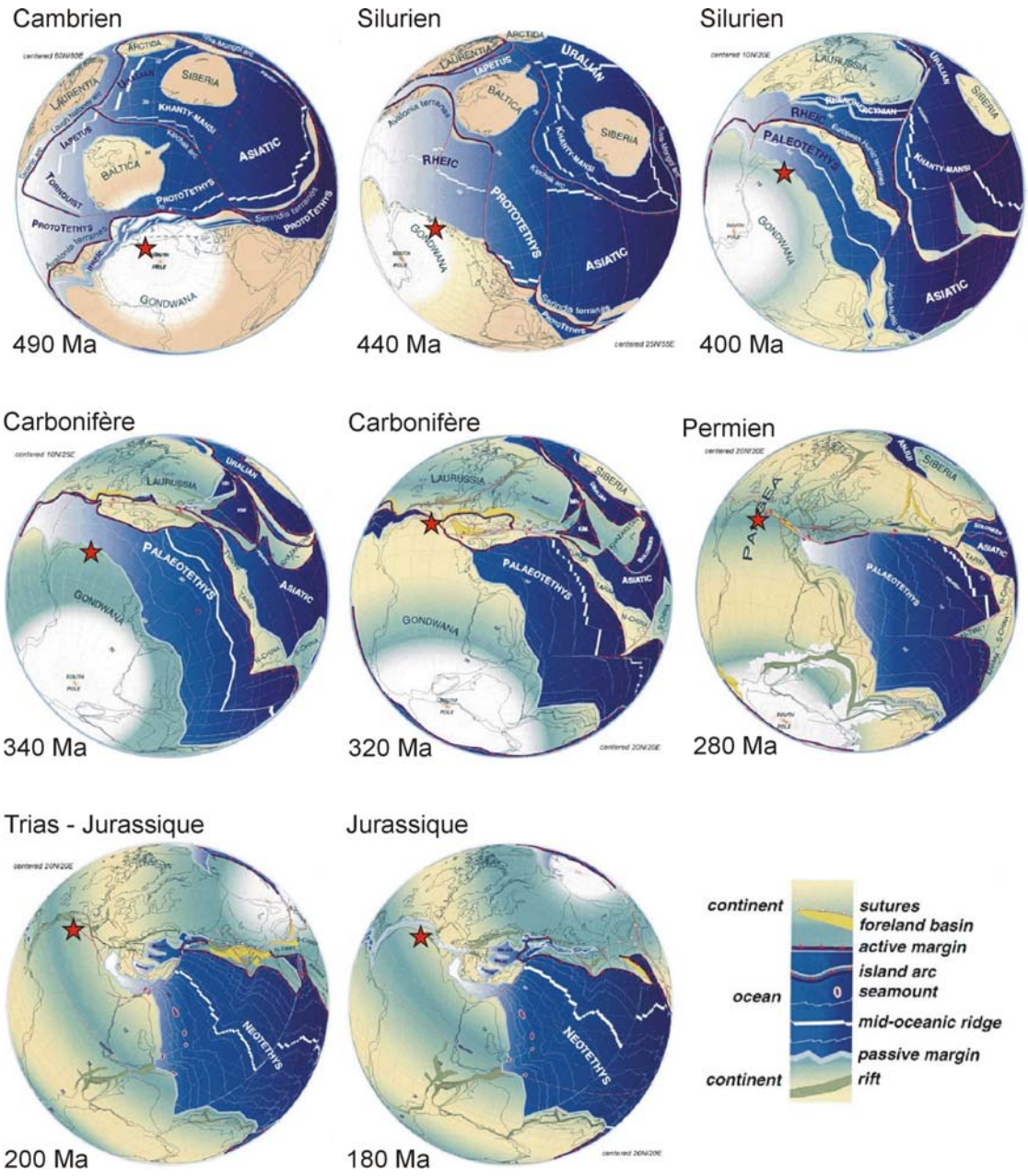

Figure 4. Paléogéographies de Stampfli et Borel (2002). L'étoile indique la position de l'Anti-Atlas.

Si l'Anti-Atlas est toujours à proximité des limites actives, il faut noter qu'il ne se situe jamais sur ces limites. Les séries plus marines correspondent à des niveaux marins élevés. La forme du bassin Anti-Atlas peut être représenté par un indentation marine ou un golfe. Toujours sur le continent Gondwana, cette zone enregistre plus ou moins intensément les événements tectoniques, mais ne les subit pas de manière directe.

2.2. Eléments morpho-géologiques de l'Anti-Atlas oriental

La carte de la Figure 5 représente les grandes formes géologiques de l'Anti-Atlas oriental.

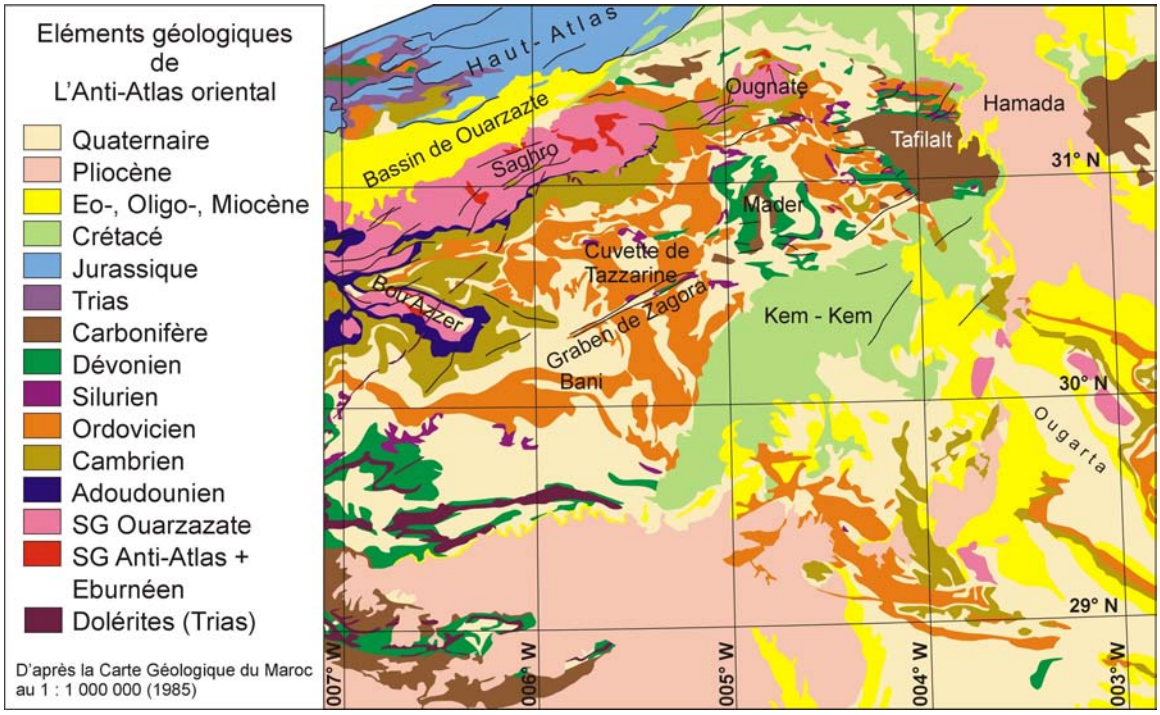

Figure 5. Eléments géologiques de l'Anti-Atlas oriental. D'après la Carte Géologique du Maroc au 1 : 1'000'000 (1985).

Le socle apparaît sous la forme de boutonnières. D'ouest en est : la boutonnière de Bou Azzer (Anti-Atlas central), celle du Saghro et celle de l'Ougnate. Avec son orientation NNW-SSE, la boutonnière de Bou Azzer dévie de l'orientation générale (NE-SW) des boutonnières de l'Anti-Atlas (Figure 1, p.2). Le plissement de la couverture paléozoïque est mis en valeur par la formation du Bani, crête

ordovicienne qui peut être suivie dans tout l'Anti-Atlas. L'image à grande échelle du Paléozoïque montre une série de dômes et bassins. D'ouest en est : la cuvette de Tazzarine, les « bassins » du Mader et du Tafilalt. Cette structure concorde avec celle de la chaîne de l'Ougarta d'orientation NW-SE. De grandes structures d'extension tel que le graben de Zagora apparaissent dans les niveaux rigides de la couverture. Le tout est scellé par des sédiments du Crétacé ou plus récents. On distingue le plateau Crétacé des Monts Kem-Kem au sud-est, la Hamada du Guir Mio-Pliocène à l'est, le Crétacé du nord de l'Ougnate et le bassin Cénozoïque de Ouarzazate sur la bordure NW du Saghro. Au nord-ouest de l'Anti-Atlas, le Haut Atlas est limité au sud par la faille sud atlasique. Ces formes géomorphologiques sont visibles sur les vues tridimensionnelles de la Figure 6.

6 A : Vue vers le nord

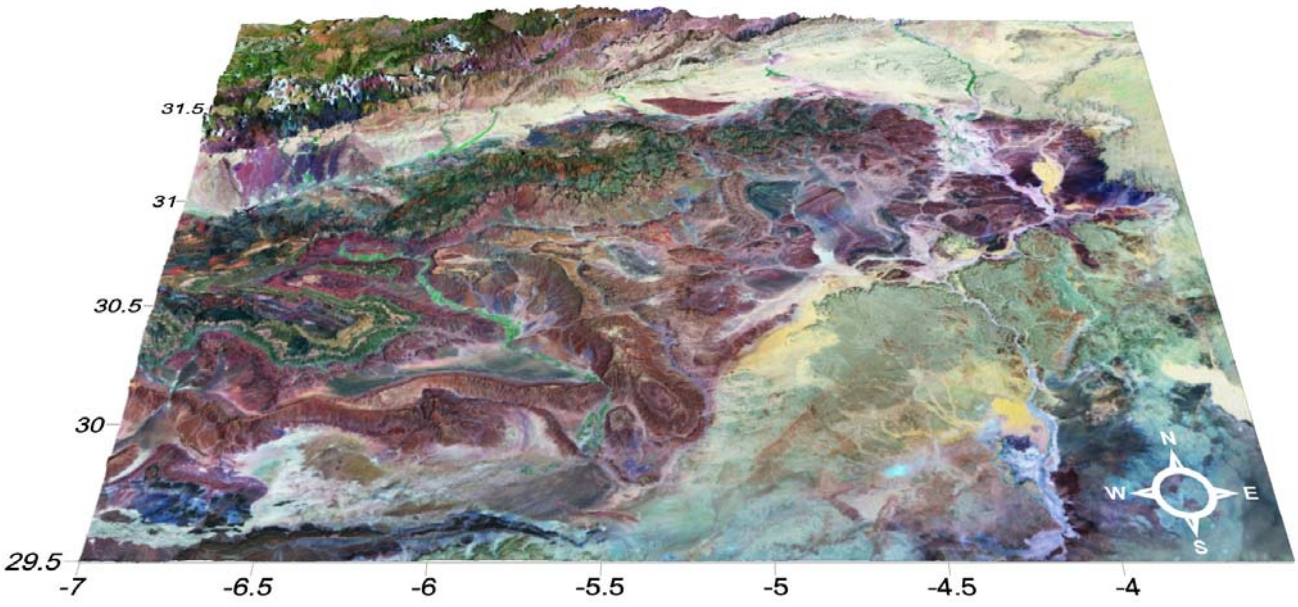

6 B : Vue vers l'ouest

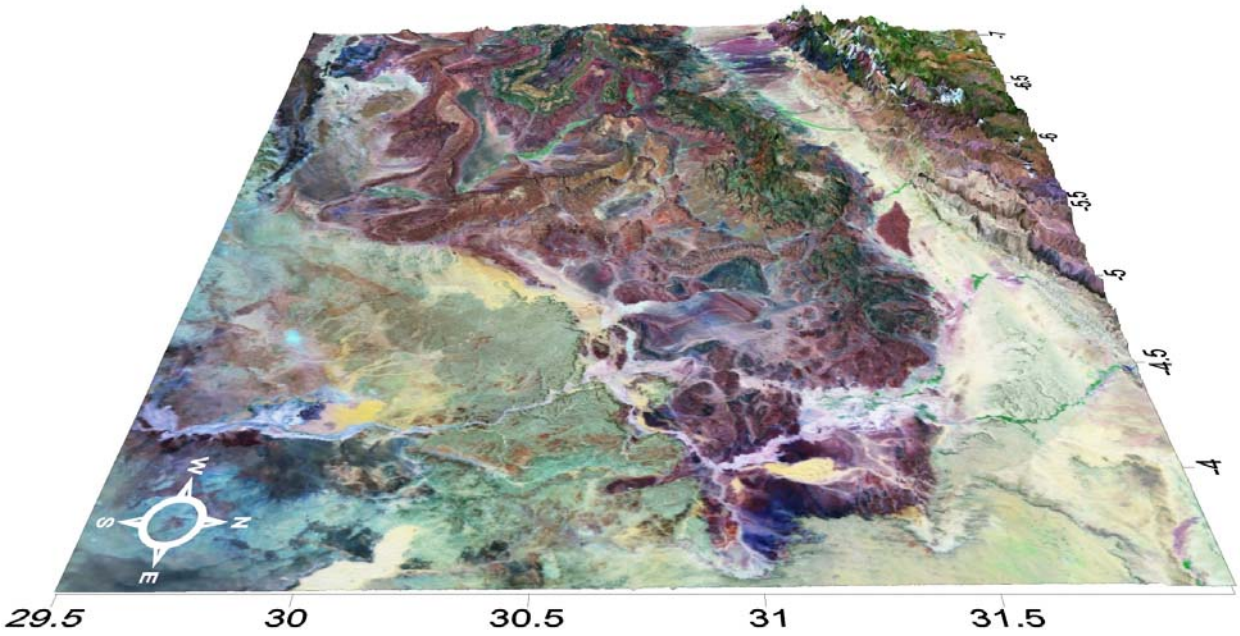

6 C : Vue vers le sud

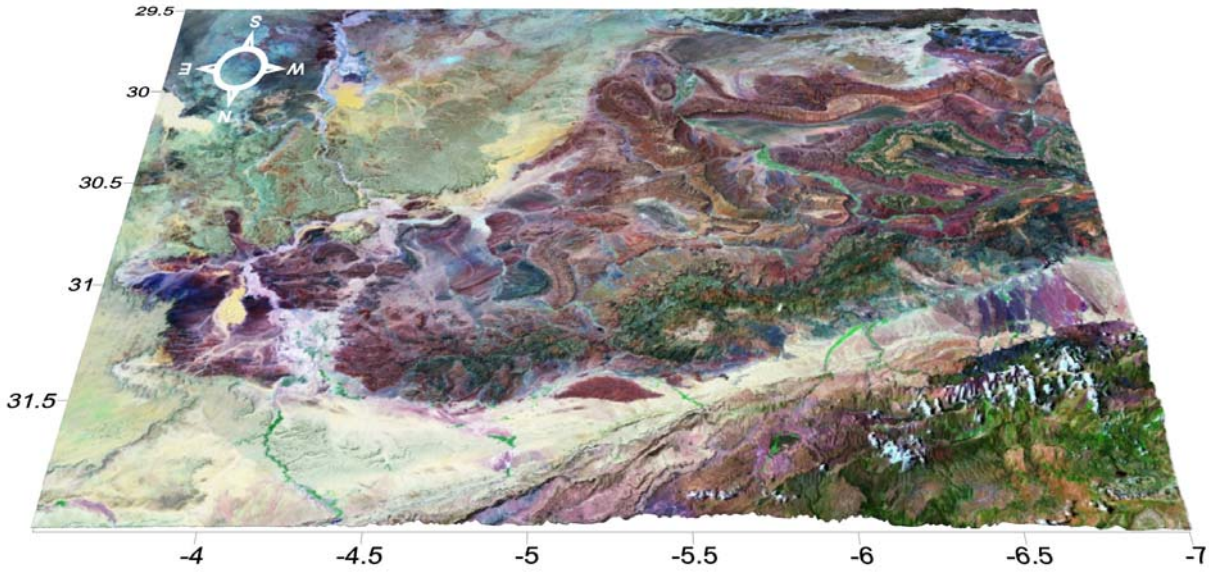

6 **D** : Vue vers l'est

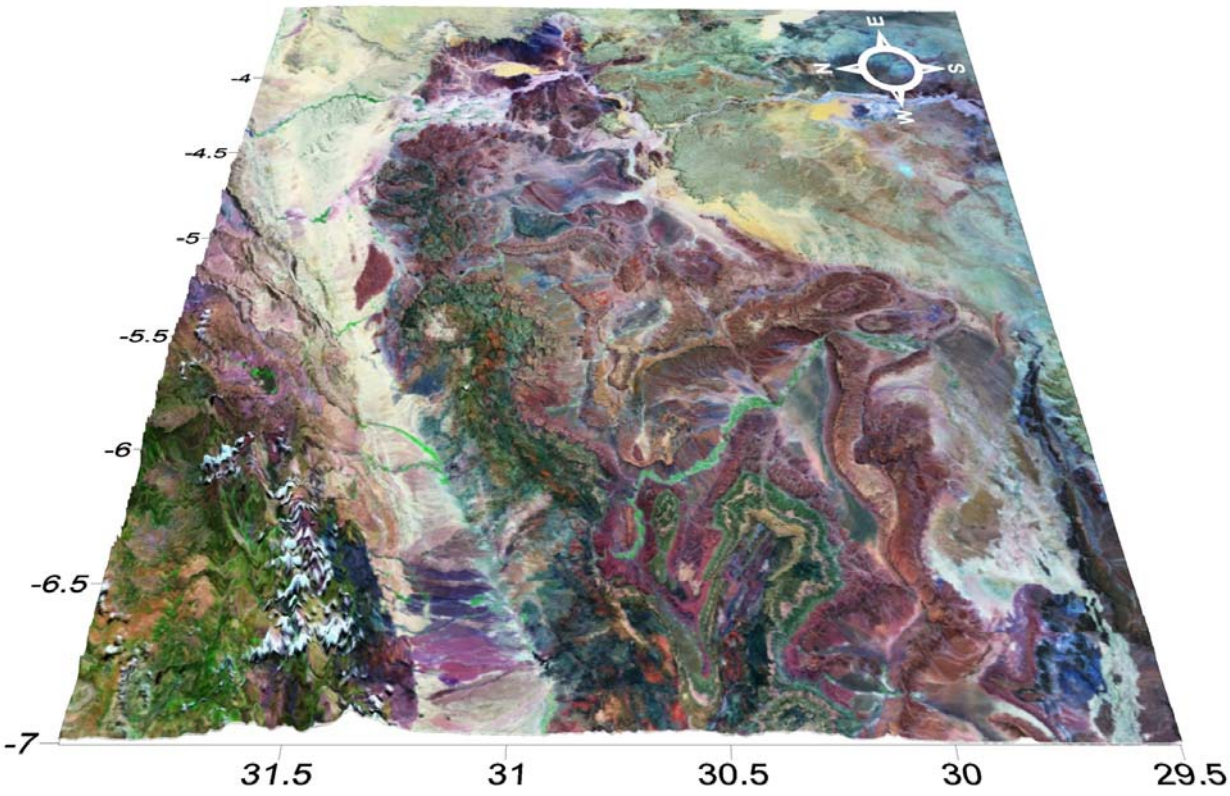

Figure 6. Vues tridimensionnelles de l'Anti-Atlas oriental. Modèle numérique de terrain : GTOPO30 avec plaquage de l'image satellite Landsat 7.

2.3. Le socle

Avec une impressionnante variété de roches, le socle est le témoin d'une activité géologique multiphasée qui explique sa complexité. D'un point de vue « varisque », le socle comprend toutes les roches antérieures aux sédiments déposés lors du rift Précambrien (début du cycle de Wilson varisque). Il n'en va pas toute à fait de même en terme de rhéologie et de déformation.

Pour les chercheurs s'intéressant au Précambrien , l'orogenèse Anti-Atlasique désigne celle du cycle Pan-Africain. Les roches du socle de la présente étude sont subdivisées en trois parties (Thomas *et al.*, 2004 ; Gasquet *et al.*, 2005) : (1) Le socle éburnéen Paléoprotérozoïque (~2 Ga) composé principalement de

granitoïdes intrusifs dans des séries métamorphiques complexes, (2) le super-groupe de l'Anti-Atlas comprend des roches volcano-sédimentaires, ophiolitiques et intrusives impliquées dans l'accrétion Pan-Africaine au Néoprotérozoïque, et (3) le super-groupe de Ouarzazate est composé de roches volcaniques, intrusives (Barbey *et al.*, 2004) et détritiques dans un contexte fini- à post-collisionnel. Des sédiments syn-rift indiquent l'extension Post-Panafricaine (Piqué *et al.*, 1999 ; Piqué, 2003 ; Soulaïmani *et al.*, 2003).

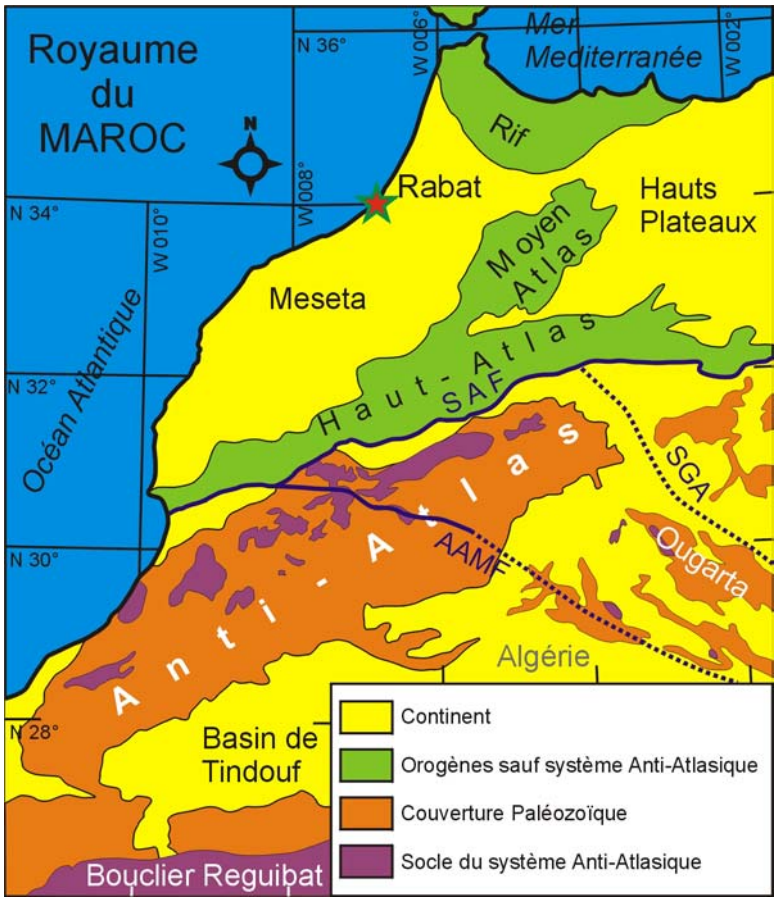

Figure 7. Limites cratoniques de l'Anti-Atlas. SAF : *South Atlas Fault* (Faille sud atlasique), AAMF : *Anti-Atlas Major Fault* (Accident Majeur), SGA : *Saoura gravimetric anomaly* (Anomalie gravimétrique du Saoura).

Suivant le linéament du Tibesti (Guiraud *et al.*, 2000), l'Accident Majeur (Choubert et Faure-Muret, 1971) (AAMF, Figure 7) est certainement la plus importante trace de l'orogène Pan-Africain dans l'Anti-Atlas. Anciennement considérée comme la suture délimitant le nord du craton ouest africain

(Saquaque *et al.*, 1989), cette structure est aujourd'hui décrite comme la limite australe d'un bassin aulacogène du Néoprotérozoïque inférieur (Hefferan *et al.*, 2000 ; Ennih & Liégeois, 2001; 2003). Les ophiolities trouvées sur cet accident, sont en fait charriées sur le craton (et le bassin aulacogène) lors de l'accrétion Pan-Africaine d'un arc volcanique. Ainsi la limite septentrionale du craton ouest-africain est la faille sud-atlasique (SAF). La zone intermédiaire peut être qualifiée de métacratonique (Liégeois *et al.*, 2005). La limite orientale de ce métacraton semble coïncider avec l'anomalie gravimétrique du Saoura (SGA, Figure 7) (Bayer et Lesquer, 1978 cités dans Ennih et Liégeois, 2001).

La nouvelle phase de rift du Néoprotérozoïque terminal utilise peut-être d'anciennes structures, mais crée en tous cas d'importantes hétérogénéités dans ce socle varisque sous la forme de failles normales. Cette compartimentalisation ou préstructuration jouera un rôle essentiel lors de la déformation varisque.

2.4. La couverture Paléozoïque

La série sédimentaire Paléozoïque de l'Anti-Atlas est impressionnante par sa puissance. Elle atteint plus de 10 km dans le sud-ouest. Dans la partie orientale, l'épaisseur est de 8 km à l'ouest et décroît jusqu'à 4 km à l'est (Figure 8). Ceci est dû à la réduction des formations elles-mêmes mais également à la disparition de certains niveaux (Figure 9). La puissance de la couverture décroît également vers le nord. La mesure des épaisseurs s'y complique par la présence du Haut Atlas et de roches sédimentaires récentes. Sur la bordure nord-ouest de la boutonnière du Saghro, les sédiments Paléozoïques sont masqués par le bassin Cénozoïque de Ouarzazate (Figure 5). Au nord de l'Ougnate, ce sont les roches Crétacées qui recouvrent une partie du Paléozoïque et même des pointements de socle comme le suggèrent de petits affleurements de Néoprotérozoïque dans la partie nord-est du Tafilalt.

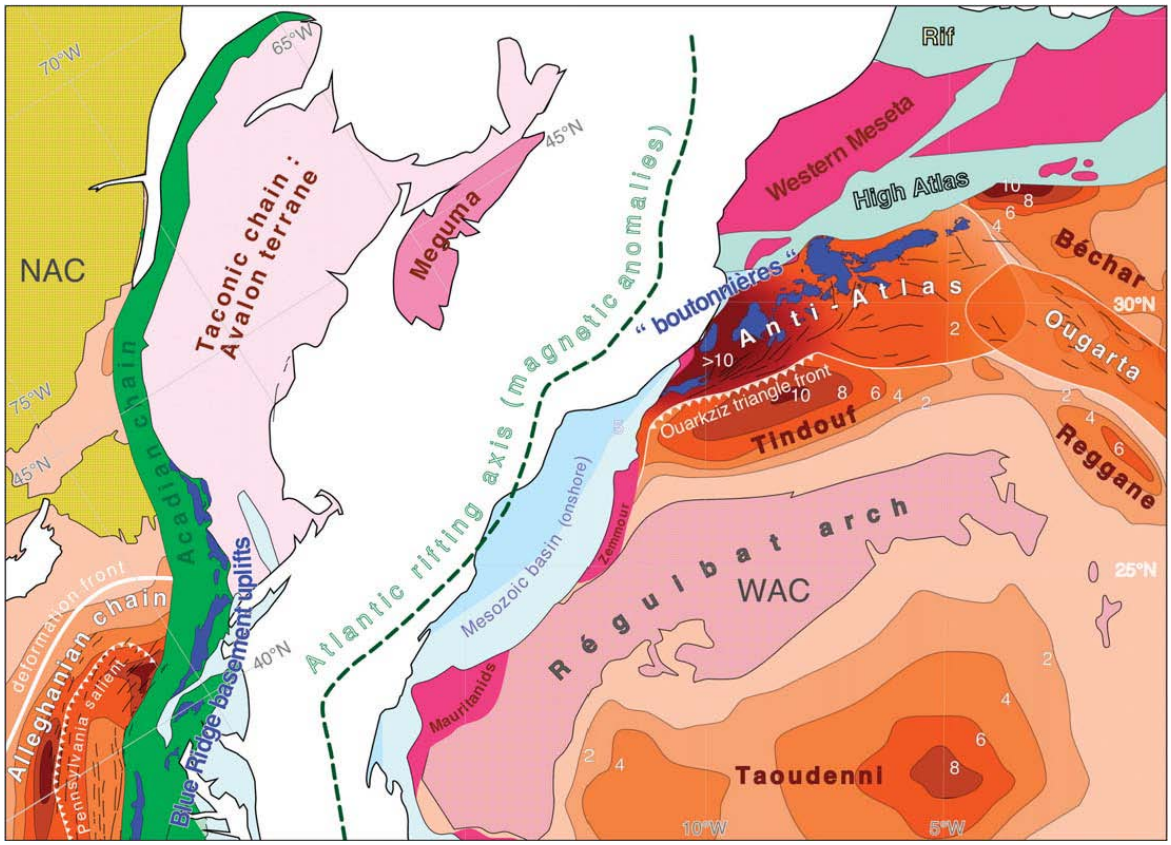

Figure 8. Situation de l'Anti-Atlas par rapport à la chaîne des Appalaches à la fin du Paléozoïque. Les contours isopaques (en km) sont données pour les bassins sédimentaires paléozoïques qui n'ont subi que peu ou pas de déformation. Le même code couleur est appliqué à la chaîne plissée de l'Anti-Atlas afin d'indiquer la profondeur estimée de ce bassin avant son inversion. Les massifs de socle alléghaniens sont indiqués en bleu. Les parties internes, métamorphiques et plus anciennes, de la chaîne des Appalaches-Mauritanides-Meseta marocaine sont colorées en vert et en rose.

Toute la série Paléozoïque est dominée par des sédiments déposés dans un environnement de mer peu profonde. L'absence de sédiment de bassin, de talus ou de plate-forme externe exclut une interprétation de marge passive. L'environnement de dépôt de l'Anti-Atlas s'apparente plutôt à un bassin de type intracontinental (Burkhard et al., 2006), dû à une subsidence thermique post-rift. Mais le régime thermique, la structuration pré-rift et les effets d'une compression lointaine qui contrôlent la formation du bassin (Cloething *et al.*, 1995 ; Ziegler et Cloething, 2004) sont mal contraints. Le bassin Paléozoïque de l'Anti-Atlas est la partie tectonisée du gigantesque bassin de Tindouf (Coward et Ries, 2003).

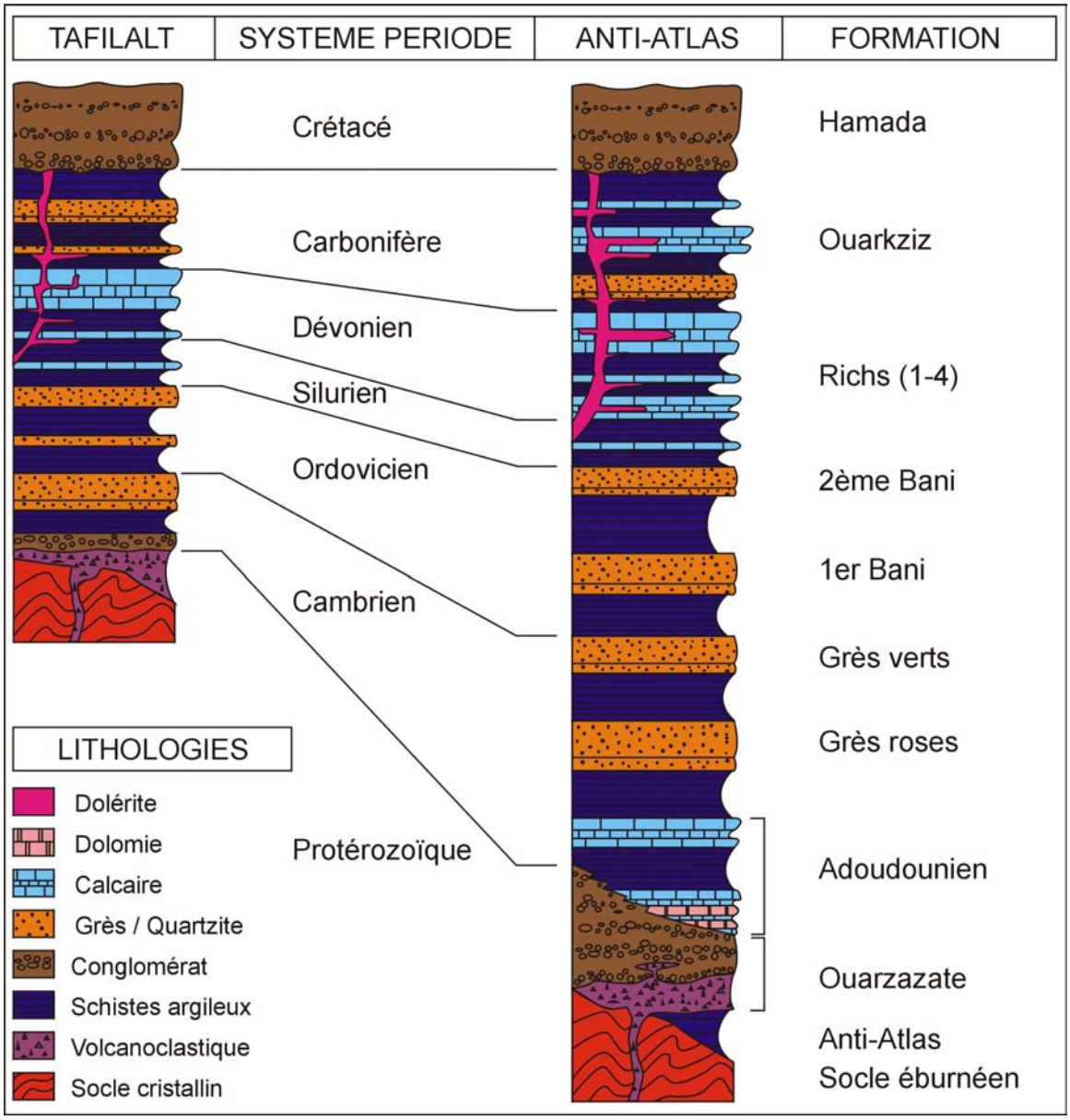

Figure 9. Formations et colonne stratigraphique de l'Anti-Atlas. Colonne de droite est dessinée d'après Soulaïmani *et al.*, 1997. Elle est typique de l'Anti-Atlas occidental.

Cambrien

La série de l'Adoudounien (Buggish et Flügel, 1988 ; Algouti *et al.*, 2001) se dépose après les Conglomérats de base couronnant le super-groupe de Ouarzazate. L'Adoudounien comprend les Calcaires inférieurs, la série Lie de vin et les Calcaires supérieurs (Figure 9). Dans le sud-ouest, des signes du rifting amorcé au Néoprotérozoïque terminal persistent jusqu'à la fin du Cambrien inférieur (Benssaou et Hamoumi, 2003). Cette série est fortement réduite dans

l'Anti-Atlas oriental et même absente à son extrémité la plus orientale (Figure 5, p.11). Ensuite, une série de schistes argileux se termine par le niveau marqueur des Grès roses. Le sommet des Grès roses marque la fin du Cambrien inférieur, absent sous cette forme à l'est de l'Ougnate. Les premiers sédiments présents sur l'ensemble du domaine anti-atlasique sont les Schistes à Paradoxides (trilobites) et les Grès verts, ensemble correspondant au Cambrien moyen. Tout à l'est, les grès trouvés à la base du Cambrien moyen sont attribués au Cambrien inférieur et non au super-groupe de Ouarzazate. Le hiatus du Cambrien supérieur correspond à la phase de rift qui sépare les terrains avaloniens du Gondwana par l'ouverture de l'océan Rhéic.

Ordovicien

L'Ordovicien demeure toujours à tendance détritique. L'Ordovicien inférieur débute par une puissante série de schistes argileux et se termine par les grès et quartzites du 1er Bani. L'Ordovicien supérieur ressemble beaucoup à l'inférieur, mais d'une plus petite épaisseur. Le niveau marqueur qui le couronne est le 2ème Bani. Il comprend des microconglomérats et des surfaces érodées témoignant d'une glaciation (Choubert et Faure-Muret, 1983).

Silurien

Tectoniquement, cette période correspond à l'ouverture de l'océan Proto- et Paléotéthys et à la dérive des terrains Huniques. Après la dominance du détritisme provenant du craton africain, le Silurien marque le passage à une sédimentation carbonatée. Ce changement est expliqué par une hausse du niveau marin qui commence par déposer une épaisse série de *black shales*, constituant une importante roche mère en Afrique du nord (MacGregor, 1996 ; Boote *et al.*, 1998). S'ensuit l'apparition de bancs calcaires qui vont dominer durant le Dévonien.

Dévonien

Durant cette période, la marge du Gondwana bénéficie d'un calme tectonique. Les Richs Dévoniens témoignent d'un niveau marin toujours haut. La composante calcaire est plus développée dans la partie orientale. Les calcaires

gris-bleutés à noirs terminent la formation des Richs. Ces niveaux condensés abritent une riche faune paléontologique de goniatites et d'orthocères notamment. Ceci témoigne d'une élévation du niveau marin et d'un environnement marin plus ouvert.

Carbonifère

Les sédiments Carbonifères témoignent d'un retour marqué du détritisme. Après une épaisse série de schistes argileux, la tendance devient gréseuse. Des figures de chenaux, des marques de courant et des bioturbations décrivent un environnement deltaïque. On trouve dans la partie nord de l'Anti-Atlas oriental des figures sédimentaires interprétés comme des tempestites. Les calcaires couronnant la série dans le sud-ouest sont absents dans la partie orientale.

La Figure 10 est une charte chronostratigraphique. Elle montre linéairement la répartition des dépôts sédimentaires selon le temps (et non selon l'épaisseur). Elle met en évidence les périodes de dépôt et de hiatus. Attention toutefois car les « trous » (hiatus apparent) peuvent également provenir de la tectonique par l'érosion de structures.

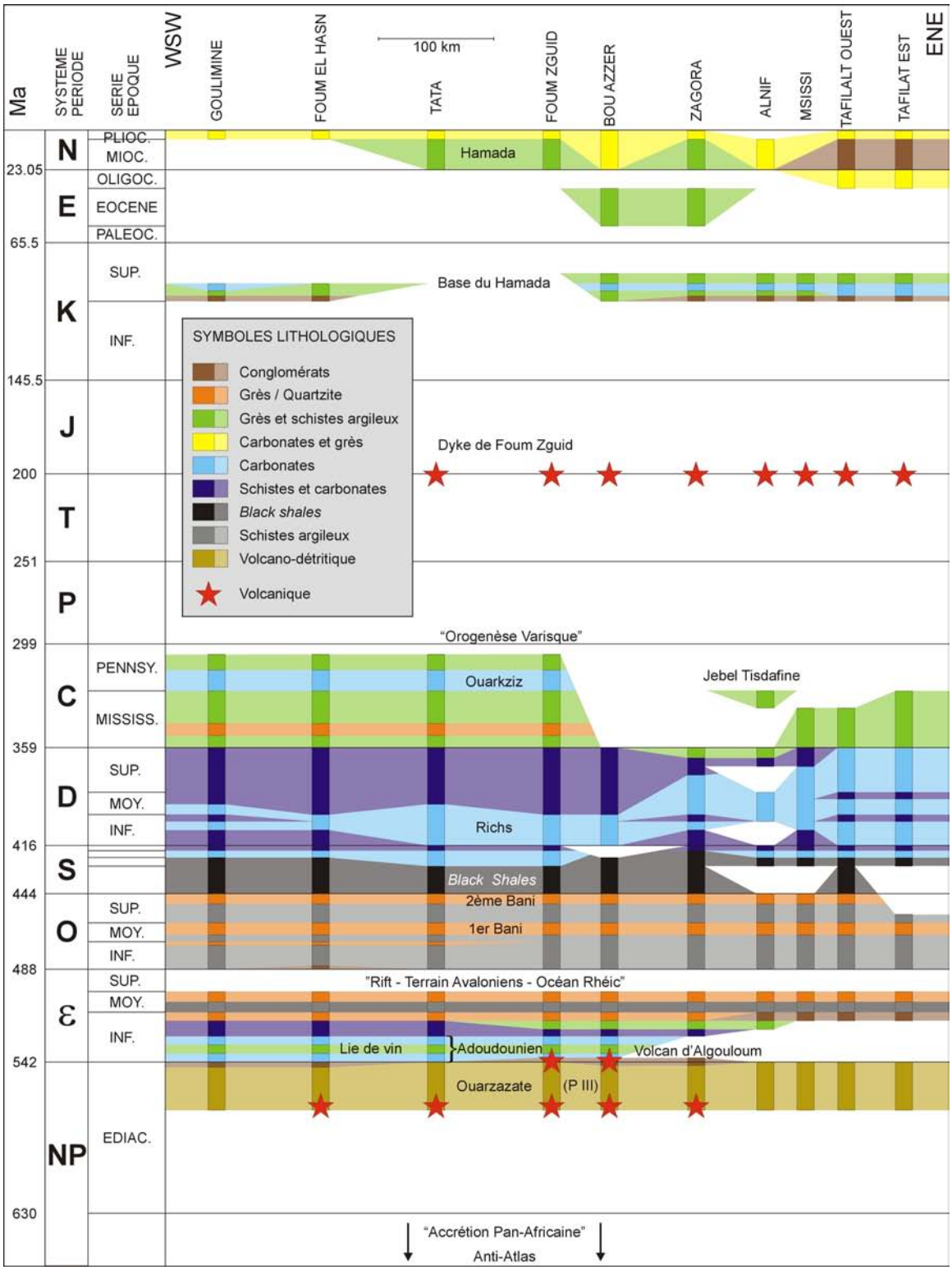

Figure 10. Schéma chronostratigraphique de l'Anti-Atlas. Compilation d'après les cartes géologiques au 1 : 200'000.

2.5. L'orogène Varisque

La chaîne de l'Anti-Atlas est une partie externe de l'orogène varisque (Appalaches-Ouachita-Mauritanides) (Figure 8, p.17). En terme de style tectonique, de chronologie et de géodynamique, les relations entre la chaîne de l'Anti-Atlas et les parties internes de cet orogène restent à élucider.

La compression varisque affecte l'Anti-Atlas vraisemblablement au Carbonifère supérieur. La datation relative de cet événement est difficile à contraindre puisque l'orogène varisque marque le début d'une longue période de non sédimentation. Les prochaines roches à sceller cette déformation, par recoupement de structures, sont des dolérites. Elles apparaissent principalement sous la forme de dykes. Mais elles se développent également en sills, ce qui peut être déroutant, car ils épousent la forme des plis. L'âge de mise en place de ces dolérites est daté à la limite Trias – Jurassique entre 206 et 195 Ma (Sebai *et al.*, 1991). Les plus anciennes roches sédimentaires à post-dater le plissement sont du Crétacé. Pour l'instant la date la plus plausible de cet événement est donnée par les compilations tectoniques globales, telles que celles de Stampfli et Borel (2002). Elles proposent un âge d'environ 320 Ma pour la collision des continents Laurussia et Gondwana au niveau de l'actuelle Afrique du Nord.

S'il est vrai que la Meseta (Figure 8, p.17) fait également partie de l'édifice varisque, des corrélations avec l'Anti-Atlas sont hasardeuses. Malgré sa proximité actuelle, sa position dans l'orogène varisque a été nettement plus interne. Elle a subi des déformations bien avant l'Anti-Atlas (Hoepffner *et al.*, 2005). Aujourd'hui la relation géométrique qui lie l'Anti-Atlas à la Meseta est masquée par le Haut Atlas.

2.6. Les événements post-varisques

Du Permien au Jurassique, aucun sédiment ne se dépose sur le domaine de l'Anti-Atlas. En revanche dans le Haut-Atlas central (au Nord de l'Anti-Atlas

oriental), plusieurs kilomètres de sédiments syn-rift se déposent du Trias à la fin du Jurassique (Manspeizer et al., 1978 ; Beauchamp *et al.*, 1999). On trouve également dans cette série sédimentaire des roches intrusives basaltiques, contemporaines des dolérites de l'Anti-Atlas, aux alentours de la limite Trias – Jurassique (Sebai *et al.*, 1991). Ces intrusions sont les prémices de l'ouverture de l'Atlantique centrale au Jurassique inférieur et moyen (Aït Brahim *et al.*, 2002).

Les prochains sédiments à se déposer dans l'Anti-Atlas, scellant la déformation varisque, sont d'âge Crétacé supérieur. Ils forment la base du Hamada. Ils débutent par des grès grossiers et des conglomérats ; suivent des marnes rouges, puis des calcaires. Aucun sédiment Paléocène n'est présent sur l'Anti-Atlas et la Hamada. Après ce hiatus, des sédiments continentaux et lacustres se déposent durant le Miocène, puis au Pliocène.

Sur la bordure nord de l'Anti-Atlas oriental (sud du Haut Atlas) la série Cénozoïque est plus complète. Elle enregistre l'inversion du Haut Atlas. Les conglomérats, calcaires marins et marnes rouges du Crétacé supérieur correspondent à la phase post-rift atlasique (Beauchamp *et al.*, 1999). Ils sont suivis par des sédiments Paléocènes et Eocènes d'environnement laguno-continental (calcaires lacustres, marnes gréseuses, oolithes). La première des deux phases d'inversion du Haut Atlas a lieu dès l'Eocène supérieur et durant l'Oligocène. Les sédiments Oligo-Mio-Pliocènes continentaux (molasses du bassin de Ouarzazate) se déposent ensuite (Görler *et al.*, 1988). La deuxième et la plus importante phase d'inversion du Haut Atlas intervient durant le Pléistocène et le Quaternaire inférieur (Frizon de Lamotte *et al.*, 2000 ; Ellouz *et al.*, 2003). Le raccourcissement de l'inversion du Haut Atlas est plus important sur les bords du bassin atlasique en particulier sur sa limite sud (Teixell *et al.*, 2003). Mais cette déformation n'affecte pas directement l'Anti-Atlas oriental.

Le relief particulièrement développé du Haut Atlas central est partiellement dû à l'inversion et à un épaississement crustal (Arboleya *et al.*, 2004). Une origine thermique est responsable de la topographie actuelle de l'Anti-Atlas et pour une

partie du Haut Atlas (Saddiqi *et al.*, 2005 ; Ayarza *et al.*, 2005). Les modèles géophysiques (gravimétriques) de Missenard *et al.* (2006) démontrent un amincissement lithosphérique (<70 km) orienté NE-SW. Cette anomalie est oblique par rapport au système atlasique et correspond géographiquement au volcanisme alcalin Néogène et Quaternaire, ainsi qu'à une bande d'activité sismique. Initiée par remontée mantellique durant le Miocène (Missenard *et al.*,2006), l'anomalie est actuellement davantage entretenue par la convergence tectonique des plaques Ibéro-Africaine et du craton saharien (Teixell *et al.*,2005).

3

STRUCTURES

Description des observations

3.1. Introduction

L'Anti-Atlas oriental est analysé selon différentes structures.

- La structure générale s'observe sur la carte géologique générale (Figure 5, p.11 et Figure 11), sur les vues Landsat (Figure 12). Elle est décrite par les coupes de la Figure 17, p.33).
- Par structures compressives et extensives, on entend celles que l'on observe sur le terrain. Elles sont typiquement métriques à hectométriques (représentées par les photographies). Vu leurs petites tailles, elles ne figurent pas sur les coupes ; en revanche leur mesure permet de caractériser l'orientation de la déformation. La Figure 22 (p.40) représente une partie des mesures effectuées.
- Sans parler de structures, une analyse spécifique de la bordure de l'Anti-Atlas oriental permet d'étudier ses relations avec les roches sédimentaires crétacées et cénozoïques.

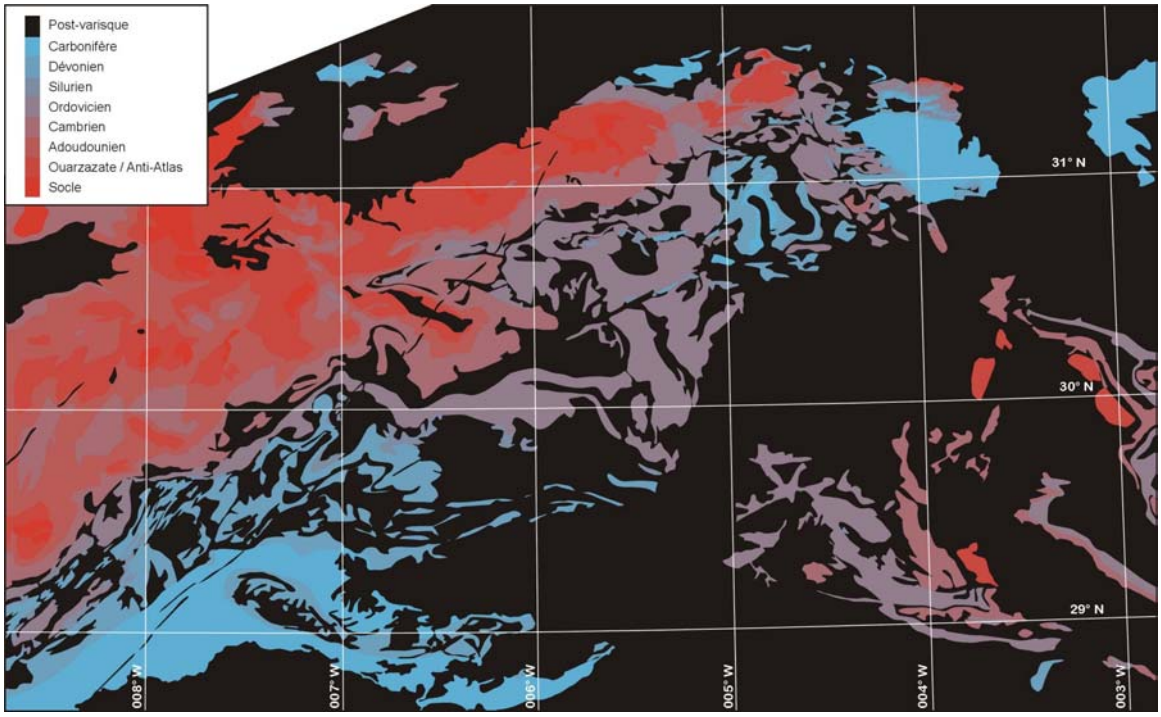

Figure 11*. Carte géologique de l'Anti-Atlas central et oriental. Cette carte n'illustre que les roches incorporées à la déformation varisque. Ainsi toutes les roches post varisques apparaissent en noir. Le rouge a été attribué aux roches les plus anciennes, le bleu aux roches les plus jeunes.

Figure 12. Image satellite Landsat avec la mise en valeur de certains contacts.

3.2. Stratigraphie mécanique

Le comportement mécanique des roches est mise en valeur par l'analyse des structures. Elle sera néanmoins discutée au préalable, puisqu'elle est un des principaux paramètres qui contrôlent le style de déformation.

Socle

Malgré une composition des plus hétérogènes et une forte anisotropie, les blocs de socle réagissent de manière homogène, comme des unités rigides avec de très faibles déformations internes. Ceci est visible sur les images Landsat (Figures 3 et 12). Mise à part la boutonnière de Bou Azzer, aucune relation géométrique directe ne lie la surrection des boutonnières et les différents éléments qui les composent, autant en terme d'âge (Eburnéen, super-groupe de l'Anti-Atlas ou de Ouarzazate) qu'en terme pétrologique (métamorphique, plutonique, volcanique ou sédimentaire). Par contre, les failles normales développées lors du rift précambrien prédéfinissent la structure du rejeu de la déformation varisque. Elles n'affleurent malheureusement pas dans l'Anti-Atlas oriental, mais certaines structures dans la couverture fournissent des indices sur leurs positions. Pour la partie orientale, le rift précambrien est davantage déduit de l'analyse de la nature des sédiments que de l'observation directe de structures. Il n'est pas non plus exclu que ces structures extensives soient déjà héritées d'événements Pan-Africains ou Eburnéens.

Contact socle - couverture

Dans les premiers temps de l'étude, un accent a été mis sur l'observation de cette limite et la série incompétente sus-jacente pouvant potentiellement contenir un décollement basal. Mais, outre certaines discordances angulaires, ce contact ne montre ni chevauchement, ni décollement basal. La Figure 13 montre ce contact sur différents sites. Cette absence de décollement basal est certainement la caractéristique la plus intrigante de la chaîne plissée de l'Anti-Atlas.

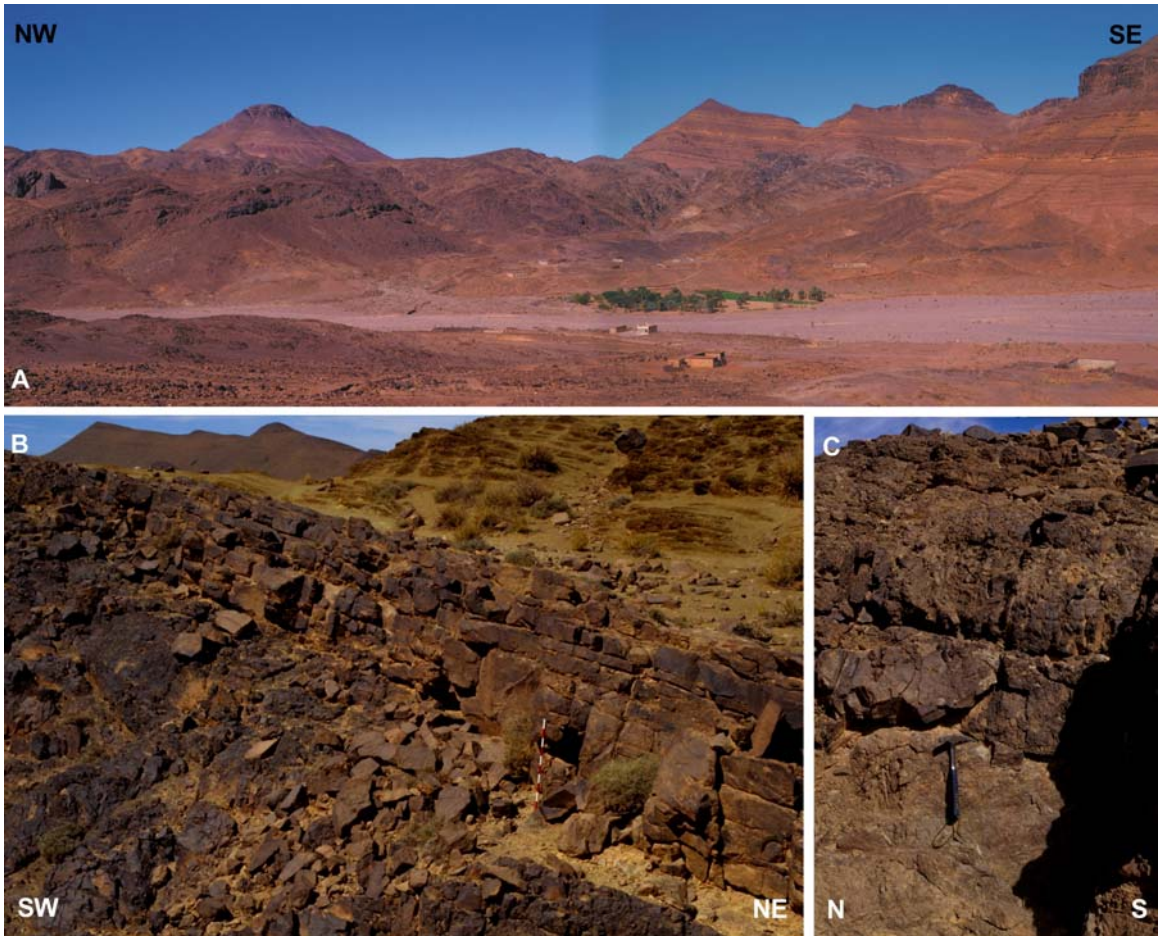

Figure 13. Contact socle-couverture. A : à Tazelaft, sud-est de la boutonnière du Saghro. Le socle est composé d'andésite et la couverture débute par les schistes argileux du Cambrien inférieur, surmonté des Grès roses ; B : sur la bordure nord du Saghro, le bâton rouge et blanc mesure 1 m, sa base repose sur la discordance, le socle est andésitique, suivent 2.50 m de Grès roses (conglomératiques) puis les schistes à Paradoxides du Cambrien moyen ; C : à l'extrémité est de la boutonnière de l'Ougnate. Rhyollite surmontée de grès conglomératiques.

Couverture

La couverture paléozoïque est très nettement dominée par de puissantes séries de faible compétence. Elle est ponctuée de niveaux marqueurs compétents. Ceci explique la morphologie typique de la couverture sous la forme de succession de cuestas (Figure 14).

Figure 14. Cuesta au sud de la boutonnière de l'Ougnate. Ici sous le 2ème Bani (Ordovicien supérieur).

Unités lithologiques structurales

La rhéologie des roches impliquées dans la déformation varisque est représentée dans la Figure 15. Cette colonne est une compilation des séries les plus complètes de l'Anti-Atlas oriental. Le tracé « *soft-stiff* » décrit la compétence relative des roches. Elle a été déterminée d'après les observations de terrain, les coupes et des critères de morphologie des affleurements (topographie).

Chaque unité lithologique structurale comprend un membre dominant dont la compétence et l'épaisseur relative au matériel environnant déterminent le comportement de l'unité. Les limites des unités sont comprises dans les intervalles incompétents. Les membres ou unités de conformation sont ceux dont la forme est imposée par un membre dominant. Selon ces termes définis par Currie *et al.* (1962), les deux membres dominants majeurs sont le socle et le 1er Bani. Les autres membres compétents sont davantage des membres de conformation, puisque leur forme générale épouse celle des membres dominants. Toutefois à plus petite échelle, chaque membre développe sa propre forme de structure de raccourcissement interne (*layer-parallel shortening*). Autrement dit, les structures de déformation interne sont caractéristiques de chaque membre dominant et indépendantes des membres sous- et sus-jacents.

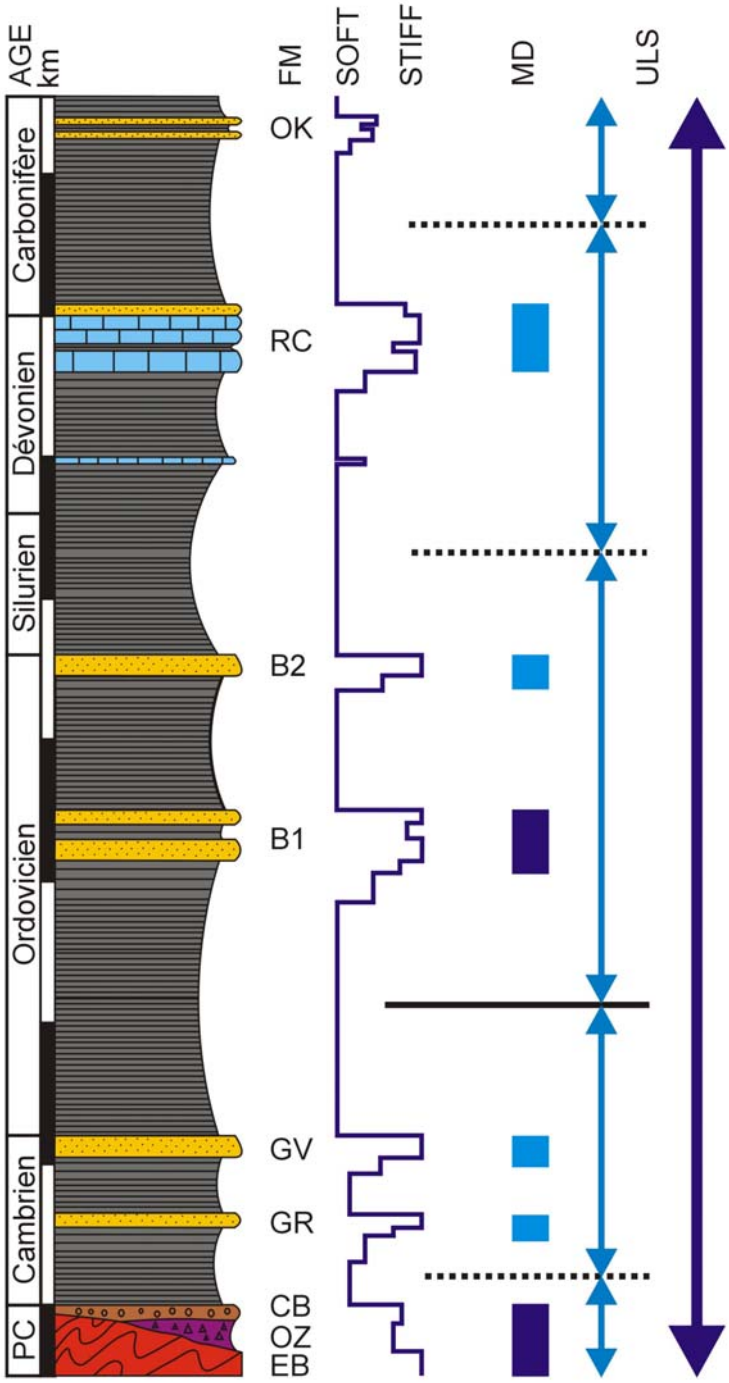

Figure 15. Stratigraphie mécanique et unités lithologiques structurales du socle et de la couverture varisque de l'Anti-Atlas oriental. FM : formations ; *Soft-Stiff* : Incompétent-compétant ; MD : membre dominant ; ULS : unité lithique structurale. EB ; socle éburnéen ; OZ : super-groupe de Ouarzazate et l'Anti-Atlas ; CB : Conglomérats de base ; GR : Grès roses ; GV : Grès verts ; B1 : 1er Bani ; B2 : 2ème Bani ; RC : Richs ; OK : Ouarkziz.

En ce sens on peut parler de déformation disharmonique et découper la colonne (Figure 15) en cinq unités lithiques structurales, avec une limite plus marquée dans les argiles de l'Ordovicien inférieur. A grande échelle, néanmoins, toute la

couverture paléozoïque se conforme au socle. L'ensemble de ces roches ne constitue ainsi qu'une seule grande unité lithologique structurale. La couverture est drapée sur les mouvements relatifs des blocs de socle. Ainsi dans le cas d'un pli forcé (Figure 16), cette mécanique prévoit un modèle avec des blocs de socle rigides forçant une série incompétente et créant dans les séquences de la couverture une déformation disharmonique.

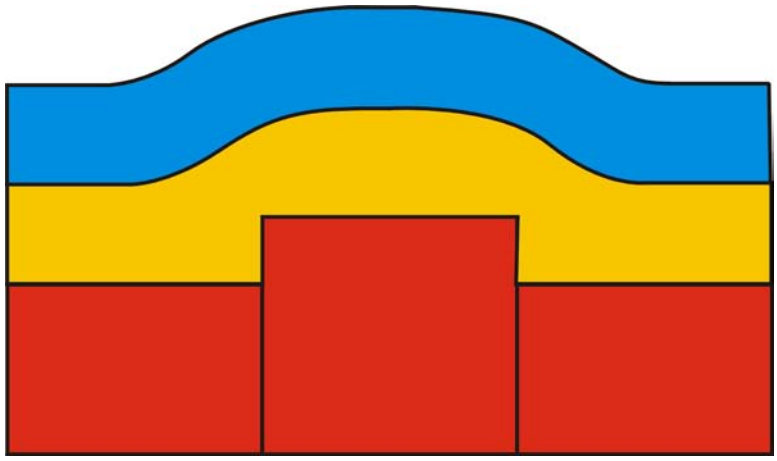

Figure 16. Effet de la mécanique sur un pli forcé ou de drapage (d'après Groshong, 2002). En rouge : unité rigide, en jaune : série incompétente, en bleu : de compétence intermédiaire.

Cette mécanique particulière explique en partie l'absence de chevauchement majeur. Les puissantes séries incompétentes permettent à la couverture de se déformer de manière plastique. Ce phénomène d'amortissement s'observe également dans les structures en extension.

3.3. Structure générale - Coupes

La Figure 12 permet de se rendre compte de la structure générale de l'Anti-Atlas oriental. L'affleurement des boutonnières donne la structure globale à savoir une forme anticlinale d'orientation ENE-WSW à l'ouest puis E-W à l'est (structure antiforme majeure). Au cœur de cet anticlinal se trouve le socle, puis de part et d'autre la couverture paléozoïque. Les affleurements sur le flanc nord sont

réduits, car la couverture est elle-même réduite, mais aussi parce qu'ils ont été masqués par l'inversion du Haut Atlas.

L'analyse du tracé du sommet de l'Ordovicien supérieur (2ème Bani) et celui de l'Ordovicien inférieur (1er Bani) montre une structure d'un ordre inférieur (structure majeure secondaire). Une succession de synclinaux et d'anticlinaux dont les axes sont orientés globalement N-S à NW-SE et plongent vers le sud-est. Mise en valeur par les membres dominants de l'Ordovicien, cette structure est également soulignée par les affleurements de socle (resserrement du Saghro, ensellement Saghro-Ougnate et dépression entre l'Ougnate et l'affleurement de l'extrémité est) et par les différents « bassins » Dévoniens et Carbonifères (Cuvette de Tazzarine, « bassin » de Mader et « bassin » du Tafilalt). Cette structure globale est également visible grâce à la carte géologique remaniée (Figure 11, p.26).

Construction des coupes

La structure de l'Anti-Atlas oriental est représentée par dix coupes (Figure 17) perpendiculaires à l'axe de l'anticlinal donné par l'alignement des boutonnières. Originellement, elles ont été construites par dessin à une échelle de 1 : 50'000. Le profil topographique provient des cartes topographiques du Maroc au 1 : 100'000. Les données géologiques proviennent d'abord des données de terrain, puis des cartes géologiques au 1 : 200'000 couplées aux vues satellites (limites lithologiques, failles) et aux cartes topographiques (calcul de pente sur les pentes structurales). Les interprétations en profondeur et au-dessus de la topographie ont été faites par simple projection. Sans preuves de variation, les épaisseurs ont été maintenues constantes. De même, l'orientation des failles normales a été conservée en profondeur. En revanche lors d'indications latérales évidentes, certaines failles ont été amorties en remontant dans la série ou inversement des failles ont été dessinées sous des structures non faillées. Aucune distinction stratigraphique n'a été faite dans le socle.

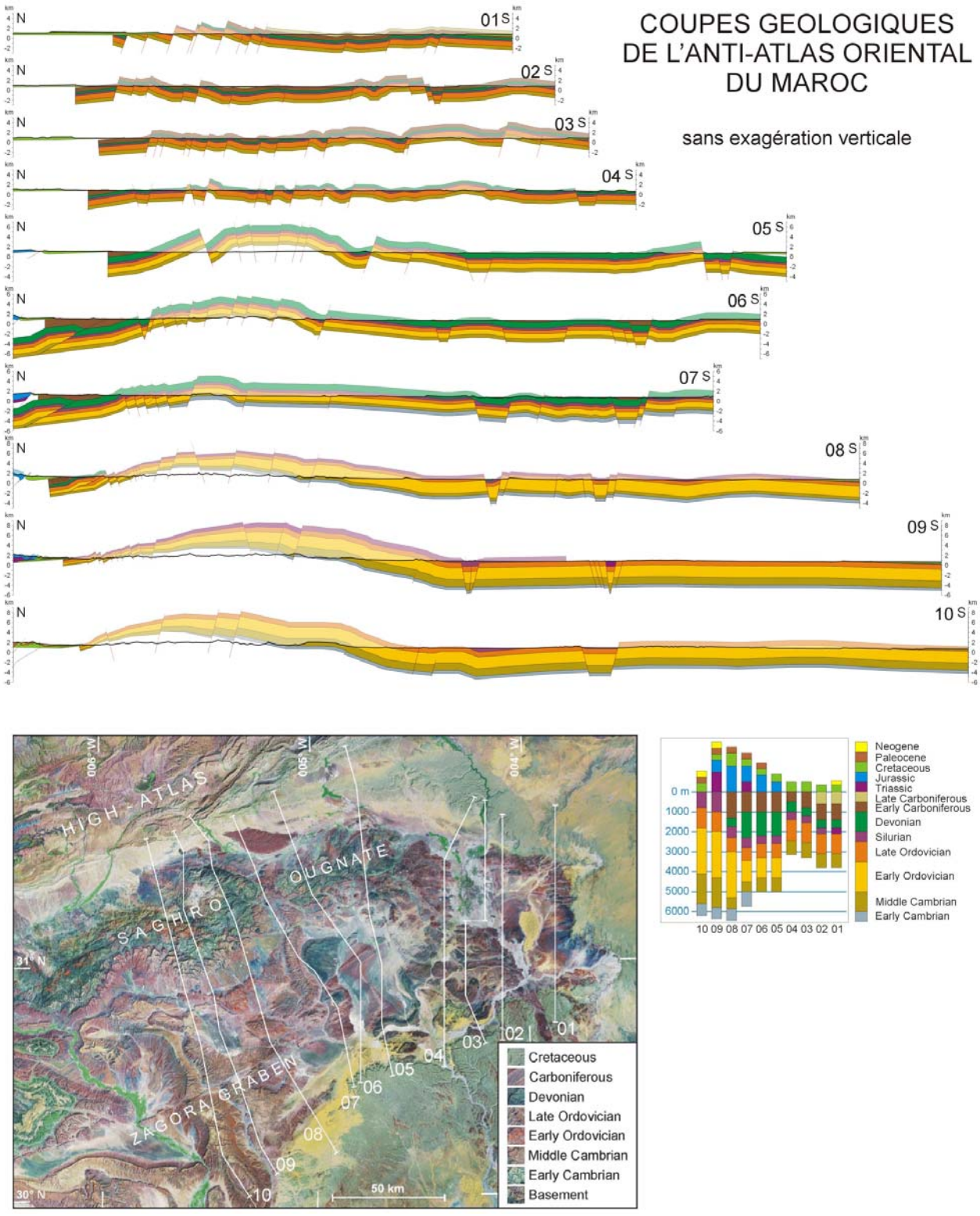

Figure 17*. Coupes géologiques de l'Anti-Atlas oriental. Image Landsat avec la position des coupes. Epaisseurs des séries dans les différentes coupes.

Description des coupes

Alors que les cartes géologiques et les images satellites fournissent une image d'un plissement modéré, les coupes font apparaître une structure générale particulièrement hachée par des failles normales. Sur le terrain, ces failles normales sont bien ou peu apparentes selon la série. Elles sont très marquées depuis le socle jusqu'au sommet de l'Ordovicien (1er Bani). Beaucoup d'entre elles sont amorties par le Silurien et le Dévonien inférieur (séries particulièrement incompétentes). Seuls des rejets importants permettent aux failles de traverser les séries Dévoniennes et Carbonifères.

Les failles normales tendent à minimiser la structure générale de cette partie de la chaîne. La structure anticlinale est bien visible sur les coupes 5 à 10, bien que son amplitude soit diminuée par l'effet des failles normales. Les coupes 1 à 4 paraissent plus monotones et il faut restaurer les failles normales pour voir apparaître cette structure principale. La coupe 1 montre toutefois une remontée de socle un peu plus importante qui étaye l'idée de la présence d'une boutonnière plus à l'est, aujourd'hui sous la Hamada.

Les coupes occidentales (10 à 5) montrent des failles normales très localisées créant notamment le graben de Zagora. A l'est (coupes 1 à 4), les failles normales sont plus nombreuses, mais avec des rejets plus faibles.

Les plis sur rampe dans la partie nord des coupes 6 et 7 sont une interprétation. Ils servent à contre-balancer la déformation particulièrement intense des sédiments Carbonifères dans cette zone. Le pli sur rampe – chevauchement de la coupe 8 est lui observé en surface ; sa géométrie en profondeur reste toutefois interprétative.

Les parties du Haut Atlas sont dessinées à partir des coupes de Frizon de Lamotte *et al.* (2000).

3.4. Structures compressives

Les observations à l'échelle de l'affleurement des différents bancs marqueurs ont permis de mettre en évidence plusieurs types de structures compressives. On distingue ici deux types : les plis et les failles chevauchantes. Les unes ou les autres apparaissent selon la puissance et la compétence des roches en présence.

Figure 18. Raccourcissement interne de la couverture. Chevauchement des bancs compétents et plissement des bancs incompétents. Interpénétration en « queue de poisson » (*Fishtail structure*). Dévonien moyen. Vue vers le SE. Bordure ouest du Tafilalt. N 31°16.800' / W 004°20.400'. Marteau dans le synclinal du banc incompétent.

La Figure 18 montre les deux cas. Les bancs de calcaire sont plus cassants, la déformation provoque un chevauchement. Au-dessus de cette structure, la lithologie est plus incompétente, le banc n'est « que » plissé. La déformation est diffuse, elle se répartit dans tout le volume de la couche. Lorsque les conditions d'affleurement permettent l'observation des séries incompétentes, on distingue une multitude de petits chevauchements presque parallèles au litage (Figure 19).

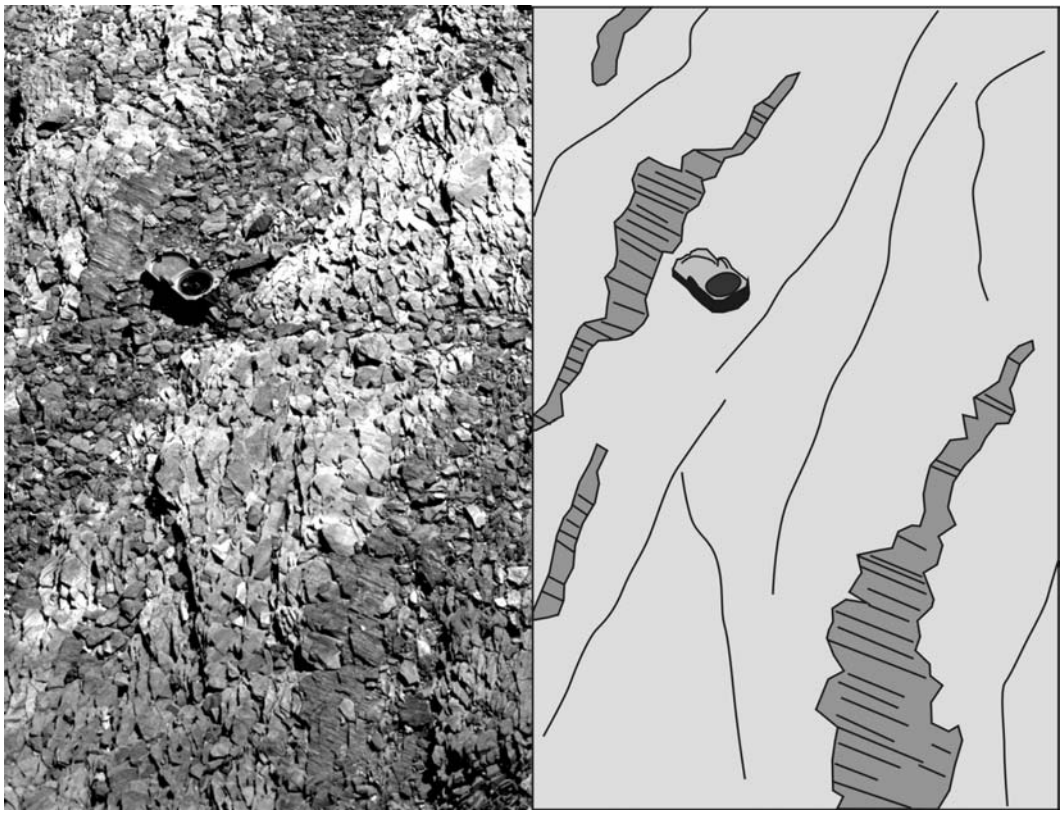

Figure 19. Plans striés de chevauchements mineurs dans des schistes argileux (Ordovicien inférieur), illustrant le style caractéristique de déformation interne dans les séries incompétentes. Sur la bordure nord du Saghro : N 31°24.361' / W 005°30.192'. La boussole est orientée au Nord.

La déformation (pli ou chevauchement) est extrêmement localisée, latéralement le long du même banc et à l'intérieur d'une succession de bancs. Ainsi un banc peut être très régulier et seule une portion limitée peut être affectée par un pli ou un chevauchement (Figure 20). D'autre part dans une série de bancs séparés par des intervalles incompétents, seul un banc peut être déformé localement, la déformation du prochain banc se situant ailleurs.

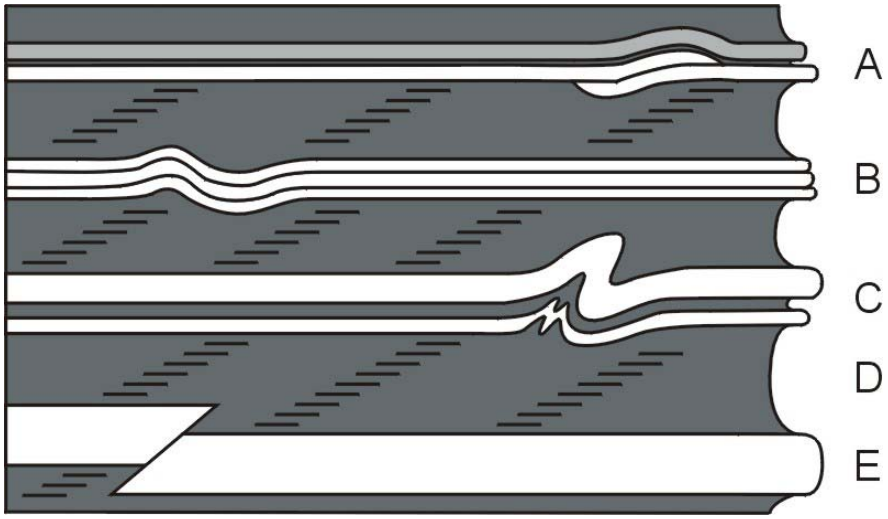

Figure 20. Schéma illustrant l'indépendance des petites structures et leur différentes formes en relation avec leur compétence. A : Structure en « queue de poisson » (*Fishtail*), illustrée par la Figure 17. B : Plissement harmonique de type « *buckling* ». Présence de cisaillement banc sur banc. C : Plissement d'un banc dominant, présentant des poly- ou des disharmonies. D : Multitude de microchevauchements sub-parallèles à la stratification (Figure 19). E : Faille inverse dans un banc massif.

Les « petits »plis

Au sud des boutonnières, les plis sont isolés. Ils ne montrent pas de vergence particulière. Au nord des boutonnières par contre, ils apparaissent beaucoup plus régulièrement, voire en continu. Leur vergence est clairement orientée vers le sud. La Figure 21 montre quelques plis typiques. Les mesures des plis sont représentées par les stéréogrammes jaunes en hémisphère inférieur (Figure 22). Dans une zone donnée, les mesures de plusieurs plis sont reportées sur un seul stéréogramme. Les points sont des pôles de plans de stratification mesurés dans ces plis. L'axe du pli est le pôle (perpendiculaire) du plan dessiné par la somme des pôles de la stratification. Les axes ne sont pas dessinés sur la Figure 22. Les données sont brutes, donc non retro-basculées par rapport au pendage général des bancs dans lesquels les plis ont été mesurés. Ceci explique le caractère bimodal du stéréogramme au sud de l'Ougnate (à l'est de la longitude W005°00'). Dans cette zone, les mesures des plis ont été prises dans des bancs avec un pendage général plongeant tantôt vers le sud, tantôt vers le nord.

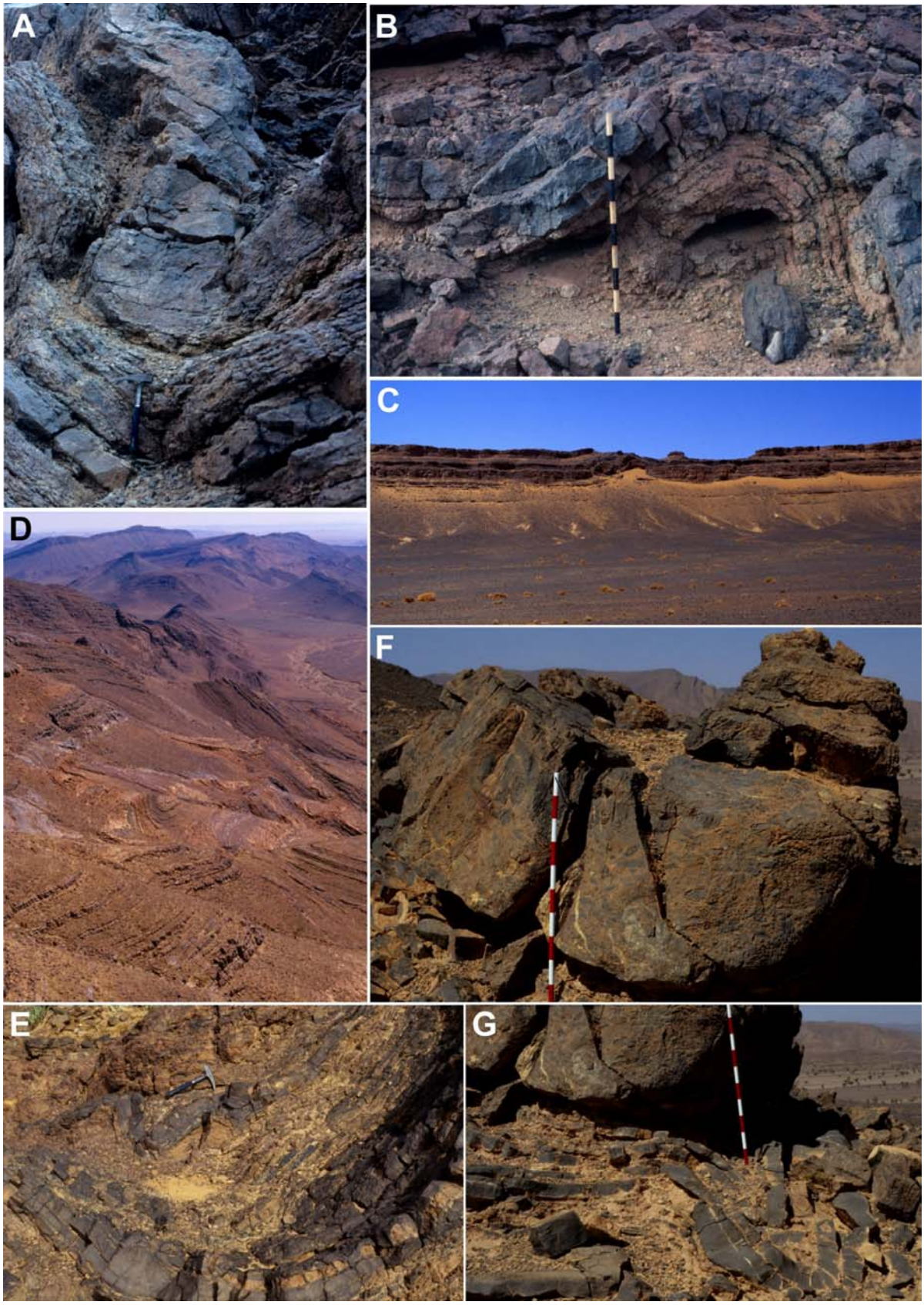

Figure 21. Photographies de petits plis (Planche 1/2).

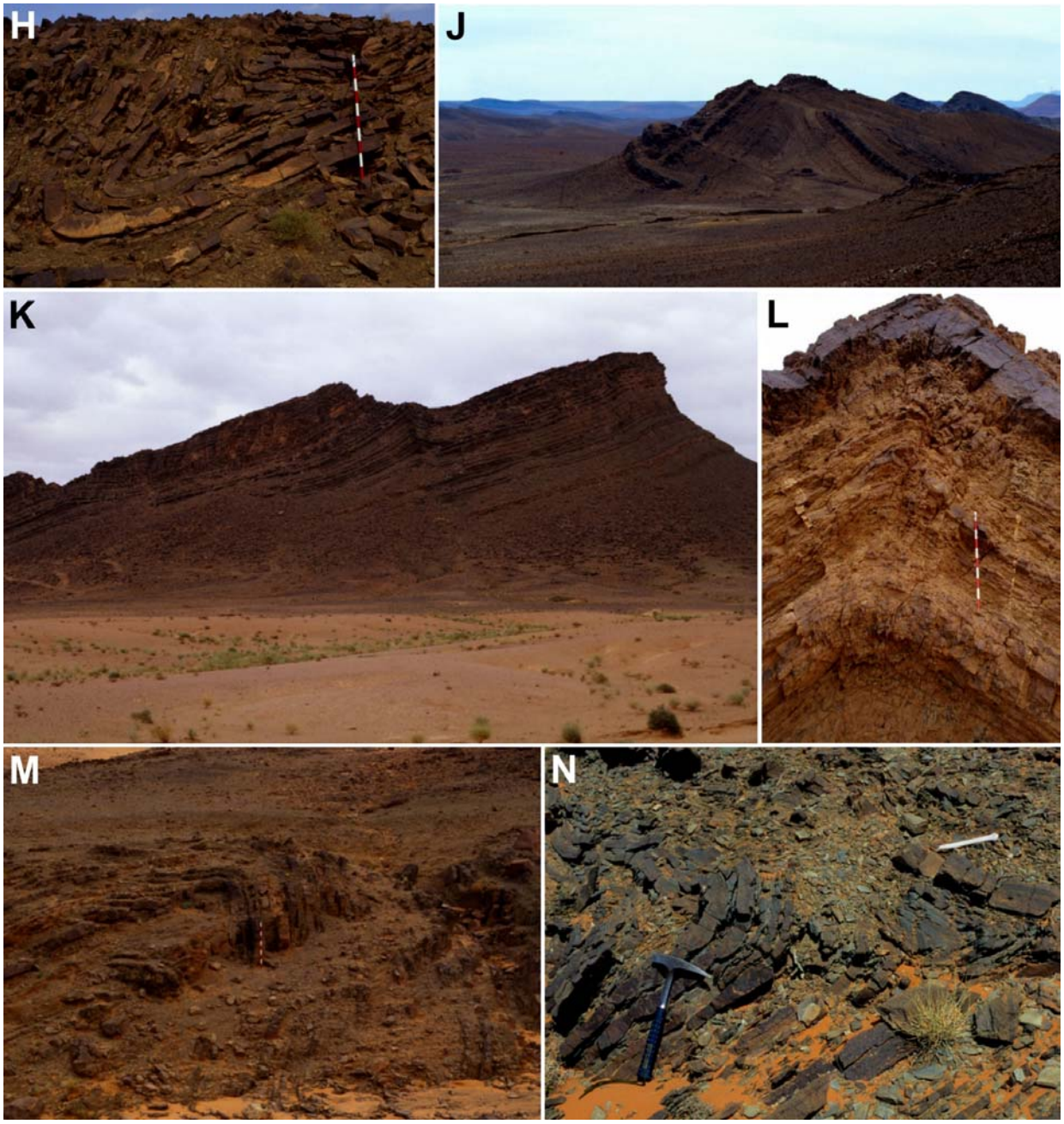

Figure 21. (Planche 2/2).

Légendes de la Figure 20 :
A : Plis dans le Dévonien moyen. Vue vers le SE. Bordure ouest du Tafilalt.
N 31°16.800' / W 004°20.400'. Marteau en bas de l'image.
B : Pli dans le Dévonien moyen. Vue vers le NW. Bordure ouest du Tafilalt.
N 31°15.750' / W 004°23.400'. Echelle 1 m.
C : Pli dans le Dévonien moyen. Vue vers le NW. Bordure ouest du Tafilalt.
N 31°15.550' / W 004°23.540'. La falaise fait 200 m de long.
D : Structure majeure secondaire et petits plis dans le Cambrien moyen. Vue vers le SE. Appendice Cambrien au sud de l'Ougnate. Depuis N 31°17.194' / W 004°55.591'. Le synclinal au premier tiers inférieur mesure environ 10 m de large.
E : Plis disharmoniques dans le Dévonien. Vue vers le Nord. Sud de l'Ougnate.
N 31°15.020' / W 004°48.360'. Marteau au centre.
F + G : (la vue G est à la base de la vue F) Plis dans le Dévonien. Vue vers le NW et NNW. Au sud de l'Ougnate. N 31°13.220' / W 004°53.760'. Echelle 1 m.

H : Plis dans le Carbonifère. Vue vers le NE. Jebel Tisdafine (Carbonifère au nord de l'ensellement Saghro – Ougnate). N 31°27.150' / W 005°18.950'. Echelle 1 m.
J : Pli-faille dans le 1er Bani. Vue vers le WSW. Bordure NNW du Saghro. Depuis N 31°24.120' / W 005°37.640'. L'anticlinal fait 100 m de large.
K+L : (vue générale et détail) Pli dans le Carbonifère. Vue vers le NE. Jebel Asdaf, lambeaux Carbonifère isolé dans l'Oued Todra à l'ouest de l 'Ougnate. N 31°25.455' / W 005°12.368'. K : 250 m de large, L : échelle 1 m.
M : Pli déversé vers le SE dans le Dévonien. Vue vers le NE. Au nord du Saghro. N 31°27.240' / W 005°30.950'. Echelle 1 m.
N : Pli couché dans le Dévonien. Vue vers l'est. Au nord du Saghro.
N 31°28.200' / W 005°31.400'. Marteau en bas à gauche.

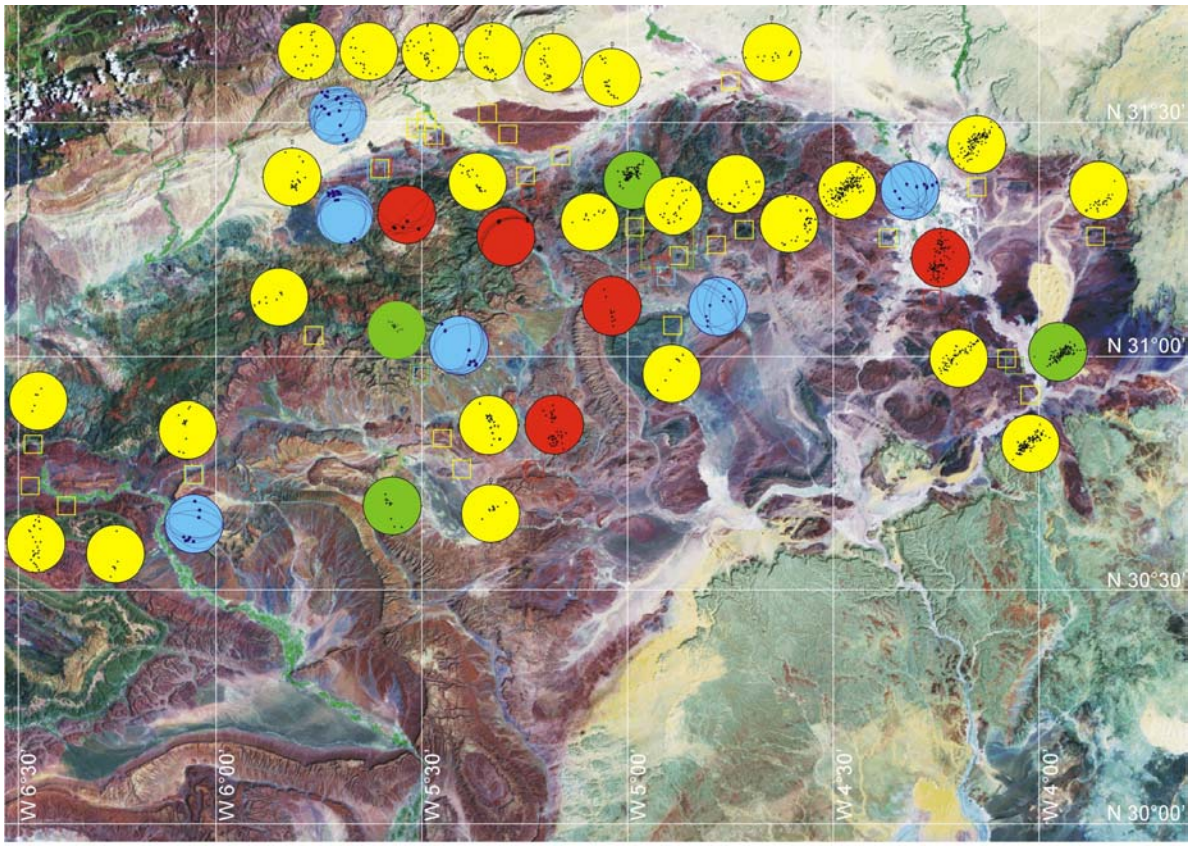

Figure 22*. Stéréogrammes des structures mesurées. Jaune : petits plis. Bleu : chevauchements. Rouge : structures extensives. Vert : structure générale.
Projection de Wulff, hémisphère inférieur.

L'analyse de l'orientation de ces petits plis met en évidence deux orientations préférentielles. L'une à axe E-W (les pôles des plans de stratification sont alignés N-S) l'autre à axe NW-SE (pôles des plans de stratification alignés NE-SW). Les petits plis à axe NW-SE dominent la moitié est, au sud des boutonnières (à l'est de la longitude W005°00' et au sud de la latitude N31°30'). Les deux orientations coexistent dans la région de Tazzarine (entre W005° et

W006° de longitude et N30°30' et N31°00' de latitude), alors qu'à l'ouest de W006° l'orientation E-W domine. Cette dernière domine également au nord des boutonnières avec une tendance ENE-WSW, à l'exception d'un cas isolé au nord de l'Ougnate qui présente un axe N-S.

Failles chevauchantes - inverses

Les chevauchements sont plus rares que les plis. Les structures en « queue de poisson » (*Fishtail*) sont un encastrement de bancs plus massifs. Dans les séries massives des failles inverses très raides se développent. Alors que dans les série de faible compétence, les chevauchements ont tendance à se paralléliser à la stratigraphie. Il n'est pas rare de voir le plan de faille se matérialiser par une minéralisation, généralement siliceuse. Ceci donne lieu à des plans striés résistants à l'érosion. Les cristaux de roche (Quartz) y abondent. Au nord des boutonnières, les petits chevauchements sont beaucoup plus intenses, en terme de nombre et de rejet. La Figure 23 montre quelques exemples de chevauchements. Leurs stéréogrammes apparaissent en bleu sur la Figure 22. Les grands cercles représentent les plans de failles et les points, les stries. Les chevauchements se développent dans les séries plus compétentes et massives. De part et d'autre de la lithologie rigide, le chevauchement « se perd » dans les séries incompétentes. On observe trois directions de contrainte principale. Une contrainte d'orientation NE-SW domine la partie est, elle correspond aux plis d'axe NW-SE. Une deuxième orientation est perpendiculaire à la première avec une contrainte orientée NW-SE. Elle est très marquée au nord des boutonnières et coïncide avec les orientations des petits plis et de la structure générale. Une troisième orientation dans l'ouest traduit des contraintes N-S.

En terme de structures compressives, notons encore la présence d'une schistosité (Figure 24) au nord des boutonnières. Elle est absente dans le reste de l'Anti-Atlas oriental. Cette schistosité est très raide et plonge vers le Nord. Son orientation suit celle des petits plis de cette zone.

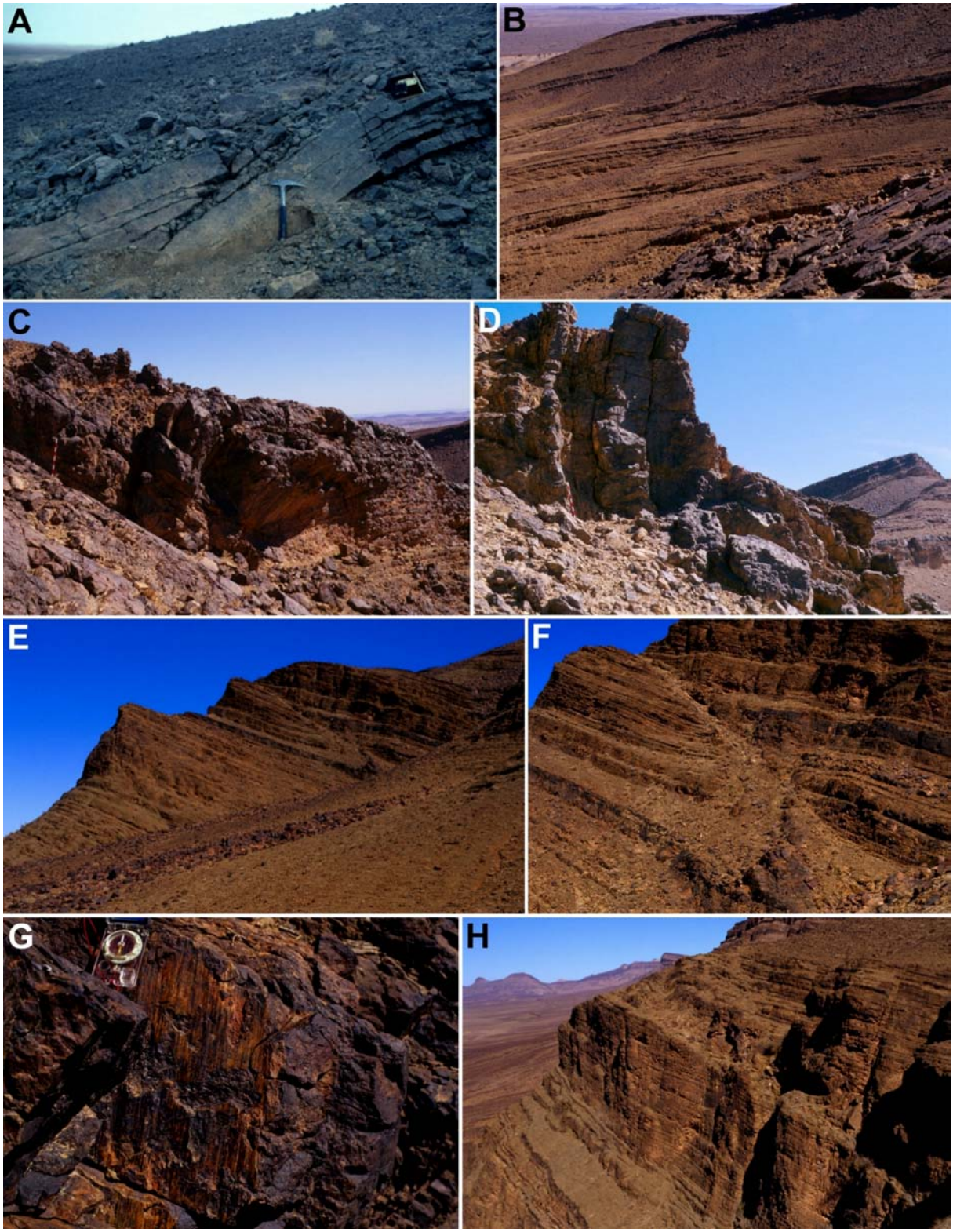

Figure 23. Photographies de chevauchements (Planche 1/2).

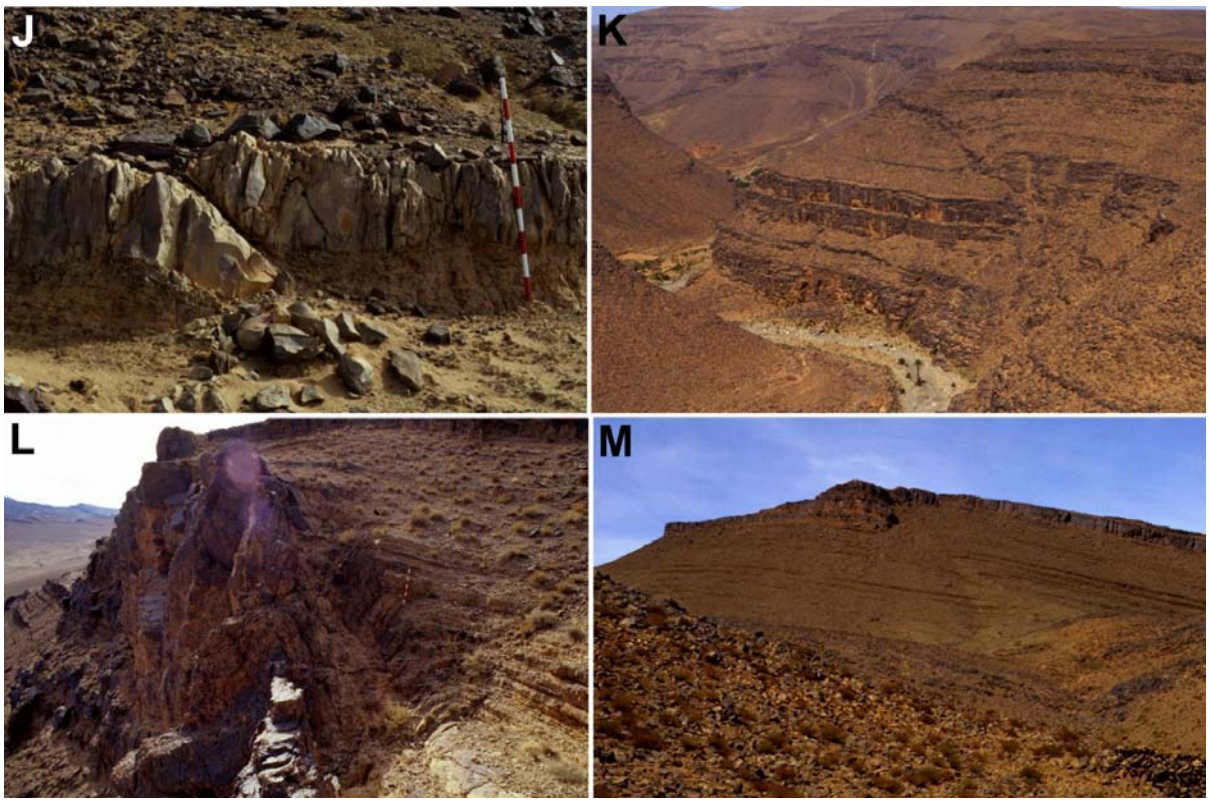

Figure 23. (Planche 2/2).

Légendes de la Figure 22 :
A : Chevauchement dans un banc massif du Dévonien moyen. Vue vers le SE. Centre du Tafilalt. N 31°19.900' / W 004°10.050'. Marteau au centre.
B+C+D : Chevauchements dans le 2ème Bani. Sud de l'Ougnate. N 31° 11.250' / W 004°55.250'. B : Plan de chevauchement avec un angle aigu par rapport à la stratification, le plan de faille est matérialisé par une minéralisation siliceuse, vue au SSE, le second plan est à 100 m. C + D : Chevauchement et crochon dans le toit, vue au SE, bâton 1 m.
E+F+G+H : Chevauchement dans le 1er Bani à l'ouest de Tazzarine. N 30°44.250' / W 006°04.450'. E+F : Chevauchement et crochon, vue vers le SE, le chevauchement mesure 30 m. G : Plan strié dans le crochon, vue vers le Sud, boussole orientée. H : Crochon supérieur, « diffusion » du chevauchement, vue vers l'est, longueur du chevauchement 30 m.
J : Structure *Fishtail* dans le Dévonien. Sud de l'Ougnate. N 31°15.000' / W 004°48.375'. Echelle 1 m.
K : Faille inverse et chevauchement dans le Cambrien. Vue vers le NE. Au SE du Saghro (nord de Tazzarine). Depuis N 30°56.610' / W 005°31.210'. Palmier dans l'oued.
L : Faille inverse minéralisée et crochon supérieur dans l'Ordovicien inférieur. Vue vers le WSW. Bordure NNW du Saghro. N 31°24.115' / W 005°37.525'. Echelle 1 m.
M : Chevauchement et « pli sur rampe » dans le Cambrien moyen. NNW du Saghro. N 31°23.320' / W 005°37.930' (sommet). La falaise fait 200 m de long.

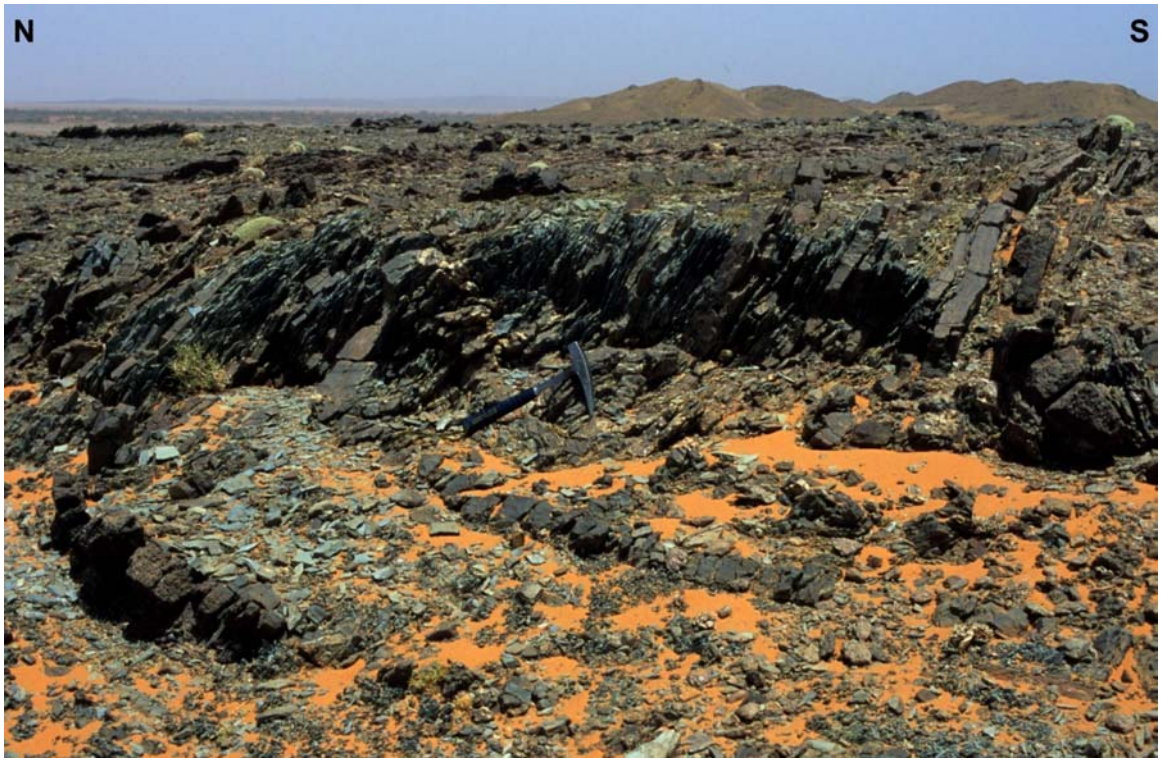

Figure 24. Schistosité dans les plis déversés Dévoniens. Vue vers l'est. Au nord de la boutonnière du Saghro. N 31°28.200' / W 005°31.400'. Marteau au centre.

3.5. Structures extensives

Les observations directes des failles normales sont rares. La Figure 25 en représente quelques exemples. Les failles normales ont davantage été mises en évidence par des zones de contact de deux formations contrastées espacées dans la colonne lithostratigraphique. Leur rejet est estimé grâce à la connaissance des puissances des formations. La plupart des mesures de l'orientation des failles normales ont été prises non pas sur la faille principale, mais sur des failles secondaires dans la zone de faille avec des rejets plus petits.

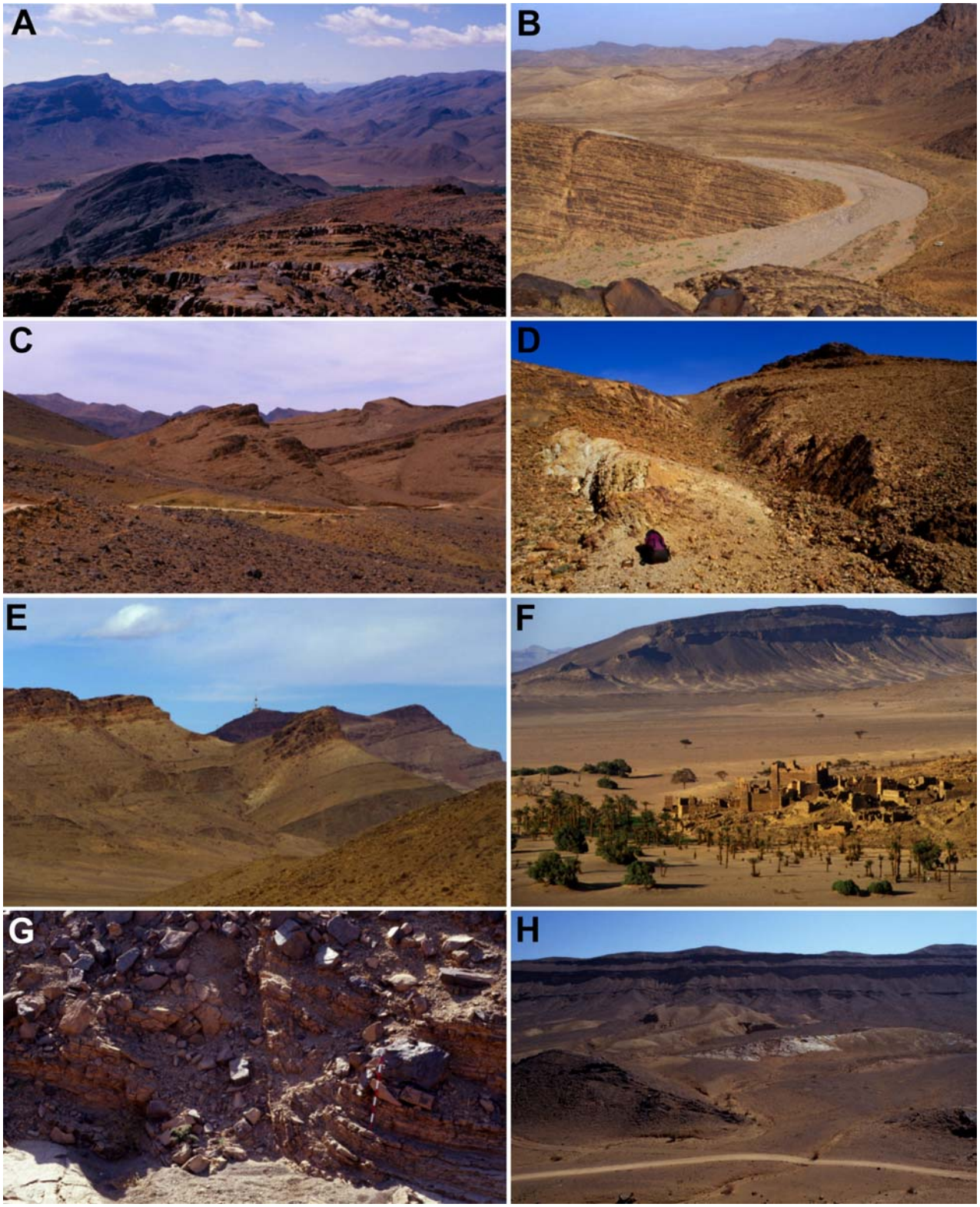

Figure 25. Photographies des structures extensives (Planche 1/2).

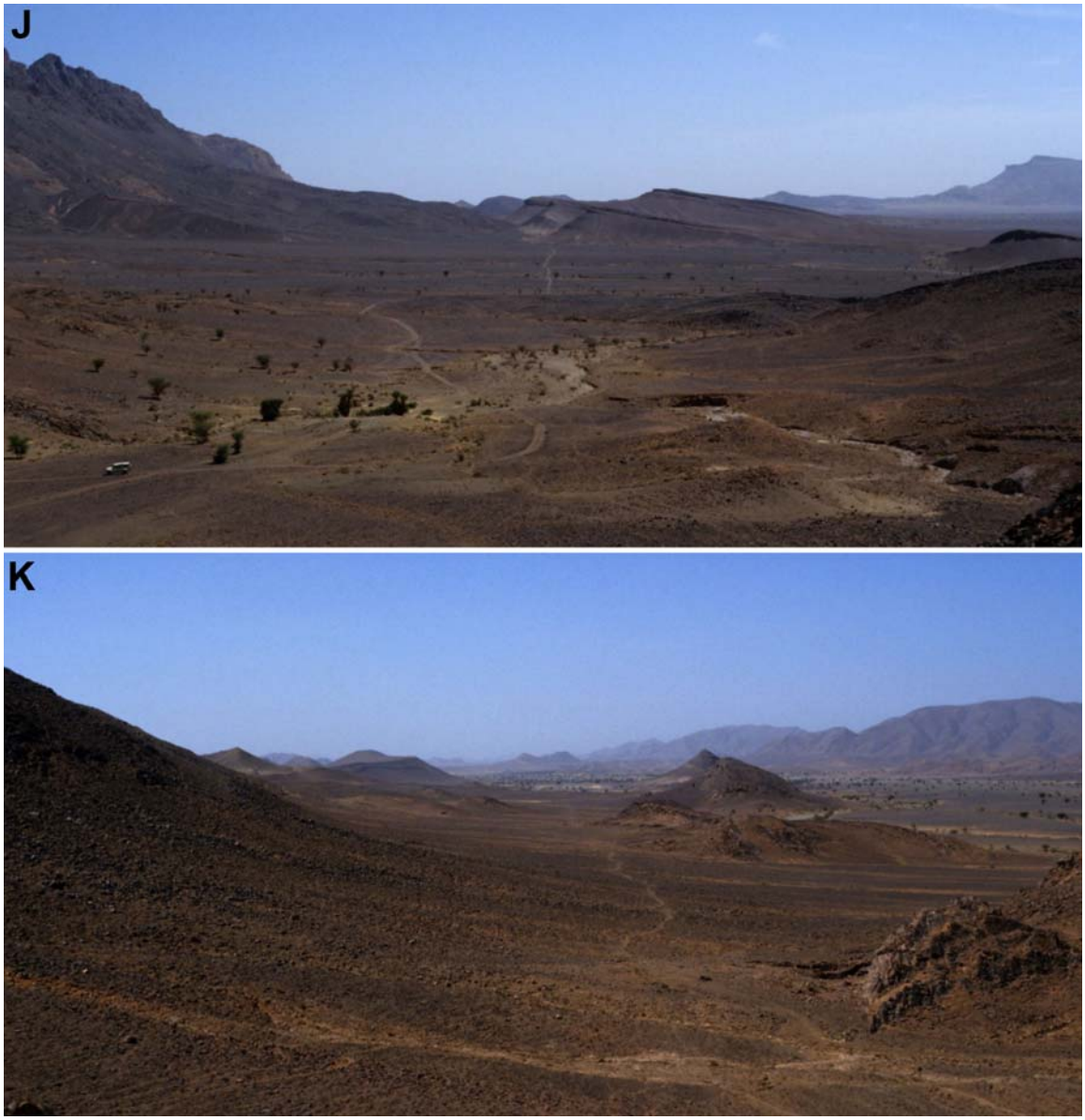

Figure 25. Photographies des structures extensives (Planche 2/2).

Légendes de la Figure 24 :
A : Faille normale dans le sud de l'Ougnate. Vue vers l'ouest. Depuis N 31°16.590' / W 004°56.025'. Le sommet de gauche est à 4 km. Sans considérer le premier plan, les deux cuestas (au sud et au nord) sont du Cambrien moyen. Cette répétition est due à une faille normale qui plonge au nord. On trouve du socle au pied de la falaise de gauche.
B : Faille normale dans l'Ougnate. Vue vers l'est. Depuis N 31°20.945' / W 005°00.800'. Landrover en bas à gauche. La faille normale plonge au nord et met en contact le socle et la cambrien inférieur.
C+D : Faille normale au nord de l'ensellement Saghro-Ougnate. N 31°20.300' / W 005°16.850'. C : vue vers l'ouest, le bloc central (à 300 m) est le 1er Bani de l'Ordovicien, il est en contact (au sud) avec du Cambrien moyen, la faille normale plonge vers le Nord. D : vue vers l'est, la faille normale est dans l'Ordovicien inférieur, la particularité est que les stries de la faille normale sont sur-imprimées de stries indiquant un mouvement dextre. Sac à dos pour échelle.
E : Faille normale dans l'Ordovicien inférieur. Vue vers le NE. Bordure nord du Saghro. Depuis N 31°23.995' / W 005°37.360'. La faille plonge au SE.
F+G+H : Graben à l'est de la cuvette de Tazzarine. Zone N 30°45' / W 005°13'. F : Limite nord du graben. Vue au Nord. Au fond les falaises du 1er Bani, plus en avant la faille normale

plongeant au SSE, la plaine avec quelques affleurement de Dévonien et Silurien et à nouveau le sommet du 1er Bani sous la khasbah. G : Faille normale et pli d'entraînement dans le Dévonien aux abords de la limite sud du graben. Echelle 1 m. H : Limite sud du graben. Vue vers le sud, la falaise est le 1er Bani qui plonge au sud, devant la falaise la faille normale plonge au nord, au premier plan les affleurements Dévoniens plongent au nord.
J+K : Vues sur l'importante faille normale du sud de l'Ougnate. Depuis N 31°15.480' / W 004°45.990'. J : Vue vers l'est. La faille sépare le Dévonien moyen (au nord) du Cambrien moyen (au sud). Le Dévonien plonge localement au nord, le Cambrien plonge au sud, la série est régulière et continue, au loin à droite les falaises du 1er Bani. K : Vue vers le WSW. Au sud la cuesta de Cambrien supérieur plonge au sud. Les différents affleurements sur la droite sont du Dévonien qui plonge globalement au nord. A droite au loin sort une cuesta du 2ème Bani (Ordovicien supérieur), plongeant au sud. En plein centre au loin un synclinal perché de Dévonien témoigne de la faille.

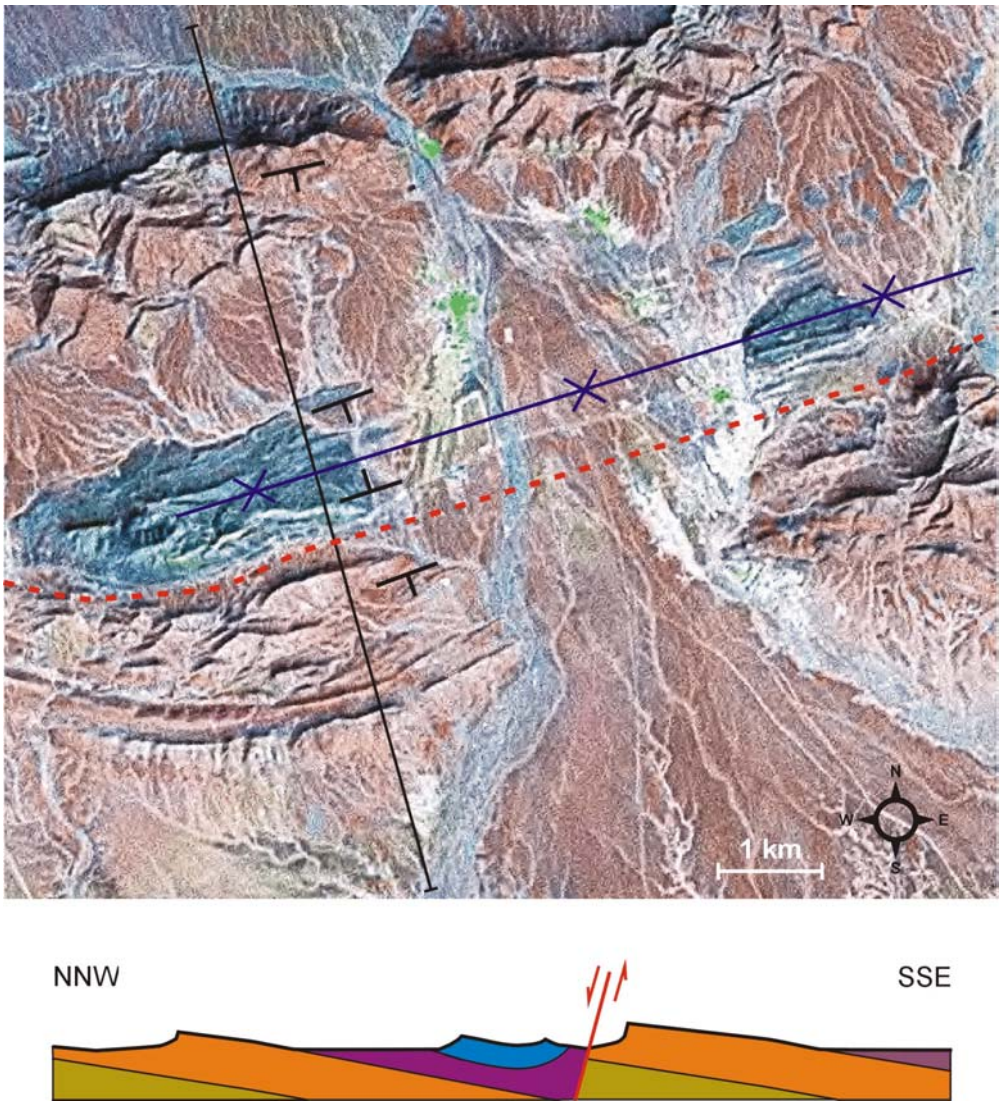

Figure 26. Vue Landsat et en coupe d'un synclinal lié à une faille normale au sud de la boutonnière de l'Ougnate.

Une toute autre manière de signaler leur présence sont les synclinaux que les failles normales provoquent dans les formations du toit, lorsque ces dernières, de faible compétence, « glissent » sur des roches du mur très rigides. Ces plis d'entraînement ont souvent été interprétés comme plis varisques. Ces structures liées à l'extension sont d'autant plus déroutantes que comme tous les plis, elles présentent du cisaillement chevauchant entre les bancs. Ces synclinaux sont plus ou moins horizontaux. Cela varie en fonction de la configuration de la structure majeure. Ils se caractérisent par un flanc limité par la faille (généralement le plus raide) et un flanc en concordance avec le reste de la série (Figure 26). Ces structures ont été observées dans le système du rift de la Mer Rouge (Khalil et McClay, 2002) et sont connues dans d'autres systèmes en extension (Schlische, 1995). Elles sont également décrites dans des modèles expérimentaux (Withjack *et al.*, 1990 ; Hardy et McClay, 1999 ; Finch *et al.*, 2004). Les modèles avec une couverture ultra-incompétente semblent le mieux correspondre à la configuration observée dans l'Anti-Atlas oriental. Selon Xiao et Suppe (1992), le développement de ces structures est induit principalement par une géométrie de faille de type listrique.

Toutes les failles normales observées sont très raides, leur plongement est typiquement compris entre 70 et 80°. L'orientation de leur trace est constante dans tout l'Anti-Atlas oriental : E-W avec de légères variations de WSW-ENE à WNW-ESE. Aucune autre orientation n'a été observée. Outre les grabens symétriques, une majorité des failles normales plongent vers le nord, à l'exception de la partie nord des boutonnières où les plongements sud dominent.

Les données de structures extensives sont représentées en rouge sur la Figure 22 (p.40). Un seul stéréogramme représente directement les failles avec leur grand cercle et leur strie. Les autres stéréogrammes montrent les pôles de stratification mesurés dans les synclinaux provoqués par ces failles. L'axe de pli que l'on peut déduire, donne la direction de la trace de la faille. Le très fort pendage, que peut obtenir le flanc en contact tectonique, témoigne du fort plongement de la faille normale.

3.6. Relations avec les roches récentes et topographie

Les premières roches à réellement sceller la déformation de l'Anti-Atlas sont des conglomérats crétacés. Cette discordance tectonique est bien visible à grande échelle sur les cartes géologiques (Figures 5 et 11). Elle est particulièrement bien mise en évidence à l'est du Tafilalt où les roches de la base de la Hamada côtoient successivement toutes les formations de la série paléozoïque et même des parties de socle.

Cette discordance est visible au nord du Saghro (photographies A et B de la Figure 27). Une discordance relativement plate sépare le Carbonifère intensément déformé, des sédiments crétacés. Ces couches conglomératiques ont aujourd'hui un faible pendage vers le nord, mais elles reposent sur la surface érosive de manière conforme, sans discordance angulaire. Cette configuration n'est toutefois pas applicable à l'ensemble du domaine. En effet, si l'on projette linéairement le plan de stratification crétacé, il butte contre les affleurements de socle. Malgré des recherches, ce contact socle – Crétacé n'a pas été directement observé, l'érosion provoquant le retrait des cuestas de Crétacé (Figure 27 D).

Au-dessus des sédiments crétacés, reposent en concordance, des couches du Paléogène. Elles sont suivies des sédiments néogènes, avec une importante discordance angulaire sur une limite érosive, permettant par endroit leur dépôt directement sur le Crétacé. Aux abords nord de la boutonnière du Saghro, les sédiments crétacés et paléogènes ont typiquement des pendages de 10 à 15° vers le nord, alors que les sédiments néogènes plongent de 5° (Figure 27 C et D). Notons encore la présence de galets de rhyolite provenant du socle varisque dans les conglomérats néogènes (également observés par Schmidt 1988 et 1992).

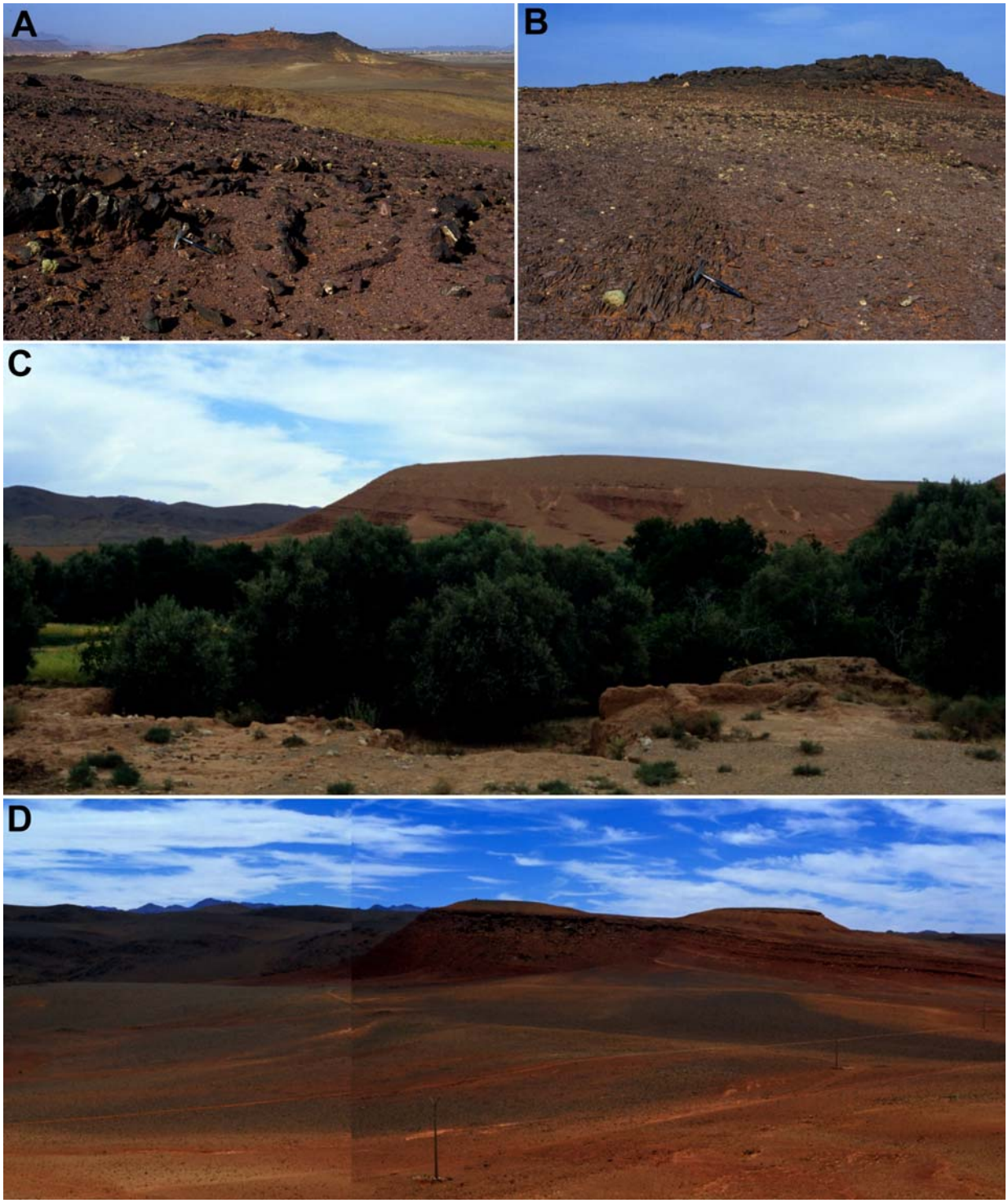

Figure 27. Photo des sédiments post-varisques.
A+B : Conglomérats Crétacés recouvrant en discordance des plis Carbonifère. Au nord du Saghro. Vue vers le ENE. N 31°28.450' / W 005°33.100'. Marteau pour échelle.
C : Butte présentant une discordance angulaire entre les sédiments Eocènes (10°) et Moi-pliocènes (< 5°). Au loin à gauche la boutonnière de Saghro. Vue vers le WSW. N 31°22.310' / W 5°48.410'. La butte est à 400 m.
D : Contact érodé Anti-Atlas – sédiments post-varisque. Vue vers le sud-ouest. A gauche des Rhyollites du Super-groupe Ouarzazate (plongement 18°). Au centre et à droite les couches rouges conglomératiques du Crétacé (12°) surmontées de conglomérats Moi-Pliocènes (6°) en discordance angulaire. Depuis N 31°21.103' / W 005°48.860'. La butte du centre est à 450 m.

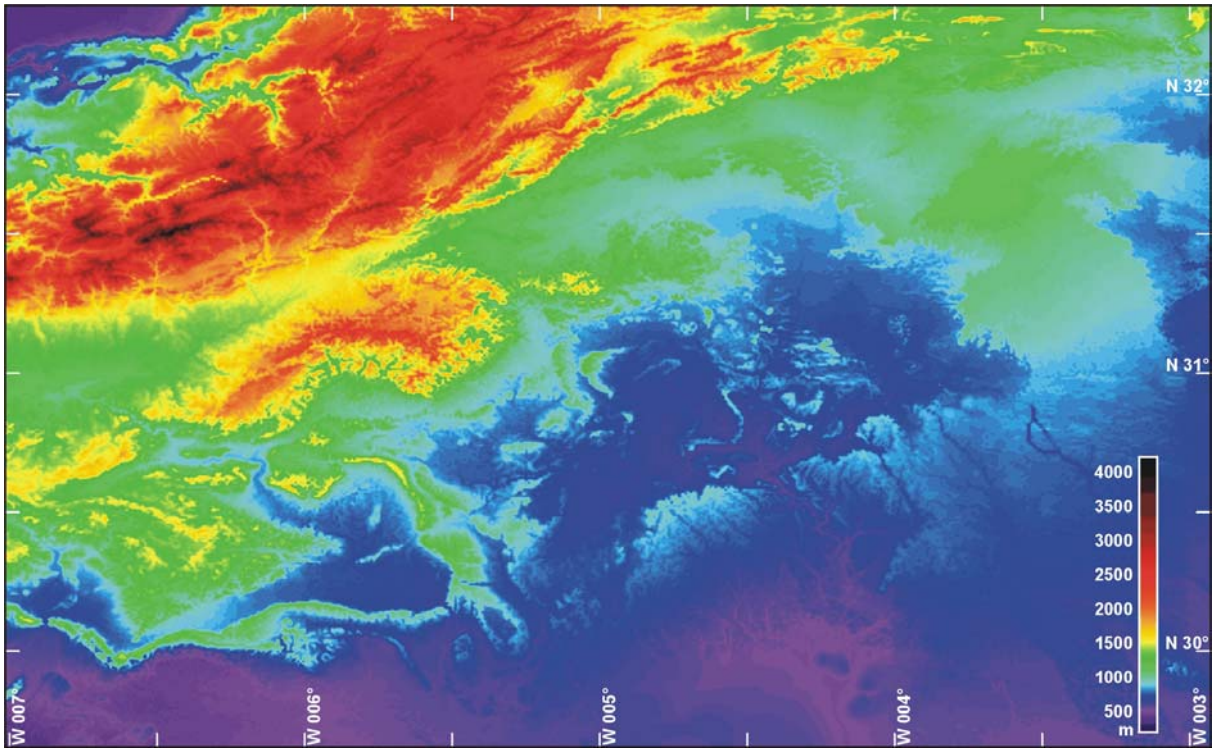

Figure 28*. Modèle numérique de terrain de l'Anti-Atlas oriental. Données de GTOPO 30.

La Figure 28 permet de se rendre compte de la topographie développée de l'Anti-Atlas oriental et plus particulièrement de la boutonnière du Saghro et de son voisin septentrional, le Haut Atlas central. L'analyse de l'orientation des couches du pourtour nord, est et sud de l'Anti-Atlas oriental, montre un bombement général, visible également par l'arrangement radiaire des réseaux hydrographiques (modèle numérique de terrain Figure 28 et vues Landsat Figures 3 et 6). Les couches des Monts Kem-Kem au sud et du Hamada à l'est plongent globalement en direction du sud-est. Au nord de l'Ougnate, les couches crétacées plongent au nord.

4

MODELE GEOMETRIQUE

Interprétation des observations

4.1. Style structural

L'affleurement des boutonnières et des roches profondes de la couverture, prouve l'implication du socle lors de la formation de la chaîne de l'Anti-Atlas. Ainsi cette inversion massive est de type *thick skin*. L'inversion des blocs de socle provoque la déformation dans la couverture qui réagit de manière passive, exception faite de la partie nord où l'on observe de véritables chevauchements à l'intérieur de la couverture.

Les modèles numériques « *trishear* » (Figure 29) de Erslev (1991), Allmendinger (1998), Johnson et Johnson (2002, A) ou Finch et al. (2003) semblent très bien correspondre à la géométrie globale des structures compressives. Le fait que l'on observe pas directement la faille inverse de la base rigide découle de trois faits : (1) l'inversion des failles normales induit des raccourcis dans le mur de la faille, vraisemblablement dans les sédiments syn-rift, de manière que la faille s'horizontalise avant l'intersection du contact socle-couverture (Figure 30, stade C). Ceci amène à considérer une géométrie de faille de type listrique. L'inversion induit le raccourci à l'endroit où la faille normale devient trop abrupte (l'angle

entre la préstructuration et la contrainte est trop obtus) (Bump, 2003 ; Yamada & MacClay, 2003). (2) Une part importante du raccourcissement horizontal n'est pas localisée en un seul horizon, mais est accommodée de manière diffuse dans l'important volume de roche incompétente. (3) Le niveau d'érosion actuel ne permet pas encore d'observer ces failles inverses. Elles se trouvent « au large » des boutonnières, sous la couverture. La présence et la localisation de ces failles inverses sont toutefois trahies par les failles d'extension tardive qui affectent la couverture au moins jusqu'au 1er Bani.

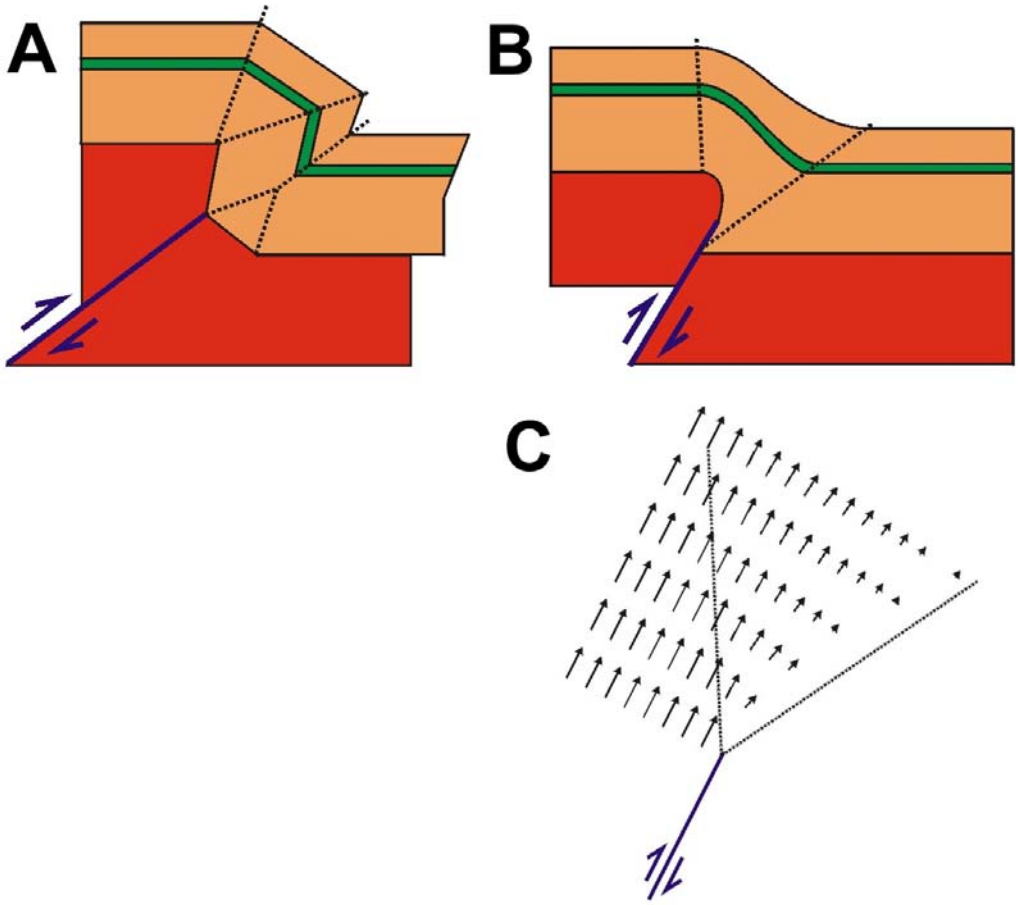

Figure 29. Principe de trishear (d'après Erslev, 1991). A : Solution classique. Elle nécessite un décollement basal. Il en résulte un excès de volume de la couverture. B : Le modèle trishear palie à ces problèmes. C : Répartition des vecteurs de déplacement dans la zone triangulaire.

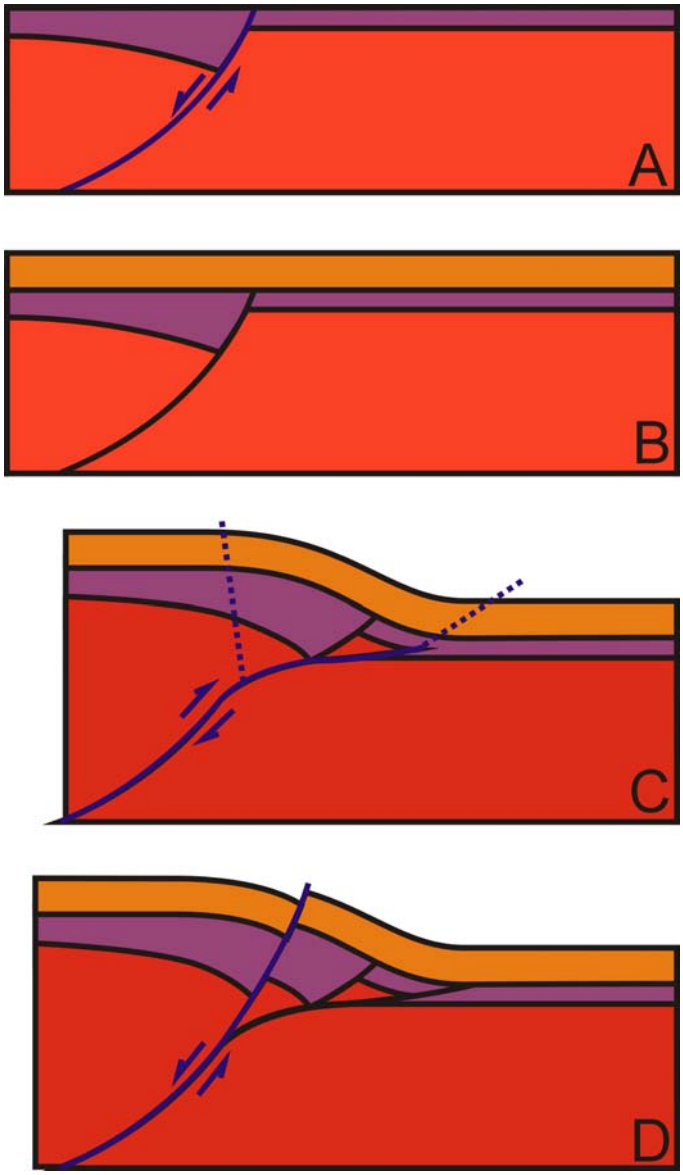

Figure 30. Modèle évolutif du style structural de l'Anti-Atlas oriental (stades A à C repris de Bump, 2003). A : Rift et sédiments syn-rift. B : Dépôt des sédiments post-rift. C : Inversion avec raccourcis dans le socle et drapage de la couverture (trishear). D : Extension. Les failles normales recoupent la couverture.

Différence majeure avec l'Anti-Atlas du sud-ouest

Malgré une stratigraphie globalement similaire, le style structural de la partie orientale et celui du sud-ouest sont différents. Dans l'Anti-Atlas occidental, des détachements se produisent dans la majeure partie des séries incompétentes. La série y comprend quatre membres dominants : le socle, les calcaires du Cambrien inférieur (Adoudounien), le Bani Ordovicien et les Richs Dévoniens. Chacun de ces membres développe sa propre fréquence et amplitude de

plissement, ce qui aboutit à un plissement polyharmonique multi-couches (Helg *et al.*, 2004). Dans la géométrie globale de l'Anti-Atlas oriental, la couverture se comporte comme une couche unique drapant les mouvements verticaux du socle (Soulaïmani *et al.*, 1997).

4.2. Restaurations et calcul de la profondeur de détachement

Choix de la coupe

Le calcul de la profondeur de détachement a été appliqué sur la coupe 8. Cette coupe a été choisie, car elle offre le niveau d'affleurement le plus bas dans la série. Ainsi le minimum d'erreur d'interprétation sur la morphologie du contact socle-couverture est garanti. La coupe 8 montre un bon développement de la structure anticlinale majeure. Ceci implique qu'elle coupe un bloc de socle en son milieu. La coupe 7 passant dans l'ensellement entre les boutonnières du Saghro et de l'Ougnate, n'aurait pas été significative, puisque ce secteur peut être interprété comme une zone de transition entre les deux blocs.

Restauration

La Figure 31 illustre les différents stades dans la restauration de la coupe. Afin d'établir la situation à la fin du paroxysme varisque, il faut tout d'abord restaurer les failles normales tardives (passage du stade B au stade C). Ce profil est ensuite remis à plat (D). A cette étape, les couches contiennent encore une composante importante de raccourcissement interne. Il faut par conséquent les étirer pour obtenir la configuration à la fin de la sédimentation Paléozoïque. Le profil A montre l'effet de la surrection Néogène. Ces données proviennent du modèle développé par Missenard *et al.* (2006) à partir de données gravimétriques. Cette composante récente est présente dans le relief actuel et doit être déduite du profil pour obtenir la configuration réelle du paroxysme varisque.

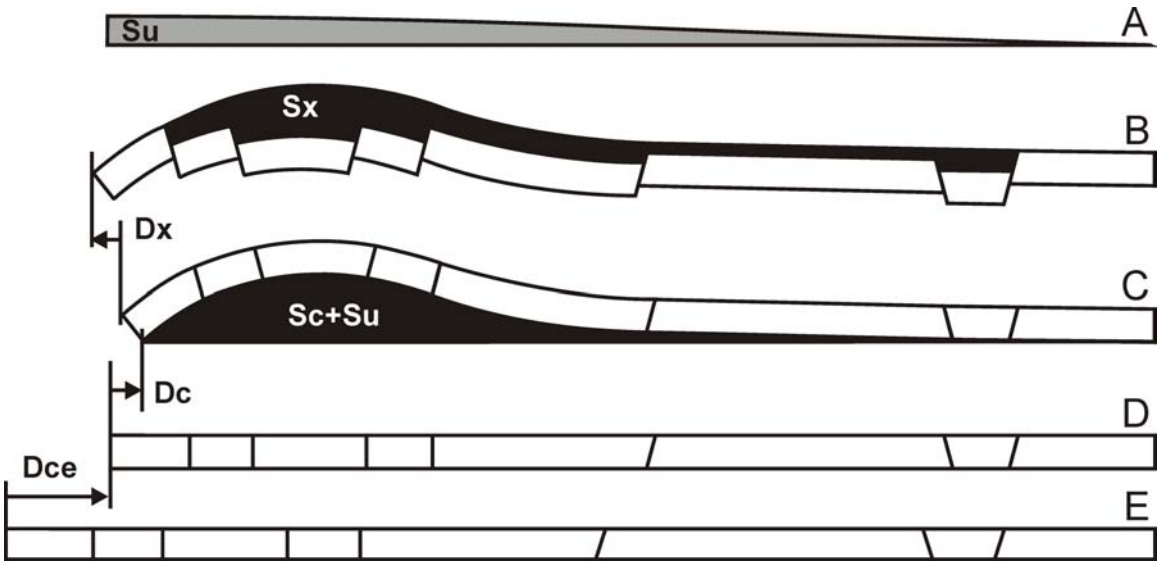

Figure 31. Restauration de la coupe 8. A : Surface différentielle due à la surrection Néogène Su, déduite de Missenard *et al.* (2006, Figure 6.C, profil oriental). B : Coupe actuelle ; Sx est la surface en défaut due à l'extension tardive. C : Coupe de la fin de l'événement varisque. Ce profil contient toutefois encore l'effet de la surrection récente. D : Coupe restaurée montrant la situation avant l'inversion mais comprenant encore le raccourcissement interne. E : Coupe restaurée, sans raccourcissement interne.

Principe du calcul de la profondeur de détachement

Pour estimer la profondeur du détachement, on utilise la méthode des surfaces déplacées (Epard et Groshong, 1993 ; Groshong, 1994, 2002). Cette méthode d'équilibrage analyse, sur une coupe en deux dimensions, la surface en excès provoquée par une compression ou une surface en défaut, dans le cas d'une extension par rapport au niveau régional virtuel représentant le niveau non déformé. Le principe est que cette surface en excès ou en défaut est égale à la surface déplacée, qui est elle-même définie par la profondeur du détachement multipliée par le déplacement horizontal. Cette méthode ne donne toutefois aucune information sur la géométrie ni sur la dynamique de la mise en place du détachement. Ainsi décrite, la méthode ne prend en compte aucune déformation interne.

Le principe de notre démarche est de calculer tout d'abord la profondeur de détachement grâce aux structures extensives. La première hypothèse est que

l'extension ne provoque aucune déformation interne. On peut donc simplement appliquer le calcul comme décrit ci-dessus. Pour traiter le cas de la compression nous modifions la méthode pour qu'elle prenne en compte la déformation interne, nous ajoutons ainsi une inconnue. La seconde hypothèse est que les structures profondes et donc la profondeur de détachement, sont les mêmes dans le cas de l'extension tardive que dans le cas de l'inversion varisque. Nous pouvons réduire d'une inconnue, notre nouvelle formule, en injectant la profondeur de détachement trouvée et ainsi déduire le raccourcissement interne provoqué par l'inversion varisque.

Calcul de la profondeur du détachement par les structures extensives

La surface en défaut provoquée par l'extension tardive est appelée Sx. Elle est définie comme la différence d'aire entre le profil actuel (B dans la Figure 31) et le profil restauré sans les failles normales (C). A ce stade de la restauration, la surface provoquée par le soulèvement récent (Su) n'a pas besoin d'être prise en compte puisqu'elle est implicitement contenue dans les deux profils.

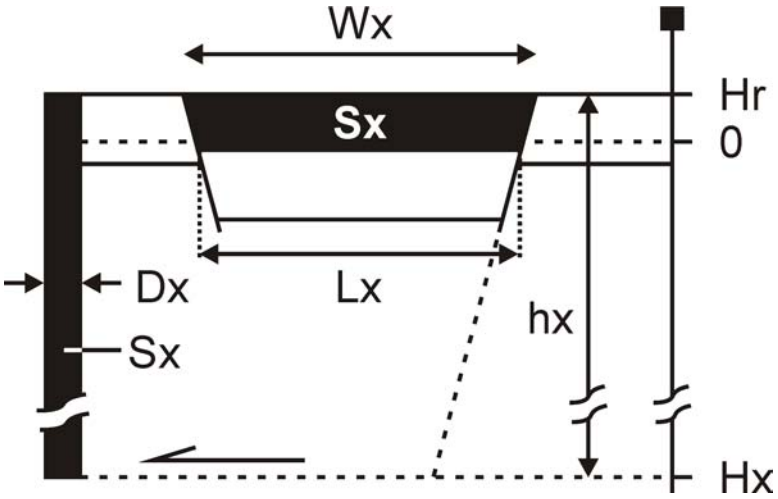

Figure 32. Détachement provoqué par extension. Définition des éléments géométriques utilisés dans le calcul de la profondeur de détachement.

La surface en défaut Sx, située sous le niveau régional Hr (Figure 32) résulte d'une extension. Elle est compensée par la surface déplacée définie par la longueur du déplacement horizontal Dx multipliée par hx la profondeur du détachement sous le niveau régional Hr :

(1) $Sx = Dx \cdot hx$ ainsi $hx = \frac{Sx}{Dx}$

Le déplacement horizontal Dx est la différence entre la longueur originale Lx et Wx la largeur de la structure :

(2) $Dx = Lx - Wx$

La profondeur du détachement en absolu, par rapport à l'altitude 0 m, est donnée par :

(3) $Hx = Hr - hx = Hr - \frac{Sx}{Lx - Wx}$

Notez que dans le cas de l'extension, Sx et Dx sont tous deux négatifs.

Cette profondeur de détachement a été calculée pour différentes structures de la coupe 8 : le graben de Zagora, la boutonnière du Saghro et la coupe entière. Pour chaque structure le calcul a été appliqué aux différents horizons. Le Tableau 1 présente les mesures et les résultats.

La profondeur de détachement pour le graben de Zagora varie de -12 à -18 km. Les valeurs les plus profondes sont obtenues pour le Silurien et l'Ordovicien supérieur qui sont les mieux contraints puisqu'ils sont affleurants. Le Graphique 1 représente la relation surface-profondeur. On reporte l'altitude de chaque niveau régional (Hr) en fonction de sa surface en défaut (Sx). Ce graphique permet d'extrapoler la profondeur du détachement basal. Cette profondeur est définie comme celle à laquelle la surface en défaut est nulle (Sx = 0 km^2). Ainsi

la droite pointillée désigne une profondeur de -16 km. La pente de cette droite donne l'inverse du déplacement (1/Dx). On obtient une valeur pour Dx de 0.204 km ce qui concorde avec les valeurs mesurées.

Niveau	Hr (km)	Sx (km^2)	Dx (km)	hx (km)	Hx (km)
Graben de Zagora					
Silurien	1.920	3.743	-0.185	-20.232	-18.312
Ordovicien supérieur	1.330	3.533	-0.185	-19.097	-17.767
Ordovicien inférieur	0.725	3.290	-0.185	-17.784	-17.059
Cambrien moyen	-1.555	3.047	-0.260	-11.719	-13.274
Cambrien inférieur	-2.125	2.840	-0.245	-11.592	-13.717
Socle	-2.735	2.500	-0.250	-10.000	-12.375
Saghro					
Silurien	5.000	28.279	-1.245	-22.714	-17.714
Ordovicien supérieur	4.460	30.285	-1.435	-21.105	-16.645
Ordovicien inférieur	3.815	30.317	-1.490	-20.347	-16.532
Cambrien moyen	1.500	30.850	-1.490	-20.705	-19.205
Socle	0.355	25.623	-1.355	-18.910	-18.555
Coupe entière					
Silurien	2.100	68.000	-2.155	-31.555	-29.455
Ordovicien supérieur	1.445	92.000	-2.365	-38.901	-37.456
Ordovicien inférieur	0.800	135.000	-2.480	-54.435	-53.635
Cambrien moyen	-1.425	135.000	-2.545	-53.045	-54.470
Socle	-2.560	144.000	-2.635	-54.649	-57.209

Tableau 1. Profondeur de détachement sur les structures extensives.

La profondeur de détachement obtenue par la boutonnière du Saghro varie de -17 à -19 km. Contrairement au graben de Zagora, ce sont les horizons inférieurs qui sont les mieux contraints.

Les résultats obtenus sur la totalité de la coupe sont irrationnels. La profondeur de détachement varie de -29 à -57 km. En terme de relation surface-profondeur, le niveau le plus élevé (ici le Silurien) devrait obtenir une surface en défaut supérieure au niveau le plus bas (socle). Cette déviation résulte certainement des raisons suivantes. (1) L'orientation des failles normales. Avec notre interprétation des failles normales (avec des plongements de 70 à 80° maintenus constants en profondeur), les déplacements horizontaux Dx sont faibles. Avec

des déplacements absolus plus grands, la profondeur de détachement serait moindre. Pratiquement, le déplacement change selon la géométrie de la faille normale. L'aplatissement des failles en profondeur (type listrique) génère deux effets : des déplacements horizontaux plus grands et des surfaces en défaut plus petites par rapport à des failles droites. (2) Aucune déformation interne n'a été considérée. En réalité, la longueur mesurée Lx (Figure 32) est plus longue que la longueur initiale avant l'extension (étirement). Si l'on applique la formule (7') développée pour les structures compressives (voir paragraphe suivant), une faible déformation interne suffit pour changer significativement le résultat de la profondeur de détachement. Avec une déformation interne de 3 %, la profondeur de détachement calculée pour le sommet du Cambrien inférieur passe de -54 km à seulement -19 km. L'influence de l'amincissement des bancs sur la surface en défaut est négligeable puisque l'amincissement vertical est compensé par l'allongement horizontal (volume constant).

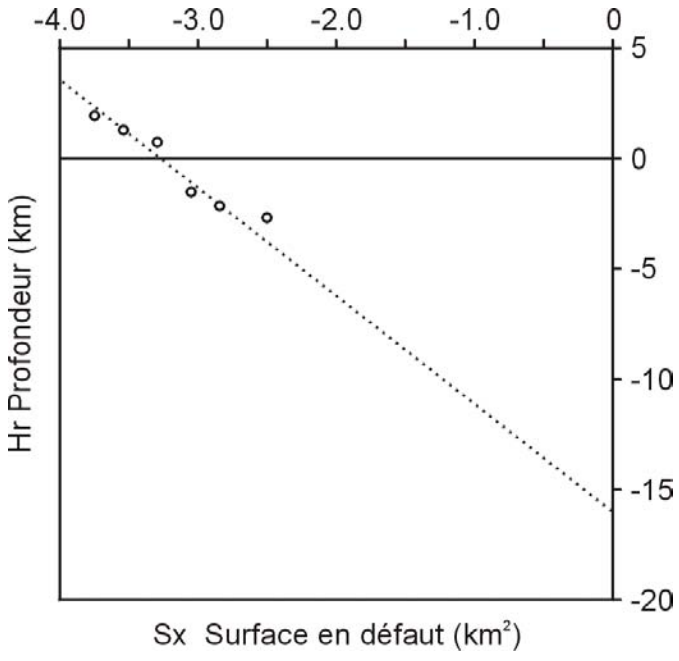

Graphique 1. Relation surface – profondeur sur le graben de Zagora.

Profondeur de détachement et déformation interne sur les structures compressives

Les calculs sont effectués sur un profil restauré, montrant la géométrie supposée de la fin de l'inversion varisque. Pratiquement, les failles normales et leurs effets ont été restaurés pour obtenir une géométrie régulière. Le niveau régional Hr (Figure 33) a été défini à l'extrémité sud de la coupe. La surface différentielle due à la surrection tardive (Su) a été soustraite de la surface en excès mesurée. La valeur de Su pour la partie Saghro est de 12.9 km^2 et de 61.2 km^2 pour la totalité de la coupe.

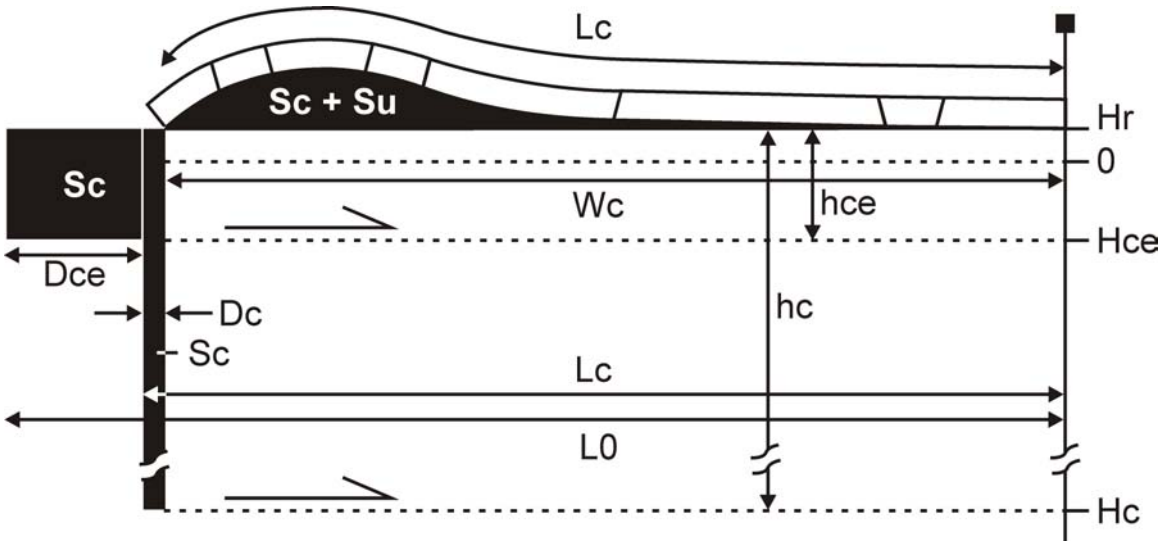

Figure 33. Détachement par compression. Cas de figure sans et avec raccourcissement interne (Dce).

Le calcul de la profondeur de détachement sur les structures compressives sans déformation interne utilise des équations semblables à celles démontrées pour l'extension.

(1) $Sc = Dc \cdot hc$ ainsi $hc = \frac{Sc}{Dc}$

Le déplacement Dc est défini comme étant la différence entre la longueur originale Lc et la largeur de la structure Wc.

(2) $Dc = Lc - Wc$

Dans le cas de la compression, Dc et Sc sont positifs. La profondeur de détachement par rapport au niveau de la mer est donnée par l'équation suivante :

(3) $$Hc = Hr - hc = Hr - \frac{Sc}{Lc - Wc}$$

Appliquée telle quelle, cette formule fournit des valeurs extrêmement profondes de -111 à -126 km pour le partie Saghro et de -172 à -212 km pour la coupe entière (Tableau 2). Etant donné les excellentes conditions d'affleurement, l'absence totale de chevauchement ou d'autres grandes structures est un fait avéré. L'équilibrage de ces coupes nécessite la considération d'une composante plus discrète. Le style structural, dicté par une rhéologie particulière, ne permet pas de changer les valeurs des déplacements horizontaux autrement que par raccourcissement interne. Cette déformation interne est par ailleurs très bien documentée par les structures de plus petite taille ne figurant pas sur les coupes.

Niveau	Hr (km)	Sc (km^2)	Dc (km)	hc (km)	Hc (km)
Saghro					
Silurien	1.550	206.090	1.730	119.595	-118.045
Ordovicien supérieur	1.000	212.090	1.725	122.951	-121.951
Ordovicien inférieur	0.340	222.090	1.925	115.371	-115.031
Cambrien moyen	-1.890	249.090	2.005	124.234	-126.124
Socle	-3.030	264.090	2.425	108.903	-111.933
Coupe entière					
Silurien	0.650	454.785	2.590	175.593	-174.943
Ordovicien supérieur	0.075	449.785	2.445	183.961	-183.886
Ordovicien inférieur	-0.585	411.785	2.400	171.577	-172.162
Cambrien moyen	-2.805	431.785	2.445	176.599	-179.404
Socle	-4.000	458.785	2.205	208.066	-212.066

Tableau 2. Profondeur de détachement sur les structures compressives.

Pour prendre en compte le changement de longueur dans le calcul de la profondeur de détachement, nous incluons le raccourcissement e :

(4) $e = \frac{Dce}{Lo}$ ainsi $Dce = Lo \cdot e$

Où la longueur Dce est le raccourcissement absolu et Lo la longueur originale (voir Figure 32).
La longueur Lc est mesurable, elle est définie comme la longueur originale moins le raccourcissement :

(5) $Lc = Lo - Dce$

En introduisant l'équation (4) dans la (5), on obtient :

(6) $Lc = Lo - Lo \cdot e = Lo(1-e)$ or $Lo = \frac{Lc}{1-e}$

On introduit ensuite cette composante de raccourcissement interne, l'équation (1) de la profondeur de détachement devient :

(7) $hce = \frac{Sc}{Dc + Dce}$

Dc est remplacé par l'équation (2), Dce par la (4) et Lo par la (6). Cette équation se simplifie ensuite comme suit :

(7') $hce = \frac{Sc}{Lc - Wc + Lo \cdot e} = \frac{Sc}{Lc - Wc + \frac{Lc}{1-e} \cdot e} = \frac{Sc}{Lc\left(1 + \frac{e}{1-e}\right) - Wc}$

Finalement pour calibrer la profondeur du détachement à l'altitude :

(8) $Hce = Hr - hce$

Le Tableau 3 donne les valeurs de la profondeur de détachement (Hce) pour chaque niveau avec une déformation allant de 0 à 0.25 (gamme compatible avec les observations de terrains). Ces résultats sont reportés sur le Graphique 2.

Considérant une profondeur de détachement raisonnable de -18 à -20 km (déterminée sur les structures en extension), on obtient des valeurs de déformation interne de 0.11 à 0.17.

e	Silurien	Ordov.sup	Ordov.inf	Camb.moy	Socle
0.00	-174.943	-183.886	-172.162	-179.404	-212.066
0.01	-109.169	-112.435	-104.84	-110.83	-126.226
0.02	-78.801	-80.501	-75.032	-80.175	-90.015
0.03	-61.313	-62.402	-58.216	-62.798	-70.045
0.04	-49.945	-50.748	-47.416	-51.609	-57.391
0.05	-41.962	-42.617	-39.895	-43.802	-48.655
0.06	-36.049	-36.621	-34.356	-38.045	-42.262
0.07	-31.492	-32.017	-30.107	-33.624	-37.380
0.08	-27.874	-28.371	-26.744	-30.122	-33.530
0.09	-24.931	-25.411	-24.016	-27.280	-30.416
0.10	-22.490	-22.961	-21.759	-24.928	-27.846
0.11	-20.434	-20.900	-19.860	-22.948	-25.688
0.12	-18.677	-19.141	-18.241	-21.259	-23.851
0.13	-17.159	-17.623	-16.844	-19.801	-22.269
0.14	-15.834	-16.299	-15.626	-18.530	-20.890
0.15	-14.667	-15.135	-14.555	-17.412	-19.680
0.16	-13.633	-14.103	-13.606	-16.421	-18.608
0.17	-12.709	-13.181	-12.759	-15.536	-17.652
0.18	-11.878	-12.354	-11.998	-14.741	-16.794
0.19	-11.128	-11.607	-11.311	-14.024	-16.021
0.20	-10.447	-10.929	-10.688	-13.373	-15.319
0.21	-9.826	-10.311	-10.120	-12.779	-14.680
0.22	-9.257	-9.745	-9.601	-12.236	-14.095
0.23	-8.734	-9.226	-9.123	-11.737	-13.558
0.24	-8.252	-8.746	-8.683	-11.277	-13.064
0.25	-7.806	-8.303	-8.276	-10.851	-12.606

Tableau 3. Profondeur de détachement (km) en fonction de la déformation compressive (e) pour les différents niveaux de la coupe 8.

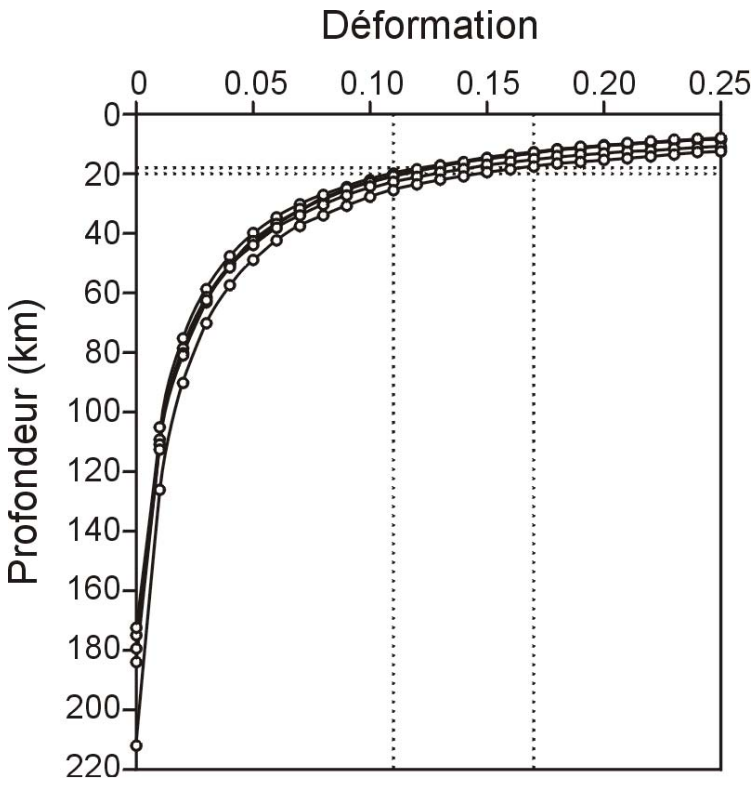

Graphique 2. Profondeur de détachement des différents niveaux sur la coupe entière en fonction de la déformation compressive.

4.3. Interférence et gradient de déformation

L'analyse de l'orientation des petits plis et des chevauchements représentés dans la Figure 22 (p.40) permet les interprétations suivantes :

- Les plis à axe NW-SE, qui dominent la moitié orientale au sud des boutonnières, peuvent être associés à la déformation de la chaîne de l'Ougarta. Ils correspondent également à la structure secondaire majeure.
- Les plis à axe E-W (tendance ENE-WSW) au nord des boutonnières sont parallèles à la structure antiforme majeure de l'Anti-Atlas.
- Les plis d'orientation E-W (tendance ESE-WNW) sont le résultat de la somme de la formation de la structure antiforme majeure (Anti-Atlas) et de la structure majeure secondaire (Ougarta). En effet les faisceaux ougartiens divergent. Ainsi

ils sont perpendiculaires à la structure antiforme majeure dans la partie orientale et pratiquement parallèles à cette dernière dans la partie occidentale.
- A échelle égale, les deux orientations de plis E-W et NW-SE coexistent dans la région de Tazzarine (N 31°00' / W 005°30'). L'orientation E-W est attribuée à la structure antiforme majeure, l'orientation NW-SE à l'Ougarta. Les chevauchements au nord de Tazzarine, avec des contraintes orientées NW-SE sont également attribués à la structure anticlinale majeure.
- L'exception au nord de l'Ougnate avec une orientation N-S est attribuée à la déformation d'orientation ougartienne. Elle pourrait également provenir d'un poinçonnement d'un coin de socle provoquant des plis de drapage.

L'image globale de la compilation de ces interprétations est représentée par la Figure 33. C'est l'interférence des deux orientations (Anti-Atlas et Ougarta) qui donne cette structure en dômes et bassins. Cette particularité de l'Anti-Atlas oriental est due au fait de la proximité de l'Ougarta et à la perpendicularité des deux orientations dans cette zone. Ceci conforte également le concept de métacraton pour cette partie du craton ouest-africain.

Considérant la direction anti-atlasique (ENE-WSW), le nord des boutonnières et le Jebel Tisdafine en particulier (Carbonifère au nord de l'ensellement Saghro-Ougnate), sont caractérisés par un plissement beaucoup plus intense qu'ailleurs dans l'Anti-Atlas oriental. Les couches y sont déformées sur toute leur longueur et non pas uniquement en un segment très localisé. Le déversement des plis vers le nord, les chevauchements et le développement d'une schistosité sont autant de particularités propres à cette région nord de l'Anti-Atlas oriental. Ces observations amènent à décrire un fort gradient de déformation qui décroît du nord au sud.

La direction ougartienne présente également un gradient de déformation. Ce gradient est moins marqué que celui de l'Anti-Atlas. Il n'apparaît pas par l'analyse des observations de terrains, mais par l'interprétation géologique à grande échelle (Figures 11 ou 12, p.26). Si l'on considère la structure majeure secondaire d'orientation ougartienne, on s'aperçoit que les plis de la partie

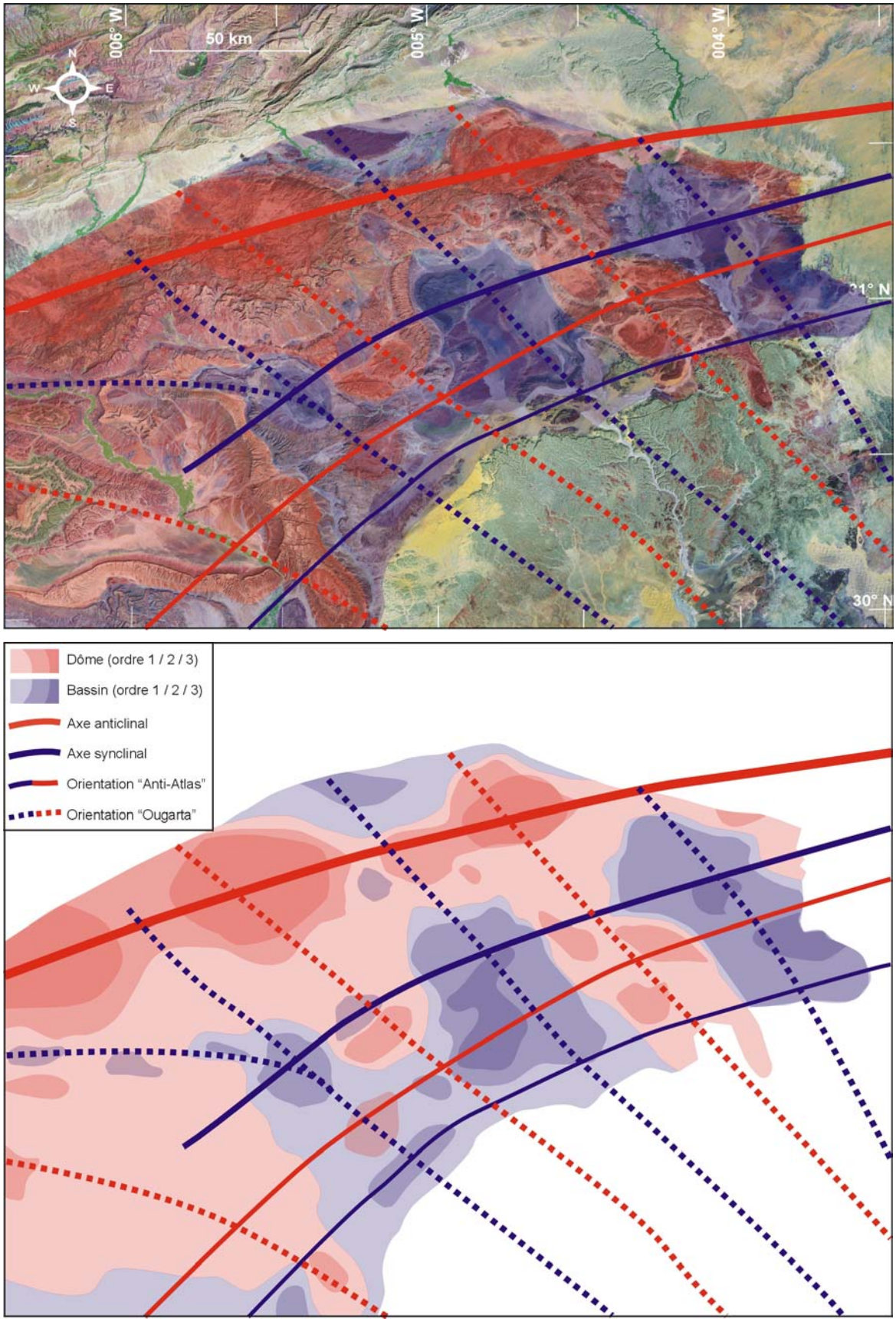

Figure 34* : Faisceaux dans l'Anti-Atlas oriental. Avec et sans le fond Landsat.

orientale sont caractérisés par une longueur d'onde plus courte et une amplitude supérieure par rapport à la zone plus à l'ouest. En effet, l'anticlinal séparant le Tafilalt du Mader est nettement plus étroit que celui séparant le Mader et la cuvette de Tazzarine (longueur d'onde). Les variations d'amplitude sont montrées par l'affleurement des roches plus ou moins profondes. Dans la partie orientale, des roches profondes (Cambriennes au moins) se trouvent à proximité géographique de roches Carbonifères, alors que dans la partie occidentale, les affleurements varient du 1er Bani (Ordovicien) au Dévonien (voire même jusqu'au Silurien uniquement). Cette observation peut être expliquée par les variations d'épaisseur qui affectent la couverture. Il est évident que si la couverture est plus fine, la probabilité de voir affleurer des roches plus ancienne est plus grande. Mais cette constatation est réfutée par l'observation des pendages. Les pendages sont en effet beaucoup plus forts à l'est et plus plats à l'ouest. Ces observations démontrent également l'implication du socle dans la déformation d'orientation ougartienne. L'interférence obtenue dans cette partie de la chaîne découle donc du croisement de deux déformations toutes deux de type *thick skin*.

4.4. Structures d'extension tardive

Les failles plongeant au nord sont majoritaires, on les interprète comme les principales, alors que les failles qui plongent au sud sont leurs conjuguées. Cette interprétation est influencée, mais également supportée, par la connaissance de la configuration du craton.

Malgré le fait que toutes ne recoupent pas toujours l'entière série Paléozoïque, les failles normales sont attribuées à une extension post-varisque. La rhéologie particulière de la couverture explique le fait qu'elles n'affleurent pas systématiquement. Le modèle *trishear* en extension de la Figure 35 illustre ce phénomène. Les niveaux marqueurs suffisamment séparés de la faille par des séries incompétentes, forment des plis de drapage ou plis de revêtement. Ceci explique l'absence de faille normale dans les sédiments supérieurs de la

couverture. Certains larges plis sont interprétés comme étant le seul résultat des failles normales, comme par exemple les plis Dévoniens et Carbonifères dans et sur la bordure sud-ouest du Mader (voir au tiers sud de la coupe 7). Le fait que ces failles affectent des formations plus jeunes dans l'est qu'à l'ouest, s'explique par le simple fait que la couverture y est moins épaisse.

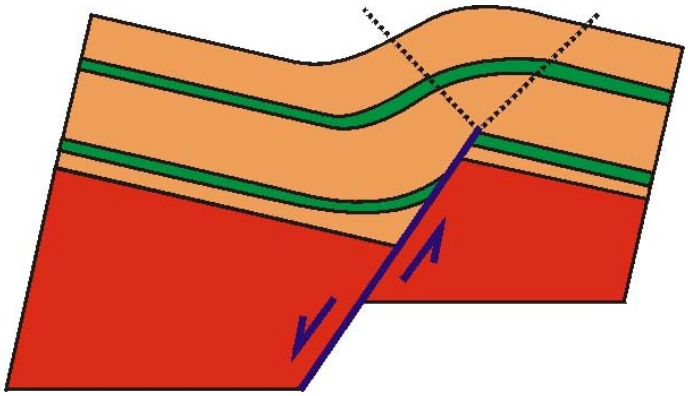

Figure 35. Modèle trishear en extension.

Avec l'hypothèse que ces failles réutilisent les anciennes discontinuités du socle, leur emplacement permet la localisation de ces structures profondes. La forte inclinaison des failles normales dans la couverture permet une extrapolation aisée. Toutefois, mise à part la projection, ces failles ne définissent pas directement le front des blocs inversés lors de l'événement varisque. Tout comme les failles inverses prennent un raccourcis dans le socle, les failles normales empruntent un chemin légèrement différent. Elles se développent de manière verticale et recoupent la couverture (Figure 30.D, p.55), sans utiliser le chemin créé par l'inversion. La faille inverse étant trop plate en surface (Faccenna et al., 1995).

Toutes les failles normales suivent l'orientation anti-atlasique, aucune faille n'indique une orientation ougartienne. Le Tafilalt montre un nombre de failles normales plus important qu'ailleurs. Ceci explique les répétitions de cuestas d'une même formation. Les rejets sont plus faibles, mais la fréquence des failles

est plus grande. On peut en déduire que la taille des blocs de socle est inférieure dans cette zone et donc que le socle y est plus fracturé qu'ailleurs. Il est possible que cette intensité de fracture traduise un interférence des structures profondes des deux orientations (Anti-Atlas et Ougarta).

Cette phase extensive n'affecte que l'Anti-Atlas oriental. Elle est interprétée comme le témoignage de l'ouverture du bassin adjacent du Haut-Atlas. Ceci explique le fait que cette phase n'apparaisse pas dans le reste de l'Anti-Atlas. Les premiers sédiments à se déposer dans ce bassin datent du Trias. Toutefois comme aucun sédiment Triassique ou Jurassique ne se dépose sur l'Anti-Atlas, il est possible que cette extension soit uniquement un effet de bord et que cette extension n'affecte pas forcément l'Anti-Atlas dans les premiers stades de l'ouverture de ce bassin.

4.5. Relations Anti-Atlas – roches Post-varisques

La base des sédiments Crétacés décrit une surface de pénéplaine. Exception faite des abords des boutonnières, les cuestas des formations compétentes montrent des crêtes d'une grande régularité topographique, témoignant d'un « paléo » niveau d'érosion. L'observation de la discordance tectonique, séparant les roches Carbonifères plissées et les conglomérats Crétacés, permet d'affirmer que l'intense déformation, observée dans les sédiments Paléozoïques de la partie nord, est due exclusivement à la phase varisque et non à l'inversion du Haut Atlas. Les différents pendages mesurés dans les sédiments post-varisques témoignent toutefois d'une certaine surrection. L'évolution chronologique de ce soulèvement est mis en valeur par la discordance angulaire séparant les sédiments Crétacés-Paléogènes et Néogènes. Les calculs de Schmidt (1988 ; 1992) sur le recul des cuestas indiquent le début de la surrection à l'Eocène supérieur.

Considérant la projection des couches Crétacées dans la partie nord, deux configurations du contact socle – Crétacé sont possibles. (1) Soit les sédiments Crétacés buttent sur le socle, décrivant ainsi une discordance angulaire ; le socle apparaissant alors comme une île dans cette surface Crétacée. (2) Soit les couches Crétacées épousent la topographie du socle, montrant ainsi une surrection tardive (partielle) des boutonnières. L'analyse du pendage des sédiments Crétacés et Cénozoïques parle en faveur de cette configuration. La présence de roches du socle varisque dans et par-dessus les sédiments Paléogènes prouve l'existence d'une « île » de socle (configuration 1). La situation réelle est donc une configuration intermédiaire. Cette théorie se limite aux boutonnières du Saghro et de l'Ougnate. Dans l'extrémité orientale (à l'est du Tafilalt), le Crétacé repose sur le socle montrant exclusivement la surrection tardive (configuration 2).

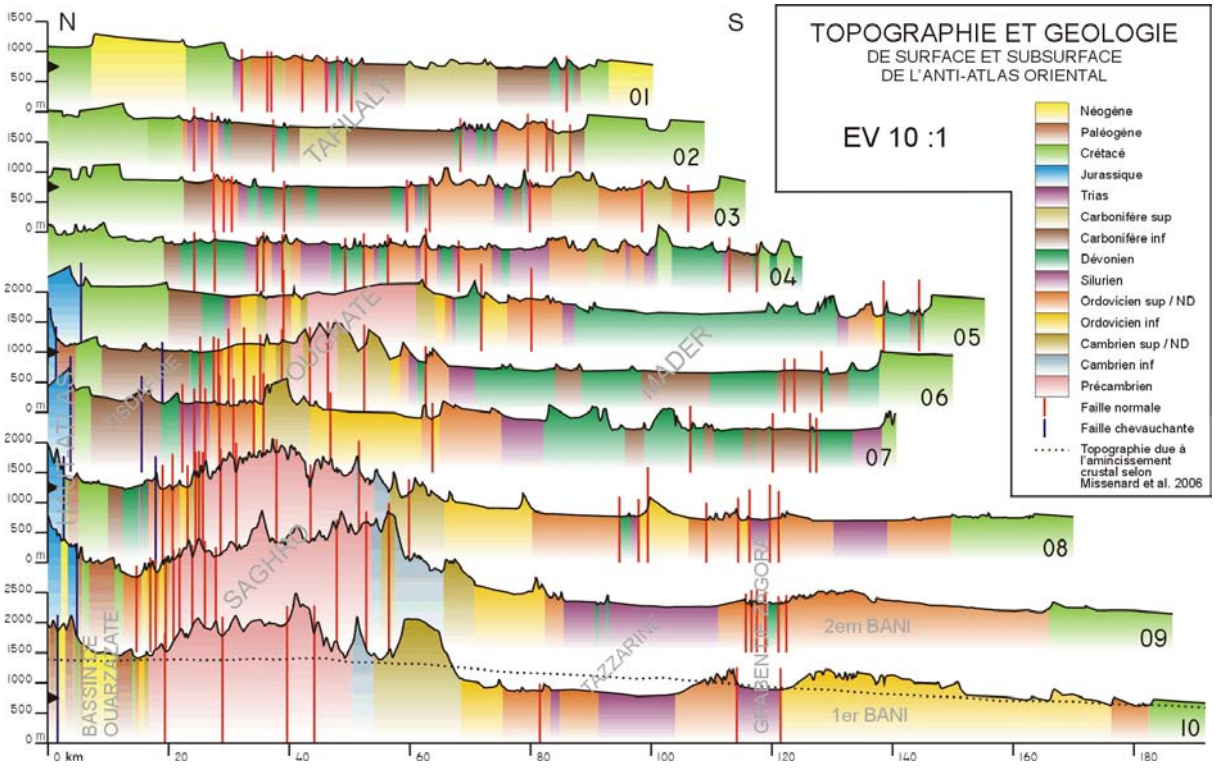

Figure 36*. Topographie et géologie de surface selon les coupes de l'Anti-Atlas oriental. La coupe 10 comprend également une courbe montrant l'influence de la surrection Néogène (dessinée d'après Missenard *et al.* (2006, Figure 6.C, profil oriental).

Le bombement, observable par l'analyse de l'orientation des couches post-varisques sur les vues satellite (Figure 3, p.7) et le modèle numérique de terrain (Figure 27, p.51), provient du soulèvement récent dû à une anomalie thermique (Missenard et al., 2006), mais il n'est pas l'unique responsable de la forte topographie. La courbe du soulèvement modélisé par Missenard et al. (2006) a été reportée sur le profil topographique de la coupe 10 (Figure 36), calée au sud, à la base des sédiments Crétacés. Il apparaît que la topographie du Bani et de la boutonnière du Saghro dépasse de cette limite érosive théorique. Ces hauts reliefs ont donc dû constituer des « îles » dès la fin de l'inversion varisque.

4.6. Interprétations des données sismiques

Le modèle géométrique est étayé par l'analyse de trois lignes sismiques réalisées par l'ONAREP (actuellement ONHYM) dans la région du Tafilalt. RS 8 et RS 10 sont orientées N-S (Figure 37). La ligne RS 3 n'a pas pu être clairement positionnée. Elle a une orientation E-W, passant vraisemblablement au sud de Rissani. La ligne RS 8 permet une excellente corrélation avec les données de surface, c'est pourquoi elle a été choisie pour l'interprétation. RS 10 laisse une trop grande part à l'interprétation étant donné l'épaisse séquence de Carbonifère qui en compose la surface.

RS 8 est perpendiculaire à l'extension et oblique par rapport aux deux structures majeures : WSW-ENE dans la partie nord et NW-SE dans la partie sud. Le dix premier kilomètres (Figure 38) depuis le sud montrent de larges plis. Ils sont interprétés comme détachés du socle à la base de la pile paléozoïque, le raccourcissement de la couverture étant compensé par l'inversion des anciennes failles normales dans le socle. Ces plis correspondent à l'orientation ougartienne.

Le reste du profile est dominé par des failles normales tardives. Une série de « pseudo-bassins » (p. ex. km 25) ont été anciennement interprétés comme des

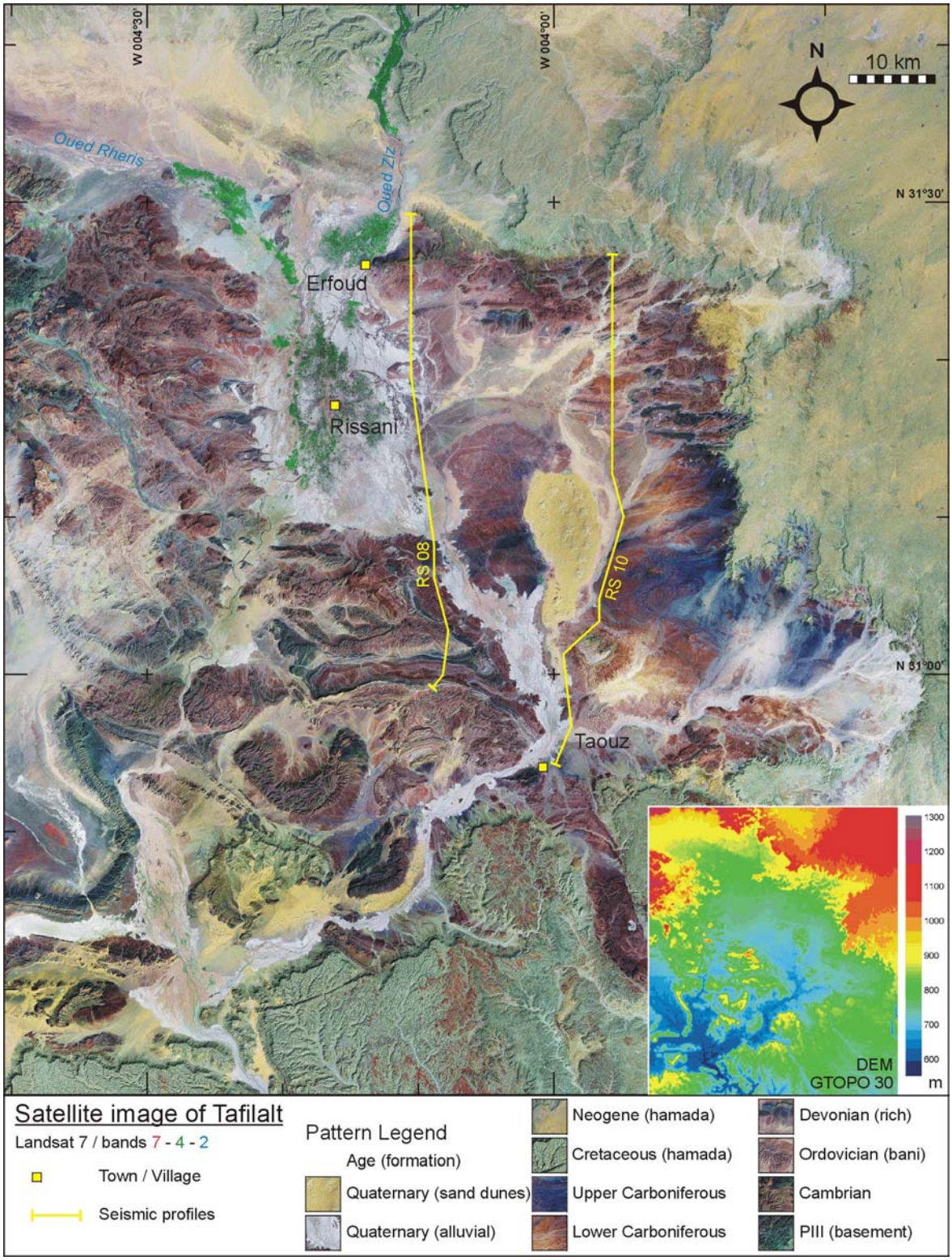

Figure 37. Image satellite du Tafilalt avec la position des lignes sismiques RS 8 et RS 10.

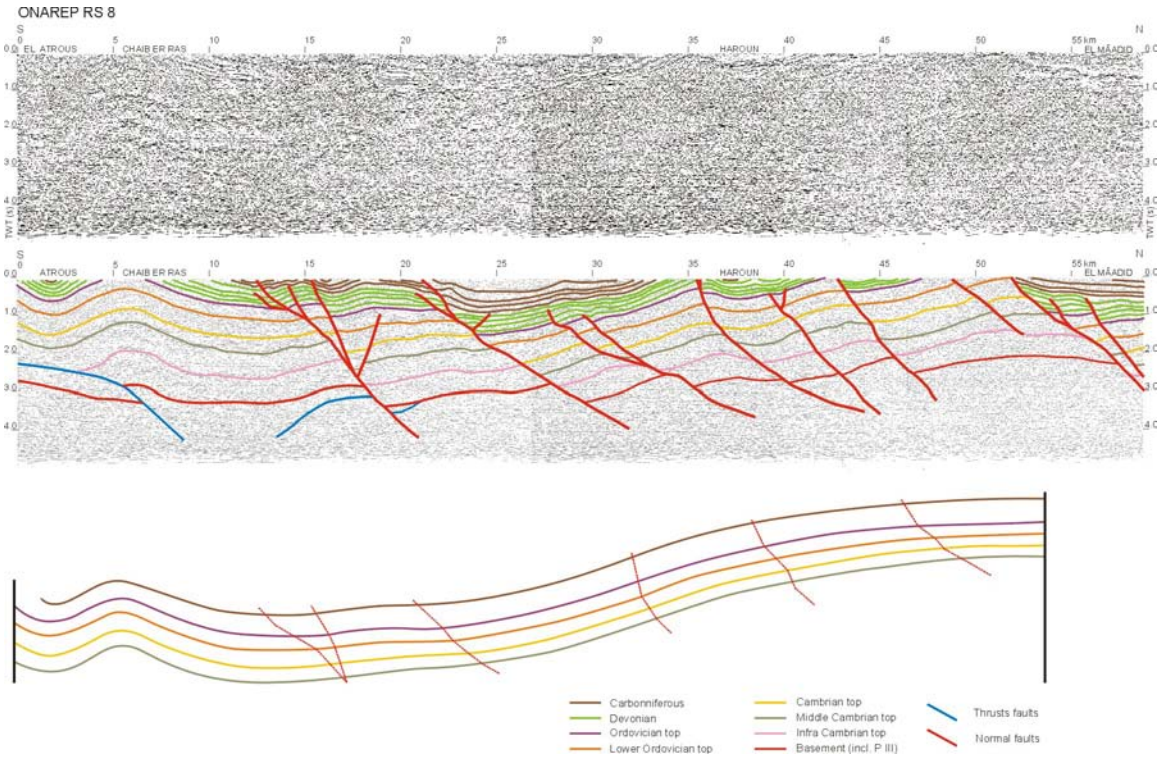

Figure 38*. Ligne sismique RS 8. En haut : vierge. Au centre : interprétation en profondeur d'après les données de surface (terrain et carte géologique). En bas : profile après restauration des failles normales.

bassins syn-sédimentaires de chevauchements. Notre interprétation prévoit un modèle en extension, dans lequel la géométrie de ces « pseudo-bassins » est expliquée comme la conséquence d'une couverture particulièrement incompétente additionnée d'un artefact sismique. Premièrement, l'amincissement des couches du toit de la faille et l'épaississement de celles du mur est un fait observé spécialement dans les modèles « couverture incompétente sur socle rigide » (Finch *et al.*, 2004). Deuxièmement, l'axe z des lignes sismiques est donné en temps (*Two Ways Time*) et non en profondeur. La vitesse des ondes dans les marnes et argiles du Carbonifère doit être extrêmement faible (probablement inférieure à 2000 m/s), alors qu'elle peut atteindre 3000 m/s dans les couches compétentes telles que dans celles des calcaires dévoniens et des quartzites ordoviciennes. Cette différence de vitesse provoque un artefact (*velocity pull down*) qui tend à exagérer la profondeur de ces « pseudo-bassins ».

La troisième partie de la Figure 38 est le profile restauré qui illustre la configuration présumée avant la mise en place des failles normales. Le raccourcissement mesuré avoisine les 10 %, mais il ne prend pas en compte le raccourcissement interne observé à plus petite échelle.

5

MODELE DYNAMIQUE

Chronologie des événements

5.1. Structuration Précambrienne

L'orogène Pan-Africain (650 – 580 Ma) termine l'assemblage du Gondwana (Boote *et al.*, 1998). Si cet événement n'a pour ainsi dire aucune influence sur la pré-structuration de l'événement varisque dans l'Anti-Atlas occidental, il n'en va pas de même pour ce qui est de la partie orientale. En effet, le socle de l'Anti-Atlas oriental peut être schématisé en une zone triangulaire, limitée au NNW par la faille sud atlasique, à l'est par l'anomalie du Saoura et au SSW par l'Accident Majeur. Cette dernière structure découle directement de l'édifice Pan-Africain. Son orientation coïncide avec le linéament du Tibesti qui traverse l'Afrique en direction ESE. Si cette structure est décrite comme une suture, le socle de l'Anti-Atlas oriental n'est pas pour autant allochtone par rapport au craton ouest-africain. Cette zone découlant d'un bassin aulacogène du Néoprotérozoïque inférieur, correspond plutôt à une bordure moins rigide du craton, d'où cette qualification de métacratonique.

Le rift débutant au Néoprotérozoïque terminal et qui dure jusqu'au Cambrien moyen, marque le début du super-cycle du Gondwana (Boote *et al.*, 1998). Cette phase d'extension affecte tout l'Anti-Atlas. La préstructuration en blocs par des failles normales est un des paramètres déterminant la géométrie de l'inversion

varisque. La présence de zones de faiblesse crustale permettra l'inversion en type *thick skin*. La trace des failles normales suit la structure générale de l'Anti-Atlas. Les failles plongent le plus généralement vers l'extérieur du craton soit vers le nord (Figure 39, stade A). Les plongements symétriques sont interprétés comme leurs conjugués. Les sédiments associés au rift (Figure 30, stade A, p.55), très puissants dans la partie occidentale, fournissent d'importants horizons de décollement potentiel. Cet aspect ne concerne toutefois pas l'Anti-Atlas oriental, où ces séries sont fortement réduites voire absentes.

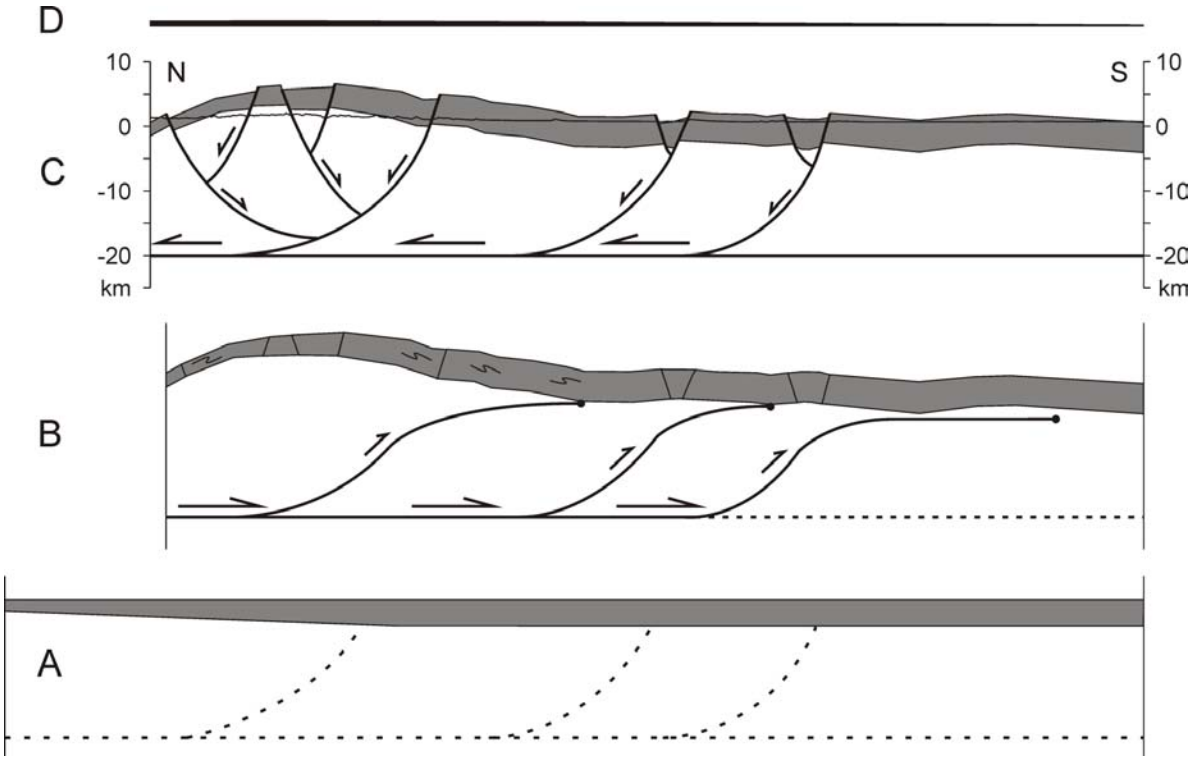

Figure 39. Modèle du détachement médio-crustal pour la coupe 8. Sans exagération verticale. La couverture comprend le Cambrien, l'Ordovicien et le Silurien. A : Profil avant la compression avec les failles normales héritées du rift Précambrien. B : Profil au paroxysme de l'inversion varisque. Les failles normales sont réutilisées mais recoupent le socle et s'aplatissent avant d'atteindre la couverture. C : Extension. Les failles normales atteignent la couverture. D : Soulèvement différentiel récent dû à une anomalie thermique (donnée de Missenard et al. 2006, Figure 6.C).

5.2. Bassin Paléozoïque

Durant pratiquement la totalité du Paléozoïque, une puissante série de sédiments se dépose d'une manière régulière dans cette partie septentrionale du bassin de Tindouf. Quelques hiatus reflètent probablement une activité tectonique distante (Burkhard *et al.*, 2006). La variété de sédiments est faible. L'environnement de dépôts passe d'un milieu dominé par le détritisme jusqu' à l'Ordovicien supérieur à un milieu carbonaté avant un retour du détritisme à la fin du Dévonien (Figure 10, p.21). Aucun sédiment ne traduit des conditions de mer profonde, ce qui conforte l'idée d'un bassin de type intracontinental au même titre que d'autres bassins nord africains comme celui de l'Ougarta, de Reggane ou de Taoudenni par exemple (Figure 3, p.7).

La puissance de cette couverture atteint 8 km dans l'Anti-Atlas oriental et mis à part quelques bancs marqueurs, la série est très incompétente (Figure 15, p.30). Ce sont ces deux caractéristiques particulières qui vont dicter le style de la déformation dans la couverture.

5.3. Inversion et interférence varisques

L'événement varisque provoque une inversion massive de type *thick skin* (Figures 39, stade B et 30 C, p.55). Les anciennes failles normales rejouent en failles inverses sans affecter directement la couverture. La datation de cet événement est difficile à contraindre, mais on peut le dater raisonnablement à la fin du Carbonifère inférieur, selon les extrapolations à grande échelle de Stampfli et Borel, 2002 (Figure 4, p.10) ou de Veevers, 2004.

La chronologie relative des deux déformations d'orientations différentes (Anti-Atlas et Ougarta) n'a pas été établie de façon certaine. Des indices d'axes de plis replissés dans la région de Tata dans l'Anti-Atlas occidental (Caritg *et al.*, 2004), indiquent que l'orientation anti-atlasique (axe NE-SW) précéde la déformation d'orientation ougartienne (E-W). Mais pour autant que ces directions

soient correctement interprétées (Figure 40), cette chronologie relative n'est pas forcément identique dans l'Anti-Atlas oriental, vu également la proximité qui lie l'Anti-Atlas oriental à la chaîne de l'Ougarta. D'ailleurs, dans sa partie la plus orientale, la préférence est donnée pour une orientation ougartienne précédant la déformation anti-atlasique. En effet, les axes des petits plis d'orientation ougartienne sont basculés par la structure majeure de la déformation anti-atlasique (voir le stéréogramme le plus oriental de la Figure 22, p.40). Dans la région de Tazzarine, l'analyse des deux stéréogrammes de petits plis semble indiquer le contraire. Les petits plis d'orientation ougartienne ont un axe de pli horizontal, alors que l'axe des petits plis d'orientation anti-atlasique est basculé vers l'ouest. Ce basculement étant provoqué par la structure majeure secondaire attribuée à la déformation ougartienne. Mais ceci peut être expliqué par le fait que les déformations internes (petits plis) précèdent la déformation de plus grande envergure (structure majeure). Au sud de la boutonnière de l'Ougnate ces relations sont brouillées par les synclinaux provoqués par l'extension à venir.

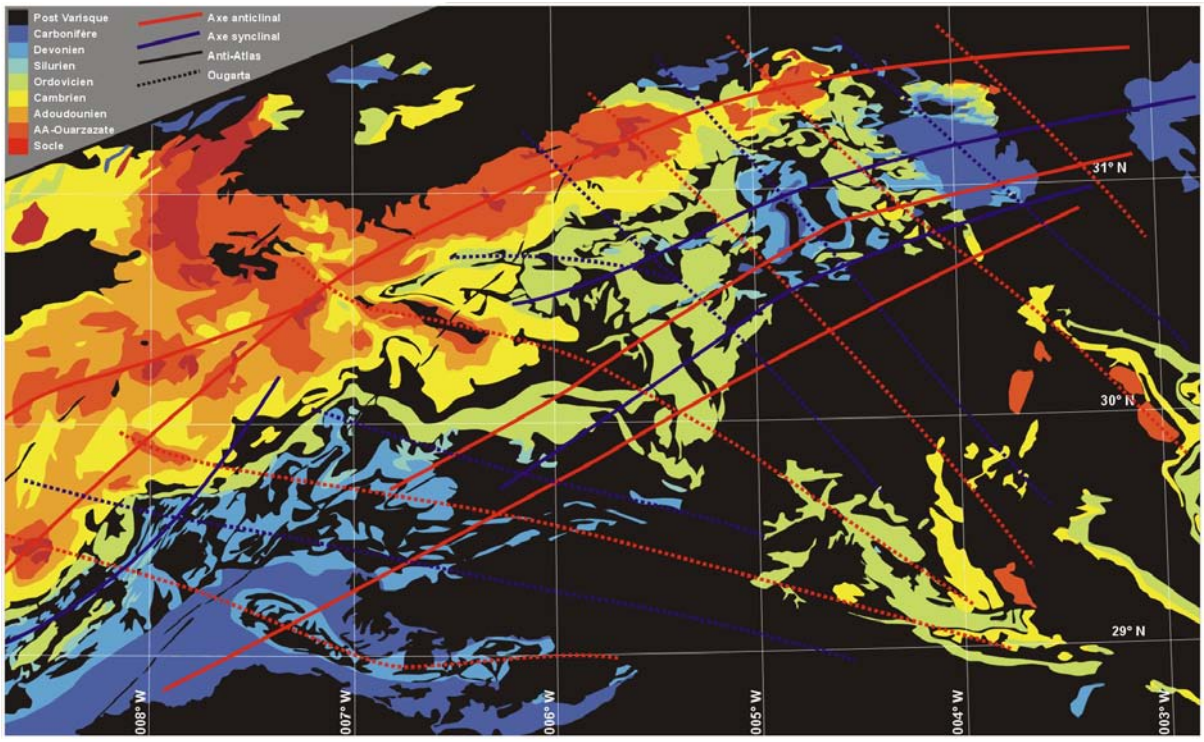

Figure 40*. Interprétation à grande échelle de la carte géologique en terme de plis ou de faisceaux.

5.4. Extension Mésozoïque

La formation de failles normales affectant la couverture est post-varisque, car elles recoupent les structures majeures anti-atlasiques et ougartienne (Figure 39, stade C, p.78 et Figure 30, stade D, p.55). De plus les synclinaux créés dans le toit des failles normales replissent les axes des petits plis varisques. Ces failles normales ne recoupent pas toujours la totalité de la couverture Paléozoïque, mais elles l'affectent néanmoins. En effet, le rejet est parfois amorti dans les séries sommitales, créant ainsi des plis « d'effondrement » drapant les mouvements verticaux de la même manière que lors de l'événement varisque. Cette extension n'affecte pas les sédiments Crétacés. Le fait que l'on trouve ces failles uniquement dans la partie bordant le Haut Atlas permet raisonnablement d'attribuer cette phase d'extension à l'ouverture du bassin du Haut Atlas au Trias supérieur. Quelques cas montrent une réactivation de ces failles dans un système dextre.

5.5. Réjuvénation Cénozoïque

L'inversion du Haut Atlas ne provoque pas de déformation telle que plissement ou chevauchement dans l'Anti-Atlas oriental. Mais il induit un soulèvement progressif identifiable par les différentes discordances angulaires observées entre les séries Crétacées, Eocènes et Mio- Pliocènes sur la bordure nord de l'Anti-Atlas oriental. Ces étapes dans le soulèvement correspondent à celles de l'inversion du Haut Atlas. Ce bombement lisible par l'analyse de l'orientation des sédiments Crétacés et Cénozoïques (Figure 41) provient de surcroît d'une surrection actuelle due à une anomalie thermique. Cette conjonction explique la topographie développée de l'Anti-Atlas oriental et plus particulièrement celle du Saghro. Cela n'annule toutefois pas les effets de l'édifice varisque puisque l'analyse des constituants des sédiments post-varisques démontre que la boutonnière du Saghro du moins, a toujours été émergeante depuis l'événement varisque, expliquant ainsi l'absence de sédiments Triasiques et Jurassiques sur

le domaine de l'Anti-Atlas alors en extension. Ceci est également démontré par la comparaison de l'uplift modélisé (Missenard *et al.*, 2006) avec le relief actuel (Figure 36, p.72).

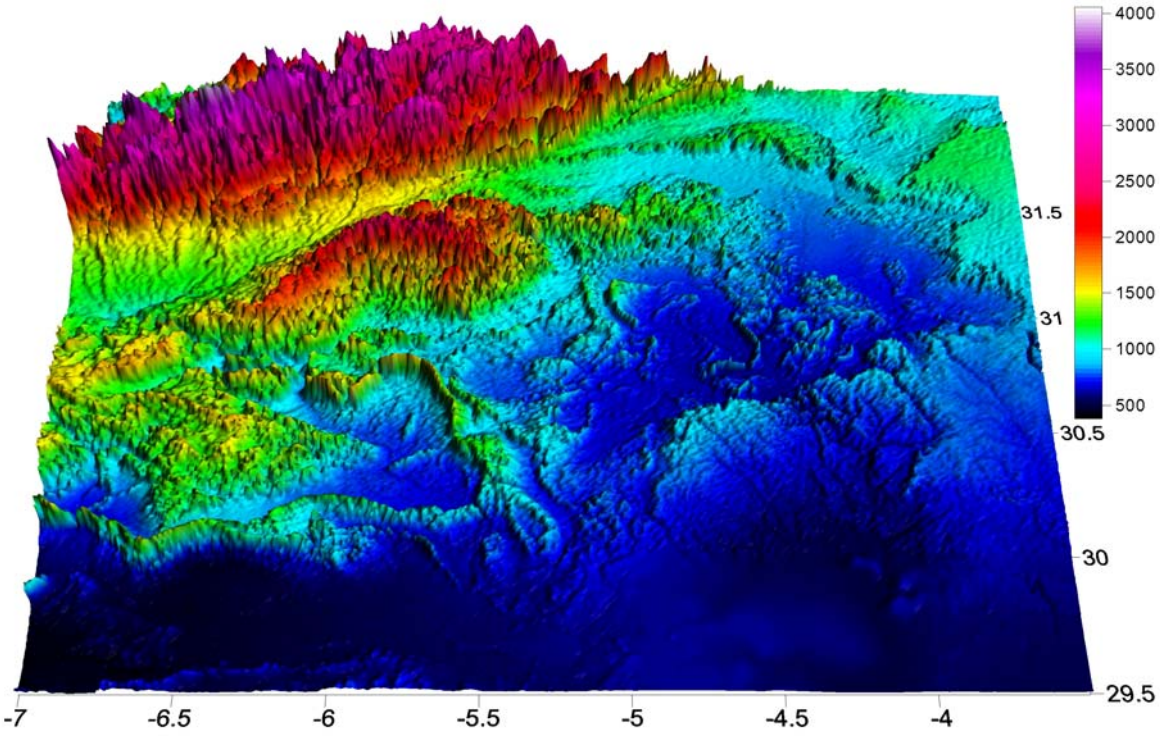

Figure 41*. Modèle tridimensionnel du modèle numérique de terrain. Exagération verticale 10 :1. Données GTOPO 30.

6

CONCLUSIONS

Apports de l'étude

6.1. Style structural

Le style structural est contrôlé par deux paramètres principaux :

Pré-structuration du socle. Les failles normales du rift Néoprotérozoïque – Cambrien constituent des zones de faiblesse qui seront réactivées lors de l'inversion varisque et lors de l'extension Mésozoïque. Le fait que le socle de l'Anti-Atlas oriental soit métacratonique, le différencie du reste de la chaîne et favorise l'interférence Anti-Atlas – Ougarta.

Rhéologie de la couverture. L'incompétence de la série Paléozoïque permet l'amortissement des mouvements de socle, lors de l'inversion varisque selon le modèle trishear. Ce drapage est également observé, dans la partie supérieure de la couverture, lors de l'extension tardive. Cette incompétence rend possible un important raccourcissement interne discret à grande échelle : 3 km de raccourcissement observé (2%) contre 11 à 17 % de déformation interne (16 à 25 km). Elle explique l'absence de décollement majeur.

La différence de style structural avec l'Anti-Atlas occidental provient du fait que la série y est encore plus épaisse et que les séries incompétentes comprennent des détachements qui permettent le *buckling* polyharmonique.

6.2. Structures

L'inversion varisque est de type *thick skin*. On ne trouve aucun décollement majeur au contact socle – couverture, ni dans d'autres horizons de décollement potentiel. Le détachement s'enracine en milieu de croûte (-18 à -20 km). Les failles inverses se prolongent en chevauchements horizontaux, probablement localisés dans les sédiments syn-rift du sommet du « socle » (Figure 39, stade B, p.78). Ceci peut toutefois créer, au front de la structure majeure, une déformation de type *thin skin*. La géométrie globale de la couverture est donc un drapage induit par les mouvements relatifs des blocs de socle.

Une multitude des petites structures compressives plus ou moins isolées témoigne d'une part importante de déformation interne dans la couverture.

L'analyse de l'orientation des structures majeures et des petites structures montre une image d'interférence due au croisement de deux déformations d'orientations distinctes : anti-atlasique et ougartienne. Cette partie de la chaîne est donc davantage un carrefour plutôt qu'un arc relayant l'Anti-Atlas à l'Ougarta (Figure 40, p.80).

L'intensité de la déformation indique clairement un gradient décroissant vers le sud pour ce qui est de l'orientation anti-atlasique. Un gradient ougartien décroissant vers l'ouest est moins marqué.

Une phase d'extension tardive crée des failles normales dans la couverture et provoque localement des synclinaux (anciennement interprétés comme plis varisques). Ces structures extensives très raides permettent d'extrapoler les limites des blocs de socle.

6.3. Tectonique

Le caractère métacratonique du socle de l'Anti-Atlas, la suture Pan-Africaine et les failles normales du rift Néoprotérozoïque – Cambrien sont autant de structures déterminantes dans l'agencement de l'inversion varisque.

L'Anti-Atlas est la partie déformée du bassin de Tindouf. L'analyse sédimentologique et la corrélation avec d'autres bassins nord-africains, permettent de conclure à un bassin intracontinental. Il bénéficie d'une subsidence régulière durant le Paléozoïque, certaines variations étant attribuées à des fluctuations du niveau marin, à des événements climatiques ou à des phases orogéniques lointaines. Il se distingue des autres bassins par une inversion plus massive et une déformation plus intense. Il est néanmoins connecté aux chaînes inversées des bordures du craton ouest africain, comme l'Ougarta ou l'Ahnet-Mouydir (Haddoum *et al.*, 2001).

L'Anti-Atlas oriental enregistre l'ouverture du bassin du Haut Atlas par la formation de structures extensives. Mais l'inversion alpine ne provoque aucune déformation directe dans l'Anti-Atlas oriental, excepté un soulèvement général combiné à l'effet d'une anomalie thermique récente.

6.4. Implications et Perspectives

D'après son style structural, l'Anti-Atlas a des analogues tels que les bassins inversés de l'orogénèse Laramide de Uinta ou de Wind River, décrits par Mitra et Mounts (1998) ou Stone (1999). Ils ont en commun une déformation de type trishear, induite par des mouvements verticaux de blocs de socle rigides, forçant une couverture de faible compétence. L'Anti-Atlas dévie pourtant de ces exemples, par l'aplatissement en surface des failles inversées. Ceci est rendu possible grâce aux séries post-Panafricaines et syn-rift qui caractérisent la partie

supérieure du socle varisque. Cette déviation de toute autre chaîne décrite jusqu'à présent, fait de l'Anti-Atlas un objet géologique particulier. Cela peut être intéressant dans le domaine appliqué de la recherche de ressources énergétiques et pourrait amener à (ré)interpréter la structure d'autres bassins.

La nouvelle méthode de calcul de la profondeur de détachement, prenant en compte le raccourcissement interne, permettra la comparaison avec d'autres bassins inversés. Elle pourrait être testée sur des chaînes mieux connues et de styles structuraux différents.

L'entreprise d'une comparaison avec les autres bassins nord-africains en terme de style structural et de raccourcissement interne pourrait aider à la compréhension de l'assemblage de la Pangée.

L'étude de la dénudation tectonique du Saghro par des méthodes d'analyse de traces de fission ou de rayonnements cosmiques permettrait de définir plus précisément l'histoire de sa topographie.

Enfin, des essais en modèles analogiques, jouant les multiples réactivations des blocs de socle, en variant la compétence et la puissance de la couverture, seraient une expérience fort intéressante.

REFERENCES

AIT BRAHIM L., P. CHOTIN, S. HINAJ, A. ABDELOUAFI, A. EL ADRAOUI, C. NAKCHA, D. DHONT, M. CHARROUD, F. SOSSEY ALAOUI, M. AMRHAR, A. BOUAZA, H. TABYAOUI, A. CHAOUNI (2002), Paleostress evolution in the Moroccan African margin from Triassic to present, *Tectonophysics*, 357, pp. 187-205.

ALGOUTI AB., AH. ALGOUTI, B. CHBANI, M. ZAIM (2001), Sédimentation et volcanisme synsédimentaire de la série de l'Adoudounien infra-cambrien à travers deux exemples de l'Anti-Atlas du Maroc, *Journal of African Earth Sciences*, Vol. 32, N° 4, pp. 541-556.

ALLMENDINGER R.W. (1998), Inverse and forward numerical modeling of trishear fault-propagation folds, *Tectonics*, Vol. 17, N°. 4, pp. 640-656.

ARBOLEYA M.L., A. TEIXELL, M. CHARROUD, M. JULIVERT (2004), A structural transect through the High and Middle Atlas of Morocco, *Journal of African Earth Sciences*, 39, pp. 319-327.

AYARZA P., F. ALVAREZ-LOBATO, A. TEIXELL, M.L. ARBOLEYA, E. TESÓN, M. JULIVERT, M. CHARROUD (2005), Crustal structure under the central High Atlas Mountains (Morocco) from geological and gravity data, *Tectonophysics*, 400, pp. 67-84.

BARBEY P., F. OBERLI, J.-P. BURG, H. NACHIT, J. PONS, M. MEIER (2004), The Palaeoproterozoic in western Anti-Atlas (Morocco): a clarification, *Journal of African Earth Sciences*, 39, pp. 239-245.

BAYER R., A. LESQUER (1978), Les anomalies gravimétriques de la bordure orientale du craton ouest-africain: géométrie d'une suture pan-africaine, *Bull. Soc. Géol. Fr*. 20, pp. 863-876.

BEAUCHAMP W., R.W. ALLMENDINGER, M. BARANZAGI, A. DEMNATI, M. EL ALJI, M. DAHMANI (1999), Inversion tectonics and evolution of the High Atlas Moutains, Morocco, based on a geological-geophysical transect, *Tectonics*, Vol. 18, N° 2, pp. 163-184.

BENSSAOU M., N. HAMOUMI (2003), The lower-Cambrian western Anti-Atlasic graben: tectonic control of palaeogeography and sequential organisation, *C. R. Geoscience*, 335, pp. 297-305.

BOOTE D.R., D. CLARK-LOWES, M. TRAUT (1998), Palaeozoic petroleum systems of North Africa. In: Macgregor, D.S., Moody, R.T.J. & Clark-Lowes, D.D. (eds). Petroleum Geology of North Africa. Geological Society, London, Special Publication No. 132, pp. 7-68.

Buggish, W., E. Flügel (1988), The Precambrian / Cambrian boundary in the Anti-Atlas (Morocco) discussion and new results, in *The Atlas System of Morocco*, edited by V.H. Jacobshagen, *Lecture Notes Earth Sci*., vol. 15, pp. 361-404, Springer-Verlag, New-York.

BUMP A.P. (2003), Reactivation, trishear modeling, and folded basement in Laramide uplifts: implications for the origins of intracontinental faults, *GSA Today*, pp. 4-10.

BURKHARD M. S. CARITG, U. HELG, C. ROBERT-CHARRUE, A. SOULAÏMANI (2006), Tectonics of the Anti-Atlas of Morocco, *Comptes Rendus Geoscience*, 338, pp. 11-24.

CARITG S., M. BURKHARD, R. DUCOMMUN, U. HELG, L. KOPP, C. SUE (2004), Fold interference patterns in the Late Palaeozoic Anti-Atlas belt of Morocco, *Terra Nova*, 16, pp.27-37.

CHOUBERT G., A. FAURE-MURET (1971), Epoque hercynienne, *In*: *Tectonique de l'Afrique*, Sciences de la Terre, Paris, 6, UNESCO, Paris, France, pp. 353-371.

CHOUBERT G., A. FAURE-MURET (1983), Anti-Atlas, *In*: *Lexique Stratigraphique International, Nouvelle série n°1, Afrique de l'Ouest*, J. Fabre (Editor), Pergamon, pp. 80-95.

CLOETINGH S., J.D. VAN WEES, P.A. VAN DER BEEK, G. SPADINI (1995), Role of pre-rift rheology in kinematics of extensional basin formation: constraints from thermomechanical models of Mediterranean and intracratonic basins, *Marine and Petroleum Geology*, Vol. 12, N° 8, pp. 793-807.

COWARD M., A. RIES (2003) Tectonic development of North African basins in : Arthur, T. J., MacGregor, D. S. & Cameron, N. R. (eds) *Petroleum Geology of Africa : New Themes and Developing Technologies*. Geological Society, London, Special Publications, 207, 61-83.

CURRIE J.B., H.W. PATNODE, R.P. TRUMP (1962), Development of folds in sedimentary strata, *Geological Society of America Bulletin*, v. 73, pp. 655-673.

ELLOUZ N., M. PATRIAT, J.-M. GAULIER, R. BOUATMANI, S. SABOUNJI (2003), From rifting to Alpine inversion: Mesozoic and Cenozoic subsidence history of some Moroccan basins, *Sedimentary Geology*, 156, pp. 185-212.

ENNIH N., J.-P. LIÉGEOIS (2001), The Moroccan Anti-Atlas: the West African craton passive margin with limited Pan-African activity. Implications for the northern limit of the craton, *Precambrian Research*, 112, pp. 289-302.

ENNIH N., J.-P. LIÉGEOIS (2003), Discussion, The Moroccan Anti-Atlas: the West African craton passive margin with limited Pan-African activity. Implications for the northern limit of the craton: reply to comments by E.H. Bouougri, *Precambrian Research*, 120, pp. 185-189.

EPARD J.-L., R.H. GROSHONG (1993), Excess area and depth to detachment, *The AAPG bulletin*, v. 77, No. 8, pp. 1291-1302.

ERSLEV E.A. (1991), Trishear fault-propagation folding, *Geology*, v. 19pp. 617-620.

FACCENNA C., T. NALPAS, J.-P. BRUN, P. DAVY (1995) The influence of pre-existing thrust faults on normal fault geometry in nature and in experiments, *Journal of Structural Geology*, Vol. 17, N° 8, pp. 1139-1149.

FINCH E., S. HARDY, R. GAWTHORPE (2003), Discrete element modelling of contrational fault-propagation folding above rigid basement fault blocks, *Journal of Structural Geology*, 25, pp. 515-528.

FINCH E., S. HARDY, R. GAWTHORPE (2004), Discrete-element modelling of extensional fault-propagation folding above rigid basement fault blocks, *Basin research*, 16, pp. 489-506.

FRIZON DE LAMOTTE D., B. SAINT BEZAR, R. BRACÈNE, E. MERCIER (2000), The two main steps of the Atlas building and geodynamics of western Mediterranean, *Tectonics*, Vol. 19, N° 4, pp. 740-761.

FRIZON DE LAMOTTE D.,CRESPO-BLANC A., SAINT-BEZAR B.,COMAS M., FERNANDEZ M., ZEYEN H., AYARZA P., ROBERT-CHARRUE C., CHALOUAN A., ZIZI M., TEIXELL A., ARBOLEYA M.L., ALVAREZ-LOBATO F., JULIVERT M., MICHARD A. (2004) TRANSMED Transect I. In: Cavazza W, Roure F, Spakman W, Stampfli GM, and Ziegler PA (eds) *The TRANSMED Atlas: the Mediterranean Region from Crust to Mantle*, Springer Verlag, 2004, XXIV, 141 pp. ISBN : 3-540-22181-6.

GASQUET D.,G. LEVRESSE, A. CHEILLETZ, M.R. AZIZI-SAMIR, A. MOUTTAQI (2005), Contribution to geodynamic reconstruction of the Anti-Atlas (Morocco) during Pan-African times with the emphasis on inversion tectonics and metallogenic activity at the Precambrian–Cambrian transition, *Precambrian Research*, 140, pp. 157-182.

GÖRLER K., F.-F. HELMDACH, P. GAEMERS, K. HEISSIG, W. HINSCH, K. MÄDLER, W. SCHWARZHANS, M. ZUCHT (1988), The uplift of the central High Atlas as deduced from Neogene continental sediments of the Ouarzazate province, Morocco, in *The Atlas System of Morocco*, edited by V.H. Jacobshagen, *Lecture Notes Earth Sci.*, vol. 15, pp. 361-404, Springer-Verlag, New-York.

GROSHONG R.H. (1994), Area balance, depth to detachment, and strain in extension, *Tectonics*, v. 13, No. 6, pp. 1488-1497.

GROSHONG R.H., 2002, 3-D structural geology: 2nd printing, Springer-Verlag, 324 p.

GUIRAUD R., J.-C. DOUMNANG MBAIGANE, S. CARRETIER, S. DOMINGUEZ (2000), Evidence for a 6000 km length NW-SE-striking lineament in northern Africa: the Tibesti Lineament, *Journal of the Geological Society, London*, Vol. 157, pp. 897-900.

HADDOUM H., R. GUIRAUD, A. MOUSSINE-POUCHKINE (2001), Hercynian compressional deformations of the Ahnet-Mouydir Basin, Algerian Saharan Platform: far-field stress effects of the Late Palaeozoic orogeny, *Terra Nova*, 13, pp. 220-226.

HARDY S., K. MCCLAY (1999), Kinematic modelling of extensional fault-propagation folding, *Journal of Structural Geology*, 21, pp. 695-702.

HEFFERAN K.P., H. ADMOU, J.A. KARSON, A. SAQUAQUE (2000), Anti-Atlas (Morocco) role in Neoproterozoic Western Gondwana reconstruction, *Precambrian Research*, 103, pp. 89-96.

HELG U., M. BURKHARD, S. CARITG, C. ROBERT-CHARRUE (2004), Folding and inversion tectonics in the Anti-Atlas of Morocco, *Tectonics*, Vol. 23, TC4006, doi:10.1029/2003TC001576.

HOEPFFNER C., A. SOULAIMANI, A. PIQUÉ (2005), The Moroccan Hercynides, *Journal of African Earth Sciences*, 43, pp. 144-165.

JOHNSON K.M., A.M. JOHNSON (2002, A), Mechanical models of trishear-like folds, *Journal of Structural Geology*, 24, pp. 277-287.

KHALIL S.M., K.R. MCCLAY (2002), Extensional fault-related folding, northwestern Red sea, Egypt, *Journal of Structural Geology*, 24, pp. 743-762.

LIÉGEOIS J.-P., A. FEKKAK, O. BRUGUIER, E. ERRAMI, N. ENNIH (2005) Lower ediacaran age (630-610 Ma) for the Sarhro group. Implications for the metacratonic evolution of the Anti-Atlas, correlations with the Tuareg shield and the evolution of the pan-african orogeny in the NW Africa (abs.), *4ème Colloque International 3Ma, Agadir 2005*, Abstract Volume, pp. 2.

MACGREGOR D.S. (1996), The hydrcarbon systems of North Africa, *Marine and Petroleum Geology*, Vol. 13, N° 3, pp. 329-340.

MANSPEIZER W., J.H. PUFFER, H.L. COUSMINER (1978), Separation of Morocco and eastern North America: A Triassic-Liassic stratigraphic record, *Geological Society of America Bulletin*, v. 89, pp. 901-920.

MISSENARD Y., H. ZEYEN, D. FRIZON DE LAMOTTE, P. LETURMY, C. PETIT, M. SÉRBIER, O. SADDIQI (2006), Crustal versus asthenospheric origin of relief of the Atlas Mountains of Morocco, *Journal of Geophysical Research*, Vol. 111, B03410, 13 p.

MITRA S., V.S. MOUNT (1998), Foreland Basement-Involved Structures, *AAPG Bulletin*, V. 82, N°. 1, pp. 70-109.

PIQUE A., M. BOUABDELLI, A. SOULAÏMANI, N. YOUBI, M. ILIANI (1999), Les conglomerates du P III (Néoprotérozoïque supérieur) de l'Anti-Atlas (Sud du Maroc): molasses panafricaines, ou marqueurs d'un rifting fini-protérozoïque ?, *C. R. Acad. Sci. Paris, Sciences de la Terre et des planètes*, 328, pp. 409-414.

PIQUE A. (2001) Geology of Northwest Africa, Beiträge zur regionalen Geologie der Erde ; Bd. 29, Gebrüder Borntraeger, 310 p.

PIQUÉ A. (2003) Perspective, Evidence for an important extensional event during the latest Proterozoic and Earliest Paleozoic in Morocco, *C. R. Geoscience*, 335, pp. 865-868.

ROBERT-CHARRUE C., M. BURKHARD (soumis), Variscan inversion tectonics and interference pattern in the Tafilalt, Anti-Atlas, Morocco, *Journal of African Earth Sciences*.

SADDIQI O., N. ZIAD, Y. MISSENARD, D. FRIZON DE LAMOTTE, B. GOFFE, P. LETURMY, R. EL MAMOUN, S. SEBTI, G. POUPEAU (2005), Age Miocène moyen supérieur du soulèvement thermique du Haut-Atlas Central : apport des traces de fission sur apatite, *4ème Colloque International 3Ma, Agadir 2005*, Abstract Volume, pp. 45.

SAQUAQUE A., H. ADMOU, J. KARSON, K. HEFFERAN, I. REUBER (1989), Precambrian accretionary tectonics in the Bou Azzer-El Graara region, Anti-Atlas, Morocco, *Geology*, v. 17, pp. 1107-1110.

SCHLISCHE R.W. (1995), Geometry and Origin of Fault-Related Folds in Extensional Settings, *AAPG Bulletin*, V. 79, N°. 11, pp. 1661-1678.

SCHMIDT K.-H. (1988), Rates of scarp retreat: a means of dating neotectonic activity, in *The Atlas System of Morocco*, edited by V.H. Jacobshagen, *Lecture Notes Earth Sci.*, vol. 15, pp. 445-462, Springer-Verlag, New-York.

SCHMIDT K.-H. (1992), The tectonic history of the Pre-Saharan depression (Morocco) – a geomorphological interpretation, *Geologische Rundschau*, 81/1, pp. 211-219.

SEBAI A., G. FERAUD, H. BERTRAND, J. HANES (1991), $^{40}Ar/^{39}Ar$ dating and geochemistry of tholeiitic magmatism related to the early opening of the central Atlantic rift, *Earth and Planetary Science Letters*, 104, pp. 455-472.

SOULAÏMANI A., C. LE CORRE, R. FARAZDAQ (1997), Déformation hercynienne et relation socle/couverture dans le domaine du Bas-Drâa (Anti-Atlas occidental, Maroc), *Journal of African Earth Sciences*, Vol. 24, N° 3, pp. 271-284.

SOULAÏMANI A., M. BOUABDELLI A. PIQUE (2003), L'extension continentale au Néo-Protérozoïque supérieur – Cambrien inférieur dans l'Anti-Atlas (Maroc), *Bull. Soc. Géol. France*, 174 (1), pp. 83-92.

STAMPFLI , G.M., G.D. BOREL (2002), A plate tectonic model for the Paleozoic and Mesozoic constrained by dynamic plate boundaries and restored synthetic oceanic isochrones, *Earth and Planetary Science Letters*, 196, pp 17-33.

STONE D.S. (1999), Foreland Basement-Involved Structures: Discussion, *Discussion & Reply, AAPG Bulletin*, V. 83, N°. 12, pp. 2006-2016.

TEIXELL A., M.-L. ARBOLEYA, M. JULIVERT, M. CHARROUD (2003), Tectonic shortening and topography in the central High Atlas (Morocco), *Tectonics*, Vol. 22, N° 5.

TEIXELL A., P. AYARZA, H. ZEYEN, M. FERNANDEZ, M.-L. ARBOLEYA (2005), Effects of mantle upwelling in a compressional setting:the Atlas Mountains of Morocco, *Terra Nova*, 17, pp. 456-461.

THOMAS R.J., A. FEKKAK, N. ENNIH, E. ERRAMI, S.C. LOUGHLIN, P.G. GRESSE, L.P. CHEVALLIER, J.-P. LIÉGEOIS (2004), A new lithostratigraphic framework for the Anti-Atlas Orogen, Morocco, *Journal of African Earth Sciences*, 39, pp. 217-226.

VEEVERS J.J. (2004), Gondwanaland from 650-500 Ma assembly through 320 Ma merger in Pangea to 185-100 Ma breakup: supercontinental tectonics via stratigraphy and radiometric dating, *Earth-Science Reviews*, 68, pp. 1-132.

WITHJACK M.O., J. OLSON, E. PETERSON (1990), Experimental Models of Extensional Forced Folds, *AAPG Bulletin*, V. 74, N°. 7, pp. 1038-1054.

XIAO H., J. SUPPE (1992), Origin of Rollover, *AAPG Bulletin*, V. 76, N°. 4, pp. 509-529.

YAMADA Y., K. MCCLAY (2003), Application of geometric models to inverted listric fault systems in sandbox experiments. Paper 2: insights for possible along strike migration of material during 3D hanging wall deformation, *Journal of Structural Geology*, 25, pp. 1331-1336.

ZIEGLER P.A., S. CLOETINGH (2004), Dynamic processes controlling evolution of rifted basins, *Earth-Science Reviews*, 64, pp. 1-50.

Cartes géologiques

S.E. M. Fetah, M. Bensaïd, M. Dahmani (1986) carte géologique du Maroc 1:200'000, Tafilalt – Taouz (N° 244), Ministère de l'Energie et des Mines, Royaume du Maroc. J. Destombes, H. Hollard.

S.E. M. Fetah, Bensaïd, M. Dahmani (1988) carte géologique du Maroc 1:200'000, Todrha – Ma'der (N° 243), Ministère de l'Energie et des Mines, Royaume du Maroc. R. du Dresnay, G. Dubar, J. Hindermeyer, G. Choubert, A. Emberger, J. Caïa, J. Destombes, H. Hollard.

S.E. M. Fetah, Bensaïd, M. Dahmani (1989) carte géologique du Maroc 1:200'000, Zagora – Coude du Dra – Hamada du Dra (p.p.), Ministère de l'Energie et des Mines, Royaume du Maroc. G. Choubert, A. Faure-Muret, J. Destombes, H. Hollard.

S.E. M. Saadi, E.A. Hilali, M. Bensaïd (1975) carte géologique du Maroc 1:200'000, Jebel Saghro – Dadès (N° 161), Ministère de l'Energie et des Mines, Royaume du Maroc. J. Hindermeyer, H. Gauthier, J. Destombes, G. Choubert, A. Faure-Muret, E. Roch, G. Dubar, P. Fallot, E. Laville, J.L. Lesage, R. du Dresnay.

S.E. M. Saadi, E.A. Hilali, M. Bensaïd (1982) carte géologique du Maroc 1:200'000, Bou Haïara – Zegdou (N° 259), Ministère de l'Energie et des Mines, Royaume du Maroc. J. Destombes, H. Hollard.

Sites Internet

[1] http://www.geomag.bgs.ac.uk/mercator.html

[2] https://zulu.ssc.nasa.gov/mrsid/

[3] http://edc.usgs.gov/products/elevation/gtopo30/gtopo30.html

TABLES DES FIGURES TABLEAUX ET GRAPHIQUES

Figures Page

---

* Figures également représentées dans l'annexe D en format plus grand.

Tableaux Page

Graphiques Page

REMERCIEMENTS

Mes remerciements posthumes à Martin Burkhard qui m'a toujours fait confiance et encouragé dans toutes mes entreprises. A celui qui m'a inculqué la géologie structurale, la cartographie, la géologie des Alpes. A celui qui m'a rendu attentif à l'importance de la géologie dans notre société, aux problèmes environnementaux et politiques, à la vulgarisation. A celui qui m'a permis de découvrir un bout du monde.

Au Fonds National de la Recherche Scientifique. Pour le financement des projets N° 21-52516.97 et 20-63790.00.

Au Fonds Matthey-Dupraz pour le soutien financier lors de mon travail de diplôme.

Au ministère de l'Industrie, de l'Energie et des Mines de Rabat, Maroc. Notamment à MM Dahmani et Haddane chefs de la Division de la Géologie, ainsi que leur secrétaire et M. Scalante.

A l'ONHYM (anciennement ONAREP) pour nous avoir fournit les données sismiques. A MM B. Bally et M. Zizi pour leurs interprétations.

A Dominique Frizon de Lamotte pour m'avoir fait participer au le projet Transmed, pour son avis critique et son soutient.

A MM les jurés A. Soulaïmani et M. Zizi pour avoir accepté de faire partie de mon jury de thèse, pour leur critiques constructives.

Au Pr Jean-Paul Schaer pour ses conseils éclairés et nos discussions encourageantes.

Au Pr Jean-Paul Liègeois, pour ses échanges intéressants lors du congrès 3Ma 2005 à Agadir et lors de sa visite à Neuchâtel.

Au Pr Karl Föllmi d'avoir spontanément pris le relais de directeur de thèse.

Au Pr Thierry Adatte pour ses corrections pertinentes et constructives.

A l'Institut de Géologie pour les belles années passées. Une thèse étant également le fruit de tout un environnement. :

A Mme la directrice le Pr A. Kalt, aux secrétaires Sabine et Franca, à André, à Eli, à Manu.

A mes collègues et amis assistants, enfants de l'institut (anciens et nouveaux) : Baba, Nat, Kaspar, Rachel, Séverine, Urs, Jack, Julien, Feddi, Bas, Alex (Corinne), Stéphane (Justine), Beni (sixpack), Stafele (Gaminou), Mary-Alix (arc-en-ciel de l'institut, avec qui j'ai aimé partager mon bureau), Laurette (bonne humeur de l'institut, photophile et super co-pilote en Tunisie), Flurin (10 nights in Tunisia), Laure, Laurent, Haydon, Cécile, Pascal, Raoul, Nico, Séverine, Christina ainsi qu'aux paléo-maîtres-assistants Virginie et Erwan.

A mes collègues de volées : Lionel, Pauline, Christophe, Philippe (2x), Stork, Gregory, Meryem, Virginie, Yves, Galaad, Julien, Métro, ...

Aux étudiants avec qui j'ai partagé TP et excursions : Aline, Pauline, Lucien, Laurent, Réza, Patrick, Samuel, Tomaso, Roger, Robin, Esther, Laureline, Jean-Luc, Johann, Jonathan (2x), Vincent (3x), Baptiste, Claude, Gaël, Naomi, Marina, Mickael, Amstutz, Cédric, Géraldine (2x), Martine, Ivan, Pascal, Pascale, Affoltre, Christophe, Anne, Nicolas, Ekim, Tiziano, Yannick, Bérénice, Sophie, Laurent, Rodrigo, Paul, Samuel, Raphaël, Guillaume, Clara-Marine, Clémentine, Cristobal, Julien, Philipp ... et j'en oublie.

A mes amis d'hydrogéologie : Franz, Romain, Michiel, Ludovic, Daniel, Vincent, Stéphane, François-David, François Z, ...

A toute l'équipe du Garage Blaser pour mon initiation à la mécanique.

A tous les Marocains, amis de longue date ou d'un instant, pour leur chaleur et leur hospitalité. Hassane, Abdulla, Redoine, Tarik, Smaïl, Mohammed, Ahmed, Mansour, Mehdi, Somia, Kaoutar, Isham, Amine, Adnane, Abdulwahed, Aziz, ...

A mes parents

A Rachel

A

DONNEES BRUTES DE LA FIGURE 22

PETITS PLIS

Stéréogrammes jaunes

Plan de stratification :
Données : Azimut (000-360°) et Plongement (00-90°) de la ligne de plus grande pente.
Représentation sur les stéréogrammes : Pôle du plan, hémisphère inférieur.

Kreb Lethel N31°20' / W003°50'

356	54	032	79	004	66	330	46
306	54	002	71	030	60	339	52
024	68	338	46	240	64	012	48
311	43	287	52	031	77	017	45
002	53	331	59	306	47	002	43
294	41	018	56	344	53		
358	38	005	64	324	49		

Aoufital N30°55' / W004°05'

058	38	069	30	035	10	208	39
054	42	053	19	062	45	039	35
043	15	046	28	069	19	202	27
044	55	225	20	149	08	055	22
247	39	226	28	052	23	225	33
059	34	228	35	073	44	112	21
079	42	198	30	094	46	075	40
056	60	173	16	109	24	254	12
225	64	207	72	166	25	079	34
075	28	253	38	168	18	077	24
064	32	005	18	222	26	215	19
081	20	358	28	049	15	228	18
154	10	033	22	075	18	234	52
243	61	060	30	039	51	087	36
253	69	309	18	230	56	074	39
097	47	341	19	187	14	057	36
062	17	045	22	218	23	230	51
228	30	048	51	201	48	211	22
042	21	082	24	049	54	043	55
045	26	198	22	095	25	221	40
178	23	248	27	153	21	224	39

083	11	231	12	207	56	217	21
057	39	252	41	061	49	057	44
044	40	053	20	052	44	225	55
050	31	236	40	044	38	064	37
047	78	053	19	209	48	063	20
054	60	231	37	212	53		
217	16	049	58	055	26		

Tamjrani N31°00' / W004°10'

042	60	227	79	217	68	053	34
047	61	225	69	062	56	087	22
229	83	057	64	207	33	121	23
228	32	226	84	090	20	152	32
066	48	049	47	241	39	166	46
078	37	048	78	051	65	172	44
083	29	067	30	228	71	228	59
190	22	142	14	054	74	192	22
234	37	197	21	237	53	067	28
063	34	222	38	091	56	204	33
063	55	019	24	226	60	103	47
071	53	062	74	191	28	089	40
074	26	228	69	136	20	075	59
124	17	193	25	075	29	219	55
168	15	054	53	051	34	229	73
216	43	227	84	048	63		

Bou Tchrafine N31°25' / W004°10'

173	26	149	25	078	23	215	40
161	38	186	32	059	34	029	86
060	51	214	48	052	30	042	84
057	75	346	28	045	43	045	59
073	32	093	63	029	66	043	66
125	25	224	53	033	42	233	88
190	40	167	27	025	60	221	76
192	42	142	22	038	15	215	47
195	39	213	36	019	57	213	48
043	57	149	34	359	42	039	49
189	24	122	31	220	15	214	10
039	21	127	37	189	34	060	06
207	60	229	60	152	14	041	53
197	38	077	33	190	13	043	49
155	10	062	63	099	20	022	37
212	85	053	22	206	30	111	30
044	46	065	16	236	49	074	59
038	32	063	19	230	50	239	24
222	42	215	42	158	19	258	35
209	28	212	48	097	22	172	63
107	29	214	54	227	45	121	30
058	87	219	37	212	44		
228	63	179	20	232	45		
111	14	073	32	235	40		

Jebel Irhs N31°20' / W004°20'

171	35	046	21	238	32	064	19
205	53	041	54	249	41	069	31
199	58	037	45	186	34	060	61
206	77	146	18	242	42	110	20
059	53	110	24	090	08	105	31
103	24	220	44	276	48	208	83
181	44	227	64	093	60	042	43
197	18	152	13	272	58	240	40
193	20	218	59	090	42	045	43
196	12	226	82	097	30	062	78
048	71	041	38	077	33	035	27
064	25	089	22	065	29	019	20
207	71	205	42	208	06	239	82
235	29	203	47	242	20	003	40
231	47	172	11	311	04	280	47
225	73	124	12	175	30	229	61
223	57	084	10	102	43	260	43
111	29	059	19	235	55	023	49
086	67	054	20	113	22	281	21
103	78	055	26	057	39	255	48
156	29	052	28	057	58	244	45
207	32	056	23	188	28	254	53
225	41	057	21	141	27	074	80
226	30	220	37	080	38	221	18
095	09	205	36	207	23	075	58
224	47	203	35	044	35	243	24
217	30	215	87	125	12	252	40
040	43	175	18	051	41	059	51
031	29	193	46	233	70	063	62
189	64	139	36	051	79	063	59
161	13	029	67	218	53	061	49
045	26	112	19	209	47	228	22
047	46	077	33	088	55	228	50
201	46	074	36	048	56	210	53
204	83	117	13	066	45		
025	84	116	05	202	36		
040	72	242	20	091	10		

Jebel Rheris N31°20' / W004°40'

253	58	256	52	270	57	010	62
316	72	255	56	234	65	019	60
265	61	258	52	312	77	351	49
222	50	279	50	177	82	327	45
195	78	257	64	270	46	287	65
258	68	288	49	276	45	269	63
261	81	295	60	338	54	013	65

Msissi est N31°20' / W004°45'

042	79	049	70	352	55	299	60
019	62	265	70	051	84	005	67

258	31	005	30	270	31	035	74
318	26	015	61	283	37		
018	58	002	69	265	60		

Msissi ouest N31°15' / W004°50'

247	41	355	23	200	74	223	77
331	42	108	19	192	65	020	43
357	46	180	44	175	29	211	51
279	17	013	51	050	33	016	52
342	29	297	19	056	45	342	20
227	70	257	30	042	44	219	59

Fezzou N31°10' / W004°50'

156	11	197	45	041	64	211	42
210	65	045	25	204	44		

Toufassemane N31°20' / W004°55'

143	07	234	46	232	54
156	25	088	50	220	40
148	21	116	17	213	24

Tazzarine est N30°45 / W005°20'

201	21	163	12	055	29	226	28
225	15	166	08	197	21		
212	18	234	55	215	12		

Tazzarine nord N30°50' / W005°25'

243	17	168	27	187	28	324	52
326	09	173	25	205	19	333	25
202	09	351	59	339	42	320	52
184	25	307	09	334	24	321	49
181	12	175	23	278	17	277	27
197	19	168	19	203	17		
214	16	198	25	158	68		

Nekob nord N31°05' /W005°45'

42	10	71	78	228	10
64	40	76	59	194	13
72	61	88	38	206	14

Achmas N30°45 / W006°05'

141	22	011	68	172	26	182	63
164	22	185	70	022	68		
153	17	148	50	157	21		
156	24	159	27	011	25		

Tamnougalt N30°10' / W006°25'

012	69	002	44	010	38
345	23	183	67	003	40

Agdz N30°45' / W006°30'

354	82	257	13	174	53	017	50
358	71	196	43	156	03	006	59
001	63	152	42	338	11	007	89
011	37	174	49	020	23	179	68
349	42	154	37	004	29	186	80
349	28	152	19	010	33	188	65
338	22						

Agdz nord N30°50' / W006°30'

172	17	042	16	031	33
155	19	193	36		

Touroug N31°40' / W004°40'

308	25	062	23	045	35	072	41
298	20	348	24	351	14	282	11
280	52	078	81	267	57	273	54

Asdaf N31°25' / W005°10'

039	11	353	52	015	27	156	45
153	60	055	23	013	39	162	59
152	72	044	19	025	27	002	49
344	62	154	59	034	29	013	41
352	59						

Tizi'n Boujou N31°25 / W005°15'

337	28	174	17	348	18	127	35
15	10	142	41	1	14	138	64
135	42	320	33	122	27	335	17
347	25	343	17	135	74	158	38
335	16	342	25	120	52		

Tisdafine sud N31°30' / W005°20'

003	60	014	46	107	36	130	31
058	18	015	68	021	48	149	47
022	38	014	37	025	57	092	22
146	70	164	43	036	39	009	40
084	33	158	89	106	27		

Tisdafine ouest N31°10' / W005°20'

006	59	163	65	061	39	172	58
001	52	022	45	016	49	156	40
171	50	040	21	054	27	082	35
358	55	014	53	354	82	027	50
001	50	352	67	174	59	006	87
178	78						

Tineghir sud-est N31°30' / W005°25'

009	27	021	21	182	34	105	72
060	19	051	09	236	09	112	83

083	27	174	85	033	26	356	55
110	51	072	12	334	50	009	33
119	68	173	80	028	19	044	24
015	40	178	54	094	67	129	45

Tineghir sud N31°35' / W005°30'

103	53	033	42	357	65	015	63
130	60	067	48	105	39	046	50
020	40	342	72	087	15	015	50

Tineghir SSW N31°30' / W005°30'

240	30	201	62	295	33	162	57
302	20	195	57	012	58	065	37
342	40	204	35	003	40	027	56
351	83	195	48	132	20		

Tineghir sud-ouest N31°25' / W055°40'

003	22	346	88	272	37	328	24
341	29	165	77	304	27	335	25
003	29	353	12	215	55	294	18
354	26	349	28	299	23	200	64
341	38	228	21	340	32		

CHEVAUCHEMENTS

Stéréogrammes bleus

Plans de chevauchements :
Données : Azimut et plongement de la ligne de plus grande pente.
Représentation sur stéréogrammes : Grand cercle, hémisphère inférieur.

Stries :
Données : Azimut et plongement de la direction de la strie.
Représentation sur stéréogramme : Direction de la strie, hémisphère inférieur.

Jebel Irhs N31°20' / W004°20'

Plans de chevauchement

100	32	227	64	064	35	095	30
182	26	056	85	138	45	231	40
078	61	159	30	126	15		

Stries

078	28	230	41	082	29	267	36
201	23	074	02	068	34		
063	60	332	64	077	13		

Msissi N31°10' / W004°50'

Plans de chevauchement

074	36	233	40	278	68	050	59
068	33	047	71	051	54		
152	35	226	54	273	52		

Stries

035	27	207	24	278	68	032	57
032	29	044	69	230	47		
215	39	070	51	295	20		

Tazzarine nord N30°50' / W005°25'

Plans de chevauchement

133	27	114	17	101	60	261	18
113	29	123	12	132	33	332	33

Stries

135	27	137	15	116	59	321	08
152	26	140	12	144	33	317	32

Achmas N30°45 / W006°05'

Plans de chevauchement

222	25	001	52	018	70	192	53
176	34	182	44	183	50	011	25

Stries

206	35	022	48	038	68	198	49
182	39	200	40	218	42	002	23

Tineghir sud N31°35' / W005°30'

Plans de chevauchement

119	65	005	45	321	46	331	40
046	20	332	72	105	23	352	79
343	45	338	59	160	10	325	50
002	31	341	21	339	11	302	24
170	31						

Stries

165	61	355	44	002	38	021	28
326	03	279	65	159	14	020	77
299	36	016	55	162	10	296	48
331	28	328	20	337	11	291	23
164	30						

Tineghir sud-ouest N31°25' / W055°40'

Plans de chevauchement

353	19	092	24	339	30	004	35
341	29	013	27	348	21	017	23
348	29	321	13	295	23	327	19
010	49	068	30	349	47	256	20

Stries

342	17	157	09	350	29	330	28
344	28	333	21	346	21	326	15
334	27	334	12	334	21	321	18
338	45	165	01	329	43	324	09

PENDAGES GENERAUX

Stéréogrammes verts

Plans de stratification :
Données : Azimut et plongement de la ligne de plus grande pente.
Représentation sur stéréogrammes : Pôle du plan, hémisphère inférieur.

Aoufital N30°55' / W004°05'

019	25	050	20	065	23	033	21
036	24	043	22	073	23	032	18
030	27	028	26	052	20	050	09
039	29	069	17	065	22	067	18
047	36	068	27	076	20	054	18
041	32	074	40	091	22	087	20
054	17	082	29	072	30	054	21
057	22	031	19	037	41	033	08
073	17	057	19	064	20	099	17
070	19	037	18	049	33	094	19
064	18	039	15	073	08	057	16
041	23	042	18	038	29	138	39
055	26	051	18	058	29	083	20
079	12	063	17	071	24	058	32

Msissi N31°15' / W004°50'

126	29	123	14	204	28	137	20
129	21	122	50	200	26	199	30
130	25	145	20	198	42	141	14
130	24	116	17	205	38	108	14
146	30	053	35	197	38	134	34
131	37	253	17	200	49	146	11
123	30	230	18	211	55	120	11

122	13	229	28	189	32	160	22
112	20	208	26	203	51	092	13
120	11	208	31	156	34	155	39
100	16	208	24	164	39	176	38
082	37	209	23	187	37	176	20
106	18	213	18	208	65	169	24
089	19	219	19	150	22	144	21
101	17	231	15	166	19	120	13
096	22	191	18	163	12	111	15
090	16	209	28	161	16	156	25
067	39	211	29	139	13	148	21
121	12						

Tazzarine nord N30°50' / W005°25'

139	30	141	12	303	03	260	16
136	14	125	10	136	08	137	35
144	09	164	17	306	04	146	26
136	17	150	12	138	18	165	11
152	17	256	09	139	11	149	10
154	15	194	15	181	09	155	27
155	12						

Tazzarine N30°45' / W005°35'

163	07	116	07	116	18	149	37
005	38	354	61	134	25		
142	11	336	69	142	21		

STRUCTURES EXTENSIVES

Stéréogrammes rouges

Failles :
Données : Azimut et plongement de la ligne de plus grande pente.
Représentation sur stéréogrammes : Grand cercle, hémisphère inférieur.

Stries :
Données : Azimut et plongement de la direction de la strie.
Représentation sur stéréogramme : Direction de la strie, hémisphère inférieur.

Tizi'n Boujou N31°20' / W005°15'

Failles

339	40	333	39	328	45	322	41	328	47

Stries

334	40	054	09	334	44	338	40	049	03

Tineghir sud-ouest N31°25' / W055°40'

Failles

190	53	161	38	137	89	138	55	164	64

Stries

176	71	141	35	225	37	196	51	220	37

Plans de stratifications des synclinaux associés à une faille normale :
Données : Azimut et plongement de la ligne de plus grande pente.
Représentation sur stéréogramme : Pôle du plan, hémisphère inférieur.

Ifarherioun N31°10' / W004°15'

153	29	032	33	335	31	012	37	034	45
180	80	202	37	170	54	016	33	061	44
032	51	219	44	194	64	026	59	006	79
139	28	331	29	185	59	016	51	004	51
146	39	343	33	059	26	012	27	028	51
188	50	330	43	202	67	351	24	007	70
175	52	333	47	032	50	277	34	043	64
181	35	023	66	001	07	157	18	051	45
023	80	012	76	182	44	176	19	038	50
210	29	002	29	019	71	103	22	033	53
039	54	184	72	352	12	263	26	040	46
031	46	193	38	191	33	250	17	031	40
007	60	221	54	192	88	219	47	022	42
024	51	171	61	247	51	180	59	030	52
027	50	187	48	182	36	178	64	349	58
029	47	189	56	169	51	345	31	037	36
013	34	008	53	008	73	207	43	173	22
049	53	181	50	004	67	205	42	354	30
049	54	173	62	354	72	040	33		
018	73	180	33	010	50	050	33		

Msissi N31°10' / W004°50'

356	59	339	17	009	13	148	30	348	40
359	31	002	19	155	52	358	44	356	30

Jebel Morf N30°45' / W005°10'

186	22	176	17	338	32	013	57	000	63
305	41	354	39	356	41	009	33	023	42
168	32	142	51	315	27	006	44	003	53
167	27	348	50	003	31	008	40	166	37
163	19	176	57	004	34	022	39	330	42
187	18	178	41	017	33	325	37	337	59
138	35	140	09	353	50	007	63		
156	20	339	21	339	78	354	58		

B

ARTICLES

- Variscan inversion tectonics and interference pattern in the Tafilalt, Anti-Atlas, Morocco. Soumis le 14.03.06 au *Journal of African earth Sciences*.

- Inversion tectonics in the eastern Anti-Atlas of Morocco. Soumis le 05.09.2006 au *AAPG Bulletin*.

- Burkhard M., S. Caritg, U. Helg, Ch. Robert-Charrue, A. Soulaimani (2006), Tectonics of the Anti-Atlas of Morocco, *C. R. Geoscience*, 338, pp. 11-24.

- Helg U., M. Burkhard, S. Caritg, and C. Robert-Charrue (2004), Folding and inversion tectonics in the Anti-Atlas of Morocco, *Tectonics*, *23*, TC4006, doi :10.1029/2003TC001576.

- Projet d'un troisième article.

Variscan inversion tectonics and interference pattern in the Tafilalt, Anti-Atlas, Morocco

Charles Robert-Charrue, Martin Burkhard*

[1] Institut de Géologie et d'Hydrogéologie, Université de Neuchâtel,

11, rue Emile-Argand, CH-2009 Neuchâtel, Switzerland

*Corresponding author. Tel. : +41 32 718 26 52 ; fax : +41 32 7182601.

E-mail address : martin.burkhard@unine.ch

Abstract

The structural style of the Anti-Atlas of Morocco is determined by two key parameters: the total thickness of Paleozoic cover series and the relative abundance of shale vs. competent marker beds. A late Proterozoic / earliest Cambrian rifting event produces a « Horst and Graben » configuration with clastic syn-rift deposits of the PII-III (Piqué et al., 1999, Piqué, 2003, Soulaimani et al., 2001). Post-rift sedimentation during most of the Paleozoic is dominated by shallow marine shale and marl deposits, alternating with periods of sandstone (Ordovician) and limestone (Devonian, lower Carboniferous) deposition. Clastic foreland basin sedimentation sets in during the middle Carboniferous and is terminated by a first tectonic compressional event in late Carboniferous times. This leads to strongly disharmonic small scale folding and minor thrust faults, by the intervention of diffuse detachments within thick shale horizons, in a trishear mode (Erslev, 1991, Bump, 2003). In the eastern Anti-Atlas, a regional gradient in deformation style, intensity and orientation is observed from north to south. A thick skinned inversion style in the north, is gradually changing southward into a thin skinned detachment folding style. An egg-box interference pattern is observed inbetween, interpreted to be linked to the shape of the West-African Craton. A Late Triassic NNW-SSE extension in relation with the onset of the Atlantic opening, reactivates the strongly compartimentalized, partly inverted basement blocks. Within the Paleozoic sediments this event leads to extensional fault-related folding above complex normal faults with stair case geometries. Upper Cretaceous sediments (Hamada du Guir) seal a peneplained Paleozoic landsurface. The topography of the eastern Anti-Atlas is only very slightly affected by Cenozoic to Quaternary inversion of the High-Atlas (Frizon de Lamotte et al., 2000). The present height of the Anti-Atlas chain in general is interpreted as due to large scale thermal uplift from middle Miocene onward (Saddiqi et al., 2005, Teixell et al., 2005).

Keywords: Anti-Atlas; Inversion tectonics; Thick vs thin skinned tectonics; Paleozoic; Variscan orogeny; Extensional fault-related folding.

1. Introduction

The Moroccan Anti-Atlas belt could be regarded as a fold-and-thrust belt in the hinterland of the Appalachian orogeny as the thin-skinned Alleghenian chain in the western foreland. The lack of major basal "décollement", deformation front or thrust fault makes the Anti-Atlas an unusual type of fold belt, which does not easily fit with classic schemes of ramp flat folding style, nor does it have any obvious analog in other well known orogens. The relationship between the basement involvement in the large inliers and the gentle folds of the surrounding cover has not found a satisfactory tectonic explanation sofar.

The aim of this study is to elucidate the tectonic evolution of this uncommon chain in terms of basement / cover relationships. Is the Anti-Atlas primarily thick skinned or is the basement involvement a late stage of an ordinary thin skinned belt ?

Detailed geological mapping has been conducted in the eastern Anti-Atlas of the Tafilalt area in order to characterize the type and orientation of folds, faults and successive generations of paleo-stress axes from fault/striae populations. The interpretation of a regional grid of reflexion seismic lines from ONAREP (National Office for Research and Oil Exploitation) provided additional constraints for the establishment of cross-sections and to establish a regional kinematic model.

2. Geological framework

2.1. Location and setting

The Anti-Atlas of Morocco is part of the larger Appalachian Orogen system, time equivalent with the Alleghenian front to the West. The Anti-Atlas appears as a huge anticlinorium oriented NE-SW (Choubert and Faure-Muret, 1971). Locally, the basement is cropping out as inliers, but the main part is made of an important Paleozoic cover, which is gently folded and of low grade metamorphism. The Anti-Atlas belt (Fig. 1) is located along the northern border of the West-African Craton (WAC). It is limited to the South by the Tindouf basin, unaffected by late Paleozoic folding, and to the North by the High-Atlas where Meso-Cenozoic sediments are involved in strong Cenozoic-lower Quaternary deformations. The

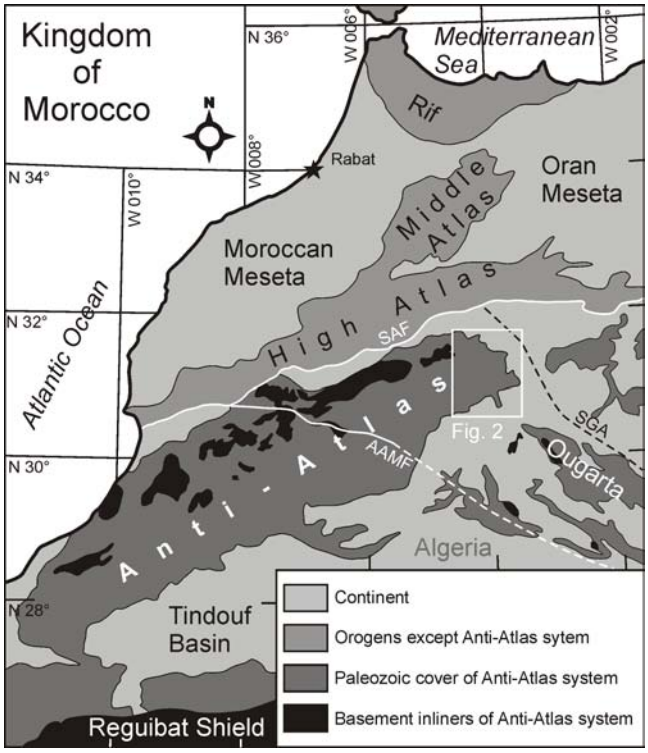

Fig. 1. Geographic situation and geological context of the Anti-Atlas. AAMF: Anti-Atlas Major Fault ; SAF: South Atlas Fault ; SGA: Saoura gravimetric anomaly.

Anti-Atlas s.s. is laterally limited by the Atlantic Ocean to the South-West and disappears eastward below the Hamada in the Tafilalt region. On a larger scale, the Anti-Atlas can also be seen as an arch (or rather a recess) continued to the South-West into the Zemour and Mauritanides thrust belts and to the South-East into the Ougarta fold belt (Haddoum et al., 2001). The studied area, the Tafilalt, is the eastern end of the Anti-Atlas s.s.. Structurally, this area differs markedly from the western part of the Anti-Atlas chain (Soulaimani et al., 1997, Helg et al., 2004, Cartig et al., 2004). In these semi-arid regions, a Landsat ™ 7 view can be used as a geologic map (see the succinct description, Fig. 2).

2.2. Stratigraphic units and lithology

Basement

In the Tafilalt area proper, basement outcrops are very sparse, limited to a few tiny outcrops of rhyolites and andesites of late P III, located along the north-east edge of the Tafilat half-window, 30 km east of Erfoud. An larger inlier is certainly hidden below the Cretaceous and Neogene sediments of the Hamada, in prolongation of an ENE alignment of inliers further west.

The crystalline basement has a complex history.

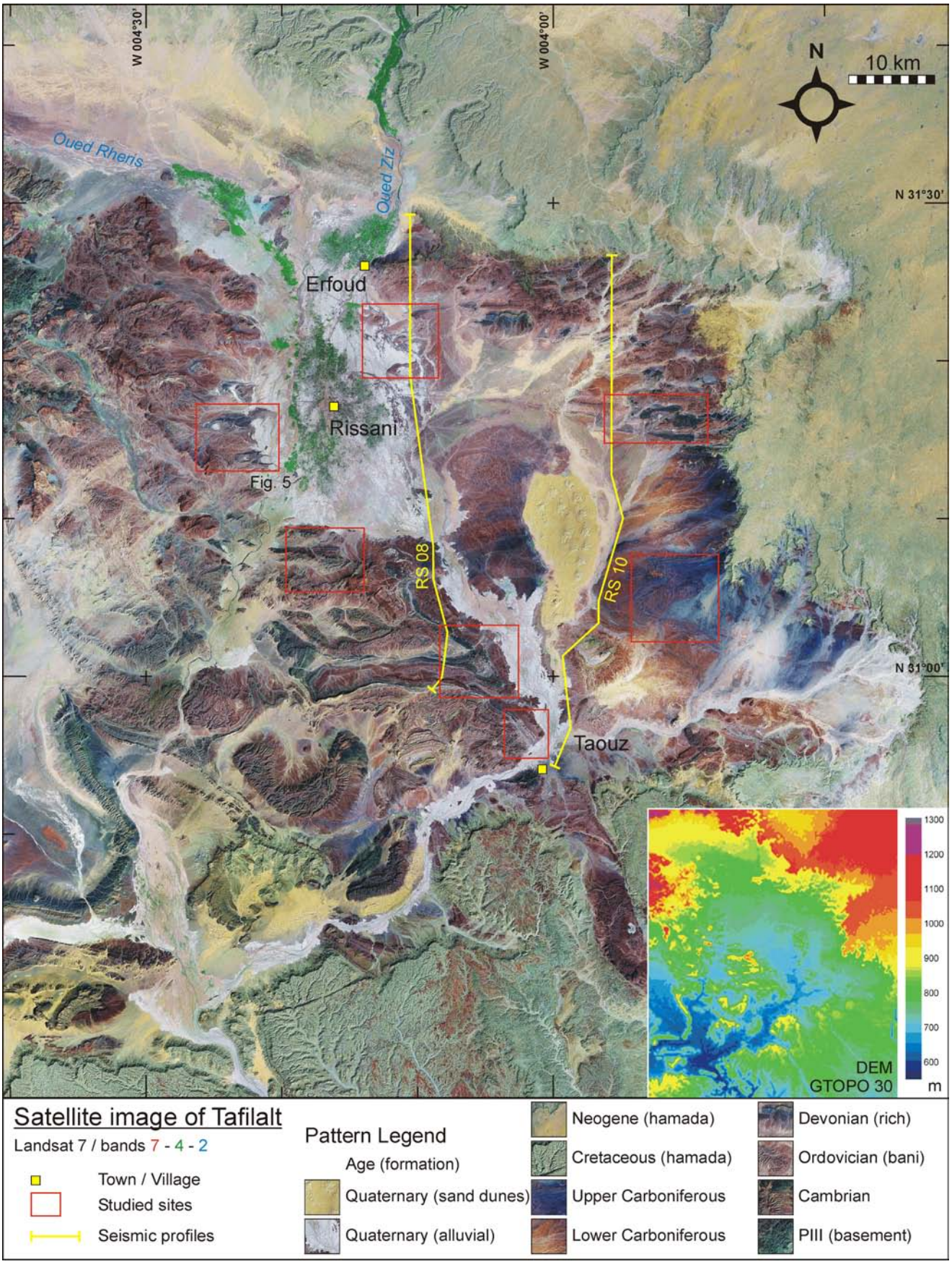

Fig. 2. Tafilalt area, eastern end of Anti-Atlas belt, viewed from Landsat 7 (NASA, 2005), false colours (downloaded from : https://zulu.ssc.nasa.gov/mrsid/). Image description: The Tafilalt Flood plain (shown by the green Palm Tree culture around Rissani and Erfoud), the Oued Ziz and Oued Rheris (oued : sporadic river) are flooding from the High-Atlas and get dry to the South, in the center of the view the Erg Chebbi sand dunes. In light green, the Neogene and Cretaceous Hamada seals the Anti-Atlas which appears as a half-window. The folded and faulted Paleozoic cover is underlined by the competent layers such as the Devonian Rich in blue, the Ordovician Bani in reddish-orange and the Cambrian sandstones in dark brown. The structural basement does not crop out in the Tafilalt region. Except some tiny outcrops in the north-east edge of half-window, it appears on the left side of the view, at latitude of Erfoud, in dark green and belongs to the Ougnat inlier.

It was last consolidated during the Panafrican orogeny. Exposed further west in the Bou Azzer inlier, the Major Anti-Atlas Suture or Anti-Atlas Major Fault (AAMF) (named "Accident Majeur") was interpreted as the old border of the african shield (Choubert and Faure-Muret, 1971). Recent workers, however, considered it as part of the "metacratonic" evolution and the northern boundary of the WAC is now defined further north, along the South Atlas Fault (Hefferan et al., 2000, Ennih and Liégeois, 2001, 2003, Liégeois et al., 2005), coincident with a major Neogene tectonic feature, the southern deformation front of the High-Atlas chain. At the end of Proterozoic, a major unconformity is interpreted as the onset of a new rifting cycle (of the Paleozoic era). The successive openings of Rheic and Paleotethys oceans (Stampfli and Borel, 2002) along the NW border of the WAC must have left their imprint in the area of the future Anti-Atlas belt. Rifting in this area was aborted early, but it is structurally very important since lead to the preconfiguration of blocks which were inverted during the Variscan orogeny. Syn-rift sediments of the P II-III unit are mainly volcaniclastics, but the thickness of this unit is very thin in the Tafilalt compared to the western Anti-Atlas. Traditionally, from a structural point of view, the basement englobes the crystalline basement and the P II-III unit.

Paleozoic cover

Throughout the Paleozoic, the Anti-Atlas "basin" is dominated by shallow marine conditions. In the western part the series reaches 12 km thickness, while in the Tafilalt it is only about 6 km thick. The major part of the Paleozoic sediments are made of fine grained detrial shales, siltstones and mudstones (Fig. 3). Competent marker beds are subordinate in abundance and thickness, and distributed among the series. These relatively thin competent beds appear morphologically as cuestas and some of these crests can be followed throughout the Anti-Atlas range. The local name of each crest has given the name to the formations (Ordovician Jebel Bani, Devonian Jebel Rich, Carboniferous Jebel Ouarkziz). These formation names are not formally accepted lithostratigraphic terms but they are very useful, widely known and applied by all the workers in the region.

In the studied area, the whole Adoudounian series (local formation name for Cambrian from Basal Conglomerates to Upper Limestones) is lacking from the stratigraphy of the Tafilalt. Above some thin basal conglomerates, the first competent layers to appear are the Cambrian Green Sandstones. The Ordovician 1st Bani is very thin compared to the Zagora region and the major Ordovician cuestas, creating the topographic heights in the Tafilalt, can be linked to the 2nd Bani, mostly made of quartzites and sandstones. The Silurian shales are very weak and outcrops are exceedingly rare. They are responsible for large valleys inbetween the two cuestas of the 2nd Bani and the Devonian Richs. However, a single limestone marker bed in the middle of the Silurian shales is well known for its echinoderms and some graptolithes at its base. This bed can be seen as the first member of a carbonate series that follows in the Devonian, in contrast to the first half of the Paleozoic series which is mainly detrial. The Devonian series is dominated by fossiliferous blueish dark carbonates. To the delight of the Filallis (Tafilalt inhabitants), slabs and handicrafts from this area are exported worldwide. The Upper Devonian is marked by a return to detrital sedimentation that dominates throughout the Carboniferous where marker beds are fluvial and/or deltaic sandstones in contrast to the carbonates found further west.

The structural style of the cover is dictated by two key-parameters, namely: the total thickness and the incompetent / competent ratio.

2.3. Variscan orogeny

The closure of Paleotethys leads to the collision of Gondwana and Laurussia to form the supercontinent Pangea. The former normal faults are reactivated and inverted. Because of its particular incompetent rheology, the Paleozoic cover folds. For this reason, the deformation is characterised by a gradient rather than by a major thrust-front. The timing of the inversion in the Anti-Atlas is hard to constrain since the oldest formation sealing the deformed Carboniferous sediments is of Upper Cretaceous age. Dolerites dykes and sills postdate the Variscan folding and occur between 206 and 195 Ma (Sebai et al., 1991) . However deformation can be estimated to late Carboniferous between 320 and 300 Ma according to the new paleoreconstructions of Stampfli and Borel (2002).

2.4. Post Variscan

The next Wilson cycle begins with tholeitic magmatism at the end of Triassic, which is the

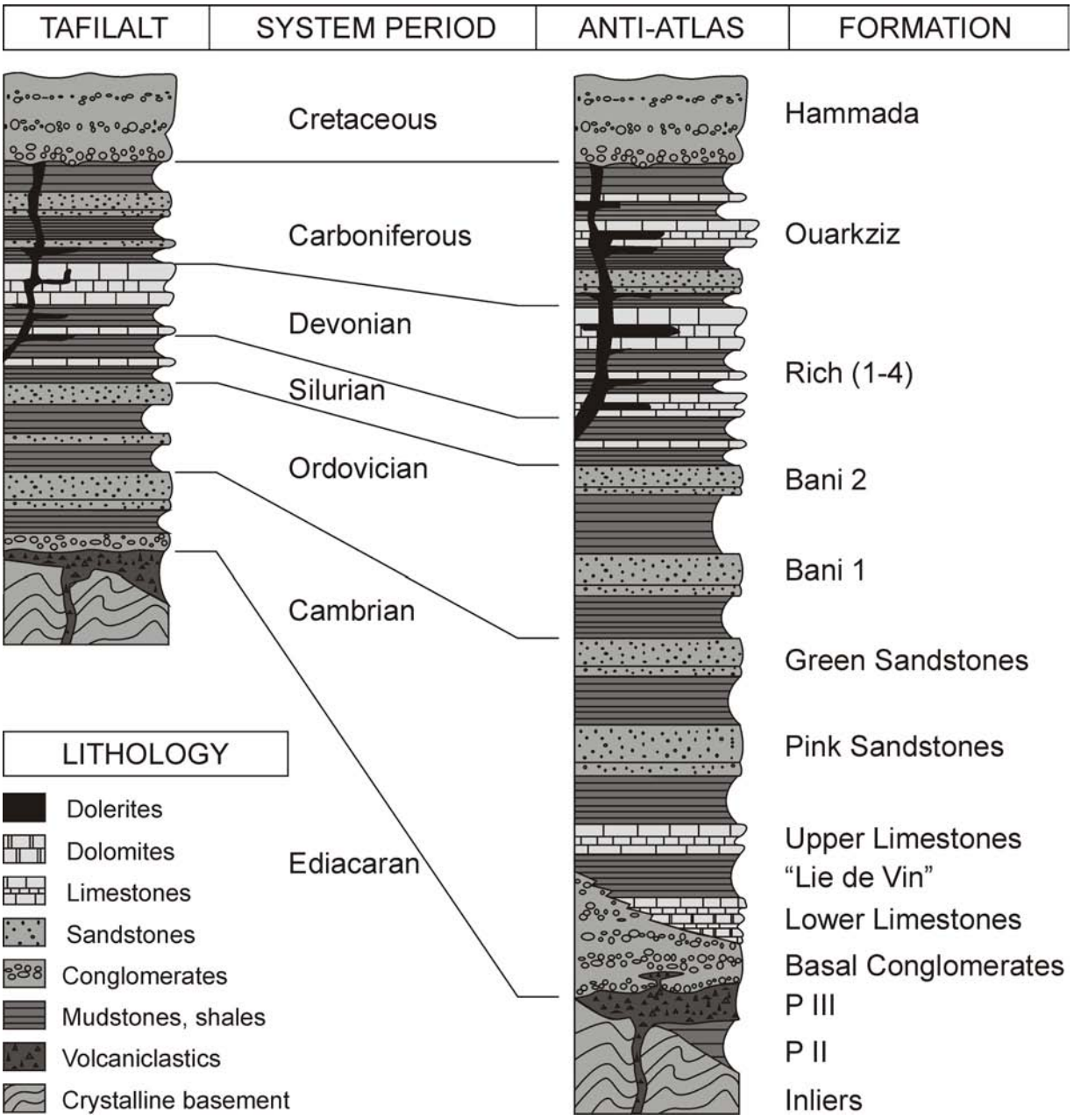

Fig. 3. Schematic lithostratigraphic logs for the Tafilalt area and the whole Anti-Atlas (modified from Soulaimani, 1997 and augmented from Tafilalt geologic map, Fetah et al., 1986). The whole series (to the end of Paleozoic) reaches 12 km in the western Anti-Atlas but is decreasing eastward to about 6 km in the Tafilalt area. Some series are reduced but others, like the infra-Cambrian Adoudounian (from Basal Conglomerates to Upper Limestones) and the Early Cambrian, are lacking. Note that the real incompetent / competent layers ratio is more important than the sketch suggests.

precursory event to the opening of the Central Atlantic ocean. The new "Mesozoic High-Atlas basin" opens just north of eastern Anti-Atlas. This extension affects the Anti-Atlas by the intrusions of dolerite dykes and sills and by normal faulting. This normal faulting corresponds to a third re-activation of faults inherited from the late Proterozoic (Piqué and Laville, 1996) (post-tectonic intrusion of dykes between 206 and 195 Ma (Sebai et al., 1991)). The Anti-Atlas Major Fault is essentially Precambrian, but must be reactivated in the Mesozoic since it produces the graben from Zagora to Taouz in the Paleozoic sedimentary cover. No Permian to Jurassic sediments are found in the Anti-Atlas. The structural basement of the High-Atlas is of Paleozoic age. It is mostly covered by a thick deformed Mesozoic series but must include Variscan deformations. So the northern part of the eastern Anti-Atlas is hidden under the High-Atlas.

The actual high topography of the Anti-Atlas (up to 2500 m) does not result from the Variscan orogeny alone. The Cretaceous and Neogene hamada east and south of Tafilalt is clearly tilted to the South and in the north of Tafilalt the Cretaceous hamada is tilted to the North-East (see Fig. 2, on the DEM

and the river patterns on the Landsat view). The scarp retreat analysis of Schmidt (1992) indicates a beginning of uplift in late Eocene times with an increase in late Miocene / early Pliocene times. These geomorphological interpretations fit nicely with structural observations in the High-Atlas and with an analysis of the deformation of Neogene sediments (Görler et al., 1988). The deformations of the High-Atlas during Eocene – Oligocene and mainly Pliocene – Pleistocene epochs (Frizon de Lamotte et al., 2000, Ellouz et al., 2003) just a few kilometres north, affects also the adjacent strongly compartmentalized Anti-Atlas basement. This rejuvenated relief could come partly from a Neogene thermal uplift (Anguita and Hernan, 2000, Saddiqi et al., 2005, Teixell et al., 2005).

3. Field data

3.1. Small scale structures

The dominant structures in the study area are apparently regular cuestas. On closer inspection, however, internal imbrications and small scale folds such as those shown in Fig. 4 are quite common. These folds and thrusts are highly localised. The spacing is on the order of 500 to 1000 m, with virtually undeformed regular intervals inbetween. Structural perturbations are not only laterally localised but seem to be confined to competent horizons within the stratigraphy. Below and above a folded or thrust competent layer, the next immediate competent layers may well be unaffected. In terms of structural style, folding and thrusting occurs within the competent bed which may be folded in one place and thrust in an other locality. Folds in competent layers are parallel class 1B folds and class 3 for the weak interbeds, resulting in a characteristic chevron fold pattern (Ramsay and Huber, 1987). Bedding parallel slickenside surfaces can be found in folded competent layers indicating flexural slip.

Thrust faults are very localised both laterally and vertically within the stratigraphy. The identification of contractional faults is limited to thick competent layers; but wherever observed, thrusts seem to be rapidly attenuated within adjacent incompetent layers. In the right picture of Fig. 4, the competent layers are seen to be duplicate by a thrust while the weaker beds above (hammer) are just folded. This example demonstrates that in absence of competent marker beds, the layer parallel shortening is hard to constrain.

In contrast to the apparent ENE-WSW global trend of the Anti-Atlas (Fig. 1), small scale structures show a clear NW-SE trend as shown on the stereogramms of Fig. 4. Note that the apparent dip of the fold axes to the south-east is

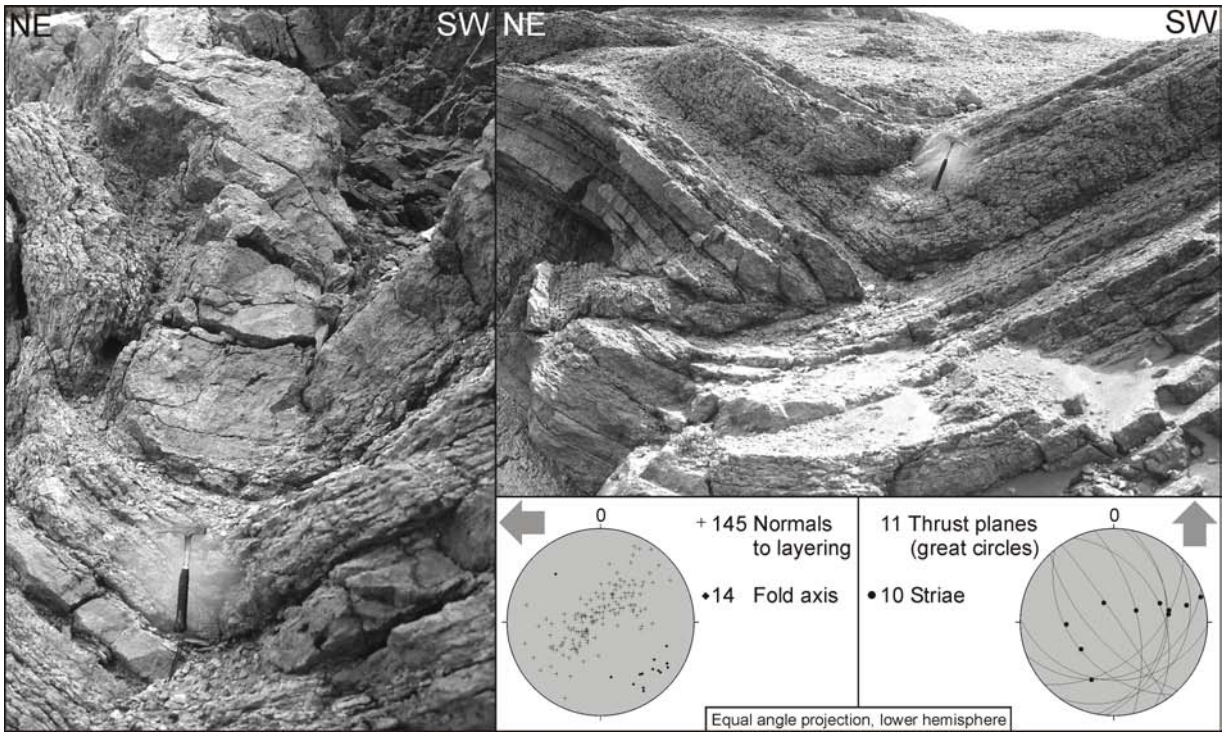

Fig. 4. Small scale structures in the cliff of Jebel Amelane (in the North-East of fig. 5). Left picture: folds in the Middle Devonian; Left stereogramm : poles of bedding planes in folds and folds axes for Jebel Amelane region; Right picture : thrust fault and layer parallel shortening; Right stereogramm : great circles of thrust-planes and striae for Jebel Amelane region.

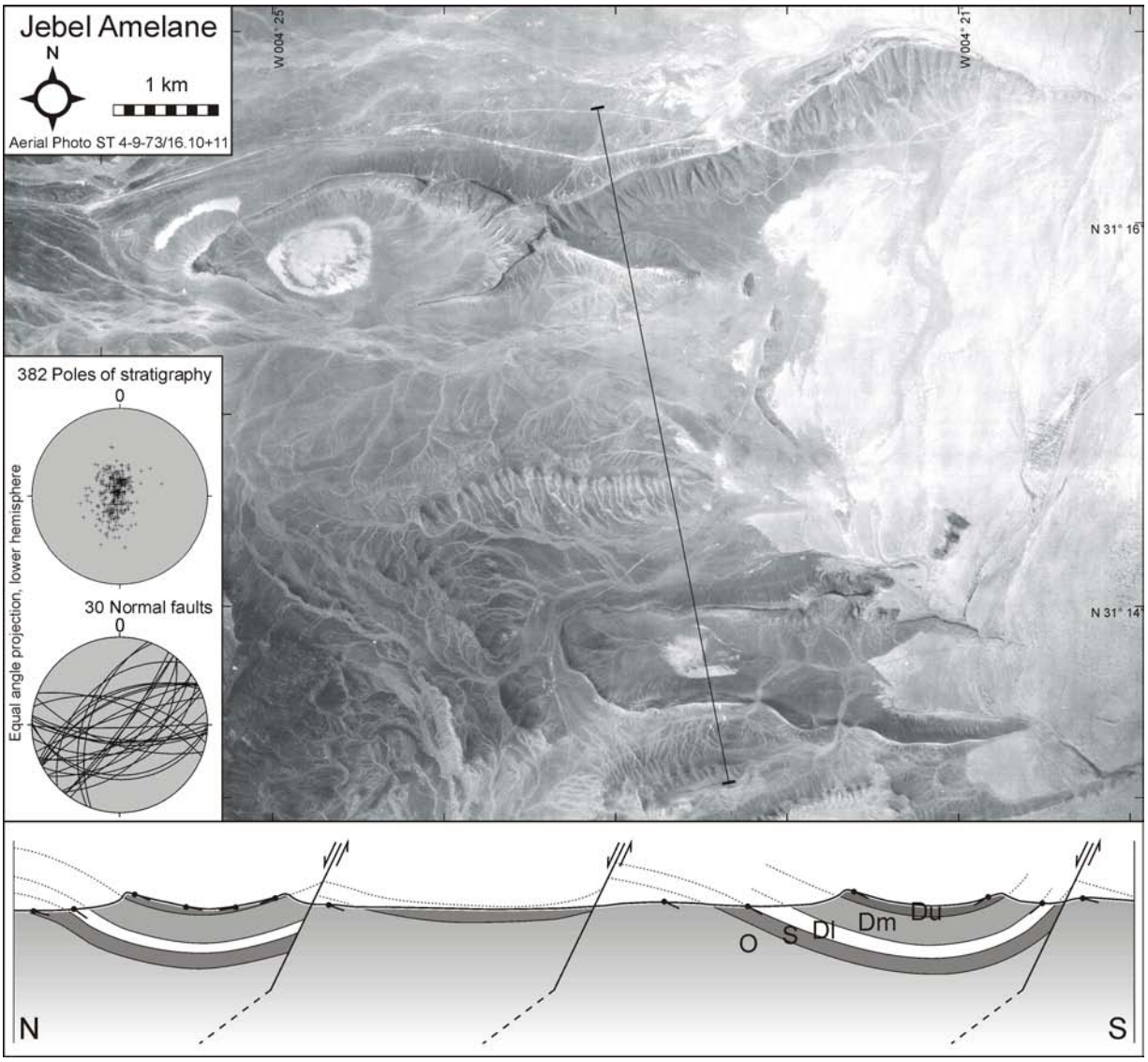

Fig. 5. Aerial mosaic view of Jebel Amelane / Jebel Mech Idrane (Service Topographique du Maroc), 10 km west of Rissani (see Fig. 2 for location); Stereogramms of bedding planes and normal faults; Cross-section.

due to the fact that a large majority of the small-scale structures has been observed on south-verging cuestas (hanging wall syncline). Tilting those limbs back to horizontal also restores the fold axes to a sub-horizontal attitude. This is a strong argument for these small-scale structures to be older then the hanging wall synclines. This applies to the entire Tafilalt area, which has been affected by a NE-SW compression throughout. This NE-SW compression direction contrasts with the overall Anti-Atlas trend, but it fits nicely with the structural trend of the Ougarta chain to the South-East.

3.2. Hanging wall synclines

The synclines shown in Fig.5 have often been mistaken as Variscan folds. Strike and dip measurements of these meso-scale structures do not fit with the results obtained from the small-scale folds and thrusts discussed above. Synclines are typically some 5 km long, 2 km wide (half wave-length) and are gently plunging to either eastward or westward. Their repetition on a north-south axis is quite intriguing (especially west of Rissani, Fig. 2). These synclinal structures are well developed only within the northern half of Tafilalt, mainly because their surface expression is related to the underlying Devonian carbonate beds of the Rich (see the three northern red squares of Fig. 2). In other words, the synclines owe their existence to a particular mechanical stratigraphy rather then a geographically distinct part of the Tafilalt basin. The same extension is expressed in a different way. Ordovician and Cambrian sandstones and quartzites are too thick and too competent for such gentle fold structures to develop. Silurian and Carboniferous shales, in the other hand, are too incompetent. Hanging wall synclines appear discreetly within Carboniferous sandstones (red square south-east of the sand

dunes on Fig. 2). In fact they are extensional fault-related folds.

A detailed study of the Jebel Amelane region revealed a bimodal distribution of the bedding plane orientations (see stereogramm of the bedding poles, Fig. 5). This is interpreted to be a result of kinked or "trisheared" layers on a normal fault as described in the northwestern Red Sea (Khalil and McClay, 2002). The fact that the synclinal axes are plunging to the east, is explained by the super-structure. The Jebel Amelane is located on the eastern flank of a huge anticlinorium. The most important evidence for extensional fault-related folding is stratigraphic, however. Minor normal faults do appear but the major fault zones are mostly obscured by a thick soft interval of Silurian shales. Major fault zones can be directly observed only where the slip places more competent layers side by side as for instance at the Jebel Bou Ifarherioun (red square, 15 km south of Rissani on Fig. 2). The dip of the faults seems to vary according to the competence, flat in incompetent, steep in competent layers. The localisation and repetition of these faults is interpreted as due to pre-existing faults in the basement. Hanging wall synclines show flexural-slip movement along bedding plane surfaces, which can be misleading since the relative shear sense of such layer parallel slip is always indicting "thrusting" independent of the underlying mechanism of folding in either compression and/or extension. These extensional fault-related folds postdate the small scale folds by folding their axis.

3.3. Superstructures

The eastern Anti-Atlas shows interference of two superimposed superstructures. First, the ENE-WSW anticlinorium trend of the entire Anti-Atlas belt is materialized by the large scale shape of basement inliers (Fig. 1). The Hamada half-window apparently sealed to by Upper Cretaceous sediments to the east, inherited this ENE-WSW trend (Fig. 1 and 2). In fact the large scale Anti-Atlas superstructure appears more like a huge monocline. From NNW to SSE rocks get increasingly younger, from basement inliers, across the folded Paleozoic cover, gradually passing into the flat lying basin fill of the Tindouf basin, partly covered by younger sediments of the Hamada. The northern limit of this superstructure is defined by the thrust front of the inverted Mesozoic sediments of the High-Atlas. The contribution of High-Atlas inversion and the thermal uplift in the exaggeration of this general large scale Anti-Atlas trend is difficult to quantify (Helg et al., 2004). Secondly, the Tafilalt region is clearly affected by folding along Ougartian NW-SE trend. This trend is materialized by the global antiform axis linking the Ougnat inlier to Taouz, separating the synforms of Tafilalt and Mader, and disappearing under the Hamada (Fig. 2). This large scale orientation is identical with the one measured in small scale structures found in the entire Tafilalt (3.1.).

While these two orientations are clearly distinguished in terms of their geometry and interference patterns, the relative chronology remains open to debate. In the Tafilalt, both structural trends are of similar, weak overall shortening intensity (estimated to ca. 10%) and intuitively either structure could be first or second. Further west, however clear evidence is found for a relative chronology between folds of the Anti-Atlas trend preceding the Ougartian trend (Caritg et al., 2004). Our own, unpublished observations in the Tata area have since provided additional strong evidence for such a relative chronology.

On the other hand rather than separate these two deformations in time, an alternative explanation could be found in the shape of the WAC boundary. The eastern Anti-Atlas is located along the northern edge of the WAC metacraton. It is limited by the South Atlas Fault (ENE-WSW) to the North and by the Saoura gravimetric anomaly (NW-SE) (Ennih and Liégeois, 2001) to the East. On the very large scale, the arc defined by the Ougarta – Anti-Atlas system thus seems to be an inherited feature, mimicking the shape of the WAC. The late Paleozoic fold belts would have been formed along the boundaries of this craton, specifically along its metacratonic borders which were once again re-mobilized in inversion tectonics during the assembly of Pangea.

4. Seismic data

The ONAREP RS8 seismic reflexion line (Fig. 6) crosses the Tafilalt with a north-south orientation (see location on fig. 2). Accordingly, this line is perpendicular to extensional folding and oblique with respect to both superstructures : WSW-ENE in the northern part and NW-SE in the southern part. The interpretation of this profile has been

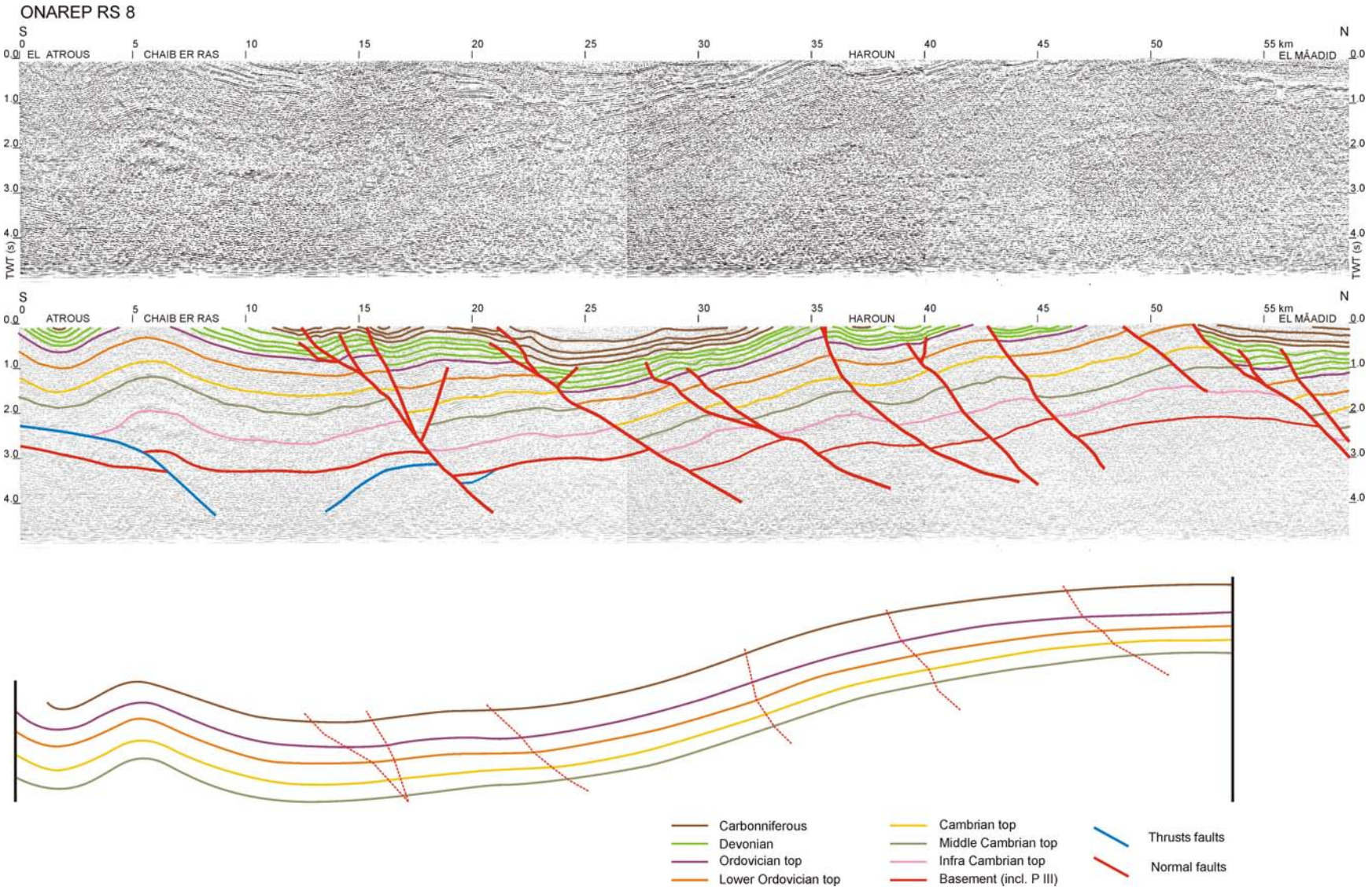

Fig. 6. Seismic line RS 8 (from ONAREP). Upper : blank; Middle : Surface from field work and geological map, interpreted at depth; Lower : reconstructed profile before normal faulting.

tied with the known surface geology, including dip measurements and inspired by our knowledge of local tectonics.

The first 10 kilometres (southern part) display large scale folds with NW-SE axes. We interpret these folds to be detached along a major décollement at the base of the Paleozoic sedimentary pile. Cover shortening is compensated below the décollement by inversion of former late Proterozoic normal faults. The resulting folding structure fits well with an Ougarta trend observed on the map scale.

The structural style remaining (northern) part of the transect (from km 10 to 60) is dominated by late normal faults. A series of pseudo-basins, e.g. one at km 25, have previously been interpreted as a syn-sedimentary "thrust top" basin. In their interpretation, an important early Variscan folding phase affected the region in Upper Devonian through early Carboniferous times, obscured by middle Carboniferous – post folding series. Such an interpretation is in conflict with field observations, and no positive evidence for a late Devonian folding phase has ever been found anywhere in the Anti-Atlas area. Our interpretation of the "pseudo-basins" seen in the seismic line is an extensional context. The geometry observed is explained as a consequence of a particularly weak cover and a seismic artefact. First, the thinning of the footwall layers and the thickening of the hanging wall layers is observed in many models specially for "ultraweak cover on rigid basement" (Finch, 2004). The image obtained by discrete-element modelling is very similar to this seismic line. Secondly, the seismic line shows the Two Ways Time and not the depth. The velocity of Carboniferous shales and mudstones must be particularly slow (probably less than under 2000 m/s), while competent layers (Devonian limestones, quartzites) may attain 3000 m/s or more. This relationship leads to a pronounced velocity pull down, which tends to exaggerate the depth of the pseudo basins.

The third part of Figure 6 is the presumed profile, restored to illustrate the situation at the paroxysm of the Variscan deformation, i.e. without the later normal faults. The overall shortening is minimum of 10 %, but this value is measured at regional scale and does not include the layer-parallel shortening observed at smaller scale. Helg et al. (2004) argue that such distributed small scale deformation add a substantial amount of shortening of similar magnitude.

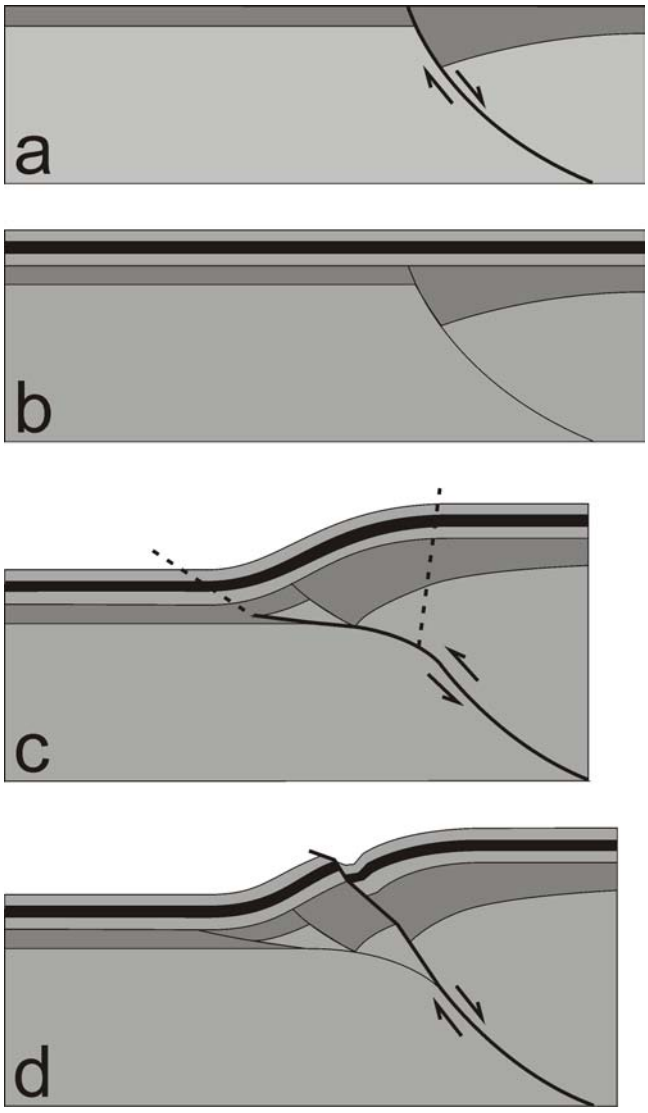

Fig. 7. Schematic illustration of the proposed kinematical model (inspired from Bump, 2003). South-North orientation perpendicular to inliers alignment. But parallel to the Ougartian trend. a: Late Proterozoic rifting with syn-rift sediments; b: Deposition of Paleozoic cover; c: Variscan inversion. The thrust fault takes a shortcut in the basement, the cover reacts in a trishear mode. The Ougartian trend do not appears on this sketch; d: New extension phase (Atlantic opening). Normal faults short cut the Paleozoic cover, its dips vary according to the competence of rocks and produce hanging wall synclines.

5. Conclusions

The eastern Anti-Atlas structure is a complex interference between two trends of Variscan folding which lead to an egg box pattern of basins and domes. This fold interference pattern is subsenquently cut by a series of normal faults most likely in response to the opening of the Atlantic in Liassic times. The ENE-WSW Anti-Atlas global trend is the best developed in terms of deformation and inversion. The Anti-Atlas is clearly thick skin. The Paleozoic cover reacts

in a “trishear way” (Fig. 7.c) to accommodate basement shortening which is inverting former late Proterozoic normal faults. The deformation gradient decreases strongly from NNW to SSE, with increasing distance from basement inliers. The NW-SE Ougarta trend is materialized throughout the Tafilalt by small scale folds and thrust faults. This deformation has a important thin skin component, detachment along weak layers; although the underlying cause is equally thick skin basement inversion. The interference between these two trends is thought to be due to the shape of the northern corner of the WAC, and particularly a renewed re-mobilisation of its ”weak” meta-cratonic borders in the late Paleozoic times. Former normal and inverted faults are again reactivated during the Atlantic opening event. This leads to the formation of new steep normal faults within the Paleozoic cover series. The overall weakness of the thick Paleozoic series favours the formation of extensional “drape” folding (Fig 7.d). The High-Atlas inversion and Neogene thermal uplift do not significatively deform the eastern Anti-Atlas. Only a light doming is underlined by the radial tilt and retreat of cretaceous cuestas.

Acknowledgments

Ongoing support by the “Ministère de l’Industrie et des Mines, Direction de la géologie” by M. Dahmani and M. Haddane and the moroccan national petroleum agency ONAREP is gratefully acknowledged. Financial support by Swiss National Science Foundation grants N° 21-52516.97 / 20-63790.00 and by the “Fonds Matthey-Dupraz” local fund for geology students.

References

Anguita, F., Hernán, F., 2000. The Canary Island origin: a unifying model. Journal of Volcanology and Geothermal Research 103, 1-26.

Bump, A.P., 2003. Reactivation, trishear modeling, and folded basement in Laramide uplifts: implications for the origins of intracontinental faults. GSA Today, 4-10.

Caritg, S., Burkhard, M., Ducommun, R., Helg, U., Kopp, L., Sue, C., 2004. Fold interference patterns in the Late Palaeozoic Anti-Atlas belt of Morocco. Terra Nova 16, 27-37.

Choubert, G., Faure-Muret, A., 1971. Epoque hercynienne. In: Tectonique de l’Afrique, Sciences de la Terre, Paris, 6, UNESCO, Paris, France, 353-371.

Ellouz, N., Patriat, M., Gaulier, J.-M., Bouatmani, R., Sabounji, S., 2003. From rifting to Alpine inversion: Mesozoic and Cenozoic subsidence history of some Moroccan basins. Sedimentary Geology 156, 185-212.

Ennih, N., Liégeois, J.-P., 2001. The Moroccan Anti-Atlas: the West African craton passive margin with limited Pan-African activity. Implications for the northern limit of the craton. Precambrian Research 112, 289-302.

Ennih, N., Liégeois, J.-P., 2003. Discussion, The Moroccan Anti-Atlas: the West African craton passive margin with limited Pan-African activity. Implications for the northern limit of the craton: reply to comments by E.H. Bouougri. Precambrian Research 120, 185-189.

Erslev, E.A., 1991. Trishear fault-propagation folding. Geology 19, 617-620.

Fetah, M., Bensaïd, M., Dahmani, M., 1986. Carte géologique du Maroc 1:200’000 Tafilalt-Taouz, Notes et Mémoires du Service Géologique du Maroc N°244.

Finch, E., Hardy, S., Gawthorpe, R., 2004. Discrete-element modelling of extensional fault-propagation folding above rigid basement fault blocks. Basin research 16, 489-506.

Frizon de Lamotte, D., Saint Bezar, B., Bracène, R., Mercier, E., 2000. The two main steps of the Atlas building and geodynamics of western Mediterranean. Tectonics 19 (4), 740-761.

Görler, K., Helmdach, F.-F., Gaemers, P., Heissig, K., Hinsch, W., Mädler, K., Schwarzhans, W., Zucht, M., 1988. The uplift of the central High Atlas as deduced from Neogene continental sediments of the Ouarzazate province, Morocco. In: V.H. Jacobshagen, Springer-Verlag (Ed.), The Atlas System of Morocco. Lecture Notes Earth Sci. 15, 361-404.

Haddoum H., Guiraud, R., Moussine-Pouchkine, A., 2001. Hercynian compressional deformations of the Ahnet-Mouydir Basin, Algerian Saharan Platform: far-field stress effects of the Late Palaeozoic orogeny. Terra Nova 13, 220-226.

Hefferan, K.P., Admou, H., Karson, J.A., Saquaque, A., 2000. Anti-Atlas (Morocco) role in Neoproterozoic Western Gondwana reconstruction. Precambrian Research 103, 89-96.

Helg, U., Burkhard, M., Caritg, S., Robert-Charrue, C., 2004. Folding and inversion tectonics in the Anti-Atlas of Morocco. Tectonics 23, TC4006, doi:10.1029/2003TC001576.

Khalil, S.M., McClay, K.R., 2002. Extensional fault-related folding, northwestern Red sea, Egypt. Journal of Structural Geology 24, 743-762.

Liégeois, J.-P., Fekkak, A., Bruguier, O., Errami, E., Ennih, N., 2005. Lower ediacaran age (630-610 Ma) for the Sarhro group. Implications for the metacratonic evolution of the Anti-Atlas, correlations with the Tuareg shield and the evolution of the pan-african orogeny in the NW Africa. 4ème Colloque International 3Ma, Agadir 2005, Abstract Volume, 2.

NASA and Earth Satellite Corporation, Landsat 7 images download website (https://zulu.ssc.nasa.gov/mrsid/), last visited 14.03.2006.

ONAREP (Office National de Recherches et d’Exploitations Pétrolières) Morocco. Seismic reflexion line RS 8.

Piqué, A., Laville, E., 1996. The central atlantic rifting : reactivation of Palaeozoic structures ?. J. Geodynamics 21 (3), 235-255.

Piqué, A., Bouabdelli, M., Soulaïmani, A., Youbi, N., Iliani, M., 1999. Les conglomerates du P III (Néoprotérozoïque supérieur) de l'Anti-Atlas (Sud du Maroc): molasses panafricaines, ou marqueurs d'un rifting fini-protérozoïque ?. C. R. Acad. Sci. Paris, Sciences de la Terre et des planètes 328, 409-414.

Piqué, A., 2003. Perspective, Evidence for an important extensional event during the latest Proterozoic and Earliest Paleozoic in Morocco. C. R. Geoscience 335, 865-868.

Ramsay, J.G., Huber, M.I., 1987. The techniques of modern structural geology, vol. 2: Folds and Fractures, Academic Press Ltd. London, pp. 462.

Saddiqi, O., Ziad, N., Missenard, Y., Frizon De Lamotte, D., Goffe, B., Leturmy, P., El Mamoun, R., Sebti, S., Poupeau, G., 2005. Age Miocène moyen supérieur du soulèvement thermique du Haut-Atlas Central : apport des traces de fission sur apatite. 4ème Colloque International 3Ma, Agadir 2005, Abstract Volume, 45.

Schmidt, K.-H., 1992. The tectonic history of the Pre-Saharan depression (Morocco) – a geomorphological interpretation. Geologische Rundschau 81 (1), 211-219.

Sebai, A., Feraud, G., Bertrand, H., Hanes, J., 1991. $^{40}Ar/^{39}Ar$ dating and geochemistry of tholeiitic magmatism related to the early opening of the central Atlantic rift. Earth and Planetary Science Letters 104, 455-472.

Service Topographique du Maroc, Aerial Photography, ST 1/40000, Mission 4-9-73, N° 16_10 / 16_11.

Soulaïmani, A., Le Corre, C., Farazdaq, R., 1997. Déformation hercynienne et relation socle/couverture dans le domaine du Bas-Drâa (Anti-Atlas occidental, Maroc). Journal of African Earth Sciences 24 (3), 271-284.

Soulaïmani, A., Piqué, A., Bouabdelli, M., 2001. La série du PII-III de l'Anti-Atlas occidental (Sud marocain) : un olistostrome à la base de la couverture post-panafricaine (PIII) du Protérozoïque supérieur. C.R. Acad. Sci. Paris, Sciences de la Terre et des planètes 332, 121-127.

Stampfli, G.M., Borel, G.D., 2002. A plate tectonic model for the Paleozoic and Mesozoic constrained by dynamic plate boundaries and restored synthetic oceanic isochrones, Earth Planet. Sci. Lett. 196, 17-33.

Teixell, A., Ayarza, P., Zeyen, H., Fernandez, M., Arboleya, M.-L., 2005). Effects of mantle upwelling in a compressional setting: the Atlas Mountains of Morocco. Terra Nova 17, 456-461.

Inversion tectonics in the eastern Anti-Atlas of Morocco

Charles Robert-Charrue, Martin Burkhard*
Institut de Géologie et d'Hydrogéologie, Université de Neuchâtel,
11, rue Emile-Argand, CH-2009 Neuchâtel, Switzerland
*Corresponding author. Tel. : +41 32 718 26 52 ; fax : +41 32 7182601.
E-mail address : martin.burkhard@unine.ch

ACKNOWLEDGMENTS

Ongoing support by the "Ministère de l'Industrie et des Mines, Direction de la géologie" by M. Dahmani and M. Haddane are gratefully acknowledged. Financial support by Swiss National Foundation grants N° 21-52516.97 / 20-63790.00.

ABSTRACT

Ten cross sections drawn from field mapping data, existing geological maps and landsat views characterize the structure of the eastern Anti-Atlas fold belt with its ENE-WSW structural grain. One of these cross sections (no. 08) is sequentially restored and used to perform depth to detachment calculations. Late, i.e. Early Mesozoic extensional structures are rooted at a mid-crustal depth of detachment of -18 to -20 km (-11 to -12 mi). We propose a novel method of integrating bed internal, layer parallel shortening deformations into depth to detachment calculations. Balancing late Variscan compressional structures of the eastern Anti-Atlas requires a substantial amount of 11 to 17 % of layer-parallel shortening within the Paleozoic cover in an early stage of the Variscan orogeny. The structural style of the Anti-Atlas is dictated by the reactivation of pre-existing structures within the basement and a predominantly weak mechanical stratigraphy of the overlying Paleozoic cover rocks. The variscan event is best described as the inversion of an intracratonic basin, rather than a classical foreland fold-and-thrust belt.

INTRODUCTION

The aim of this study is to elucidate the structure of the Eastern Anti-Atlas belt and to understand the structural style and its primary controls which govern the deformation. A specific look at the depth to detachment is used to propose a large scale model of the tectonic evolution of this chain through time. Detailed field mapping and structural analyses lead us to new a interpretation for what was for a long time considered as a fold and thrust belt. Actually, the absence of *décollement* or thrust at the basement-cover contact is one of the particularities of the Anti-Atlas fold belt.

The Paleozoic Anti-Atlas fold belt of southern Morocco is located at the northern rim of the West African Craton. Northward, the Anti-Atlas is juxtaposed against the Cenozoic High Atlas mountains along the so called South Atlas Fault (Figure 1). Southward, the Anti-Atlas forms the northern border of the Tindouf basin, filled with the same Paleozoic series, but not involved in Variscan orogeny. The Anti-Atlas appears as a huge antiform punctuated by a series of basement inliers along a general a ENE-WSW axis (Figure 1). Southeastward, the Anti-Atlas belt is connected by the NW-SE oriented Algerian “aulacogenic” Ougarta chain. In the study area the two chains intersect, leading to some intricate large scale interference pattern. The Anti-Atlas WSW-ENE trend is dominant, however, and in this paper, the subordinate Ougartan NW-SE trend will not be considered.

Figure 2 shows a Landsat scene of the Eastern Anti-Atlas. Modern false color satellite images in these arid regions compete with geologic maps in detail and accuracy. The tracks of cross sections have been chosen at a high angle to the structural grain defined by the large basement inliers cropping out along the northern border of the chain.

ANIT-ATLAS THROUGH TIME

Basement of the Anti-Atlas chain belongs to the West African Craton (WAC). Core parts of this craton consist in granites and high grade metamorphic rocks of the so-called

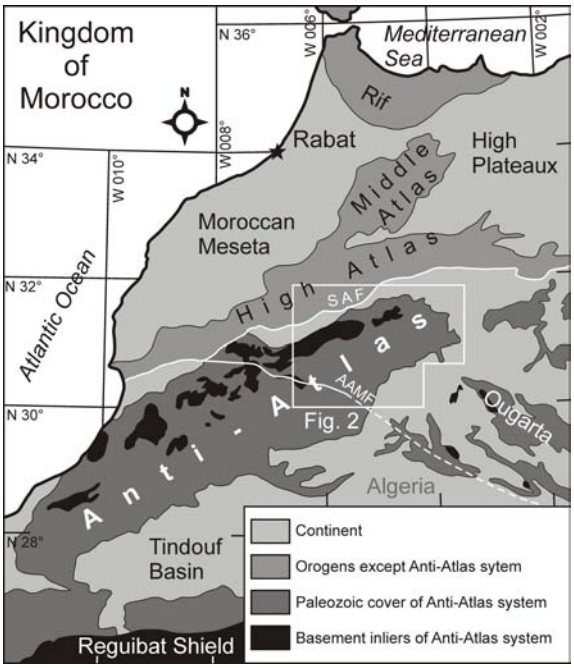

Figure 1. Situation of The Anti-Atlas.

Eburnean, 2 Ga orogeny. The final assembly and consolidation took place during the Panafrican event from 650 to 580 Ma. The Anti-Atlas Major Fault (AAMF), running in a WNW-ESE direction across the Anti-Atlas belt, is the site of a panafrican suture zone with the accretion of an oceanic island arc and associated granite intrusions (Ennih and Liégeois, 2001; Liégeois et al., 2005). The northern limit of the West African Craton, however, is located further north still and coincides with the South Atlas fault SAF (Figure 1), a long lived feature, last re-activated in Late Neogene times (Frizon de Lamotte et al., 2000).

Late Proterozoic volcaniclastic series of the so-called P II and P III document the end of the Panafrican orogeny (Benssaou and Hamoumi, 2003) and the onset of a new Wilson cycle. Evidence for active rifting is found up to Middle Cambrian. P III series of generally less than 1 km (0.6 mi) thickness are widespread in halfgrabens and patches of ill defined orientation all along the northwestern border of the West African Craton. In contrast, Cambrian series display a well defined elliptical basin of WSW-ESE orientation with up to 4 km (2.5 mi) thickness in the Western Anti-Atlas south of Agadir (Bouda and Choubert, 1972; Benssaou and Hamoumi, 2003). Post-rift series of Middle Cambrian to Middle Carboniferous build a fairly regular layercake of shallow marine

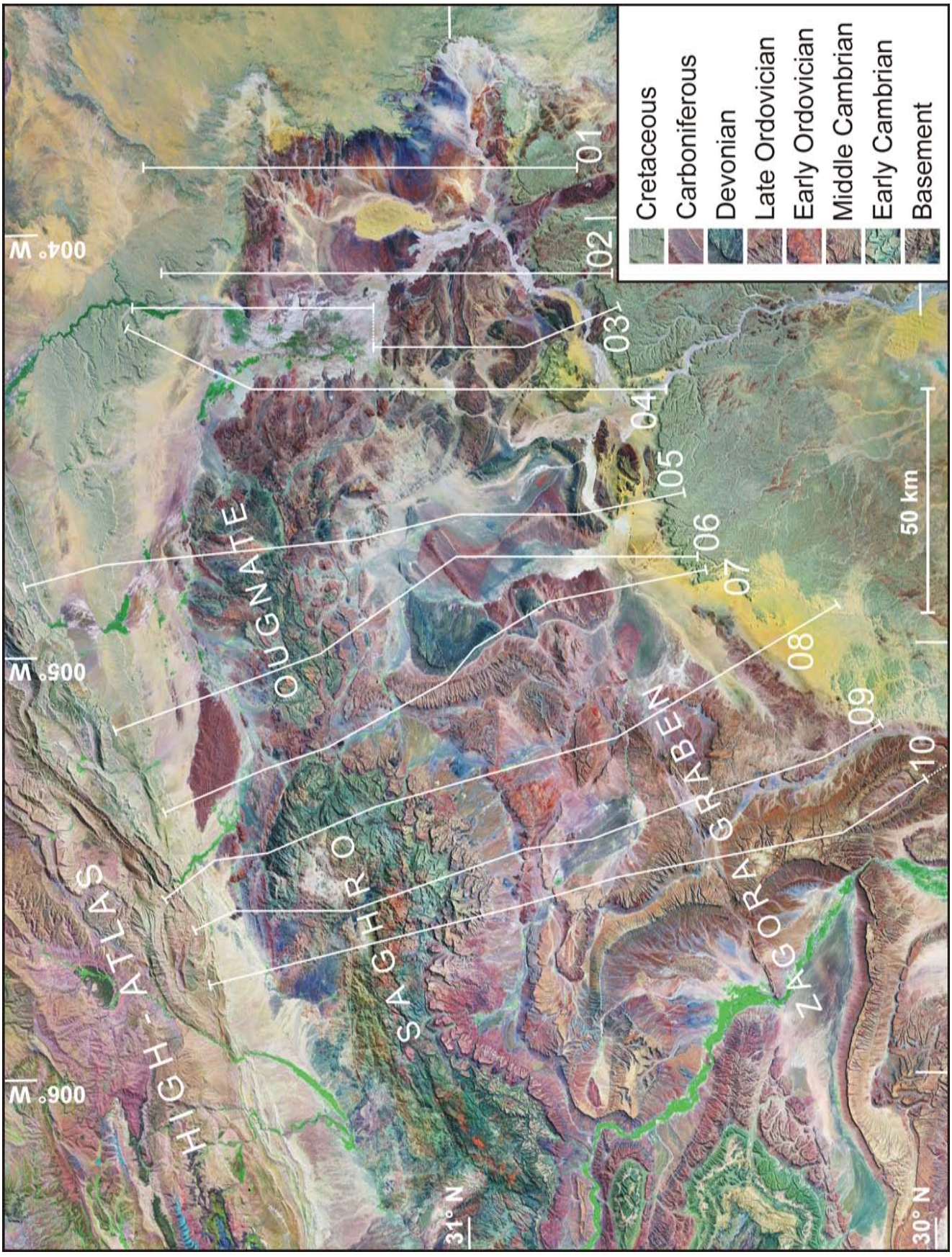

Figure 2. Landsat view of the Eastern Anti-Atlas and cross sections localization. False coulor Landsat 7 downloaded from :< https://zulu.ssc.nasa.gov/mrsid/ >.

sediments with a total thickness of 12 km (7.5 mi) in the western Anti-Atlas decreasing to less than 8 km (5 mi) in the study area, i.e. the Mader and Tafilalt. The Anti-Atlas is best described as an intracratonic basin (Burkhard et al., 2006); it can be regarded as the northern, tectonized part of the much larger Tindouf basin (Coward and Ries, 2003). The basin fill is dominated by an abundance of shales and silts deposited in a shallow marine environment (see the stratigraphic log on Figure 3). Competent and morphologically outstanding marker beds are sandstones and quartzites of the Cambrian and Ordovician. Most of the Silurian is represented by soft black shales, very rarely seen in outcrop. Carbonate plateforms dominated the Anti-Atlas sea in Lower Cambrian and again in Devonian times. The return of detrital conditions in Upper Devonian times could be interpreted as the onset of convergence in relation to Variscan tectonics. The Carboniferous is mainly made of shales and rare stiff beds are pericontinental deltaic sandstones with an abundance of flute casts figures and channel fills.

Variscan orogeny – inversion

Most if not all the Paleozoic basins of Northern Africa are involved to some degree in Variscan tectonics in Carboniferous to Permian times (Coward and Ries, 2003). The Anti-Atlas fold belt has generally be considered as a fold-and-thrust belt developed in the hinterland of the larger Appalachian – Variscan orogen. It is indeed time equivalent to and bears some structural resemblance with the Alleghenian Valley and Ridge province (Helg et al., 2004). The direct link between internal, metamorphic zones of the Variscan chain cropping out north of the South Atlas Fault and the Anti-Atlas belt remains obscure, however. No basal detachment has been observed anywhere within the Paleozoic cover series of the entire Anti-Atlas. The thick skinned involvement of the basement at very short distances behind the deformation front have been used as arguments in favour of a “basin inversion-” rather than a “frontal fold-and-thrust belt-“ deformation style of the Anti-Atlas (Burkhard et al., 2006). Anti-Atlas basin inversion is younger than middle Carboniferous as documented by the youngest sediments involved in folding and tilting along the northern border of the Tindouf basin. Anti-Atlas folds are cross-cut by the widespread Late Triassic (200 Ma) intrusions of dykes and sills (Sebai et al., 1991), in relation with Atlantic opening. The peneplained Anti-Atlas folds are sealed only by a generalized marine transgression in Upper Cretaceous times, however. Not far to the north of the Anti-Atlas, rifting in Late Triassic – Early Jurassic times lead to the opening of the High Atlas trough, filled with thick series of Triassic to Jurassic sediments (Manspeizer et al., 1978). This rifting event lead to some extensional reactivation of faults within the eastern Anti-Atlas. The major event of Cenozoic inversion responsible for uplift and folding of the High Atlas chain did not lead to any noticeable folding and/or faulting within the Anti-Atlas domain. This is documented by a smooth configuration of the basal Upper Cretaceous unconformity. The Anti-Atlas chain is standing high, however, and it has long been speculated that this renewed uplift and relief could be in response to alpine shortening deformation at a crustal scale. Alternatively, however, high present day topography in both the Anti- and High Atlas have recently been interpreted as being due to a large scale thermal anomaly located within the upper mantle (Missenard et al., 2006).

RHEOLOGY

The basement is a complex assembly of igneous, metamorphic, volcanic and sedimentary rocks. Despite these differences in composition and despite the existence of internal layering and strong anisotropy, in terms of rheology, basement blocks behave as overall rigid units, and display very little internal deformation. This is quite obvious in satellite images such as the Landsat scene shown in Figure 2. Normal faults of the Late Proterozoic - Middle Cambrian rifting event and possibly older structures, predefine the structural grain of the variscan inversion.

The Paleozoic cover series are quite weak and essentially behave as one soft layer draped over the basement blocks. Details

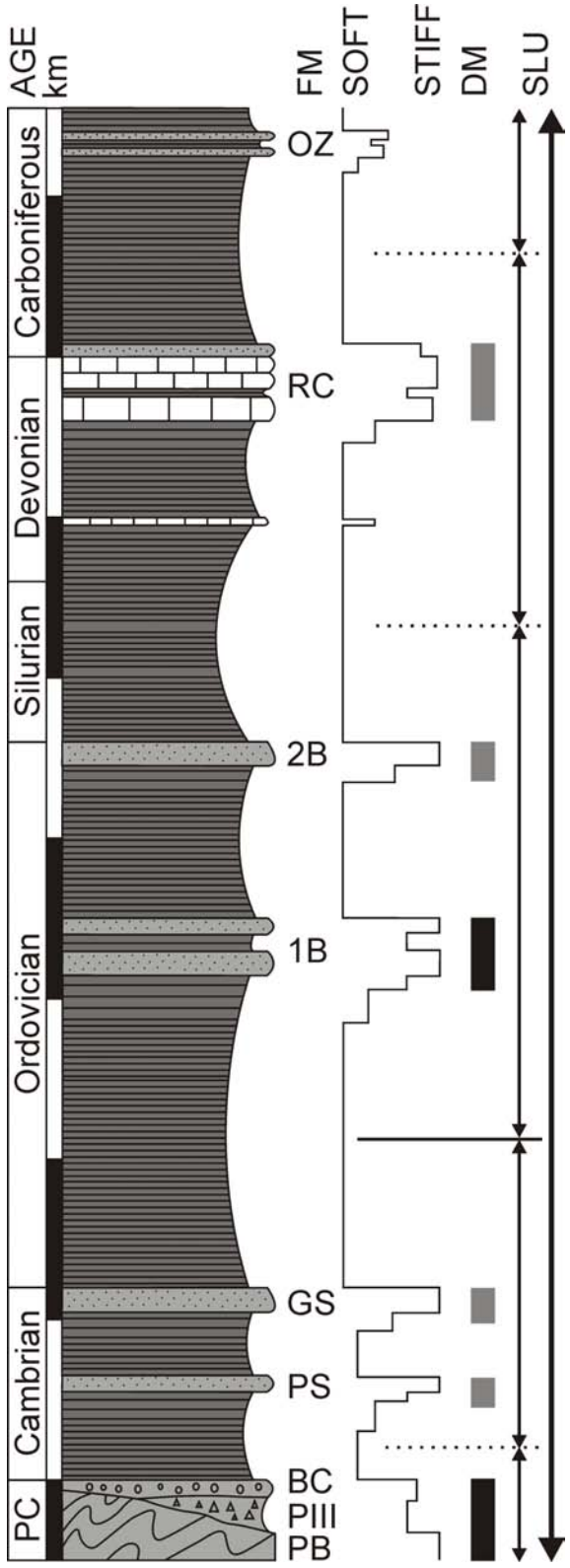

Figure 3. Synthetic stratigraphic log for the Eastern Anti-Atlas. FM: Formations, OZ: Ouarkziz, RC: Richs, 2B: Second Bani, 1B: First Bani, GS: green Sandstones, PS: Pink Sandstones, BC: Basal Conglomerates, P III: Precambrian III, PB: Pan-African basement. DM: dominant members, in black: dominant members of structural lithic unit (Currie et al., 1962), in grey: dominant members of conforming structural lithic unit. SLU: structural-lithic units, in fine arrows: conforming structural lithic units with the more marked boundary zone in Lower Ordovician, in large arrow: the dominant structural lithic unit which is the whole represented log.

of the cover rheology are shown in Figure 3. The two major dominant members (labelled DM in Figure 3) are the basement and the 1st Bani formation (Ordovician sandstones and quartzites). Remaining stiff members elsewhere in the stratigraphic column behave simply as “more dominant members within a conforming structural lithic unit” (according to the terminology of Currie et al., 1962). Our rheology log is based on field observations and cross-sections, which document the overall “conforming” geometry, matching the two major dominant members. On the smaller scale, however, dominant members of conforming structural lithic units also display their own characteristic layer parallel shortening structures such as wedging and minor buckle folding (Figure 4), clear evidence for an important component of bed-internal layer parallel shortening (LPS).

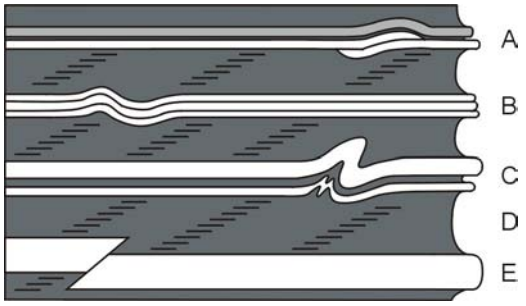

Figure 4. Effects of layer parallel shortening in competent beds. (A) Fishtail structure. (B) Buckling. (C) Disharmonic oblique fold(s). (D) Multitude of small thrusts. (E) Reverse fault.

While the rheology log of the cover can be subdivided in five conforming units, the primary structural-lithic unit is in fact the entire column of Paleozoic sediments including basement without any clear boundary zone, let alone any tectonic *décollements*. This can also be observed in the Landsat view (Figure 2) and cross sections. Despite a very similar overall stratigraphy, there is a marked difference between the eastern and the western Anti-Atlas. In the western Anti-Atlas, most of the weak units are used as detachments (boundary zones) and four distinct dominant members, namely the basement-P III, the Cambrian limestones, the Ordovician Bani, and the Devonian Rich developed their own fold geometries in what is best described as a multilayer of polyharmonic buckle folds (Helg et al., 2004).

In contrast, the overall geometry observed in the Eastern Anti-Atlas is “single layer” drape folding, dominated by the vertical component of movement of the rigid forcing member.

STRUCTURAL STYLE

Thick skinned fold belt

The lack of any basal *décollement* is probably the most intriguing feature of the entire Anti-Atlas fold belt. The basement-cover contact (Figure 5) is a major unconformity which is easily identified in satellite images, aerial photography and in the landscape. Compressional structures are increasingly abundant higher up in the stratigraphy, but even in the western Anti-Atlas, no major thrust nor any duplexing has been identified.

The geometry of compressional structures observed within the Paleozoic cover series is best explained by the trishear models of Erslev (1991) or Johnson and Johnson (2002), albeit with the difficulty to clearly identify the underlying reverse faults. This leads to conceive that most of the inverted basement faults must have induced footwall shortcuts (Bump, 2003), most likely within in Late Proterozoic syn-rift sediments, in order to horizontalize before cutting the basement-cover contact. In addition, an important component of horizontal shortening deformation is not localised but accommodated in a more diffuse manner within the volume of abundant thick soft layers of the conforming structural lithic units (Figure 4).

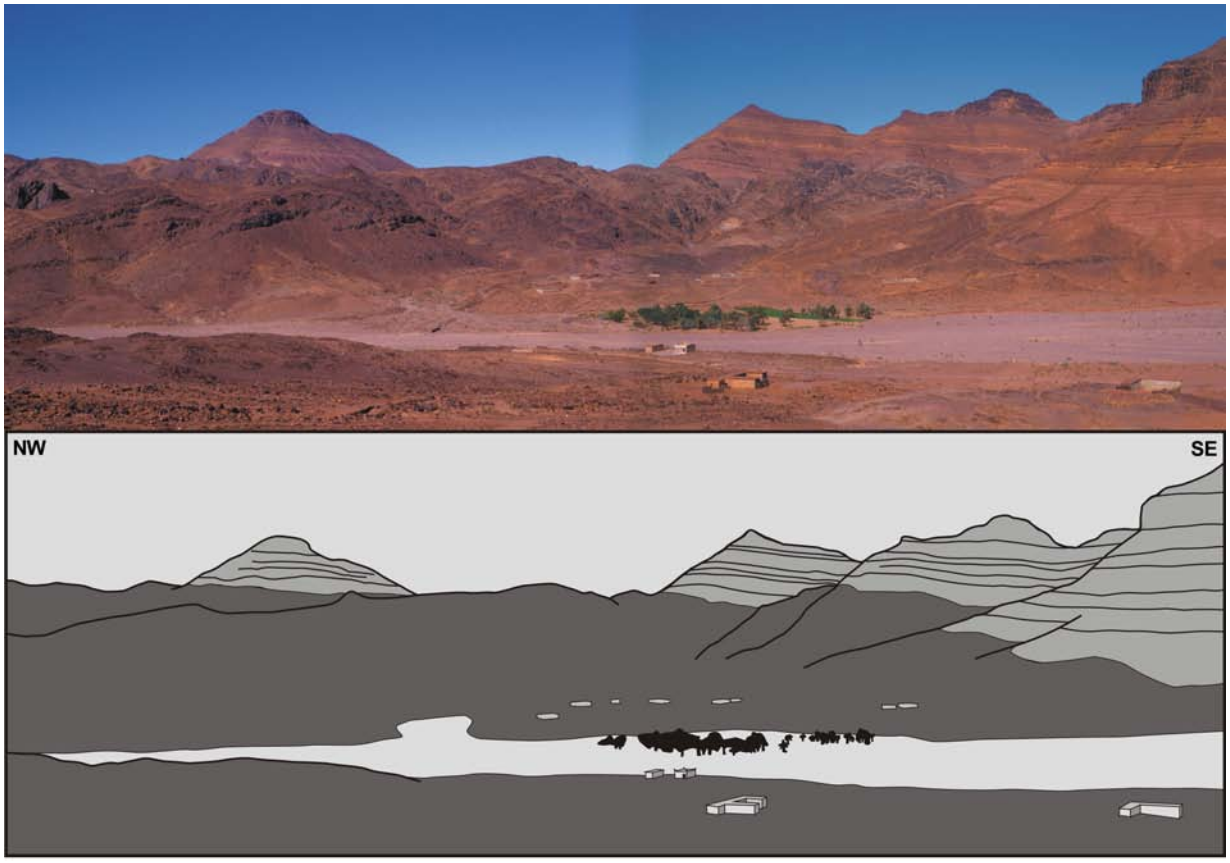

Figure 5. Basement – cover contact at the southern limit of Saghro inlier (cross section 08), view to North-East (houses for scale).

Compressional structures

On the outcrop scale, the dominant members show isolated meso-scale structures such as folds and minor wedging “fishtail structures” (Figure 6). The controlling factors are the bed thickness, the abundance of weak layers and the relative thickness of the two. The pictures A and B (Figure 6), taken from the same layers of Devonian carbonate illustrate two characteristic layer parallel shortening features, namely buckle folding and wedging (fishtail). In the fold case A, the thickness involves more layers then in case B where the thrust is limited to one single competent

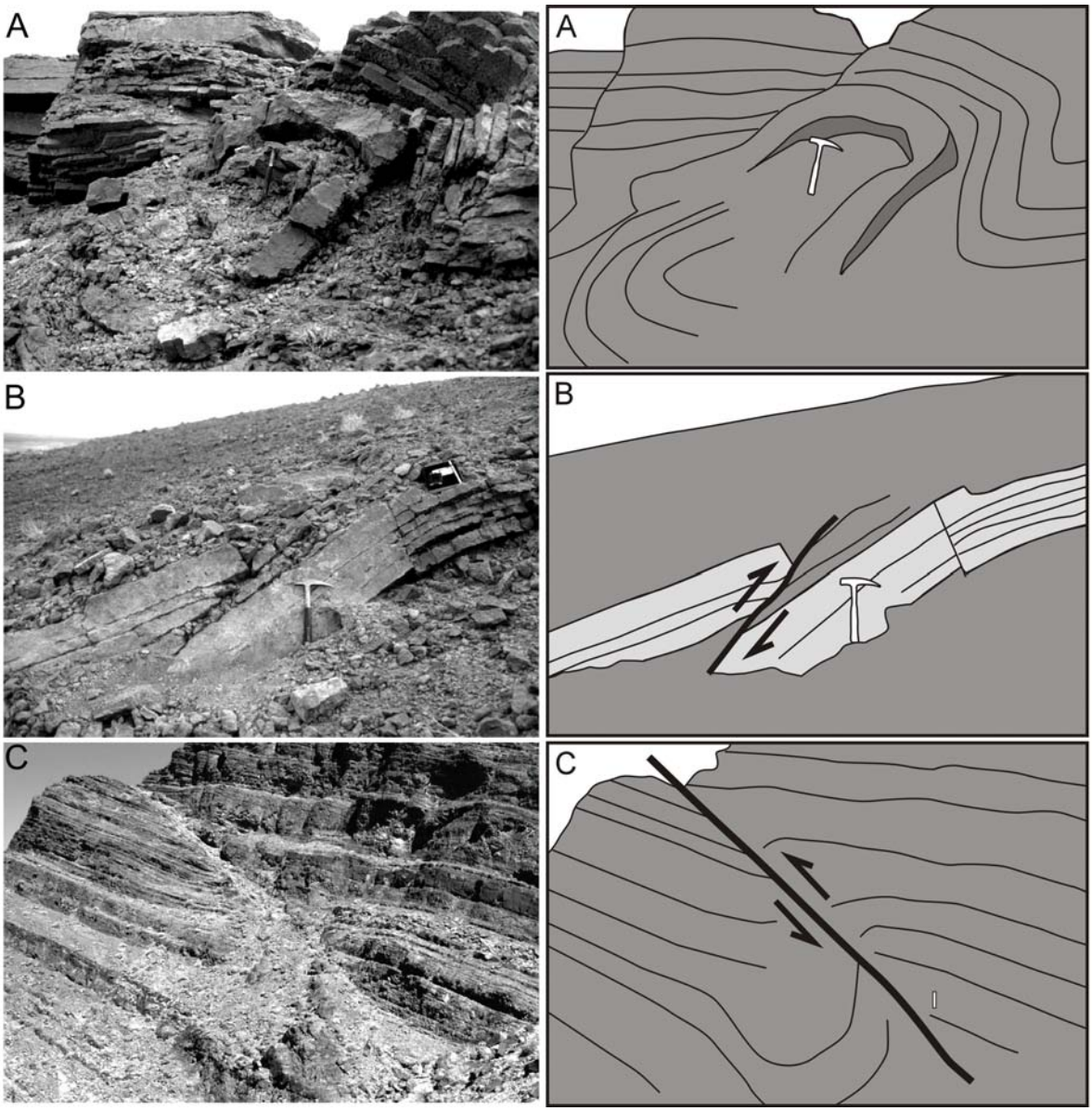

Figure 6. Compressional structures. (A) Fold in Middle Devonian limestones, cross section 03 (hammer in the centre for scale). (B) Small thrust in Middle Devonian, cross section 03 (hammer for scale). (C).: View to the East, north-vergent "back" thrusting fault with drag fold in footwall in 1st Bani, on the southern flank of cross section 10 (vertical view is 20 m).

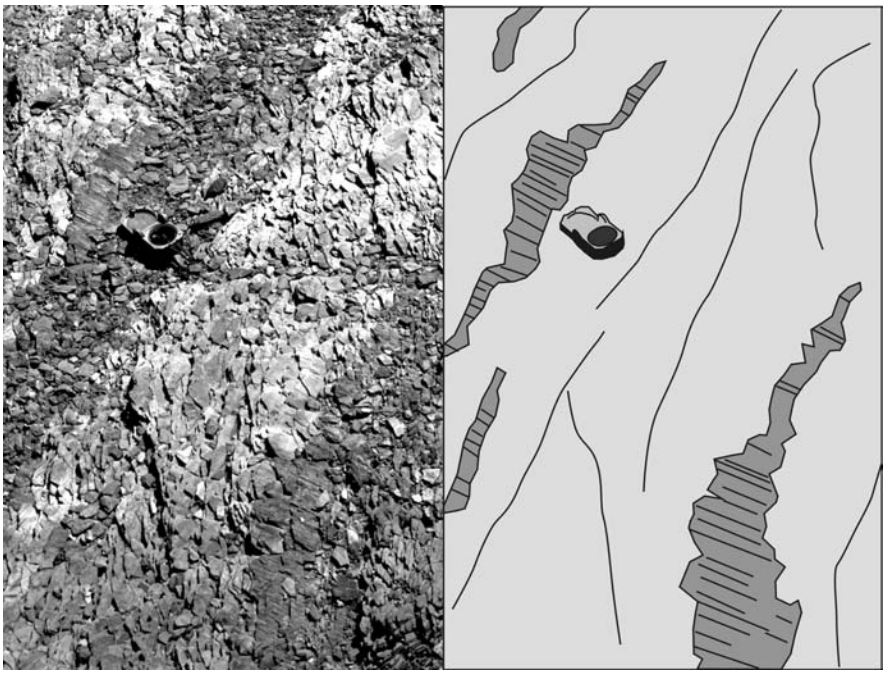

Figure 7. Small scale thrust planes with striation (in dark) within Early Ordovician shales, illustrating the characteristic style of internal layer parallel shortening deformation; location N 31°24.361' / W 005° 30.192' between cross sections 08 and 09 (compass for scale).

bed. The bigger thrust on picture C cuts off the whole lower part of the 1st Bani dominant member. Made of sandstones and quartzites this series has very few weak interlayers, and reacts as a single layer. The soft layers permit the development of a drag fold at the base of the cliff whereas the thick stiffer beds at the top don't. All these layer parallel shortening deformations are too small to appear in the cross sections, their role in balancing will be considered however.

Bed internal deformations within the thick weak zones are more subtle in appearance (Figure 7). When looking closer at shales in good outcrop conditions, they are invariably affected by a multitude of small thrusts, generally at a sharp angle with respect to bedding.

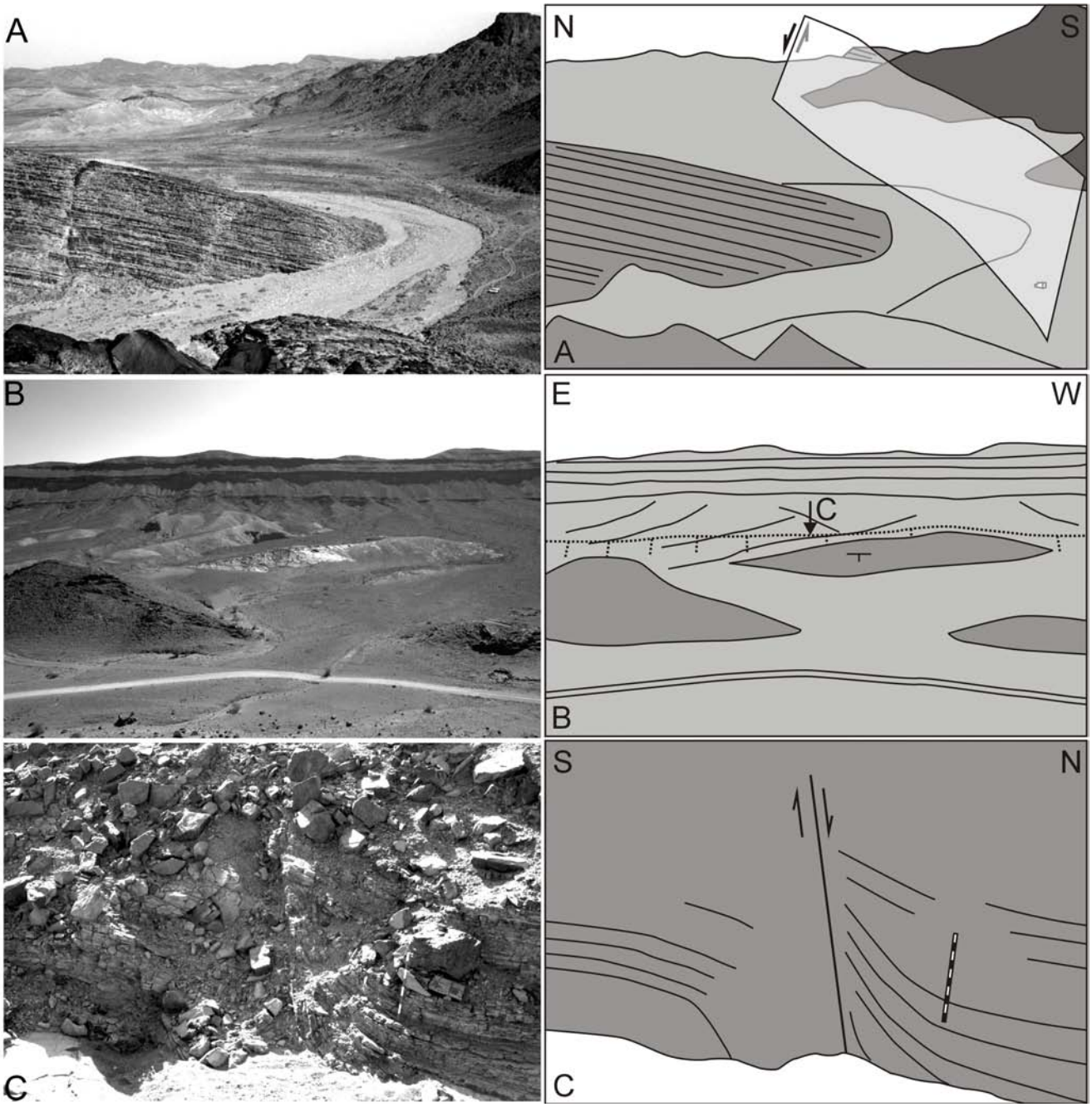

Figure 8. Extensional structures. (A) Normal fault. View to the East. The Middle Cambrian sandstones (left) dipping gently to the south abut basement on the right hand side; the normal fault is dipping steeply to the North; Ougnate inlier; cross section 06; Landrover lower right for scale. (B) View to the South. Graben structure in the middle of cross section 08. The cliff in the background is the 1st Bani (Ordovician quartzites) dipping gently to the South; the normal fault faces the viewer plunging steeply northward, drag folded layers of Devonian carbonates in the foreground dip very steeply to the North; for the scale : the trail in the foreground is 100 m (328 ft) long. (C) Drag folds along a normal fault dipping northward (fault plane: 024/68; striae : 043/65); Devonian carbonates within the oued shown in the centre of picture B; view to the West; stick on the right is one meter long.

Overall, compressional layer parallel shortening structures are best developed in the north and their abundance and intensity decreases progressively southward. This is interpreted as a regional gradient inbetween the supposed internal zones of the Anti-Atlas orogen to the north and the stable continental interior to the south. Internal parts of the Anti-Atlas orogen are obscured by, and may have been substantially shifted in position during, Mesozoic and Cenozoic events of High Atlas formation, however. The spatial relationships between the Variscan Anti-Atlas belt and the basement blocks found within and to the north of the High Atlas are a matter of ongoing debate (Hoepffner et al., 2005).

Extensional structures

The eastern Anti-Atlas of the Tafilalt and Mader basins is affected by an important "late" event of extension. This is in stark contrast to the western Anti-Atlas where no such extensional structures have been identified. Early authors (Choubert et al., 1952) depicted the general structure of the Tafilalt area as a set of tilted blocks inbetween north dipping normal faults. Normal faults are quite steep and cut mostly straight through the entire Paleozoic cover (pictures in Figure 8). Normal faults are responsible for a partial collapse of the basement inlier antiforms. Locally, extensional fault-related folds (Withjack et al., 1990; Schlische, 1995; Finch et al., 2004) and roll over folds (Xiao and Suppe, 1992) developed within weak Paleozoic cover rocks of the hanging-wall. Late normal faults are systematically rooted within the old Late Proterozoic normal faults, they were reactivated across the compressional footwall shortcut thrust of the variscan event.

CROSS SECTIONS

Cross sections have been constructed at the 1:50'000 scale, not allowing to take mesoscale deformation structures into account (Figure 9). Interpretations below and above topography have been made by simple projection (no change in fault orientation and constant layer thickness). Some features have also been laterally projected along strike such as the graben in the middle of cross sections 07 and 08. Devonian folds of cross section 07 are interpreted as forced "drape" folds resulting from extension in the underlying graben, but attenuated within the soft Silurian shales accommodating the fault throw in a trishear style.

The fault-bend fold in the northern part of cross sections 06 and 07 is an interpretation. It has been drawn such as to balance the extremely deformed Carboniferous sediments. However, the thrust in cross section 08 has been observed, but its interpretation remains ill constrained at depth. The High-Atlas structures are redrawn according to Frizon de Lamotte et al.(2000).

For calculations of the depth to detachment, the cross section 08 has been chosen because it crops out at the deepest level. Therefore, interpretation errors are minimal for the geometry of the basement-cover contact. For the reconstruction at different stages, we first restore the latest normal faults in order to establish the situation at the end of the variscan paroxysm. In a second step, the variscan folding is restored to a flat lying configuration. At this stage the layers still contain a component of early Variscan layer-parallel shortening which is compensated by stretching back to a restored configuration at the end of Paleozoic sedimentation.

DEPTH TO DETACHMENT

Depth to detachment is estimated using the displaced-area method (Epard and Groshong, 1993; Groshong, 1994, 1999). This 2-D cross-section balancing method (Figures 10 and 11) is based on the uplifted area above regional caused by compression (excess area Sc) or a downdropped area below regional caused by an extension (lost area Sx). Excess or lost area must be equal to the displaced area, which is defined by the depth to detachment times horizontal displacement. Excess or lost area is measured above or below a regional horizon (Hr in Figures 10 and 11). Such simple area balancing methods do neither require any detailed information about the shape of the detachment nor about the kinematical model. Bed-internal strains are classically assumed

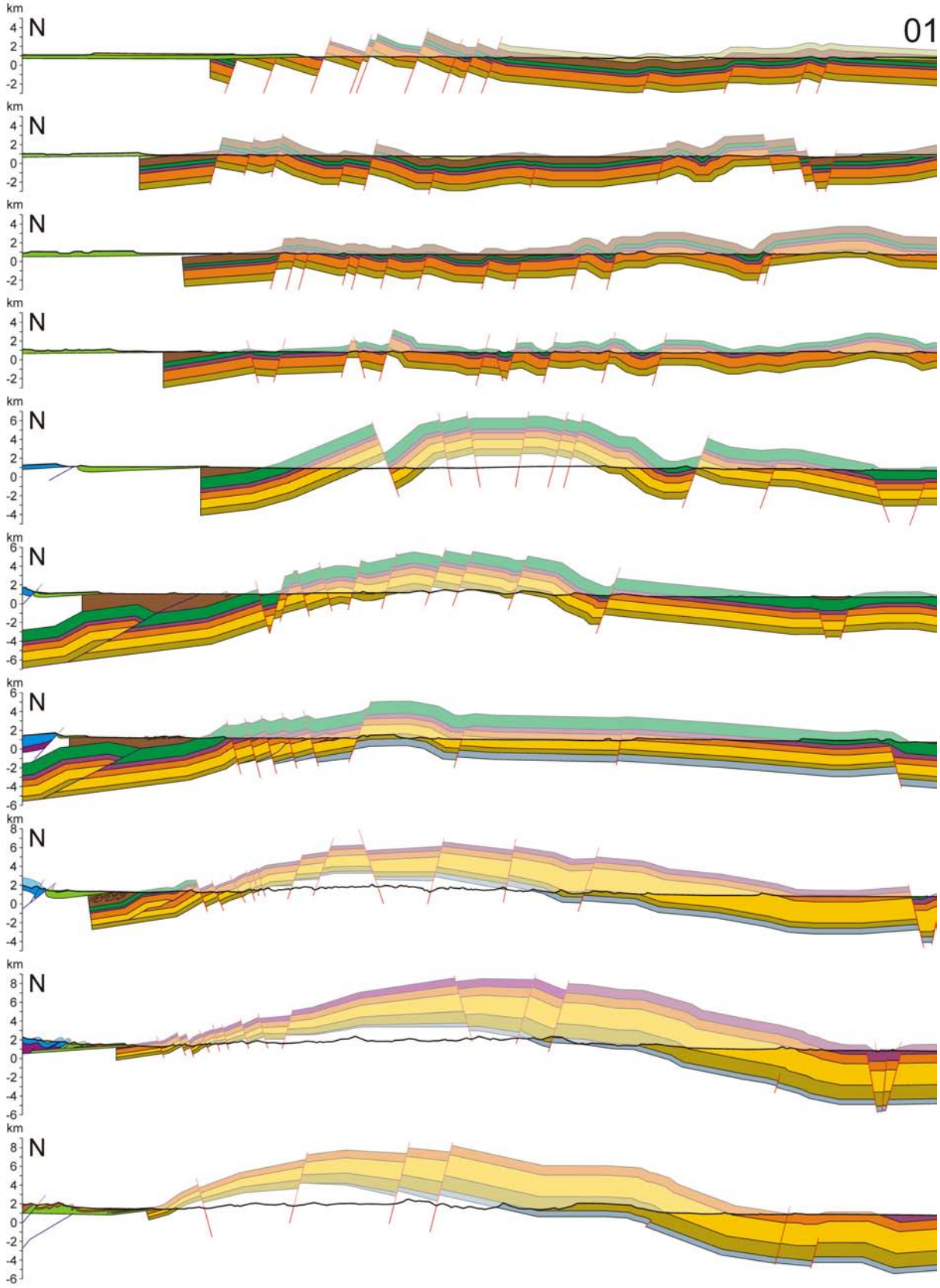

Figure 9. Cross sections.

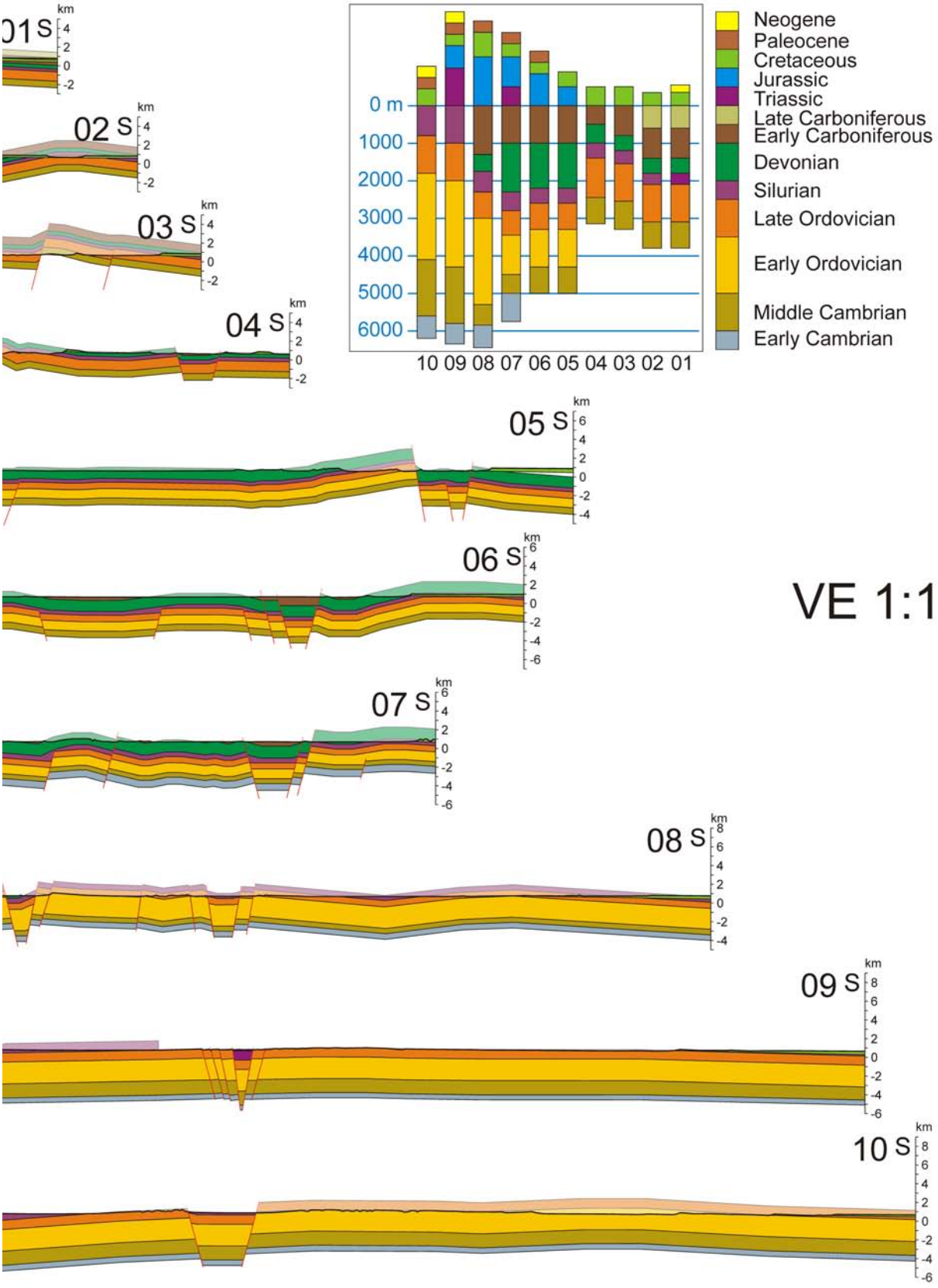
01 S
02 S
03 S
04 S
05 S
06 S
07 S
08 S
09 S
10 S
km
0 m
1000
2000
3000
4000
5000
6000
10 09 08 07 06 05 04 03 02 01
Neogene
Paleocene
Cretaceous
Jurassic
Triassic
Late Carboniferous
Early Carboniferous
Devonian
Silurian
Late Ordovician
Early Ordovician
Middle Cambrian
Early Cambrian
VE 1:1

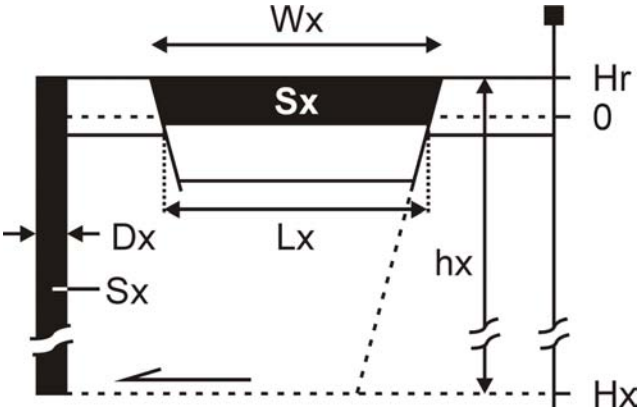

Figure 10. Extensional deformation. Definition of geometric elements used in the calculation of depth to detachment.

Figure 11. Compressional deformation. Geometric elements used in the depth to detachment calculation, including layer parallel shortening Dce.

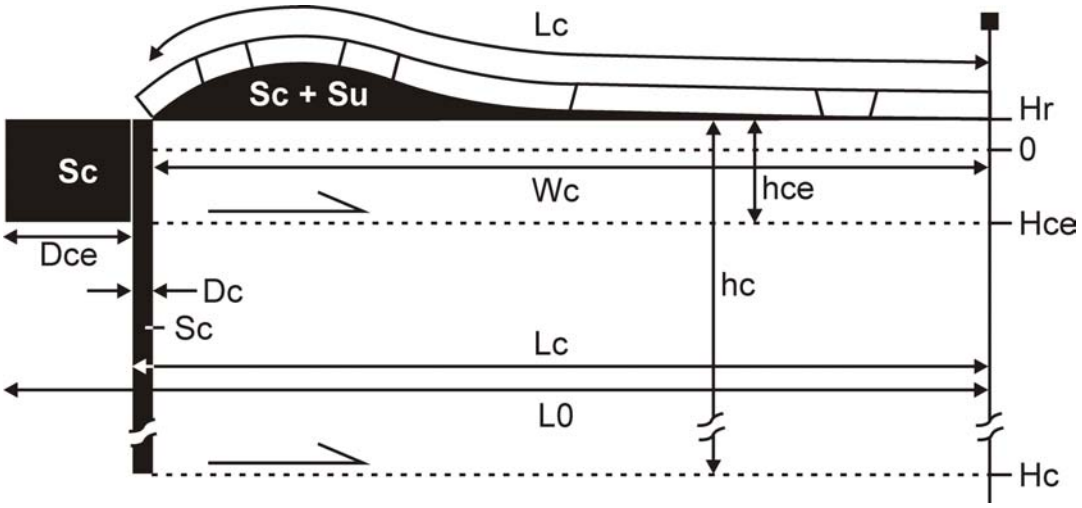

to be zero, but in the following we will develop a modified displacement area method in order to evaluate the role of layer parallel shortening. In this study, the excess and lost areas are measured from restored sections constructed for different stages of the Anti-Atlas' evolution through time (Figure 12). In the following discussion, we will concentrate on cross-section number 08, one of the best constrained and representative sections across the eastern Anti-Atlas chain. The present day cross-section has last been affected by Neogene tilting and differential uplift, without any associated faulting. The excess area resulting from this uplift (Su in Figure 12.A) has been removed from section 08 according to the lithospheric model of Missenard et al. (2006), which is based on gravity data.

The youngest faulting event in Triassic times caused the formation of the so-called Zagora graben as well as an extensional reactivation of crustal scale faults throughout the eastern Anti-Atlas anticlinorium.

The calculation of the depth to detachment is first applied to these latest extension features (stages C to B in Figure 12). The differential uplift (Figure 12.A) does not have any influence on the lost area in this stage because this uplift is identical in both profiles. However, for the next step backward, the differential uplift excess area (Su) must be subtracted from the excess area produced by compressional deformation (stage C) because the pre-compression profile D does not include the recent uplift.

Depth to detachment on extensional structures

The depth to detachment calculation for extension structures is made under the classical assumption of constant bed length. The area Sx below the regional Hr (Figure 10) resulting from extensional deformation is compensated by an equal area defined by the horizontal displacement Dx times hx the depth to detachment below the regional horizon Hr:

(1) $Sx = Dx \cdot hx$ thus $hx = \frac{Sx}{Dx}$

Where the horizontal displacement Dx is the

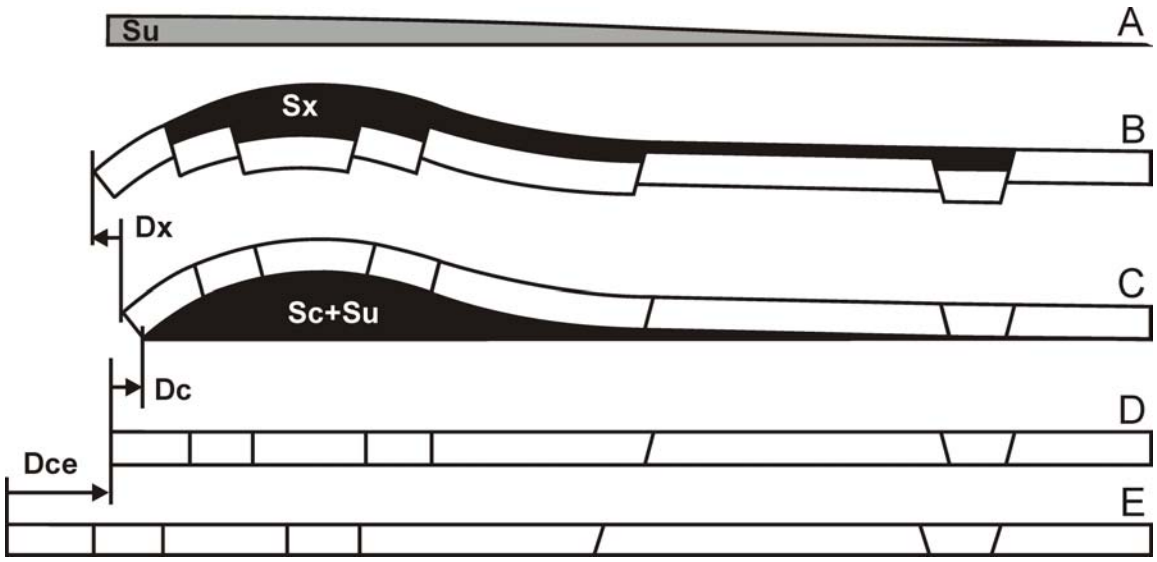

Figure 12. Restoration of cross section 08. (A) Differential uplift in Neogene to recent times; cross sectional area according to Missenard et al. (2006; figure 6.C, eastern profile). (B) Simplified present day cross section; Sx = area lost by the latest extension in Early Mesozoic times. (C) Cross section at the end of the Variscan orogeny. (D) Restored section at the onset of Variscan inversion tectonics including early Variscan layer-parallel shortening. (E) Restored section (Late Devonian, Early Carboniferous).

difference between the original bed length Lx and the width of the structure Wx:

(2) $$Dx = Lx - Wx$$

Accordingly, the depth of detachment Hx with respect to the zero altitude is given by:

(3) $$Hx = Hr - hx = Hr - \frac{Sx}{Lx - Wx}$$

Note that in the case of extension, Sx and Dx are both negative.

Such a depth to detachment calculation has been made for three different features : the Zagora graben, the Saghro inlier and the entire cross-section (Table 1; Figures 2 and 9 for localisation). For the Zagora graben detachment depth lies in the range –12 to –18 km (-7.5 to –11 mi). The higher values are those obtained from Silurian and Late Ordovician which are best constrained. The results of this depth to detachment calculation are shown in Graphic 1 by plotting the altitude of each regional level (Hr) against the lost area (Sx). Extrapolating the dotted line back to Sx = 0 km^2 yields a best fit of -16 km (10 mi) for detachment depth. The slope of this line is the inverse of the displacement (formula (1)), and yields a modest horizontal extension of D = 0.204 km (670 ft) in agreement with the measured values of Dx for the different levels.

Level	Hr (km)	Sx (km^2)	Dx (km)	hx (km)	Hx (km)
Zagora Graben					
Top Silurian	1.920	-3.743	-0.185	20.232	-18.312
Top Late Ordovician	1.330	-3.533	-0.185	19.097	-17.767
Top Early Ordovician	0.725	-3.290	-0.185	17.784	-17.059
Top Middle Cambrian	-1.555	-3.047	-0.260	11.719	-13.274
Top Early Cambrian	-2.125	-2.840	-0.245	11.592	-13.717
Top Basement	-2.735	-2.500	-0.250	10.000	-12.375
Saghro inlier					
Top Silurian	5.000	-28.279	-1.245	22.714	-17.714
Top Late Ordovician	4.460	-30.285	-1.435	21.105	-16.645
Top Early Ordovician	3.815	-30.317	-1.490	20.347	-16.645
Top Middle Cambrian	1.500	-30.850	-1.490	20.705	-19.205
Top Basement	0.355	-25.623	-1.355	18.910	-18.555
Whole cross section					
Top Silurian	2.100	-68.000	-2.155	31.555	-29.455
Top Late Ordovician	1.445	-92.000	-2.365	38.901	-37.456
Top Early Ordovician	0.800	-135.000	-2.480	54.435	-53.635
Top Middle Cambrian	-1.425	-135.000	-2.545	53.045	-54.470
Top Basement	-2.560	-144.000	-2.635	54.649	-57.209

Table 1. Depth to detachment on extensional features of cross-section 08.

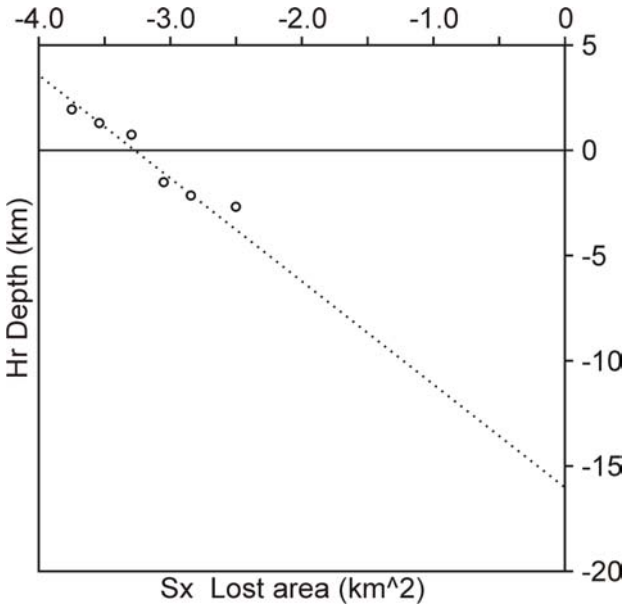

Graphic 1. Area-Depth relationship of Zagora graben.

For the Saghro inlier the calculated depth to detachment varies from –17 to –19 km. In contrast to the Zagora graben, the lower horizons (Cambrian and basement) are best constrained by outcrop observations. For the entire cross section each layer has been reconstructed individually. Simple depth to detachment calculations for this cross-section yield unreasonably high values in the range -29 to -57 km (-18 to -35 mi). From an area-depth relationship, the absolute Sx area for the top of the Silurian level should be greater then Sx of basement. These discrepancies may result from either of the following reasons. First, the overall cross section is not oriented perpendicular to all the normal faults; some of them are cut at a low angle, leading to a minimal apparent offsets and minimal Dx values. With higher absolute displacements, the detachment depth would be shifted upward. Displacement Dx is dependent on the assumed geometry of the normal faults at depth. In the interpreted cross sections, normal faults have been projected to depth with a constant angle of 70 to 80° as observed in outcrop. Assuming a listric geometry at depth would lead to greater displacements and smaller lost area with respect to the straight fault interpretation. Secondly, internal deformations (bed length change) have not been considered. In reality, the length Lx (Figure 10) is greater then the initial length before any extension and stretching. If equation (7') described in the later section on compressional structures were applied, a very small amount of strain would be sufficient to yield a significant change in the resulting depth to detachment. With a strain of only -0.03 (3 % bed internal stretching), the detachment depth calculated for the top of Early Cambrian would change from an initial -54 km (34 mi) upward to only -19 km (-12 mi). The bed thinning influence (of only three percent) on the lost area Sx is negligible.

Depth to detachment and Layer parallel shortening on compressional structures

The following calculations are made on a restored profile of the assumed geometry at the end of the variscan shortening. Practically, normal faults and their effects on the top of the sedimentary cover have been restored to a smooth unfaulted configuration. The regional horizon Hr (Figure 11) has been defined at the southern end of the cross section. The late (Neogene) differential uplift area Su has been subtracted from the measured excess area. The values of Su is 12.9 km^2 (8 mi^2) for the local Saghro section and 61.2 km^2 (38 mi^2) for the entire cross-section.

The calculation of the depth to detachment on compressional structures with constant bed length based on the very same equations as those demonstrated for extension.

(1) $Sc = Dc \cdot hc$ thus $hc = \frac{Sc}{Dc}$

Displacement Dc is defined as the difference between the originlal length Lc minus present day widths of the structure Wc.

(2) $Dc = Lc - Wc$

In the case of compression, Dc and Sc are both positive. Depth to detachment with respect to sea level, is defined by the following equation :

(3) $Hc = Hr - hc = Hr - \frac{Sc}{Lc - Wc}$

When applied to our cross-sections (Table 2) such considerations yield exceedingly high values for depth to detachment in the range -111 to -126 km (-69 to -78 mi) for the Saghro inlier and -172 to -212 km (-107 to -132 mi) for the entire cross section. Given the excellent of outcrop conditions, the complete absence of thrusting, duplexing and other large scale compressional structures is a well established fact. Balancing these cross-sections clearly requires more subtle, "hidden" components of strain to be taken into account. The structural style dictated by the particular rheology of the cover does not permit to change the displacement values other than by the assumption of an important component of layer-parallel shortening. This layer-parallel shortening is well documented in the field, but the small "meso-"scale of these deformation features does not allow them to be shown in cross-sections.

In order to take such bed length changes into account in the depth to detachment

Level	H_r (km)	S_c (km^2)	D_c (km)	h_c (km)	H_c (km)
Saghro					
Top Silurian	1.550	206.090	1.730	119.595	-118.045
Top Late Ordovician	1.000	212.090	1.725	122.951	-121.951
Top Early Ordovician	0.340	222.090	1.925	115.371	-115.031
Top Middle Cambrian	-1.890	249.090	2.005	124.234	-126.124
Top Basement	-3.030	264.090	2.425	108.903	-111.933
Whole cross section					
Top Silurian	0.650	454.785	2.590	175.593	-174.943
Top Late Ordovician	0.075	449.785	2.445	183.961	-183.886
Top Early Ordovician	-0.585	411.785	2.400	171.577	-172.162
Top Middle Cambrian	-2.805	431.785	2.445	176.599	-179.404
Top Basement	-4.000	458.785	2.205	208.066	-212.066

Table 2. Depth to detachment on compressional structures

calculation, we include the stretch e :

(4) $e = \frac{Dce}{Lo}$ thus $Dce = Lo \cdot e$

Where the length Dce is the absolute layer-parallel shortening and Lo is the original bed length (see Figure 11).

The measurable length Lc is defined as the original bed length minus shortening :

(5) $Lc = Lo - Dce$

The combination of equations (4) and (5) yields :

(6) $Lc = Lo - Lo \cdot e = Lo(1 - e)$

or $Lo = \frac{Lc}{1 - e}$

Including a component of layer-parallel shortening, equation (1) for depth to detachment is modified to :

(7) $hce = \frac{Sc}{Dc + Dce}$

Further, Dc is replaced by equation (2), Dce by equation (4) and Lo by equation (6). This yields :

(7') $$hce = \frac{Sc}{Lc - Wc + Lo \cdot e} = \frac{Sc}{Lc - Wc + \frac{Lc}{1 - e} \cdot e} = \frac{Sc}{Lc\left(1 + \frac{e}{1 - e}\right) - Wc}$$

and depth to detachment :

(8) $Hce = Hr - hce$

We examined the influence of layer-parallel shortening on the depth to detachment by varying e from 0 to 0.25, in a range compatible with observations made in outcrop and on the thin section scale. Resulting values of depth to detachment Hce are given in Table 3 and illustrated in Graphic 2.

This exercise shows that depth to detachment calculations applied to weakly folded section such as the Anti-Atlas cross-sections

are strongly dependent on layer-parallel shortening. With an assumed moderate amount of layer-parallel shortening on the order of 0.11 to 0.17, the calculated depth to detachment is shifted upward from more than -100 km to a reasonable depth of -18 to -20 km (-11 to -12 mi). This depth range is the same as the one initially determined for late extensional structures. Taking into account the observed deformation gradient, the layer-parallel shortening must be higher in the north and decreases southward.

Stretch e	Silurian	L. Ordov.	E. Ordov.	M. Camb.	Basement
0.00	-174.943	-183.886	-172.162	-179.404	-212.066
0.01	-109.169	-112.435	-104.840	-110.830	-126.226
0.02	-78.801	-80.501	-75.032	-80.175	-90.015
0.03	-61.313	-62.402	-58.216	-62.798	-70.045
0.04	-49.945	-50.748	-47.416	-51.609	-57.391
0.05	-41.962	-42.617	-39.895	-43.802	-48.655
0.06	-36.049	-36.621	-34.356	-38.045	-42.262
0.07	-31.492	-32.017	-30.107	-33.624	-37.380
0.08	-27.874	-28.371	-26.744	-30.122	-33.530
0.09	-24.931	-25.411	-24.016	-27.280	-30.416
0.10	-22.490	-22.961	-21.759	-24.928	-27.846
0.11	-20.434	-20.900	-19.860	-22.948	-25.688
0.12	-18.677	-19.141	-18.241	-21.259	-23.851
0.13	-17.159	-17.623	-16.844	-19.801	-22.269
0.14	-15.834	-16.299	-15.626	-18.530	-20.890
0.15	-14.667	-15.135	-14.555	-17.412	-19.680
0.16	-13.633	-14.103	-13.606	-16.421	-18.608
0.17	-12.709	-13.181	-12.759	-15.536	-17.652
0.18	-11.878	-12.354	-11.998	-14.741	-16.794
0.19	-11.128	-11.607	-11.311	-14.024	-16.021
0.20	-10.447	-10.929	-10.688	-13.373	-15.319
0.21	-9.826	-10.311	-10.120	-12.779	-14.680
0.22	-9.257	-9.745	-9.601	-12.236	-14.095
0.23	-8.734	-9.226	-9.123	-11.737	-13.558
0.24	-8.252	-8.746	-8.683	-11.277	-13.064
0.25	-7.806	-8.303	-8.276	-10.851	-12.606

Table 3. Detachment depth (Hce) vs stretch (e) for compressional deformation on the entire cross-section.

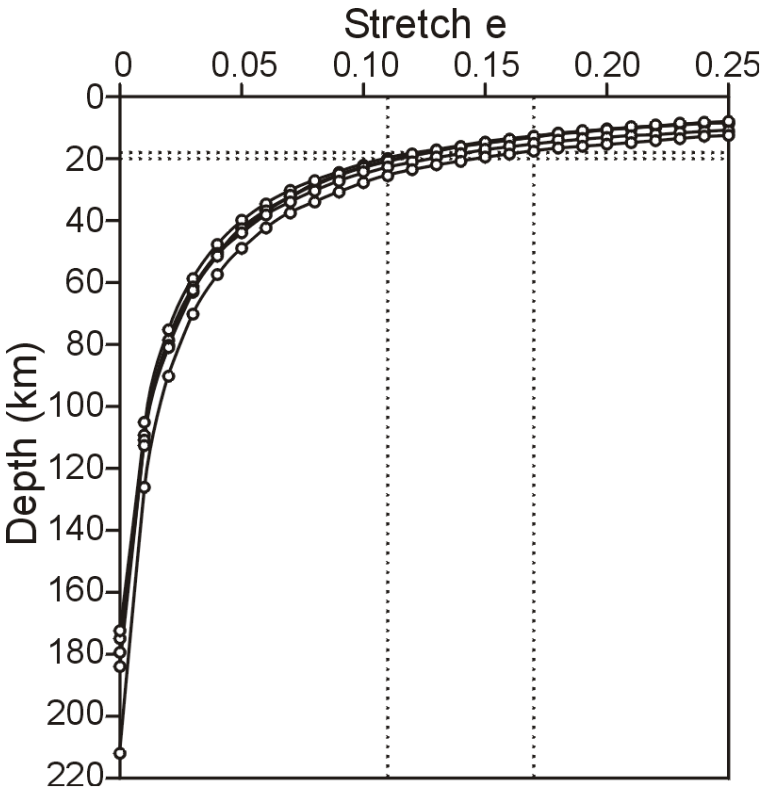

Graphic 2. Depth to detachment vs stretch for compressional deformation on the entire cross section.

CONCLUSIONS

The structural style of this inverted intracratonic basin is controlled by two properties:

1. The weak rheology of the cover. This allowed for a distributed shortening deformation within shales and siltstones and the formation of isolated mesoscale structures within competent layers. The weakness of the cover series prevented the development of any strong localization major *décollements*. This soft pile forms a single structural-lithic unit which adopts a drape fold allure with respect to the basement structures.
2. Pre-existing inherited structures within the basement. Precambrian rift normal faults constitute weak zones (Figure 13, stage A) which are repeatedly reactivated in later events be it compressional or extensional. The variscan shortening lead to the inversion of Precambrian normal faults. Thrusts faults systematically shortcut the footwalls to flatten out within Lower Cambrian shales and never step up any higher into the Paleozoic cover (Figure 13, stage B). Shortening in the cover series is accommodated by an overall drape folding and widely distributed layer-parallel shortening of up to 17 %. Extensional re-activation in Early Mesozoic times (stage C) lead to the formation of new set normal faults within cover rocks, crosscutting the variscan compressional cover structures at a high angle.

The depth to detachment calculation and its error analysis provide significant informations. On the extension structures, calculations yield a detachment depth in the range of -18 to -20 km (-11 to -12 mi). Positive deviation from this value indicates that the dip of the normal faults must decrease with depth. Alternatively, a minimal amount of 3% bed internal stretching could equally well explain the discrepancies in depth to detachment obtained from the overall cross section. Balancing Variscan shortening deformations yields unreasonably high values for depth to detachment in excess of -100 km . Taking a component of 11 to 17 % distributed layer-parallel shortening into account allows to reconcile surface observations and balancing with a reasonable depth to detachment of -18 to -20 km.

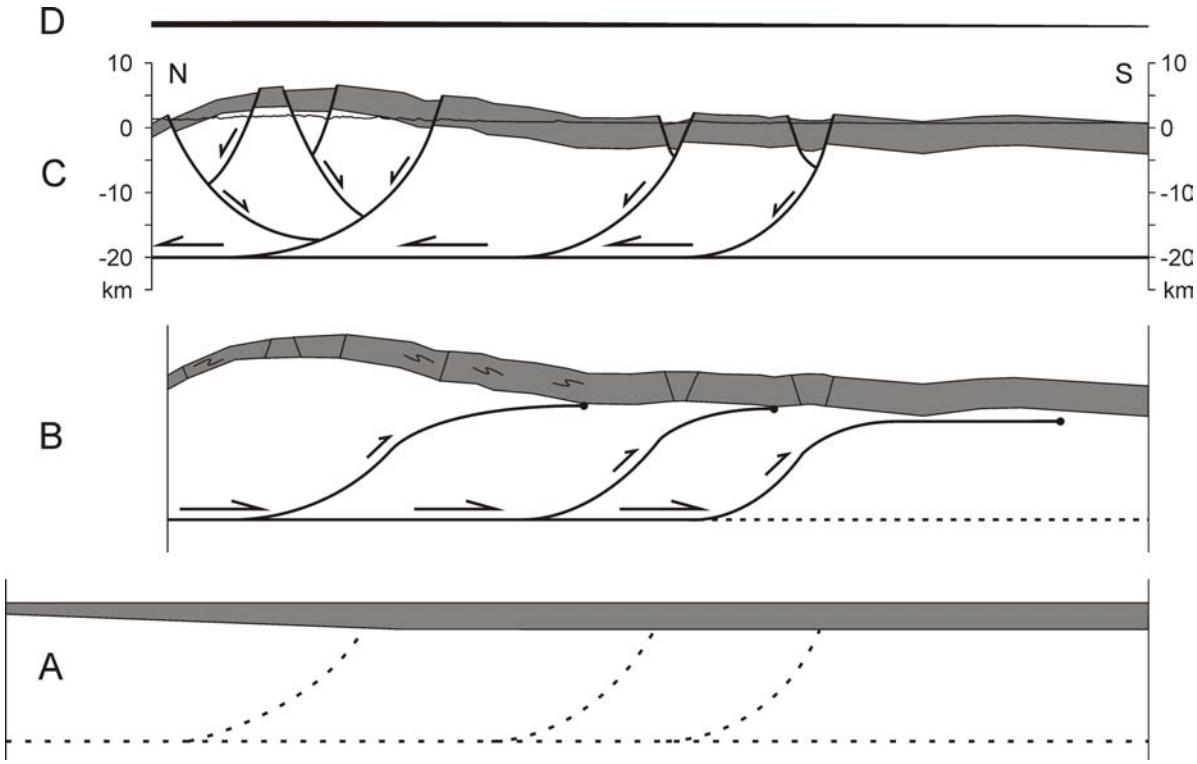

Figure 13. Mid-crustal detachment model for cross section 08. No vertical exaggeration. Cover from Cambrian to Silurian (included) (A) Profile before variscan compression with the rift inherited normal faults. (B) Profile at the paroxysm of variscan compression. The normal faults play in inversion, but do not reach the Paleozoic cover by shortcutting the normal faults where they are to steep. (C) Opening of the nearby High-Atlas basin affects Anti-Atlas. Former faults are reactivated in extension and crosscut the Paleozoic cover. (D) At scale recent uplift effect from Missenard et al. (2006).

REFERENCES CITED

Benssaou, M., N. Hamoumi, 2003, The lower-Cambrian western Anti-Atlasic graben: tectonic control of palaeogeography and sequential organisation: Comptes Rendus Geoscience, 335, p. 297-305.

Boudda, A., G. Choubert, 1972, Sur la limite inférieure du Cambrien au Maroc: C. R. de l'Académie des Sciences, Paris, Serie II 275 (1), p. 5-8.

Bump, A.P., 2003, Reactivation, trishear modeling, and folded basement in Laramide uplifts: implications for the origins of intracontinental faults: Geological Society of America Today, p. 4-10.

Burkhard, M., S. Caritg, U. Helg, C. Robert-Charrue, A. Soulaïmani, 2006, Tectonics of the Anti-Atlas of Morocco: Comptes Rendus Geoscience, 338, p. 11-24.

Choubert G., L. Clariond, J. Hindermeyer, 1952, Livret-guide de l'excursion C36, Anti-Atlas central et oriental: Congrès géologique international, XIXe session-Alger-1952, Série : Maroc N° 11, 89 p.

Coward, M.P., A.C. Ries, 2003, Tectonic development of North African basins : Petroleum geology of Africa; new themes and developing technologies. T. Arthur, S. MacGregor Duncan and N.R. Cameron, Geological Society of London. London, United Kingdom, 207, p. 61-83.

Currie, J. B., H. W. Patnode, R. P. Trump, 1962, Development of folds in sedimentary strata: Geological Society of America Bulletin, v. 73, p. 655-673.

Ennih, N., J.-P. Liégeois, 2001, The Moroccan Anti-Atlas: the West African craton passive margin with limited Pan-African activity. Implications for the northern limit of the craton: Precambrian Research, 112, p. 289-302.

Epard, J.-L., R. H. Groshong, 1993, Excess area and depth to detachment: The AAPG bulletin, v. 77, no. 8, p. 1291-1302.

Erslev, E. A., 1991, Trishear fault-propagation folding: Geology, v. 19, p. 617-620.

Finch, E., S. Hardy, R. Gawthorpe, 2004, Discrete-element modelling of extensional fault-propagation folding above rigid basement fault blocks: Basin research, 16, p. 489-506.

Frizon de Lamotte, D., B. Saint Bezar, R. Bracène, E. Mercier, 2000, The two main steps of the Atlas building and geodynamics of western Mediterranean: Tectonics, v. 19, no 4, p. 740-761.

Groshong, R. H., 1994, Area balance, depth to detachment, and strain in extension: Tectonics, v. 13, no. 6, pp. 1488-1497.

Groshong, R. H., 1999, 3-D structural geology: Springer-Verlag, 324 p.

Helg, U., M. Burkhard, S. Caritg, C. Robert-Charrue, 2004, Folding and inversion tectonics in the Anti-Atlas of Morocco: Tectonics, v. 23, TC4006, doi:10.1029/2003TC001576.

Hoepffner, C., A. Soulaimani, A. Piqué, 2005, The Moroccan Hercynides: Journal of African Earth Sciences, 43, pp. 144-165.

Johnson, K. M., A. M. Johnson, 2002, Mechanical models of trishear-like folds: Journal of Structural Geology, 24, p. 277-287.

Liégeois, J.-P., A. Fekkak, O. Bruguier, E. Errami, N. Ennih, 2005, Lower ediacaran age (630-610 Ma) for the Sarhro group. Implications for the metacratonic evolution of the Anti-Atlas, correlations with the Tuareg shield and the evolution of the pan-african orogeny in the NW Africa (abs.): 4ème Colloque International 3Ma, Agadir 2005, Abstract Volume, p. 2.

Manspeizer, W., J.H. Puffer, H.L. Cousminer, 1978, Separation of Morocco and eastern North America: A Triassic-Liassic stratigraphic record: Geological Society of America Bulletin, v. 89, pp. 901-920.

Missenard, Y., H. Zeyen, D. Frizon de Lamotte, P. Leturmy, C. Petit, M. Sérbier, O. Saddiqi, 2006, Crustal versus asthenospheric origin of relief of the Atlas Mountains of Morocco: Journal of Geophysical Research, v. 111, B03410, 13 p.

NASA and Earth Satellite Corporation, < https://zulu.ssc.nasa.gov/mrsid/ >
Accessed June 30, 2006.

Sebai A., G. Feraud, H. Bertrand, J. Hanes, 1991, $^{40}Ar/^{39}Ar$ dating and geochemistry of tholeiitic magmatism related to the early opening of the central Atlantic rift: Earth and Planetary Science Letters, 104, p. 455-472.

Schlische, R. W., 1995, Geometry and Origin of Fault-Related Folds in Extensional Settings: The AAPG Bulletin, v. 79, no. 11, p. 1661-1678.

Withjack, M. O., J. Olson, E. Peterson, 1990, Experimental Models of Extensional Forced Folds: The AAPG Bulletin, v. 74, no. 7, p. 1038-1054.

Xiao, H., J. Suppe, 1992, Origin of Rollover, The AAPG Bulletin, v. 76, no. 4, p. 509-529.

Available online at www.sciencedirect.com
SCIENCE DIRECT®
C. R. Geoscience 338 (2006) 11–24
COMPTES RENDUS GEOSCIENCE
http://france.elsevier.com/direct/CRAS2A/

Tectonics

Tectonics of the Anti-Atlas of Morocco

Martin Burkhard [a,*], Séverine Caritg [a], Urs Helg [b], Charles Robert-Charrue [a], Abderrahmane Soulaimani [c]

[a] *Institut de géologie, université de Neuchâtel, rue Émile-Argand 11, CP 2, 2007 Neuchâtel, Switzerland*
[b] *BUWAL, Bundesamt für Umwelt, Wald und Landschaf, 3003 Bern, Suisse*
[c] *Faculté des sciences Semlalia, université Cadi-Ayyad, av. Moulay-Abdellah, BP S20, Marrakech, Maroc*

Received 4 October 2005; accepted after revision 17 November 2005

Available online 4 January 2006

Written on invitation of the Editorial Board

Abstract

The Anti-Atlas is reviewed and examined in the light of its geodynamic significance as a Palaeozoic basin and fold belt. Shortening is accommodated by polyharmonic buckle folding of the cover in a thick-skinned fashion without the development of any significant thrust/duplex systems. The Anti-Atlas is heavily inverted deep intracratonic basin, rather than a former passive margin of the Palaeo-Tethys Ocean. Inversion took place in Late Carboniferous to Early Permian times. Main shortening directions changed from NW–SE to north–south and maybe NE–SW through time, leading to the development of dome and basin patterns on scales from 100 m to 10 km. ***To cite this article: M. Burkhard et al., C. R. Geoscience 338 (2006).***

Résumé

Tectonique de l'Anti-Atlas marocain. L'Anti-Atlas est revu et examiné sous l'angle de sa signification géodynamique comme bassin paléozoïque et comme chaîne plissée paléozoïque. Le raccourcissement est accommodé par le plissement polyharmonique de la couverture, avec une nette implication du socle. Aucun système significatif de chevauchement ni duplex ne s'est développé. L'Anti-Atlas est un bassin intracratonique fortement inversé plutôt qu'une partie de la marge passive de la Paléotéthys. L'inversion doit dater du Carbonifère tardif/Permien précoce. La direction du raccourcissement a changé au cours du temps depuis une direction NW–SE vers une direction nord–sud et peut-être même NE–SW, ce qui conduit à la formation de figures d'interférences de plis en dômes et bassins aux échelles allant de 100 m à 10 km. ***Pour citer cet article : M. Burkhard et al., C. R. Geoscience 338 (2006).***

Keywords: Folds and folding; Continental contractional orogenic belts; Africa; Morocco; Variscan–Hercynian

Mots-clés : Plis et plissement ; Chaînes orogéniques continentales de contraction ; Afrique ; Maroc ; Varisque–Hercynien

1. The Anti-Atlas of Morocco – Introduction

The Anti-Atlas fold belt of the south-western Moroccan desert (Figs. 1 and 2) offers vast expanses of beautifully exposed bare outcrops. This is due to a recent phase of uplift and concomitant erosion that led

* Corresponding author.
E-mail address: martin.burkhard@unine.ch (M. Burkhard).

1631-0713/$ – see front matter
doi:10.1016/j.crte.2005.11.012

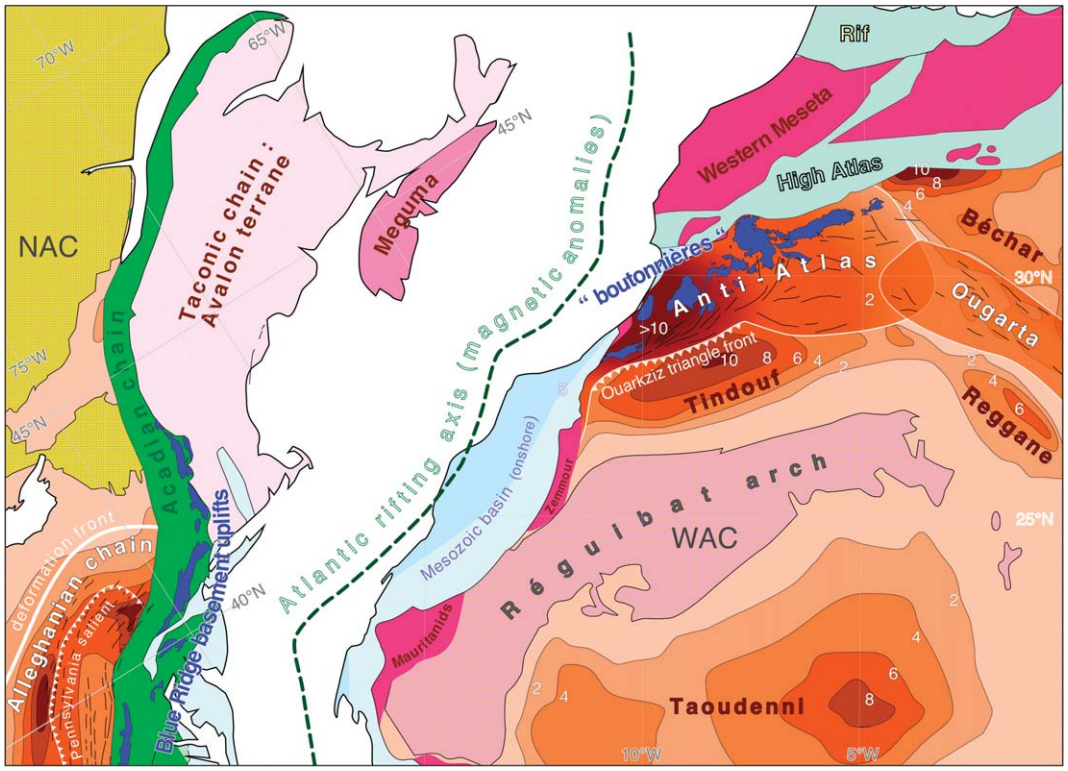

Fig. 1. The Anti-Atlas is shown in its larger context at the End of the Palaeozoic [80]. Isopach contours for total sedimentary thickness are given in kilometres for those Palaeozoic basins which have not or only weakly been involved in inversion tectonics [102]. The same colour shades are schematically superimposed onto the Anti-Atlas fold belt in order to illustrate the estimated depth of >10 km of this basin prior to inversion. Alleghenian basement uplifts are shown in blue (inspired by the Appalachian 'Blue ridge'). Internal, metamorphic and in part older portions of the Applachian–Mauritanides–Moroccan Meseta are coloured in green and pink tones [44,73].

Fig. 1. Situation de l'Anti-Atlas par rapport à la chaîne des Appalaches à la fin du Paléozoïque [80]. Les contours isopaques en kilomètres sont donnés pour les bassins sédimentaires paléozoïques qui n'ont subi que peu ou pas de déformation [102]. Le même code couleur est superposé à la chaîne plissée de l'Anti-Atlas afin d'indiquer la profondeur estimée de ce bassin avant l'inversion. Les massifs de socle alléghaniens sont indiqués en bleu (inspiré du *Blue Ridge* appalachien). Les parties internes, métamorphiques et plus anciennes, de la chaîne des Appalaches–Mauritanides–Méséta marocaine sont colorées en vert et en rose [44,73].

to a rejuvenation of relief with summits of 2500 m and higher [35,47]. Geomorphologists have coined the French term *relief appalachien* to characterize the pattern of deeply eroded fold trains, and there is indeed a striking similarity between the geomorphic expression of the Appalachian Valley and Ridge and the Anti-Atlas. Both chains are external parts of the larger Variscan Appalachian–Ouachita–Mauritanides orogen (Fig. 1). The relationship between the Anti-Atlas fold belt and the internal parts of this orogen remains to be elucidated in terms of tectonic style, timing and geodynamics.

At first sight, the Anti-Atlas shares many common features with its American counterpart of the Valley and Ridge in general and with the Alleghany Basin in particular. Both are located on the craton side of the orogen involving a thick and fairly regular layer cake of mostly shallow marine Palaeozoic sediments. Both fold provinces also have their non-folded time-equivalent intracratonic basins further inland: Michigan and Illinois on the American side, Taoudenni, Tindouf and others on the African side. On closer inspection, however, and in stark contrast to the frontal Appalachian chain, the Anti-Atlas fold belt does not easily conform with the standard anatomy of foreland fold-and-thrust belts worldwide [77]. The most striking difference is the existence of major basement domes at a very short distance behind the deformation front [76]. Similarities exist with Wind River-style basement uplifts of the frontal Rocky Mountains, but in the Anti-Atlas, the basement uplifts occur amidst a tightly folded thick Palaeozoic cover series. The style of cover folding is quite unique too, with a dominance of upright detachment folds and a complete absence of any thrusting and duplex structures [47], with the exception of the westernmost parts of the Anti-

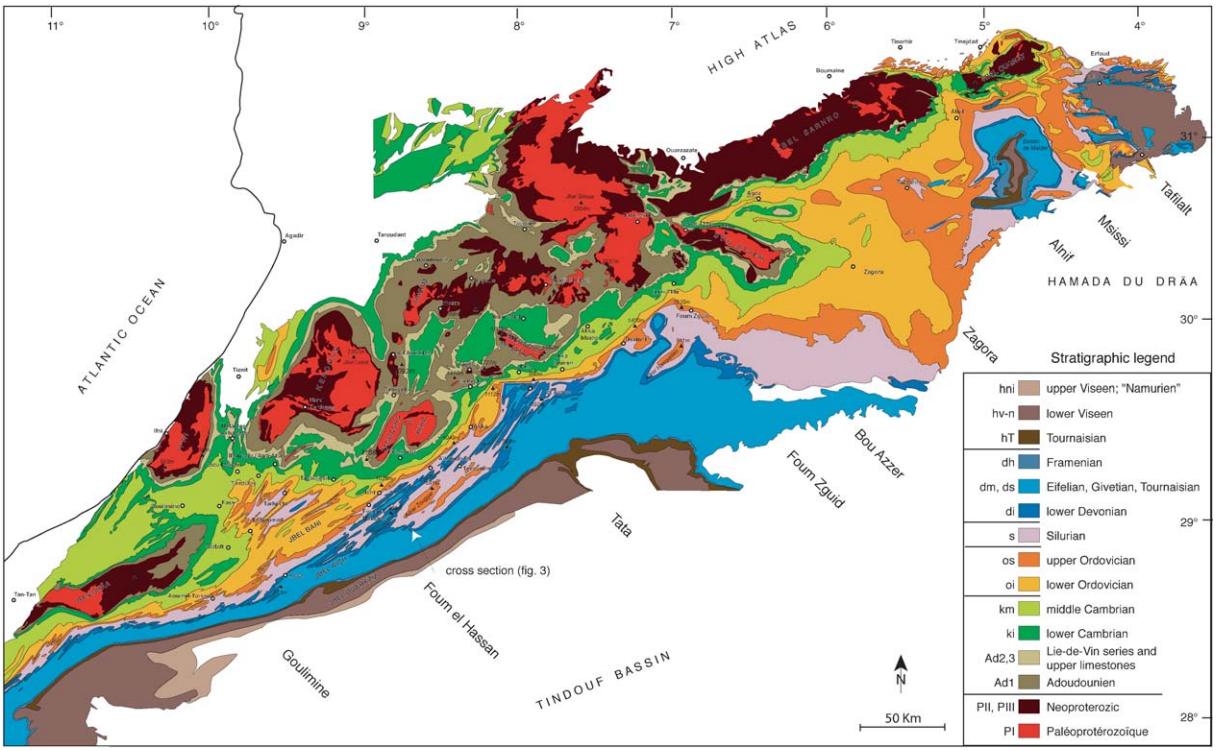

Fig. 2. Geologic overview map of the Anti-Atlas, compiled from the geologic map series (1:200 000) of the 'Service géologique du Maroc' [105–114]. NW–SE transects, used for the compilation of Fig. 4 are indicated along the southern border. A cross section through the Adrar Zouggar anticlinorium is shown in Fig. 3.

Fig. 2. Carte géologique de l'Anti-Atlas, synthétisée à partir de la série des cartes 1:200 000 du Service géologique du Maroc [105–114]. Les transects NW–SE, utilisés pour la compilation de la Fig. 4, sont indiqués le long de la bordure sud. Une coupe à travers l'anticlinorium de l'Adrar Zouggar est donnée sur la Fig. 3.

Atlas along the Atlantic coast [8,65]. There is no thin skinned basal décollement level and the western Anti-Atlas does not conform with a foreland fold and thrust belt system in the sense of Boyer and Elliott [15].

An exhaustive review of the geology of the Anti-Atlas has been presented by Michard [64]. While many authors have interpreted the Anti-Atlas fold belt in terms of a predominance of strike-slip movements [43, 61,74,99], recent structural analyses depict the western Anti-Atlas folds as highly cylindrical frontal folds related with a 'head-on' collision in a NNW–SSE direction [20,47,91].

In this paper the Anti-Atlas system is revisited in light of recent data regarding the Pre-Cambrian basement, the Palaeozoic cover, structural observations within the Anti-Atlas belt as well as plate tectonic reconstructions on a global scale. Questions of particular interest concern the Palaeozoic sedimentary basin history and subsidence mechanisms as well as the evolution of this Anti-Atlas basin near the border of the West-African Craton through time.

1.1. The basement

The Anti-Atlas basement is a complex assemblage of crystalline, metamorphic and sedimentary rocks. Note that we use the term basement here in the sense of the petroleum geologists [58], including all rocks older than the Gondwana Megacycle. The oldest rocks of the West-African Craton (WAC) are granitoids, gneisses and a complex series of metamorphic rocks, attributed to the Eburnean orogeny at around 2000 Ma [2,96, 98]. The final assembly of most of the African continental crust takes place during the Panafrican orogeny, lasting roughly from 700 to 600 Ma [46]. Remnants of a Panafrican suture zone are present as a dismembered ophiolite series in the Bou Azzer inlier of the central Anti-Atlas [45,55,81,96] – a structure recently reinterpreted as an aulacogen within the WAC [32]. Elsewhere in the Anti-Atlas, the Panafrican event left a more subtle imprint in the form of strike-slip shear zones and thrusts [43]. Post-Panafrican continental extension is well documented for the entire Anti-Atlas re-

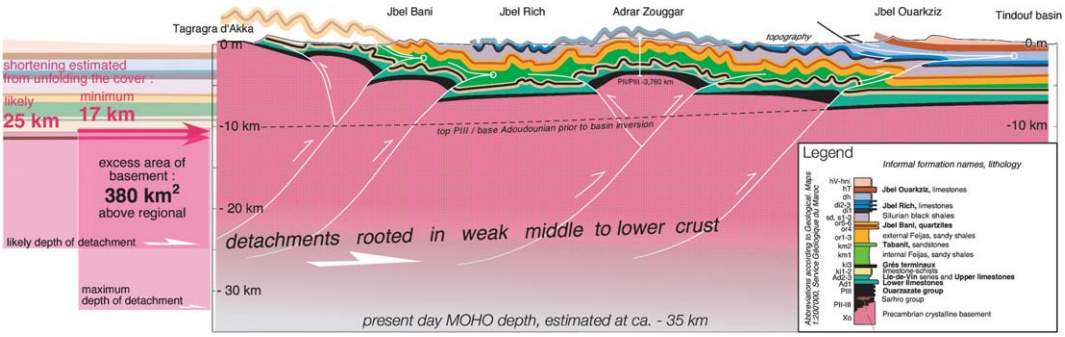

Fig. 3. Cross section through the Adrar Zouggar anticlinorium [27], see Fig. 2 for location. Surface geology is constructed from the 1:200 000 geologic map [110], augmented with our own detailed mapping and measurements of folds and other mesoscale structures [20]. Compare with Michard [64, (Fig. 20)]. This section is tentatively area-balanced. A minimum determination of map scale cover shortening is 13 to 15% from mesoscale folding alone. Additional shortening from intra-bed strains could well add another 10% or so of shortening [47]. A resulting 'likely' horizontal shortening of 25 km would need a mid-crustal décollement at about 25 km depth.

Fig. 3. Coupe à travers l'anticlinorium de l'Adrar Zouggar [27] ; pour la localisation, voir Fig. 2. La géologie de surface est construite à partir de la carte géologique à 1:200 000 [110], augmentée par nos propres cartographies et mesures de plis et d'autres structures [20]. À comparer avec Michard [64, (Fig. 20)]. Cette coupe est approximativement équilibrée en ce qui concerne les aires. Une détermination du raccourcissement horizontal minimal à l'échelle de la carte est de l'ordre de 13 à 15% par le seul plissement mésoscopique. Quelque 10% de raccourcissement additionnel par déformation intra-couche sont fort probables. Un raccourcissement total de 25 km nécessite une profondeur de décollement à 25 km de profondeur dans le socle.

gion [72,89] where indications for synsedimentary tectonics are found in the clastic series of the Saghro-group (PII^3) [92], the Ouarzazate group (PIII) and, progressively fading upward within lowermost Cambrian series. The interpretation of events during the Late Neoproterozoic (600–540 Ma) is still a matter of debate, due in part, at least, to the scarcity of reliable absolute ages. The significance of the basement/cover relationships and the geodynamic context are also still open to discussion: interpretations range from syn-orogenic, Late Panafrican molasse series shed in a collision context, to post-orogenic extension and collapse with the formation of tilted blocks and halfgrabens [55,87,91]. In a most recent interpretation [90], based on the type and volumes of volcanic rocks associated with the PIII Ouarzazate series, the Late Proterozoic extension event is compared with a basin and range extensional setting, with an important production of lower crustal melts. Soulaimani and Piqué [88] even go so far as to propose the present-day Anti-Atlas boutonnières as being re-activated former metamorphic core complexes.

1.2. The cover

Prior to folding, the Palaeozoic cover series of the Anti-Atlas must have represented a fairly regular layer cake configuration. Overall thickness reaches 10 km and more in the westernmost Anti-Atlas near Tiznit and decreases to about 6 km and less in the easternmost Anti-Atlas of the Tafilalt. In terms of rheological basement/cover relationships, the sedimentary cover series is best defined as starting with the first carbonate-bearing units of the lowermost Adoudounian, following in most places concordantly upon the coarse-grained PIII conglomerates of the Ouarzazate series. This limit makes a major colour contrast in the field and it is easily visible in satellite images. The PIII behaves as a competent basement-like unit, while the well-layered carbonates above it are increasingly detached and folded at different wavelengths from meters up to kilometres. Despite some prevailing uncertainties, the PIII/Adoudounian transition just above coincides with the Latest Proterozoic/Cambrian boundary [18,38]. There is good evidence for some extensional tectonics continuing upward into the Earliest Cambrian (Lower carbonate series of the Adoudounian) at least in the western Anti-Atlas region [3,9,10]. Lateral correlations are greatly facilitated by the presence of fossils and characteristic facies assemblages and the Anti-Atlas cover figures among the best studied Palaeozoic series worldwide [11,17,29,37,50,64,73,101]. A schematic compilation in the form of a time chart along a strike parallel line is shown in Fig. 4.

Overall, the Anti-Atlas cover series are predominantly deposited in a shallow marine environment. Important platform carbonate build-ups are observed during the Lower Cambrian of the western Anti-Atlas [13,38]. From Middle Cambrian to Late Silurian times, sedimentation is dominated by detrital input from the African craton, i.e. from the east and/or the south [17,

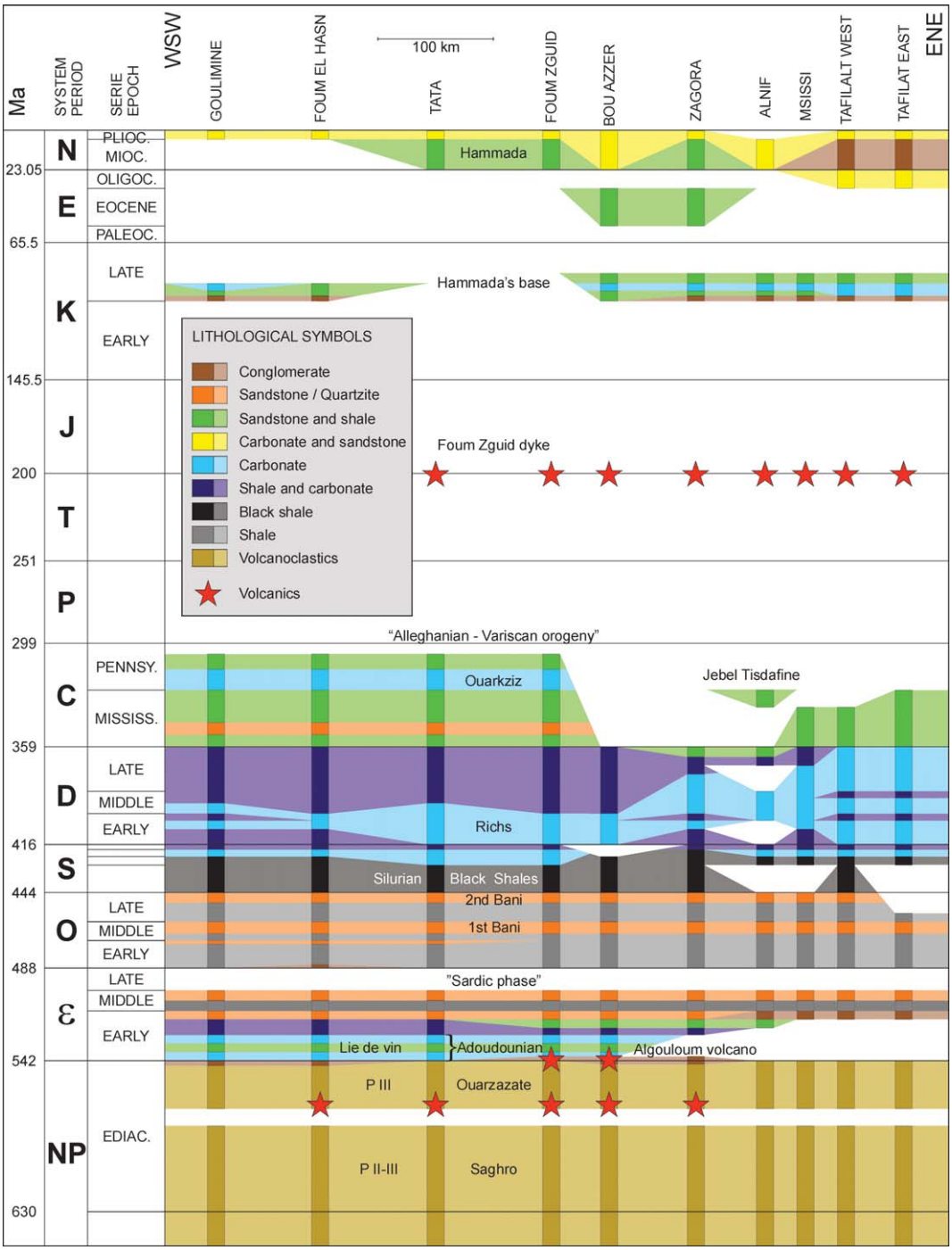

Fig. 4. Schematic chronostratigraphy of the Anti-Atlas. Vertical axis is time [40], horizontal axis is a section along strike from west to east (see Fig. 2 for locations). For each vertical column, stratigraphic data have been collected and projected from northwest (older) to southeast (younger) transects. Colour coding (see legend) is used to illustrate the dominant character of sedimentation. White is for no deposition and/or erosion. Informal formation names as well as major events are indicated.

Fig. 4. Schéma chronostratigraphique pour l'Anti-Atlas. L'axe vertical est le temps [40], l'axe horizontal est une coupe ouest–est le long de la chaîne (voir la Fig. 2 pour la localisation des transects). Pour chaque colonne verticale, les données stratigraphiques ont été compilées et projetées depuis le nord-ouest (vieux) et le sud-est (jeune). Le code couleur indique le caractère dominant de la sédimentation (voir légende). Les lacunes de non dépôt ou d'érosion sont laissées en blanc. Les appellations informelles des formations ainsi que certains événements majeurs sont indiqués.

28]. Carbonate sedimentation is resumed at the end of the Silurian [50] and lasts for most of the Devonian, being combined with clastic inputs, throughout the Anti-Atlas region and beyond [100]. The Lower Carboniferous [59] is marked by an renewed increase in detrital input from the east, south and in places from the north [66,73]. Regional-scale facies and thickness changes point toward an open ocean to the west and northwest throughout the Palaeozoic. It is therefore tempting to interpret the Anti-Atlas basin as the landward tier of the former passive margin of Gondwana, facing west and northwestward. In the preserved stratigraphic record, the shelf break, continental slope and rise of this ancient passive margin wedge are missing, however. In comparison with contemporaneous North-African Palaeozoic basins such as Tindouf, Reggane, Béchar, Ahnet, Ghadames, Illizi, Hamra, Murzuq [12], the Anti-Atlas cover series appears as just another intracratonic basin, which happened to be close enough to the continental edge to be more massively involved in Late Palaeozoic collision tectonics than its neighbours.

1.3. Cover series as a mirror of distant tectonic events?

Palaeozoic sedimentation of the Anti-Atlas region is fairly continuous throughout, and minor disconformities are most easily explained in terms of sequence stratigraphy, i.e. sea-level and/or climatic changes. Probably the most important climatic events are the Late Ordovician glaciations, recorded within the 2nd Bani microconglomerates [39,56,95] and an associated erosional discordance. The following sea-level rise is hold responsible for the deposition of the thick interval of Silurian black shales, a major source rock of the North-African realm [12,68] and a potential décollement horizon. The famous Devonian Kellwasser–event at the Frasnian/Famennian boundary [16,54] is probably a meteorite impact that left its imprint in the faunal assemblages.

As illustrated in Fig. 4, there is only one noteworthy interruption of the Palaeozoic sedimentary cycle in the Late Cambrian. Classically, it has been correlated with a sardic phase of orogeny [64] or with an epeirogenetic uplift [29]. The widespread (although not absolute) nature of this hiatus, common to all North-African basins from Morocco through Tunisia, Algeria to Libya [25] speaks for a general, eustatic, rather than a local, tectonic origin. Crossley and McDougall [26, (p. 160)] quote evidence for block faulting and marked angular unconformities in Algeria; similar evidence is missing in the Anti-Atlas of Morocco, where some lateral thickness changes are subtle at best, and strongly overprinted by later folding. Higher up in the stratigraphic column, subtle lateral facies changes, sedimentary wedges and minor erosional disconformities have long been interpreted as echoing distant tectonic phases such as Taconic, Acadian, Bretonne and Sudète [64], known from either the Appalachian or the European Variscides. New palaeogeographic reconstructions (Fig. 6) of the evolution of Gondwana and the reassembly of Pangea provide a reference frame against which such statements can be tested [83,86,93].

The Late Cambrian hiatus could be interpreted as related to a new phase of rifting further north and concomitant erosion on a southern rift shoulder. At least two important Palaeozoic rifting phases have indeed been postulated to occur along the northern border of Gondwana [93]. Avalonian (and Armorican, etc.) terranes or continental fragments are supposed to originate from the northern margin of Gondwana in Cambrian times, leading to the opening of the Rheic Ocean. A second rifting event of Hunic terranes during the Lower Silurian would have led to the formation of the Palaeo-Tethys ocean [93, (Fig. 3)]. In this proposal, future Avalonian and Hunic terranes represent former active subduction margins off the northwestern African craton. Both terranes would have drifted away after two successive stages of back-arc rifting giving way to two (Rheic, Paeothethys) Palaeozoic oceans. This proposal opens new perspectives in the interpretation of events known in the various Palaeozoic terrains of Morocco. The Anti-Atlas–Tindouf basin would not have been anywhere close to the open ocean prior to Late Silurian times. We see little evidence for rifting phases from Middle Cambrian times onward, however, and the easiest interpretation is to assume that none of those rifting events did take place anywhere close to the Anti-Atlas basin, but rather in a more external position or in a different place along the northern margin of Gondwana. The former passive margin of Gondwana would be entirely obscured by the future Atlantic rifting and hidden below the Mesozoic onshore and offshore basins. Alternatively, the Anti-Atlas basin could be interpreted as the southeastern half of an oblique back-arc basin that evolved into a passive margin in Silurian–Devonian times, after a (right lateral?) strike-slip departure of Hunic terranes.

On a local scale, geologists have also long tried to correlate events between the Meseta, north of the present-day High Atlas chain, and the Anti-Atlas [70, 73,74]. There is no direct evidence for the existence of any kind of tectonic deformation within the Anti-Atlas at least up to Middle Carboniferous times. It is thus

quite obvious that the Moroccan Meseta underwent a very different tectonic history as compared to that of the Anti-Atlas, from the Ordovician onward [69,71]. Many parts of the complex assemblage of units in the Meseta have suffered several intense phases of deformation, metamorphism including the intrusion of granites in Silurian times and from the Lower Carboniferous onward [49]. In this respect, the Meseta is comparable to the internal Appalachian chain, with its Taconic and Acadian belts. The most important question still open in this context regards the relative position of the Moroccan Meseta block with respect to the stable African craton. In the light of the most widely accepted plate tectonic models [86], the Meseta might be regarded as a small continental fragment (or terrane) rifted off the northern margin of Gondwana during an ill-defined period in the Lower Palaeozoic, comparable to Avalonia and the more recently postulated Hunic terranes [93]. Such fragments would have been accreted again to the African craton only during the latest stages of continent–continent collision in Late Carboniferous [14, 33]. Such mobilistic proposals have been made as early as 1971 by Schenk [82], but the lack of an identified suture between the Anti-Atlas domain and the Meseta and the similarities in the Lower Palaeozoic stratigraphic record are quoted as evidence against such a scenario [49,51,52,71,73,75]; a recent confirmation of the Meseta block being of African affinity is provided by crustal xenoliths found in Triassic lamprophyres [31].

2. Anti-Atlas: what kind of sedimentary basin?

The Anti-Atlas Basin has been involved in Late Palaeozoic folding, uplift and erosion and it is therefore difficult to establish its true initial shape and extent to the west and to the north, where the Alpine High Atlas is a further obstacle to restorations. East and southeastward, the transition towards the neighbouring petroleum bearing Palaeozoic basins of Bechar and Reggane are somewhat obscured by a thin blanket of Upper Cretaceous sediments (Hamada), but compilations from reflection seismics reveal the gross trends in the form of isopach contour maps shown in Fig. 1 [6,102]. The Anti-Atlas actually appears to be the northern half of the Tindouf Basin. It is not clear if the two are separated from each other by some sort of swell or basement high, nor is there any known reason for the localization of the remarkably smooth trend of the Ouarkziz chain (Fig. 1), which represents the deformation front of the Anti-Atlas belt to the SSE (Figs. 2 and 3) – and the northern border of the Tindouf basin. A strike-slip boundary (of Alpine age) has been proposed to run along Drâa lowland north of the Jbel Ouarkziz [99], but field evidence seemingly rules out any significant wrenching of any age to occur in this area [20,47,91]. To the east, the Anti-Atlas belt – or basin – turns gradually into the Ougarta chain [30,48]. Just as in the case of the Anti-Atlas belt, folding, uplift and erosion prohibit the establishment of original isopach contours for the former Ougarta Basin, but it is quite clear that this intratratonic chain is localized along a former trough of NW–SE orientation. The same structural trend is also present in neighbouring basins of Reggane and Bechar and it is generally admitted that this direction is inherited from the Panafrican orogeny [24]. Our compilation in Fig. 1 further illustrates the location of the different Palaeozoic basins with respect to the Appalachian–Variscan chain and the subsequent rifting axis of the Atlantic [80]. The question arises of what was the geodynamic setting of these different North-African basins. Is the Anti-Atlas Basin a remnant part of a passive margin of Gondwana (Fig. 6)? The total thickness of the sedimentary pile alone might be used as an argument in favour of a passive margin setting for the Anti-Atlas with the freeboard to the WNW. Other Palaeozoic basins, however, at hundreds of kilometres inboard, accumulated similar total sediment thicknesses in clearly intracratonic settings (Taoudenni > 8 km, Murzuq > 6 km). The same is true for large Palaeozoic basins on the American craton such as the Michigan (ca. 5 km) and to a lesser degree Williston, Illinois, and Hudson Bay [57]. A major argument against a passive margin interpretation is the lack of any sedimentary record for deposits from the outer shelf, talus and continental rise. Despite some general tendency to more open marine conditions westward, there are no deep water sediments preserved anywhere in the Anti-Atlas (with the exception of some debatable flysch deposits of Carboniferous age at the northern border near the High-Atlas front [66]. The determination of palaeo-water depths within the Carboniferous clastic series of the Anti-Atlas remains a matter of controversy, however. Sedimentary structures, such as graded bedding and intense convolute bedding as well as the presence of olistrostromes has been used as an indication for turbiditic flysch type sediments laid down in deep water in a compressional context [66]; we could not find any convincing flysch sequences, however, and a shallow water origin in a coastal and deltaic environment seems an equally appropriate interpretation of the sedimentary structures [41,59].

A neutral reading of the stratigraphic record of the Anti-Atlas (Figs. 4 and 5) reveals an eventless subsidence history very comparable to contemporaneous intracratonic basins of North America [7,53]. The to-

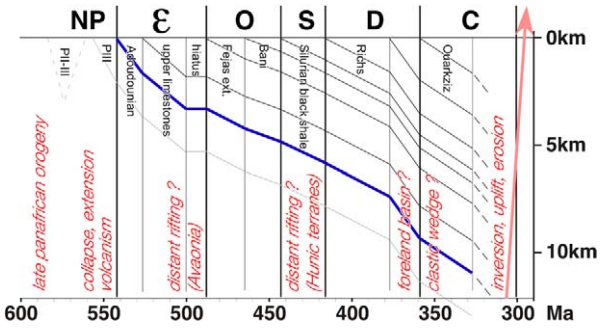

Fig. 5. Sediment accumulation curve for southwestern Anti-Atlas (between the Goulimine and Foum el Hassan transects). Horizontal axis is time [40], vertical axis is sediment thickness as observed today, compiled from a vast body of stratigraphic literature regarding the western Anti-Atlas. No decompaction, palaeo-water-depths, eustatic corrections nor back-stripping has been applied. Principal informal formation names are given along the top of the chart, while major events of the Gondwana margin are indicated at the bottom.

Fig. 5. Courbe d'accumulation sédimentaire pour l'Anti-Atlas sud-ouest entre les transects de Goulimine et de Foum el Hassan (voir Fig. 4). L'axe horizontal donne le temps, linéaire en millions d'années, l'axe vertical donne l'épaisseur des sédiments en kilomètres. Les données ont été compilées à partir d'un grand nombre de publications concernant la stratigraphie de l'Anti-Atlas occidental. Aucune correction de décompaction, de paléo-profondeur d'eau, d'eustatisme ou de délestage n'a été appliquée. Les principaux noms de formations, informels, sont donnés en haut du graphique, tandis que les événements tectoniques majeurs sur la bordure de Gondwana sont indiqués en bas.

tal accumulation curve shown in Fig. 5 illustrates the general difficulty in the interpretation of such linear on and off subsidence trends. In the case of the Anti-Atlas, more than 10 km of shallow marine sediments were accumulated over a time span of almost 200 Ma. Even though we have not applied any decompaction nor backstripping procedure, it is quite clear that this curve lacks tell-tale features of rapid tectonic rifting followed by thermal subsidence as expected in the case of a rift–drift passive margin evolution [4]. Just as in the case of the Michigan [53] and of many other intracratonic basins, the underlying mechanism of subsidence remains enigmatic [57,85]. Explanations put forward include thermal decay, uncompensated masses, imposed load as well as the far field, flexural response to tectonic compressional forces and lithospheric buckling [85,103, 104]. The only rifting phase that left its imprint in the rock record is ill constrained in its age; the terminal Proterozoic PIII–Lower Cambrian basal conglomerate and lower limestone series are all deposited in a rifting context as confirmed by a magmatic suite of calco-alkaline to tholeiite–alkaline volcanics [90]. Even this rifting event does not clearly show up in Fig. 5 either, with less than 2 km preserved thickness of PIII series, unless we assume the Late Proterozoic rifting was short and very late. Alternatively, and more probably, the Anti-Atlas was the locus of a major broad thermal dome with limited syn-rift deposits in widely distributed small graben and half-graben systems, rather than a well defined narrow rift trough with associated shoulders. Subsequently, this broad swell (or basin and range-type collapse?) would not have led to any successful rifting in the Anti-Atlas region but to a long phase of thermal subsidence throughout the Palaeozoic.

3. The Anti-Atlas chain – what kind of fold belt?

The western Anti-Atlas chain is dominated by highly cylindrical, upright fold trains. In contrast to the Appalachians and other foreland fold-and-thrust belts worldwide [77,78], there is no evidence for any thin-skinned thrusting with the exception of the westernmost parts of the Anti-Atlas along the Atlantic coast [8,65] and some blind thrusting below the Ouarkziz ridge. In our interpretation [19,47], the Ouarkziz ridge, a slightly curved monocline of more than 400 km length, is the surface expression of a triangle structure [97]. We postulate the existence of a blind thrust to end somewhere below the Tindouf Basin and a major NNW-vergent backthrust to re-emerge within a thick series of shales above the Devonian Rich, tightly folded and pushed under the Carboniferous Ouarkziz monocline (Fig. 3). This mountain front of the southwestern Anti-Atlas is progressively loosing its significance eastward, however [36]. East of Tata, Anti-Atlas fold trains are decreasing in number and individual folds are decreasing in amplitude, tightness and cylindricity. There is also a change in general orientation from SW–NE to east–west and the Anti-Atlas fold belt seems to merge with the Ougarta chain of SE–NW orientation [24,30,48].

Some layer-parallel décollements and multiple detachments are obviously required between different structural levels, each folded with its own characteristic wavelength and amplitude, but no such décollement has ever been mapped to step up in a ramp-flat geometry across competent beds. Our recent structural analyses [20,47] confirm previous studies [23,64] in the sense that individual marker beds are just folded, but never thrust upon each other in a duplex style. We conclude that the Anti-Atlas folds are a natural case of truly polyharmonic buckle folding. The abundance of incompetent shales allowed the subordinate competent beds such as the Ordovician Bani quartzites and the Devonian Richs carbonates to develop their own characteristic folds. Overall map scale shortening on the order of 10 to 20% was accommodated without (cover-)thrusting [47] and the Anti-Atlas defies any straightforward interpre-

tation in terms of a classic thin-skinned thrust system organization [15].

On the crustal scale, however, the cover shortening determined across the western Anti-Atlas fold belt, poses a serious balancing problem: where and how is this shortening accommodated within the basement? Large structural domes, the so-called *boutonnières* [22] of Proterozoic basement rocks, crop out at a very short distance behind the south-eastern front of the south-western Anti-Atlas and these basement inliers punctuate the tightly folded Palaeozoic cover. The lack of any mapped thrusts has led earlier authors to consider even these basement uplifts as just another, deeper level of crustal scale folds [22,23] dubbed *plis de fonds* by Argand (Fig. 5A–C) [5]. Balancing and rheology considerations make such a gentle folding interpretation improbable [67], however, and we infer that the Anti-Atlas basement uplifts must be associated with a series of major crustal scale reverse faults, supposedly in a Windriver-style well known in the foreland of the Rocky Mountains [67,76,94]. This uncommon proposal is illustrated in a section across the western tip of the Adrar Zouggar anticlinorium (Fig. 3) [27,110]. The backbone of this structure is made of Ordovician quartzites [27] and drilling in the 1960s has documented the existence of a basement core at −3.4-km depth, at least 2.5 km above the regional basement top (−5 km) as constructed between the synclinorium to the north and the Tindouf basin to the south. Gently plunging fold axis allows the projection of the Jbel Rich (Devonian carbonates) folds above the top of this anticlinorium. Southward, deformation ends below the Jbel Ouarkziz triangle structure, while northward, another major basement uplift of the Tagragra d'Akka boutonnière has led to a complete removal of all cover series. The tightly folded Bani (Ordovician) clearly projects above this basement uplift, however. The Adrar Zouggar and Tagragra d'Akka anticlinoria nicely illustrate the balancing problem associated with such basement 'folds'. A conservative unfolding of the well-exposed Devonian and Ordovician marker beds reveals a minimum of 12 to 15% shortening ratio – this amounts to some 17 km of minimum line-length shortening (Fig. 3). In order to compensate this shortening at the basement level, we postulate the existence of a set of rather steep (40 to 60°) faults, possibly Late Proterozoic normal faults that would have been strongly inverted. This structural style cannot be mapped in the case of the Adrar Zouggar, but it is compatible with structural observations made along the borders of more internal, deeply eroded basement inliers such as the Tagragra de Tata [21,47]. Simple area balancing considerations allow us to estimate the depths of detachment. With an excess area of ca. 380 km^2 of basement above regional, a minimum shortening estimate of 17 km requires a basal detachment in the lower crust, at ca. −32 km depth (Fig. 3). Note that present-day Moho depth is thought to be at ca. −35 km [36] at least. A more likely estimated horizontal shortening of some 25 km, taking into account layer-parallel shortening features and other bed internal strains [47], would lead to a lesser depth of detachment at mid-crustal levels of ca. −25 km (Fig. 3).

The Appalachians also used to have their basement problem in the form of the Blue Ridge (Fig. 1), a linear belt pre-Cambrian basement rocks of Grenvillian, i.e. American craton affinity [44,63,79] cropping out at some distance behind the thin-skinned frontal Valley and Ridge fold-thrust belt. While these basement uplifts have long been considered as more or less autochthonous too, crustal scale seismic reflection profiling has provided clear evidence of a truly allochthonous nature of these basement slivers, detached from the former edge of the passive margin and thrust craton-ward by up to 200 km! [44, plate 1, section C], a tectonic style anticipated by Argand [5, (Fig. 5, case E)], [63]. In comparison, our inversion interpretation of the Anti-Atlas basement domes remains very modest and autochthonous indeed and the question arises if a Blue Ridge type interpretation would not be more appropriate in the case of the Anti-Atlas? We have not found any positive arguments in favour of such an analogy, and we conclude that the similarities between the Appalachians and Anti-Atlas fold belts are not extending far below the geomorphic expression of a common Appalachian relief. We further propose the structural style of the Anti-Atlas belt being a rather unique combination of basement uplifts in a Windriver style that happened to occur below a more than 10-km-thick series of mostly soft, shale dominated sediments. Tectonic compression of this Palaeozoic basin leads to a massive inversion of the underlying basement structures and a simultaneous polyharmonic buckle folding of the basin fill. Despite its proximity to the Appalachian–Variscan chain, the Anti-Atlas is not easily classified as a foreland fold-thrust belt to this orogen. In many respects, it is rather to be considered as a severely inverted intracratonic basin – related to the orogen on a crustal to lithospheric scale, supposedly with a floor thrust at mid to lower crustal level. The Anti-Atlas belt has a direct connection to the Ougarta–Ahnet fold belts, but other North-African basins suffered a similar inversion event at the end of the Palaeozoic [24,42] in more isolated, clearly intra-cratonic settings. Some striking analogies in structural style and complexity also exist with the Iberian chain, an intraplate Cretaceous

inversion structure in the southern foreland of the Pyrenees [84].

Interestingly, there are no intracratonic structures of Palaeozoic age known cratonward of the Alleghenian mountain front of the Appalachians. However, the very same craton reacted quite sensitively to Rocky Mountain deformations and subduction along its western border, with the formation of basement uplifts and inversion of many old graben structures hundreds of kilometres eastward, well within the North American craton [60].

4. Conclusion: plate tectonic setting through time (Cambrian to Permian)

The tectonic evolution of the Anti-Atlas basin and fold belt in relation to plate tectonics on a global scale is illustrated in Fig. 6, and summarized below:

– during the Panafrican orogeny, a series of terranes are accreted to the West African craton on its northern and probably western side. While the northeastern suture (Bou Azzer) and terranes to the northeast will remain in place, northwestern and western borders are subsequently reactivated and a series of terranes or continental fragments will be ripped off again during the Palaeozoic. The southwestern Anti-Atlas, however, at the margin of the Saharan metacraton [1] remains attached to Gondwana throughout its Palaeozoic history;
– in Late Proterozoic–Early Cambrian, the Anti-Atlas area is in extension with the formation of many widely distributed graben and halfgraben structures, filled in with coarse clastics (PIII) mostly of igneous origin. The youngest volcanism is tholeiitic–alkaline and indicates an intracontinental

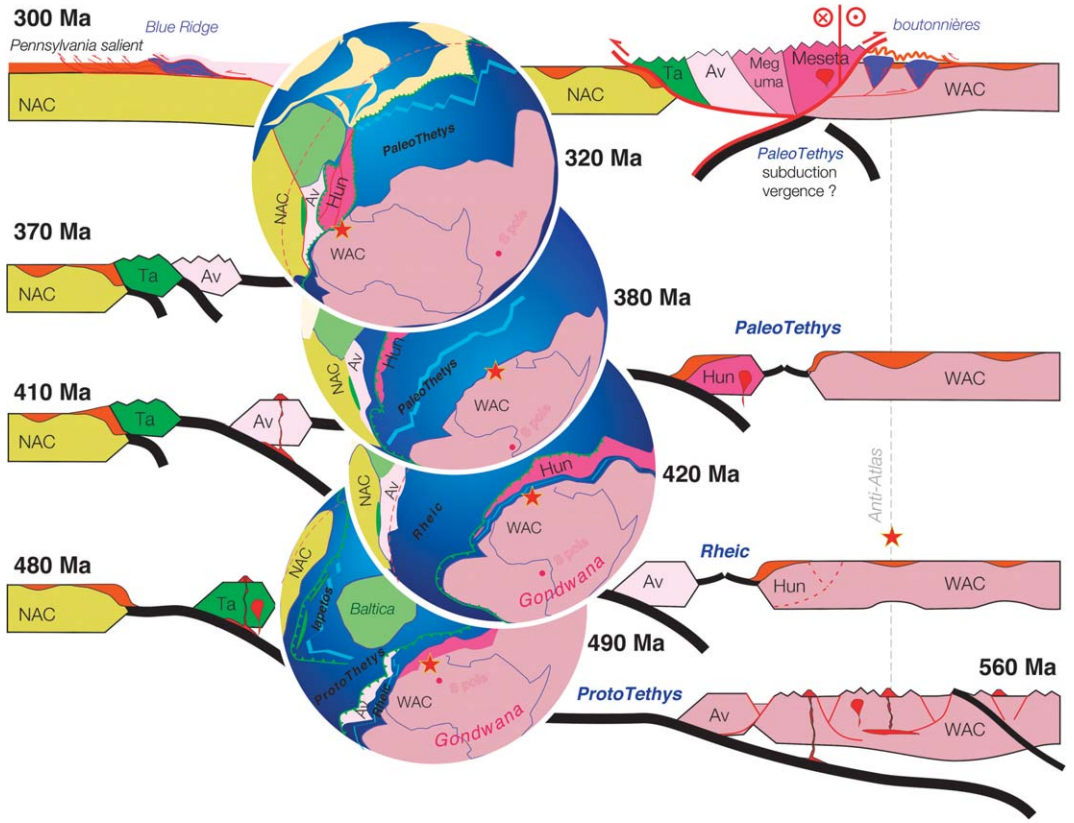

Fig. 6. Schematic evolution of the Anti-Atlas (star) in comparison with the Appalachian chain through time on a global, plate tectonic scale. Palaeo-tectonic reconstructions are redrawn and simplified from Stampfli and Borel [93]. Cross sections (cartoons) on the left-hand side (Appalachians) are according to Fichter [34].

Fig. 6. Évolution schématique de l'Anti-Atlas (étoile) en comparaison avec la chaîne des Appalaches à travers le Paléozoïque, à une échelle globale. Les cartes paléo-tectoniques ont été redessinées et simplifiées à partir de Stampfli et Borel [93]. Les coupes schématiques à gauche (Appalaches) sont selon Fichter [34].

setting. The geodynamic significance of this extensional event is not entirely clear, however. It could be related to a southeast dipping, major and long-lived subduction zone on the northwestern margin of Gondwana, causing a wide area of extension cratonward in a basin and range style. Alternatively, extension could be due to a (series of) hot spot(s) within Gondwana;

– from Middle Cambrian through Middle Carboniferous, the western Anti-Atlas basin is characterized by a strong and essentially linear subsidence trend, leading to the accumulation of more than 10 km of mostly fine-grained clastic sediments, shed into an epicontinental sea from the African craton. There is little evidence in this stratigraphic record for tectonic events postulated to have taken place along the active northwestern plate margin of Gondwana [93]. The departure of Avalon, Armorica and Hunic terranes from this margin in successive events of back-arc spreading must have brought the Anti-Atlas Sea increasingly closer to the open ocean(s) (Rheic and Palaeo-Tethys). From Silurian times onward, the Anti-Atlas Basin could thus represent the passive margin of the Palaeo-Tethys ocean, but very little if any sediments of the more distal parts of this passive margin are preserved anywhere (with the possible exception of terrains west of Guelmin [8] and near Tineghir [66]);
– in Late Carboniferous–Permian (?) compression leads to an event of strong inversion and folding. Basement is uplifted and folded into huge antiformal culminations (*boutonnières)* which punctuate the southwestern Anti-Atlas fold belt. The structural relief of the basement culminations is in excess of 10 km; minimum estimates of total shortening are 15 to 25 km. The Anti-Atlas belt does not represent a classical frontal, thin-skinned foreland fold-and-thrust-belt of the Appalachian–Variscan orogen, however, but rather an intracratonic, thick-skinned basement inversion belt. Similar time-equivalent belts occur further east into the African craton (Ougarta, Ahnet), but no such structures are known on the American side of the Appalachian chain.

In conclusion, the Anti-Atlas was a fence-rider throughout, watching the action from a distance, not paying any tribute, nor suffering too much from the events going on all along the very active margins of Gondwana [49,62].

References

[1] M.G. Abdelsalam, J.-P. Liégeois, R.J. Stern, The Saharan Metacraton, J. Afr. Earth Sci. 34 (3–4) (2002) 119–136.

[2] H. Ait Malek, D. Gasquet, J.-M. Bertrand, J. Leterrier, Géochronologie U–Pb sur zircon de granitoïdes éburnéens et panafricains dans les boutonnières d'Igherm, du Kerdous et du Bas Drâa (Anti-Atlas occidental, Maroc), C. R. Acad. Sci. Paris, Ser. IIa 327 (1998) 819–826.

[3] A. Algouti, A. Algouti, B. Chbani, M. Zaim, Sédimentation et volcanisme synsédimentaire de la série de base de l'Adoudounien infra-cambrien à travers deux exemples de l'Anti-Atlas du Maroc, J. Afr. Earth Sci. 32 (4) (2001) 541–556.

[4] P.A. Allen, J.R. Allen, Basin Analysis, Blackwell Scientific Publications, Oxford, 1990.

[5] E. Argand, La tectonique de l'Asie, in : 13th International Geological Congress, Brussels, 1924.

[6] T. Arthur, D.S. MacGregor, N.R. Cameron, Petroleum geology of Africa, new themes and developing technologies, Geological Society, London, Spec. Publ. 207 (2003).

[7] A.W. Bally, Phanerozoic basins of North America, in: A.-W. Bally, A.-R. Palmer (Eds.), The Geology of North America: An Overview, Geol. Soc. Am., 1989, pp. 397–446.

[8] M.A. Belfoul, F. Faik, B. Hassenforder, Evidence of a tangential tectonic event prior to the major folding in the Variscan belt of the western Anti-Atlas, Morocco, J. Afr. Earth Sci. 32 (4) (2002) 723–739.

[9] M. Benssaou, N. Hamoumi, The Lower-Cambrian western Anti-Atlasic graben: tectonic control of paleogeography and sequential organisation, C. R. Geoscience 335 (2003) 297–305.

[10] M. Benssaou, N. Hamoumi, Les microbialites de l'Anti-Atlas occidental (Maroc) : marqueurs stratigraphiques et témoins des changements environnementaux au Cambrien inférieur, C. R. Geoscience 336 (2004) 109–116.

[11] J. Bertrand-Sarfati, A. Moussine-Pouchkine, P. Affaton, R. Trompette, Y. Bellion, Cover sequences of the West African Craton, in: R.D. Dallmeyer, J.-P. Lécorché (Eds.), The West African Orogens and Circum Atlantic Correlatives, Springer-Verlag, Berlin, 1991, pp. 65–82.

[12] D.R.D. Boote, L.D.D. Clark, M.W. Traut, Palaeozoic petroleum system of North Africa, in: D.S. MacGregor, R.T.J. Moody, D.D. Clark Lowes (Eds.), Petroleum Geology of North Africa, Geological Society, London, 1998, pp. 7–68.

[13] A. Boudda, G. Choubert, A. Faure-Muret, Essai de stratigraphie de la couverture sédimentaire de l'Anti-Atlas : Adoudounien–Cambrien inférieur, Notes Mém. Serv. géol. Maroc 271 (1979) 96.

[14] J. Boulin, M. Bouabdelli, M. El-Houicha, Évolution paléogéographique et géodynamique de la chaîne Paléozoïque du moyen Maroc : un essai de modélisation, C. R. Acad. Sci. Paris, Ser. II 306 (1988) 1501–1506.

[15] S.E. Boyer, D. Elliott, Thrust systems, AAPG Bull. 66 (9) (1982) 1196–1230.

[16] W. Buggisch, The global Frasnian–Famennian 'Kellwasser Event', Geol. Rundsch. 80 (1) (1991) 49–72.

[17] W. Buggisch, R. Siegert, Paleogeography and facies of the 'grès terminaux'; uppermost Lower Cambrian, Anti-Atlas, Morocco, in: V.H. Jacobshagen (Ed.), The Atlas System of Morocco; Studies on its Geodynamic Evolution, Springer-Verlag, Berlin–Heidelberg–New York, 1988, pp. 107–121.

[18] W. Buggisch, E. Fluegel, The Precambrian/Cambrian boundary in the Anti-Atlas (Morocco); discussion and new results, in: V.H. Jacobshagen (Ed.), The Atlas System of Morocco; Studies on its Geodynamic Evolution, Springer-Verlag, Berlin–Heidelberg–New York, 1988, pp. 81–90.

[19] M. Burkhard, S. Caritg, U. Helg, C. Robert-Charrue, Forced, disharmonic multilayer buckle folding in the Late Variscan Anti-Atlas of Morocco, in: AAPG Annual Meeting, 2001, p. 30.

[20] S. Caritg, Géologie structurale dans l'Anti-Atlas occidental du Maroc. Implications tectoniques sur les relations entre dômes de socle et couverture plissée en front de chaîne de montagne, PhD thesis, University of Neuchâtel, 2003.

[21] S. Caritg, M. Burkhard, R. Ducommmun, U. Helg, L. Kopp, C. Sue, Fold interference patterns in the late Paleozoic Anti-Atlas of Morocco, Terra Nova 16 (1) (2003) 27–37.

[22] G. Choubert, Histoire géologique du Précambrien de l'Anti-Atlas, Notes Mém. Serv. géol. Maroc 162 (1963) 352.

[23] G. Choubert, A. Faure-Muret, Anti-Atlas (Maroc), in: Tectonic de l'Afrique, in: UNESCO Earth Sci. Series, 1971, pp. 163–175.

[24] M.P. Coward, A.C. Ries, Tectonic development of North African basins, in: T. Arthur, S. MacGregor Duncan, N.R. Cameron (Eds.), Petroleum Geology of Africa; New Themes and Developing Technologies, Geological Society, London, 2003, pp. 61–83.

[25] R. Crossley, N. Mcdougall, Lower Palaeozoic reservoirs of North Africa, in: D.S. MacGregor, R.T.J. Moody, D.D. Clark Lowes (Eds.), Petroleum Geology of North Africa, Geol. Soc. London, 1998, pp. 157–166.

[26] R. Crossley, N. McDougall, D.S.E. MacGregor, R.T.J.E. Moody, D.D.E. Clark-Lowes, Lower Palaeozoic reservoirs of North Africa Petroleum geology of North Africa, Geol. Soc. London, Spec. Publ. 132 (1998) 157–166.

[27] F. Desthieux, Etude tectonique et métallogénique du Jbel Addana, Ordovicien des plaines du Dra, Maroc présaharien, Notes Serv. géol. Maroc 268 (38) (1977) 209–236.

[28] J. Destombes, The Ordovician of the Moroccan Anti-Atlas, in: M.G. Bassett (Ed.), The Ordovician System, Univ. Wales Press and Natl. Mus. Wales, 1976, pp. 411–413.

[29] J. Destombes, H. Hollard, S. Willefert, Lower Paleozoic rocks of Morocco, in: C.H. Holland (Ed.), Lower Palaeozoic of North-Western and West-Central Africa, Trinity Coll., Dep. Geol., Dublin, Ireland, 1985, pp. 91–336.

[30] M. Donzeau, J. Fabre, Tectonique des monts d'Ougarta, in: Lexique stratigraphique international, Afrique de l'Ouest : introduction géologique et termes stratigraphiques, N.S.N., 1983, pp. 118–120.

[31] J. Dostal, J.D. Keppie, J. Hamilton, E.M. Aarab, J.P. Lefort, J.B. Murphy, Crustal Xenoliths in Triassic lamprophyre dykes in western Morocco: tectonic implications for the Rheic Ocean suture, Geol. Mag. 142 (2) (2005) 159–172.

[32] N. Ennih, J.-P. Liégeois, The Moroccan Anti-Atlas; the West African craton passive margin with limited Pan-African activity; implications for the northern limit of the craton, Precambr. Res. 112 (3–4) (2001) 289–302.

[33] H. Feinberg, T. Aifa, J.-P. Pozzi, D. Khattach, J. Boulin, Courbes de dérive apparente des pôles magnétiques de l'Afrique et de la Meseta marocaine pendant le Paléozoique, C. R. Acad. Sci. Paris, Ser. II 310 (1990) 913–918.

[34] L. Fichter, Geologic History of Virginia, http://Csmres.jmu.edu/geollab/vageol/vahist/introduc.html, http://csmres.jmu.edu/geollab/vageol/vahist/K-LatPal.html, accessed January 2005.

[35] D. Frizon de Lamotte, B. Saint-Bezar, R. Bracene, E. Mercier, The two main steps of the Atlas building and geodynamics of the western Mediterranean, Tectonics 19 (4) (2000) 740–761.

[36] D. Frizon de Lamotte, A. Crespo-Blanc, B. Saint-Bézar, M. Comas, M. Fernàndez, H. Zeyen, P. Ayarza, C. Robert-Charrue, A. Chalouan, M. Zizi, A. Teixell, M.-L. Arboleya, F. Alvarez-Lobato, M. Julivert, A. Michard, TRANSMED Transect I: Iberian Meseta–Guadalquivir Basin–Betic Cordillera–Alboran Sea–Rif–Moroccan Meseta–High Atlas–Sahara Platform, in: W. Cavazza, et al. (Eds.), The TRANSMED Atlas: The Mediterranean Region from Crust to Mantle, Springer, Berlin, 2004, p. 141 & CD-ROM.

[37] G. Geyer, E. Landing (Eds.), MOROCCO'95 – The Lower–Middle Cambrian standard of western Gondwana, Beringeria, Special Issue 2, University of Würzburg, Germany, 1995.

[38] G. Geyer, E. Landing, W. Heldmaier, Faunas and depositional environments of the Cambrian of the Moroccan Atlas region, in: G. Geyer, E. Landing (Eds.), MOROCCO'95 – The Lower–Middle Cambrian Standard of Western Gondwana, Beringeria, Special Issue 2, University of Würzburg, Germany, 1995, pp. 47–119.

[39] J.-F. Ghienne, Late Ordovician sedimentary environments, glacial cycles, and post-glacial transgression in the Taoudenni Basin, West Africa, Palaeogeogr. Palaeoclimatol. Palaeoecol. 189 (3–4) (2003) 117–145.

[40] F.M. Gradstein, et al., International Stratigraphic Chart, http://www.stratigraphy.org/chus.pdf, Stratigraphy I.C.O. Editor, 2004.

[41] J.R. Graham, Wave-dominated shallow-marine sediments in the Lower Carboniferous of Morocco, J. Sediment. Petrol. 52 (4) (1982) 1271–1276.

[42] H. Haddoum, R. Guiraud, A. Moussine-Pouchkine, Hercynian compressional deformations of the Ahnet–Mouydir Basin, Algerian Saharan Platform: far-field stress effects of the Late Palaeozoic orogeny, Terra Nova 13 (3) (2001) 220–226.

[43] B. Hassenforder, La tectonique panafricaine et varisque de l'Anti-Atlas dans le massif du Kerdous (Maroc), PhD thesis, University of Strasbourg, France, 1987.

[44] R.D. Hatcher Jr., W.A. Thomas, P.A. Geiser, A.W. Snoke, S. Mosher, D.V. Wiltschko, Alleghanian Orogen, in: R.D. Hatcher Jr., W.A. Thomas, G.W. Viele (Eds.), The Geology of North America, The Appalachian–Ouachita Orogen in the United States, Geol. Soc. Am., 1989, pp. 233–318.

[45] K.P. Hefferan, H. Admou, R. Hilal, J.A. Karson, A. Saquaque, T. Juteau, M.M. Bohn, S.D. Samson, J.M. Kornprobst, Proterozoic blueschist-bearing melange in the Anti-Atlas Mountains, Morocco, Precambr. Res. 118 (3–4) (2002) 179–194.

[46] K.P. Hefferan, H. Admou, J.A. Karson, A. Saquaque, Anti-Atlas (Morocco) role in Neoproterozoic western Gondwana reconstruction, Precambr. Res. 103 (1–2) (2000) 89–96.

[47] U. Helg, M. Burkhard, S. Caritg, C. Robert-Charrue, Folding and inversion tectonics in the Anti-Atlas of Morocco, Tectonics 23 (2004) 17, TC 4006.

[48] Y. Hervouët, G. Duée, Analyse morphostructurale par imagerie satellitaire et coupes structurales modélisées des monnts d'Ougarta (Sahara occidental, Algérie) : une chaîne hercynienne chevauchante à plis passifs, Mém. Serv. géol. Algérie 8 (1996) 127–173.

[49] C. Hoepffner, M.R. Houari, M. Bouabdelli, Tectonics of the north African Variscides (Morocco, Western Algeria), an outline, C. R. Geoscience 338 (2006).

[50] H. Hollard, Tableaux de corrélations du Silurien et du Dévonien de l'Anti-Atlas, Notes Serv. géol. Maroc (1981) 42.
[51] H. Hollard, J.P. Schaer, Southeastern Atlantic Canada, Northwestern Africa, and Continental Drift; discussion, Can. J. Earth Sci. 10 (4) (1973) 584–586.
[52] M.R. Houari, C. Hoepffner, Structures des terrains paléozoiques à la limite sud de la chaîne hercynienne du Maroc (Haut Atlas oriental), Afr. Geosci. Rev. 7 (1) (2000) 39–53.
[53] P.D. Howell, B.A. Van der Pluijm, Structural sequences and styles of subsidence in the Michigan basin, Geol. Soc. Am. Bull. 111 (7) (1999) 974–991.
[54] M.M. Joachimski, R.D. Pancost, K.H. Freeman, H.C. Ostertag, W. Buggisch, Carbon isotope geochemistry of the Frasnian–Famennian transition, in: G. Racki, M.R. House (Eds.), Late Devonian Biotic Crisis; Ecological, Depositional and Geochemical Records, Elsevier, Amsterdam, 2002.
[55] M. Leblanc, J.R. Lancelot, Interprétation géodynamique du domaine pan-africain (Précambrien terminal) de l'Anti-Atlas (Maroc) à partir de données géologiques et géochronologiques, Can. J. Earth Sci. 17 (1) (1980) 142–155.
[56] P. Legrand, Paléogéographie du Sahara algérien à l'Ordovicien terminal et au Silurien inferieur, Bull. Soc. géol. France 174 (1) (2003) 19–32.
[57] M.W. Leighton, D.R. Kolata, Selected interior cratonic basins and their place in the scheme of Global Tectonics A Synthesis, in: M.W. Leighton, et al. (Eds.), Interior Cratonic Basins, AAPG, Tulsa, 1990, pp. 729–797.
[58] D.S. MacGregor, R.T.J. Moody, D.D. Clark-Lowes, Petroleum Geology of North Africa, Geological Society London, Spec. Publ. 132 (1998).
[59] B. Mamet, G. Choubert, L. Hottinger, Notes sur le Carbonifère du Jebel Ouarkziz. Étude du passage du Viséen au Namurien d'après les Foraminifères, Notes Mém. Serv. géol. Maroc 27 (1966) 4–21.
[60] S. Marshak, K. Karlstrom, J.M. Timmons, Inversion of Proterozoic extensional faults: An explanation for the pattern of Laramide and Ancestral Rockies intracratonic deformation, United States, Geology 28 (8) (2000) 735–738.
[61] M. Mattauer, F. Proust, P. Tapponnier, Major strike-slip fault of Late Hercynian age in Morocco, Nature 237 (1972) 160–162.
[62] P. Matte, Variscides between the Appalachians and the Urals; similarities and differences between Paleozoic subduction and collision belts, in: J.R. Martinez Catalan, et al. (Eds.), Variscan–Appalachian Dynamics; the Building of the Late Paleozoic Basement, Geol. Soc. Am., 2002.
[63] J.H. McBride, J.H. Knapp, Review of seismic reflector signatures of crustal deformation in the Appalachian-Caledonide Orogen with reference to the Spanish Variscides and the Uralides, in: J.R. Martinez Catalan, et al. (Eds.), Variscan–Appalachian Dynamics; the Building of the Late Paleozoic Basement, Geol. Soc. Am., 2002, pp. 281–300.
[64] A. Michard, Éléments de géologie marocaine, Notes Mém. Serv. géol. Maroc 252 (1976) 408.
[65] A. Michard, J. Sougy, L'orogenèse hercynienne à la lisière nord-ouest de l'Afrique (Structure des chaînes primaires du Maroc au Sénégal), in : Colloque international CNRS : La Chaîne varisque d'Europe moyenne et occidentale, Rennes, France, 1977, pp. 605–640.
[66] A. Michard, A. Yazidi, F. Benziane, H. Hollard, S. Willefert, Foreland thrusts and olistostromes on the pre-Sahara margin of the Variscan Orogen, Morocco, Geology 10 (5) (1982) 253–256.
[67] G. Mitra, V.S. Mount, Foreland basement involved structures, AAPG Bull. 82 (1) (1998) 70–109.
[68] A.M. Morabet, R. Bouchta, H. Jabour, An overview of the petroleum systems of Morocco, in: D.S. MacGregor, R.T.J. Moody, D.D. Clark Lowes (Eds.), Petroleum Geology of North Africa, Geological Society, London, 1998, pp. 283–296.
[69] A. Piqué, Variscan terranes in Morocco, Spec. Pap. Geol. Soc. Am. 230 (1989) 115–129.
[70] A. Piqué, Géologie du Maroc, Les domaines régionaux et leur évolution structurale, PUMAG, Marrakech, 1998.
[71] A. Piqué, Geology of Northwest Africa, Beiträge zur regionalen Geologie der Erde, vol. 29, Gebrüder Bornträger Verlag, Berlin, Stuttgart, 2001.
[72] A. Piqué, M. Bouabdelli, A. Soulaimani, N. Youbi, M. Iliani, Upper Neoproterozoic PIII conglomerates in the Anti-Atlas, southern Morocco; Pan-African molasses, or indicators of Upper Proterozoic rifting?, C. R. Acad. Sci. Paris, Ser. IIa 328 (6) (1999) 409–414.
[73] A. Piqué, A. Michard, Moroccan hercynides: A synopsis. The Palaeozoic sedimentary and tectonic evolution at the northern margin of West Africa, Am. J. Sci. 289 (1989) 286–330.
[74] A. Piqué, J.-J. Cornée, J. Müller, J. Roussel, The Moroccan Hercynides, in: R.D. Dallmeyer, J.O.P. Lécorché (Eds.), The West African Orogens and Circum Atlantic Correlatives, Springer-Verlag, Berlin, 1991, pp. 229–263.
[75] M. Roddaz, S. Brusset, J.-C. Soula, D. Beziat, M. Ben-Abou, P. Debat, Y. Driouch, F. Christophoul, A. Ntarmouchant, J. Deramound, Foreland basin magmatism in the western Moroccan Meseta and geodynamic interferences, Tectonics 21 (5) (2002) 23.
[76] J. Rodgers, Lines of basement uplifts within cratons marginal to orogenic belts, Am. J. Sci. 287 (1987) 661–692.
[77] J. Rodgers, Fold-and-thrust belts in sedimentary rocks. Part 1: Typical examples, Am. J. Sci. 290 (1990) 321–359.
[78] J. Rodgers, Fold-and-thrust belts in sedimentary rocks. Part 2: Other examples, especially variants, Am. J. Sci. 291 (1991) 825–886.
[79] J. Rodgers, Lines of basement uplifts within the external parts of orogenic belts, Am. J. Sci. 295 (1995) 455–487.
[80] M. Sahabi, D. Aslanian, J.-L. Olivet, Un nouveau départ pour l'histoire de l'Atlantique central, C. R. Geoscience 336 (2004) 1041–1052.
[81] A. Saquaque, H. Admou, J.A. Karson, K. Hefferan, I. Reuber, Precambrian accretionary tectonics in the Bou Azzer-El Grara region, Anti-Atlas, Morocco, Geology 17 (1989) 1107–1110.
[82] P.E. Schenk, Southeastern Atlantic Canada, Northwestern Africa, and Continental Drift, Can. J. Earth Sci. 8 (1971) 1218–1251.
[83] C.R. Scotese, Paleomap project, http://www.scotese.com/Default.htm, 2005.
[84] J.L. Simon, Superposed buckle folding in the eastern Iberian Chain, Spain, J. Struct. Geol. 26 (2004) 1447–1464.
[85] L.L. Sloss, Epilog (to Interior Cratonic Basins), in: M.W. Leighton, et al. (Eds.), Interior Cratonic Basins, AAPG, Tulsa, 1990, pp. 799–805.
[86] A.G. Smith, Gondwana: its shape, size and position from Cambrian to Triassic times, J. Afr. Earth Sci. 28 (1) (1999) 71–97.
[87] A. Soulaimani, Dynamique et interactions Socle/Couverture dans l'Anti-Atlas occidental (Maroc) : Rifting fini-protérozoïque et orogenèse hercynienne, 1998.
[88] A. Soulaimani, A. Piqué, The Tasrirt structure (Kerdous inlier, Western Anti-Atlas, Morocco): a Late Pan-African transtensive dome, J. Afr. Earth Sci. 39 (2004) 247–255.

[89] A. Soulaimani, M. Bouabdelli, A. Piqué, L'extension continentale au Néo-Protérozoïque supérieur–Cambrien inférieur dans l'Anti-Atlas (Maroc), Bull. Soc. géol. France 174 (1) (2003) 83–92.

[90] A. Soulaimani, A. Essaifi, N. Youbi, A. Hafid, Les marqueurs structuraux et magmatiques de l'extension crustale au Protérozoïque terminal–Cambrien basal autour du massif de Kerdous (Anti-Atlas occidental, Maroc), C. R. Geoscience 336 (16) (2004) 1433–1441.

[91] A. Soulaimani, C. Le Corre, R. Farazdaq, Deformation hercynienne et relation socle/couverture dans le domaine du Bas-Draa (Anti-Atlas occidental, Maroc), J. Afr. Earth Sci. 24 (3) (1997) 271–284.

[92] A. Soulaimani, A. Piqué, M. Bouabdelli, La série du PII–PIII de l'Anti-Atlas occidental (Sud marocain) : un olistostrome à la base de la couverture post-panafricaine (PIII) du Protérozoïque supérieur, Earth Planet. Sci. Lett. 332 (2001) 121–127.

[93] G.M. Stampfli, G.D. Borel, A plate tectonic model for the Paleozoic and Mesozoic constrained by dynamic plate boundaries and restored synthetic oceanic isochrons, Earth Planet. Sci. Lett. 196 (1–2) (2002) 17–33.

[94] D. Stone, Morphology of the Casper Mountain uplift and related subsidiary structures, central Wyoming: Implications for Laramide kinematics, dynamics, and crustal inheritance, AAPG Bull. 86 (8) (2002) 1417–1440.

[95] O.E. Sutcliffe, J.A. Dowdeswell, R.J. Whittington, J.N. Theron, J. Craig, Calibrating the Late Ordovician glaciation and mass extinction by the eccentricity cycles of Earth's orbit, Geology 28 (11) (2000) 967–970.

[96] R.J. Thomas, L.P. Chevallier, P.G. Gresse, R.E. Harmer, B.M. Eglington, R.A. Armstrong, C.H. De Beer, J.E.J. Martini, G.S. De Kock, P.H. Macey, B.A. Ingram, Precambrian evolution of the Sirwa Window, Anti-Atlas Orogen, Morocco, Precambr. Res. 118 (2002) 1–57.

[97] I.R. Vann, R.H. Graham, A.B. Hayward, The structure of mountain fronts, J. Struct. Geol. 8 (3–4) (1986) 215–227.

[98] G.J. Walsh, J.N. Aleinikoff, F. Benziane, A. Yazidi, T.R. Armstrong, U–Pb zircon geochronology of the Paleoproterozoic Tagragra de Tata inlier and its Neoproterozoic cover, western Anti-Atlas, Morocco, Precambr. Res. 117 (2002) 1–20.

[99] R. Weijermars, Estimation of paleostress orientation within deformation zones between two mobile plates, with Suppl. Data 9329, Geol. Soc. Am. Bull. 105 (11) (1993) 1491–1510.

[100] J. Wendt, Disintegration of the continental margin of northwestern Gondwana; Late Devonian of the eastern Anti-Atlas (Morocco), Geology 13 (11) (1985) 815–818.

[101] J. Wendt, Z. Belka, E. Fluegel, Age and depositional environment of Upper Devonian (Early Frasnian to Early Famennian) black shales and limestones (Kellwasser facies) in the eastern Anti-Atlas, Morocco, Facies 25 (1991) 51–89.

[102] Tectonic Map of the World, AAPG Foundation, R.W. Wiener, F.L. Wehr, G.M. Skerlec, I.O. Norton, 1985.

[103] P.A. Ziegler, S. Cloetingh, Dynamic processes controlling evolution of rifted basins, Earth Sci. Rev. 64 (1–2) (2004) 1–50.

[104] P.A. Ziegler, S. Cloetingh, R. Guiraud, G.M. Stampfli, Peri-Tethyan platforms; constraints on dynamics of rifting and basin inversion, in: P.A. Ziegler, et al. (Eds.), Peri-Tethyan Rift/Wrench Basins and Passive Margins, Éditions du Museum national d'histoire naturelle, Paris, 2001.

Geological Maps

[105] D. Alaoui-Mdaghri, M. Bensaid, M. Dahmani, Carte géologique du Maroc 1:100 000, Bou Izakarn, Notes Serv. géol. Maroc (1992).

[106] G. Choubert, Y. Ennadifi, Carte géologique du Maroc 1:200 000, Flanc sud de l'Anti-Atlas occidental et des plaines du Dra, Akka-Tafragount-Tata, Notes Serv. géol. Maroc (1970).

[107] G. Choubert, A. Faure-Muret, Carte géologique du Maroc 1:100 000, Igherm, feuille NH-29-XVI-2, Notes Serv. géol. Maroc (1983).

[108] G. Choubert, A. Faure-Muret, Carte géologique du Maroc 1:100 000, Tafraout ; feuille NH-29-X-3, Notes Serv. géol. Maroc (1983).

[109] G. Choubert, A. Faure-Muret, Carte géologique du Maroc 1:100 000, Taroudannt, Feuille NH-29-XVI-I, Notes Serv. géol. Maroc (1983).

[110] M.A. El-Alaoui, Y.C. Chefchaouni, M. Diouri, Carte géologique du Maroc 1:200 000, Flanc sud de l'Anti-Atlas et des plaines du Drâa, Foum el Hassane-Assa, Notes Serv. géol. Maroc (1963).

[111] S.E.M. Fetah, M. Bensaid, M. Dahmani, Carte géologique du Maroc 1:200 000, Tafilalt–Taouz, ministère de l'Énergie et des Mines, royaume du Maroc (1986).

[112] S.E.M. Fetah, M. Bensaid, M. Dahmani, Carte géologique du Maroc au 1:200 000, Todrha–Ma'der, ministère de l'Énergie et des Mines, royaume du Maroc (1986).

[113] S.E.M. Fetah, M. Bensaid, M. Dahmani, Carte géologique du Maroc au 1:200 000, Zagora–Coude du Drâa–Hamada du Drâa, ministère de l'Énergie et des Mines, royaume du Maroc (1986).

[114] A. Guerraoui, M. Bensaid, M. Dahmani, Carte géologique du Maroc 1:100 000, Fask, Notes Serv. géol. du Maroc (1997).

Folding and inversion tectonics in the Anti-Atlas of Morocco

Urs Helg, Martin Burkhard, Séverine Caritg, and Charles Robert-Charrue

Institut de Géologie, Université de Neuchâtel, Neuchâtel, Switzerland

Received 25 August 2003; revised 30 April 2004; accepted 14 May 2004; published 22 July 2004.

[1] The late Variscan Anti-Atlas of Morocco shows some conspicuous deviations from the standard anatomy of foreland fold-and-thrust belts. Large basement inliers crop out at a very short distance of less than 50 km behind the southeastern front of the fold belt, reminiscent of Windriver-style basement uplifts. In contrast to the Rocky Mountain foreland, however, the Anti-Atlas basement uplifts punctuate tightly folded Paleozoic cover series similar in tectonic style to the Appalachian Valley and Ridge province. Cover shortening is exclusively accommodated by buckle folding, and the Anti-Atlas fold belt lacks any evidence for duplexing or thrust faults other than the occasional steep reverse fault found near basement inliers. Basement domes have classically been considered as the result of vertical tectonics in a horst and graben fashion, or, alternatively, as large ''plis de fond'' [*Argand*, 1924], basement folds. Unfolding of a large portion of an Ordovician quartzite marker bed reveals a minimum shortening of 17% (30 km). Balancing this section at the crustal scale indicates a lower crustal detachment level at 18 to 25 km depth. Basement shortening is inferred to be accommodated through massive inversion of former extensional faults, inherited from a Late Proterozoic-Lower Cambrian rifting phase. *INDEX TERMS:* 8005 Structural Geology: Folds and folding; 8015 Structural Geology: Local crustal structure; 8102 Tectonophysics: Continental contractional orogenic belts; 8159 Tectonophysics: Rheology—crust and lithosphere; 9305 Information Related to Geographic Region: Africa; *KEYWORDS:* Anti-Atlas, tectonics, balanced cross section, folding, foreland fold and thrust belt. **Citation:** Helg, U., M. Burkhard, S. Caritg, and C. Robert-Charrue (2004), Folding and inversion tectonics in the Anti-Atlas of Morocco, *Tectonics*, *23*, TC4006, doi:10.1029/2003TC001576.

1. Introduction

[2] The Anti-Atlas foreland fold belt of southwestern Morocco is part of the Variscan Appalachian-Ouachita-Mauretanides chain. It shows some important deviations from typical foreland fold and thrust belts [*Rodgers*, 1990]. Large structural domes, the so-called ''boutonnieres'' [*Choubert*, 1963] of Proterozoic basement rocks, crop out at a very short distance behind the southeastern front of the orogen. Detailed mapping of the Anti-Atlas did not reveal any evidence for major thrusts within this fold belt. Layer-parallel décollements or detachments are required between different structural levels, but no such décollement has ever been mapped to step up in a ramp-flat geometry. The complete lack of thrusts lead earlier authors to consider the entire basement uplifts as crustal-scale folds [*Choubert*, 1963; *Choubert and Faure Muret*, 1971], inspired by the plis de fonds of *Argand* [1924, Figures 5a, 5b, and 5c].

[3] The sedimentary cover of the Anti-Atlas includes the uppermost Proterozoic and an up to 10 km thick Paleozoic series. These mildly deformed and nearly unmetamorphosed strata of the Anti-Atlas have received much attention from stratigraphers and paleontologists [*Destombes et al.*, 1985; *Bertrand-Sarfati et al.*, 1991; *Villeneuve and Cornee*, 1994; *Piqué*, 2001]. Special attention has been given to the Proterozoic-Cambrian boundary [*Boudda et al.*, 1979; *Bertrand-Sarfati*, 1981; *Buggisch*, 1988b; *Latham*, 1988; *Geyer and Landing*, 1995; *Benssaou and Hamoumi*, 2003]. In contrast to this wealth of stratigraphical and paleontological literature, structural publications dealing with the tectonics of the western Anti-Atlas remain scarce [*Leblanc*, 1972; *Michard*, 1976; *Soulaimani*, 1998; *Guiton et al.*, 2003].

[4] On the basis of paleomagnetic observations near the South Atlas and the Tizi'n'Test faults, a strike-slip origin for the entire Anti-Atlas chain has been proposed [*Mattauer et al.*, 1972]. This view is widely shared by French authors [*Leblanc*, 1972; *Donzeau*, 1974; *Jeannette*, 1981], and folding of the sedimentary cover has mostly been explained as draping over vertically uplifted basement blocks and/or as wrenching above inherited, subvertical ''zones of weakness'' [*Faik et al.*, 2002]. Horizontal shortening in the central Anti-Atlas has been ignored, or estimated to be on the order of 5 to 10% at most [*Leblanc*, 1972; *Donzeau*, 1974]. Published cross sections of the western Anti-Atlas depict the basement inliers as horst and graben structures, indistinct broad basement domes or delimited by vertical strike-slip faults [*Michard*, 1976; *Michard and Sougy*, 1977; *Piqué et al.*, 1991]. Clearly, these cross sections imply no crustal-scale shortening within the basement, and fold trains within the synclinoria remain unexplained in terms of material balance, a question which has never been addressed in the Anti-Atlas. The striking difference between the Devonian ''Jbel Rich'' folds and the virtually undeformed Jbel Ouarkziz monocline near the southern front of

0278-7407/04/2003TC001576$12.00

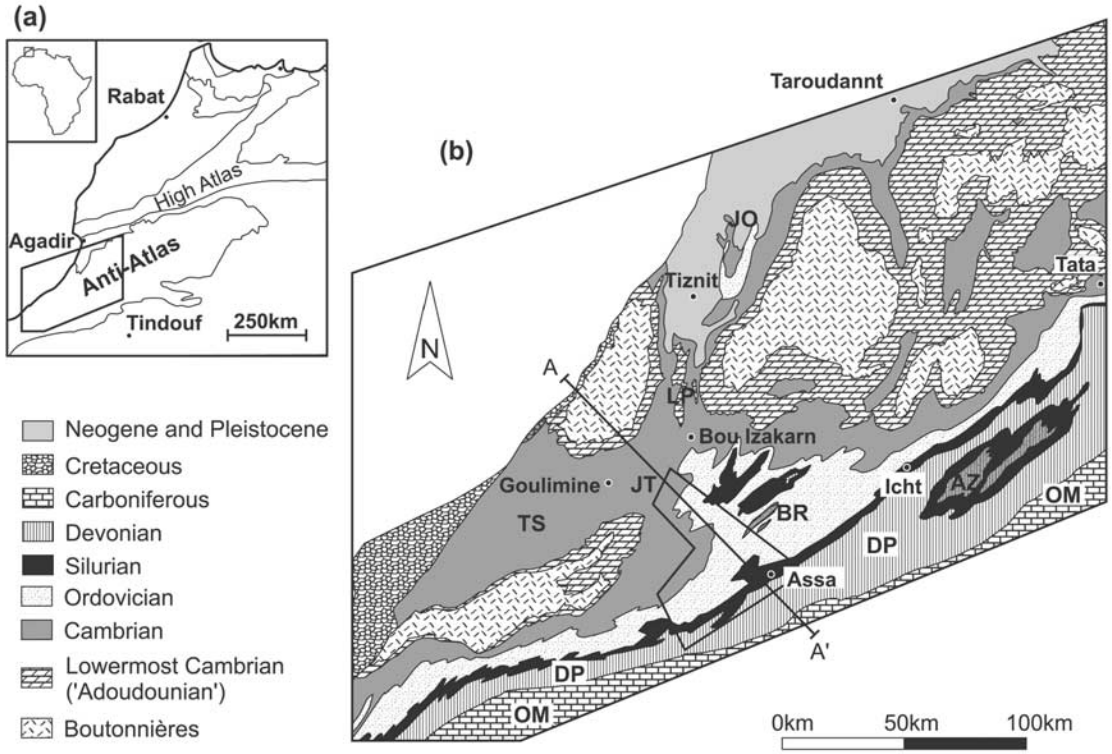

Figure 1. (a) Location of the Anti-Atlas in southwestern Morocco. The polygon represents the study area. (b) Simplified geological map of the westernmost Anti-Atlas showing the irregular shape and distribution of the structural domes. These Proterozoic ''boutonnieres'' consist of pre-Cambrian crystalline basement and Late Proterozoic volcaniclastic series of variable thickness. The black line A-A′ shows the location of the large-scale cross section of Figure 10. The polygon represents the location of the 3-D fold model shown in Figure 6. Abbreviations are as follows: AZ, Adrar Zouggar mountain; BR, Bani range; DP, Drâa plain; JO, Jebel Ouarzemine; JT, Jebel Tayyert; LP, Lakhssass plateau; OM, Ouarkziz monocline; TS, thin skin part of the ''internal'' Anti-Atlas.

the Anti-Atlas has been considered as evidence for a major strike-slip fault [*Weijermars*, 1993], of a Neogene age. The apparent ''en echelon'' arrangement of the Rich folds was further used to deduce a right lateral shear sense and amount of shear, assuming a subvertical plunge of fold axes [*Weijermars*, 1993]. In reality, however, fold axes plunges are very gentle, less than 30°, and the asymmetric fold pattern of the lower Drâa valley implies very weak, if any, wrenching deformations [*Soulaimani et al.*, 1997]; paleostress indicators are systematically orientated nearly perpendicular to the fold axial planes, rather than at an inferred angle of some 50° [*Weijermars*, 1993]. New observations in the southwestern Anti-Atlas have recently led to a general revision of the classic model of vertical and strike-slip tectonics [*Soulaimani et al.*, 1997; *Soulaimani*, 1998]. Convincing evidence exists for southwestward thrusting of the Lower Drâa inlier onto the sedimentary cover, and the dextral strike-slip boundary postulated by *Weijermars* [1993] is not substantiated by any field evidence.

[5] In this study, we present a detailed structural analysis of a large portion of the SW Anti-Atlas. A continuous fold train in a competent Ordovician quartzite bed is mapped in detail and rendered in a three-dimensional (3-D) structural model. Unfolding of this marker bed provides minimum estimates of horizontal shortening as well as a measure of regional variations in folding intensity. The consequences of this tectonic shortening are discussed at the larger, crustal scale of this ''thick skinned'' foreland fold belt.

2. Geological Framework of the Western Anti-Atlas

2.1. Basement Preconfiguration

[6] The Anti-Atlas fold belt is located at the northwestern border of the West African craton and continues southward into the Mauretanides. Large-scale basement cored domes with irregular shapes form a continuous area of positive structural relief (Figures 1 and 2). The long axis of the Anti-Atlas belt axis is oriented SW-NE and measures some 700 km.

[7] The pre-Cambrian basement has a complex geologic history. It was consolidated during the Panafrican orogeny between 620 and 580 Ma [*Choubert*, 1963; *Choubert and Faure Muret*, 1971; *Leblanc and Lancelot*, 1980; *Hassenforder*, 1987]. In detail it shows considerable

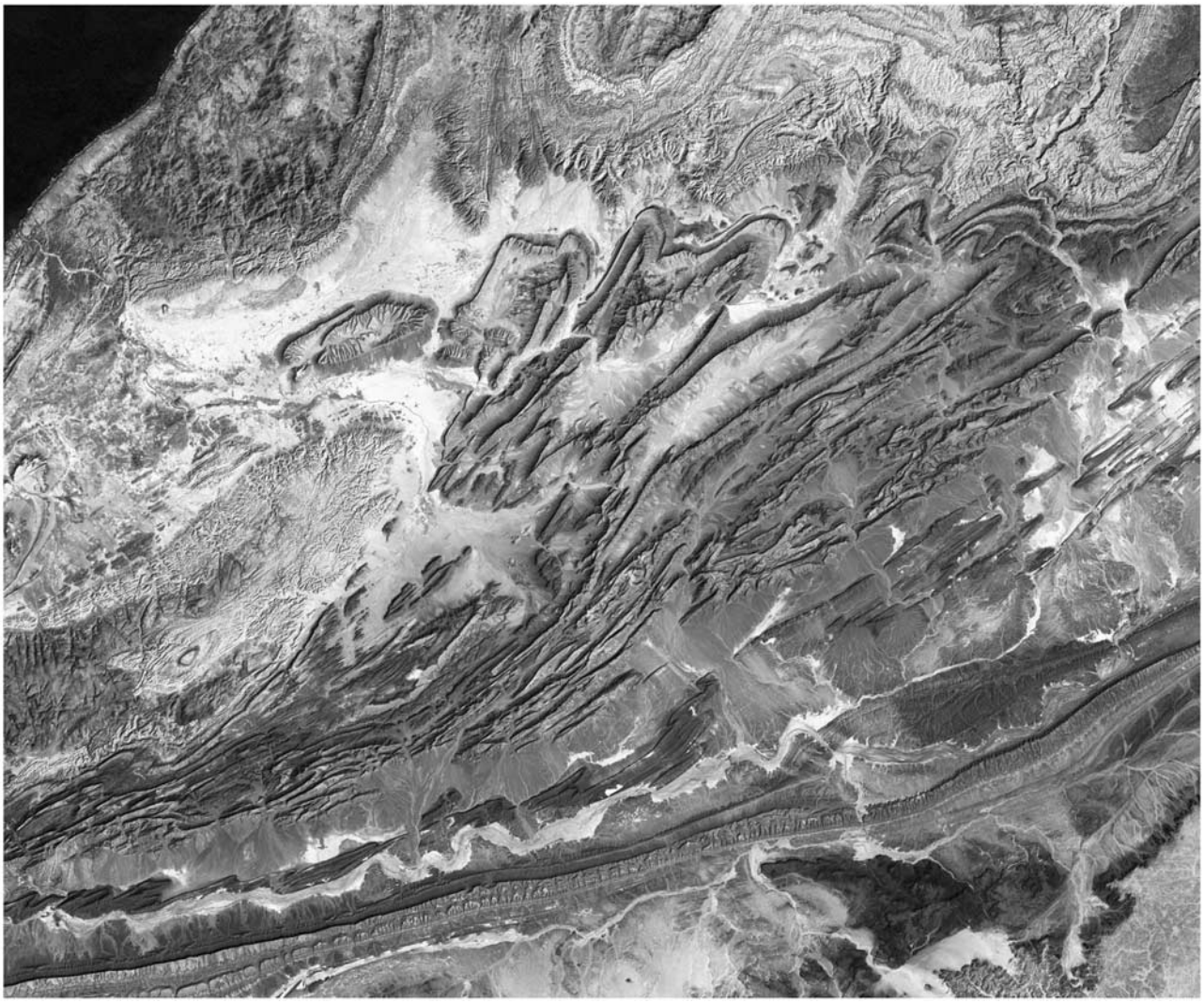

Figure 2. Landsat image of the westernmost Anti-Atlas chain. Compare with Figure 1 for major landmark features such as the basement inliers (dark green) with their ''autochthonous'' Cambrian cover in light green and tan colors. Quartz-rich lithologies of the Jbel Bani, the Jbel Rich, and Jbel Ouarkziz appear in dark purple. Image courtesy of NASA and Earth Satellite Corporation (available at http://zulu.ssc.nasa.gov/mrsid/mrsid.pl). See color version of this figure at back of this issue.

heterogeneity. It contains the suture zone between the stable West African craton and a Proterozoic mobile belt to the north. Remnants of this suture zone are exposed in several basement domes, for example in the Bou Azzer and in the El Graara inliers. In the central Anti-Atlas this suture zone is known as ''accident majeur de l'Anti-Atlas.'' Southwest of this suture zone, Eburnean (approximately 1900 Ma) augen gneisses, metadolerites, and metamorphic rocks, the so-called Zenaga and Kerdous Series, crop out in several of the structural domes. The Proterozoic rocks are further characterized by numerous synorogenic granite and granodiorite intrusions.

[8] The Panafrican orogeny is followed by an important phase of continental sedimentation, which results in locally thick clastic and volcaniclastic deposits, the so-called PII-III unit, separated from the crystalline basement by a major unconformity. The geodynamic context of the PII-III is still a matter of debate [*Piqué et al.*, 1999; *Piqué*, 2001]. In the case of the overlying PIII unit of clastics and volcaniclastics, separated by a minor unconformity from the PII, there is increasing evidence in favor of an extensional tectonic regime, in relation with a new rifting cycle starting in the Late Proterozoic [*Piqué et al.*, 1995; *Piqué*, 2001; *Soulaimani et al.*, 2003]. Extensional structures have been described within the Proterozoic basement in the westernmost Anti-Atlas [*Soulaimani et al.*, 1997] and large-scale half-grabens are documented in the central Anti-Atlas [*Azizi-Samir et al.*, 1990]. The post-Panafrican geological history of the Anti-Atlas is now considered as an aborted rift [*Piqué et al.*, 1995; *Soulaimani et al.*, 2003].

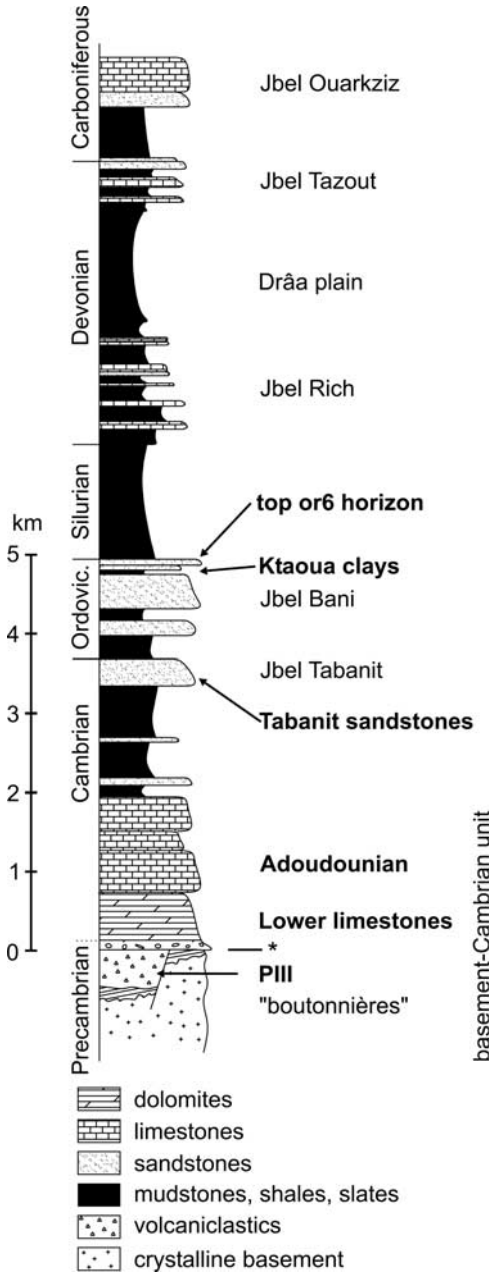

Figure 3. Synthetic stratigraphic column of the western Anti-Atlas. Incompetent units are shown in black. The asterisks marks the slight unconformity which is classically used to define the outlines of the boutonnieres (basement inliers). The commonly used, informal lithostratigraphic/mechanical units are labeled at the right-hand side; chronostratigraphy is shown to the left.

2.2. Sedimentary Cover

[9] Above the PIII conglomerates, a slight unconformity marks the onset of epicontinental shallow marine sedimentation in the Anti-Atlas, a limit often referred to as the "basement cover contact." A marked contrast in color, sediment type and rheology makes the PIII-Adoudounian contact an easy target for mapping both in the field and on satellite images (Figure 2). The same unconformity is also used to define the outline of the basement inliers.

[10] A new sedimentary cycle leading to the formation of the Anti-Atlas basin starts in the uppermost Proterozoic and ends in the upper Carboniferous. In the western Anti-Atlas, a total of up to 12 km of varied clastic and shallow marine sediments were deposited, while eastward, in the central Anti-Atlas, the thickness is decreasing to about 8 km [*Michard*, 1976; *Piqué and Michard*, 1989; *Kogbe*, 1998]. The Anti-Atlas basin fill is characterized by a high amount of fine-grained detrital, clay rich sediments: muddy siltstones and shales (Figure 3). Competent quartzites, sandstones, limestones, and conglomerates form thin but continuous beds at different stratigraphic levels. Coarse-grained beds are increasing in thickness and abundance toward the easternmost Anti-Atlas.

[11] The thin competent marker beds form very continuous spectacular crests easily visible in aerial and satellite images (Figure 2). Major stratigraphic intervals such as the Ordovician and the Devonian series have been named according to the mountain belts they form: Jbel Bani (for Ordovician), Jbel Rich (Devonian), and Jbel Ouarkziz (Carboniferous). We continue to use this terminology in order to describe the main competent units, despite the fact that they are not formally accepted "lithostratigraphic" formation names.

2.3. Variscan Orogeny

[12] The age of deformation within the western Anti-Atlas is generally considered as middle to late Carboniferous on the basis of the youngest age of (slightly) deformed and tilted sediments on the one hand, and superregional considerations and comparisons on the other hand [*Michard*, 1976; *Piqué and Michard*, 1989; *Piqué*, 1994]. The oldest sedimentary formations sealing eroded Anti-Atlas folds are of Upper Cretaceous age and do not provide any useful timing constraints. Dolerite dikes such as the famous dike of Foum-Zguid and sills clearly postdate Anti-Atlas folding [*Sebai et al.*, 1991], but their lower Jurassic age does not put any tight time constraint on the deformation age of Anti-Atlas folding either, since folding might still be anything between "middle" Carboniferous and Late Triassic. Some attempts at a direct age determination of the tectonic cleavage have been made using radiometric methods, applied to fine grained illite-muscovite assemblages of the westernmost Anti-Atlas [*Bonhomme and Hassenforder*, 1985]. Isotopic ages of 370 Ma and 290 Ma were attributed to a pre-Variscan phase of deformation and the peak of regional metamorphism, respectively. Similar results have been obtained in isotopic studies of the Variscan Meseta of northern and central Morocco [*Huon*, 1985]. Since metamorphism in many parts of the Variscan chain of Morocco is barely of lower greenschist facies, and deformation only locally penetrative, any K-Ar and Rb-Sr ages should be regarded very cautiously [*Villa*, 1998]. Correlations between the northern Moroccan Meseta and the Anti-Atlas are not straightforward either. The two

Figure 4. A gently inclined fold limb north of Assa. The entire dip slope of this fold limb is formed by one stratigraphic horizon of Upper Ordivician age: the or6c-quartzites. The foreground of the photograph shows the Drâa plain corresponding to a lowland eroded into Silurian shales; view is to the north.

provinces are separated by the South Atlas shear zone, a major terrane boundary within the Variscan chains of Morocco [*Mattauer et al.*, 1972]. An overall geodynamic interpretation of a complete Canadian-Moroccan transect through the entire Appalachian-Meseta-Anti-Atlas system has been presented as early as 1971 [*Schenk*, 1971].

2.4. Anti-Atlas Foreland Fold Belt

[13] In terms of folding and deformation style, four structural units with different wavelengths and amplitudes can be distinguished in the Anti-Atlas. They correspond to four distinct stratigraphic levels separated by the thick incompetent units of the Middle Cambrian, Silurian, and Upper Devonian respectively. None of the fold levels shows a clear and consistent vergence.

[14] The lowermost unit is represented by the basement domes and their autochthonous cover consisting of Late Proterozoic PIII conglomerates and Lower Cambrian limestones and dolomites of the so-called "Adoudounian." These basement domes have accessible, mapped amplitudes of up to 2 km, and the corresponding wavelength is on the order of several kilometers to tens of kilometers. The true "amplitude" of basement "folds" is in excess of 10 km, however, larger than the total thickness of Paleozoic cover series. Locally, thin layers of incompetent shales and evaporites within the autochthonous Adoudounian series act as minor detachment horizons, resulting in second-order folding at a much smaller scale (10 to 100 m). Toward the central Anti-Atlas the "Lie de vin" formation acts as a distinct local décollement horizon (Figure 2). Fold axis trends within the Adoudounian are strongly influenced by the preconfiguration of the underlying basement domes, and they often deviate considerably from the large-scale SW-NE Anti-Atlas orientation [*Soulaimani et al.*, 1997; *Soulaimani*, 1998]. Higher up in the stratigraphic column, two structural units are characterized by detachment folds of the Ordovician Jbel Bani quartzites (Figure 4) and the Lower Devonian Jbel Rich limestones, respectively. In the western Anti-Atlas they are separated from each other by about 1000 to 1500 m of Silurian shales and mudstones. The folding style of these two units is very similar, albeit with different wavelengths and amplitudes. Spectacular kilometer-scale Bani folds are found especially in the western Anti-Atlas between the towns of Bou Izakarn Assa and Icht (Figure 5). The Jbel Rich folds display smaller wavelengths and amplitudes at the 500 m scale. The uppermost structural unit, a thick series of Carboniferous sandstones and limestones of the Jbel Ouarkziz, is separated from the Jbel Rich folds by a thick series of Upper Devonian shales. Morphologically, the Jbel Ouarkziz defines a very continuous monocline, where the Carboniferous series dip gently south-southeastward into the adjacent Tindouf basin (Figure 2). Some authors (e.g., M. Zizi, personal communication, 2000; see also http://www.onarep.com) consider the lack of folding within the tilted Jbel Ouarkziz as evidence for a Late Devonian age of folding in the Anti-Atlas, an interpretation inspired by comparisons with northern and central Morocco and with the Canadian Appalachians [*Piqué and Michard*, 1989]. Direct field evidence in the form of an unconformity has never been identified in the sedimentary series of the Anti-Atlas, where a tectonic interpretation (décollement) is more generally accepted [*Soulaimani*, 1998]. While the deformation front of the Anti-Atlas system is classically seen at the base (NNW) of the Jbel Ouarkziz, we propose a new interpretation as a triangle structure with a forethrust ending somewhere blindly SSE of the Jbel Ouarkziz, at depth within the Tindouf basin. From this most external tip point of the Anti-Atlas thrust system, a NNW vergent backthrust climbs north-northwestward to emerge into the shale series separating the Jbel Ouarkziz monocline from the Jbel Rich fold train within the Lower Drâa valley. This interpretation is corroborated by structural observations, notably the tilting of the Jbel Ouarkziz monocline and bed internal layer

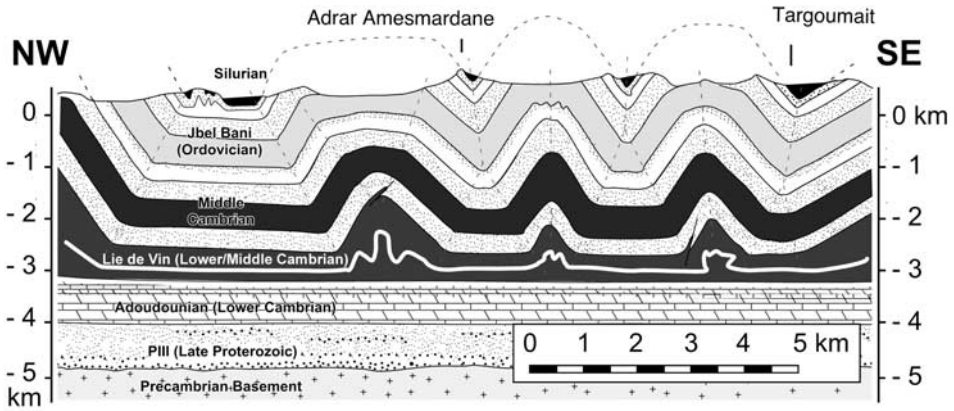

Figure 5. Intermediate-scale section across the folded Jbel Bani, in the northwestern sector of the 3-D fold model shown in Figure 6. A major décollement is inferred within the incompetent Lie de vin formation of Lower/Middle Cambrian age. The structural style below this décollement is unknown; for lack of better knowledge, it is depicted here as a flat-lying, undeformed panel of autochthonous basement-Lower Cambrian unit.

parallel shortening (LPS) deformation features within the youngest outcropping Carboniferous limestones [*Burkhard et al.*, 2001].

3. Anti-Atlas Cross-Section Balancing

3.1. Theoretical Considerations

[15] In areas of tectonic activity, deformation typically occurs at all scales, ranging from structures in crystal lattices to structures forming mountain ranges [*Ramsay and Huber*, 1983; *Mitra*, 1992; *Mitra*, 1994]. Three scales of observation are commonly used to describe structures: microscale (<0.01 m), outcrop scale (0.01–100 m), and map scale (>100 m). Primary sedimentary structures are used as proxies for the qualitative description and quantitative determination of strain at all scales.

[16] Cross-section balancing is dealing with map-scale structures such as folds, faults, and thrusts. Smaller-scale structures accommodate additional deformation, which should be considered in overall estimations of tectonic shortening. Over the years, various investigators have shown that small-scale structures do make a significant contribution to total tectonic deformation. *Mitra* [1994] measured strains in sections parallel to the transport direction across the Sevier fold-and-thrust belt. He could demonstrate that failure to include microscale deformation in the restoration of regional cross sections results in overestimation of the wedge taper for the thrust belt. Another study examined the contribution of both microscale and outcrop-scale data to regional deformation using the foreland thrust belt of the central Appalachians where small-scale structures account for more than 75% of the shortening in the roof sequence of this thrust belt [*Smart et al.*, 1997]. *Hogan and Dunne* [2001] conducted a study in the Upper Devonian Chemung-Brallier Formation boundary in the western Valley and Ridge province, where map-scale structures account for about 50% of the total shortening, whereas outcrop-scale and microscale shortening yield each close to 25% of the overall shortening.

[17] Qualitatively, layer parallel shortening features are widely recognized as predating folding and thrusting and this is very nicely demonstrated in the Jura mountains [*Plessmann*, 1972; *Homberg*, 1996].

[18] For the estimation of the total shortening in the Anti-Atlas we concentrated on map-scale and outcrop-scale structures. Since there are other important unknowns of the shortening at the scale of the orogen we were content with a qualitative assessment of microscale shortening. In order to minimize the effects of LPS, we choose a very competent quartzite horizon, devoid of any LPS features visible at the outcrop to hand specimen scale. We believe that this marker bed deformed essentially by buckling at the outcrop to map scale.

3.2. Study Area and the Ordovician Quartzite Marker Bed

[19] Our estimation of the shortening is mainly based on measurements and observations made in the Bani mountain range, an area of folded Ordovician rocks between the towns of Bou Izakarn, Aouinat Torkoz, and Icht (Figure 1b) with excellent outcrop conditions (Figure 2). The structural style is quite homogeneous, and fold trends are easily recognized.

[20] We concentrated on a very competent horizon within the so-called ''2nd Bani'' formation of Ashgillian age. This uppermost competent unit of the Jbel Bani is labeled or6c according to *Guerraoui et al.* [1997] (Figure 3); on older maps, however, this thin marker bed is not always distinguished from the immediately underlying or6b or or6s. It consists of massive microconglomeratic quartz arenites, interpreted as being of glacial origin. This particular horizon is ideal for the reconstruction of the map-scale structures: (1) It is ubiquitous in the study area and has a relatively small thickness of 50 to 90 m [*Destombes et al.*, 1985],

which is rather thin compared to the average wavelength of the folds. (2) The massive or6c quartzites are much more resistant to weathering and erosion than the Silurian shales immediately above. The top of the or6c horizon is often very well preserved and forms the present-day surface, often in the form of dip slopes. In consequence, where the or6c-quartzites crop out, the topographic contours can directly be used as structure contours (Figure 4). Owing to very favorable outcrop conditions, large areas could be checked for outcrop-scale structures through the examination of aerial photographs and verification in the field. (3) By coincidence, the present-day valley floors in the western Anti-Atlas lie close to the inflection point of the folded Jbel Bani series. The dip at the inflection point is one of the most important pieces of information for the reconstruction of a fold, especially when considering variations of fold vergence. Outcrop conditions allow for a straightforward construction of fold closures below and above topography.

3.3. Shortening Estimates Based on Folding

[21] We constructed first a structure contour map of the top or6c surface at the 1:50,000 scale, using the most recent geologic and topographic maps available, with an equidistance of 25 m. Additional information includes our field observations, bedding dip measurements, and interpreted aerial photographs.

[22] Because of the abundance and the continuity of the outcrops we were able to reconstruct most of the fold limbs and many fold closures quickly and with high accuracy. In a second step, the structure contour lines for the eroded and subsurface parts of the folds were added using auxiliary cross sections and classical techniques of down-plunge projection along the measured fold axis direction [*Ramsay and Huber*, 1987, p. 356ff]. Since the stratigraphic thicknesses of all the Ordovician formations are very well known, and not internally deformed to any measurable degree, we were able to reconstruct the hidden parts of the folds with nearly the same level of accuracy as the outcropping limbs.

[23] The structure contour map was then transformed to a digital 3-D surface with standard digitizing procedures. For most of our further analyses, we used this 3-D surface in a TIN format, in which a network of small flat, but irregular triangles approximates the real surface. In a TIN, the size of the triangles is variable and depends, in our case, on the spacing of the structure contour lines. A TIN is ideal for representing surfaces with features at variable scales since even smaller structures are adequately represented. The error stemming from replacing a curve by straight line segments (or in 3-D: a curved surface replaced by interconnected triangles) is negligible. In our case, even smaller folds consist of numerous triangles.

[24] Using a common geographic information systems software package (ArcInfo, ArcView) allowed calculation of statistics for many of the relevant fold parameters such as amplitude, wavelength, symmetry, vergence, and variations in the direction of the fold axis. Similarly, the extraction of a section at a random point in the model and the calculation of the curve's length is a more or less automatic procedure. In this way, we calculated the map-scale shortening for a virtually unlimited number of cross sections.

[25] In a second phase, sections were extracted from the model and enlarged for those locations where outcrop-scale second-order folds had been observed in the field. These structures were then added "by hand" in order to estimate their relative contribution to overall shortening.

[26] The assessment of outcrop-scale and microscale shortening is mainly based on field observations. The fieldwork had essentially two goals: (1) an assessment of the outcrop-scale structures and the estimation of their frequency and distribution and (2) the search for macroscopic indicators of microscale deformation, their description, and the estimation of their frequency and relative importance.

[27] Outcrop-scale deformation features include meter-scale minor folds and, more frequently, minor faults with displacements of the order of centimeters to decimeters. We could hardly find any indicators for microscale deformation features within the quartzites. Axial planes of folds in the Jbel Bani quartzites are materialized through the development of systematic sets of joints [*Guiton et al.*, 2003] rather than a cleavage, let alone a schistosity. Even shaly interlayers still mostly display primary bedding and the occurrence of LPS feature in the form of a weakly developed pencil cleavage or other tectonic cleavage is rather exceptional. Generally, deformation intensity increases downward in the stratigraphic pile, and the development of cleavage is more frequently observed near the basement inliers. Higher up in the stratigraphy, within limestones of the Devonian Jbel Rich and the Carboniferous Jbel Ouarkziz, we identified layer parallel stylolite peaks as clear indicators of early, layer parallel shortening in a SSE-NNW direction, at a high angle to the strike of this monocline.

4. Results

4.1. Map-Scale Shortening

[28] The top of the Ordovician or6c horizon has been reconstructed for the entire western part of the Jbel Bani (Figures 5 and 6). Our structure model covers an area of approximately 1600 km^2. It nicely illustrates the low complexity of this folded structure. Because of favorable outcrop conditions even some of the larger outcrop-scale structures are resolved, especially in the southern quadrangle (see Figure 7 for the use of "quadrangles" and "parts"). Clearly, folding is the predominant deformation style at the map scale. A few minor tear faults appear in the northern quadrangle, but they are local phenomena, normally limited to one fold limb.

[29] Throughout the area the folds show a high lateral continuity and cylindricity. Individual fold hinges are near horizontal over several kilometers. Plunging fold hinges are generally found in pairs of en echelon lateral transitions. The overall orientation of fold axes is very constant at approximately N038°.

[30] Fold limbs near the inflection point have dips between 35° and 75° (Figure 8). Most folds, irrespective of wavelength and amplitude are symmetrical and upright.

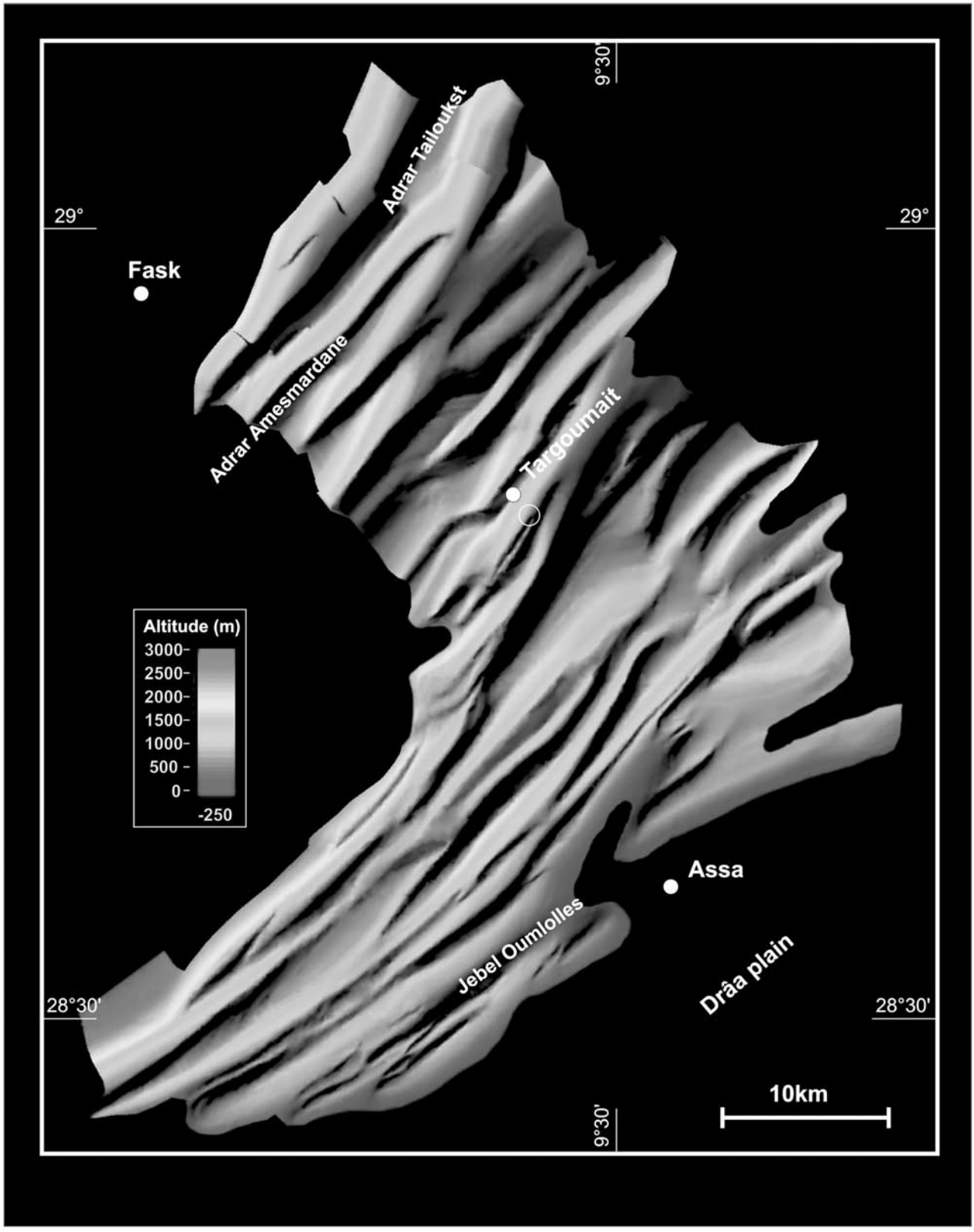

Figure 6. Three-dimensional rendering of a structure contour map constructed for the top of the or6c marker horizon in the western part of the Jbel Bani. The small white circle shows the location of the photograph of Figure 8. Note the decreasing amplitude and wavelength toward the south. See color version of this figure at back of this issue.

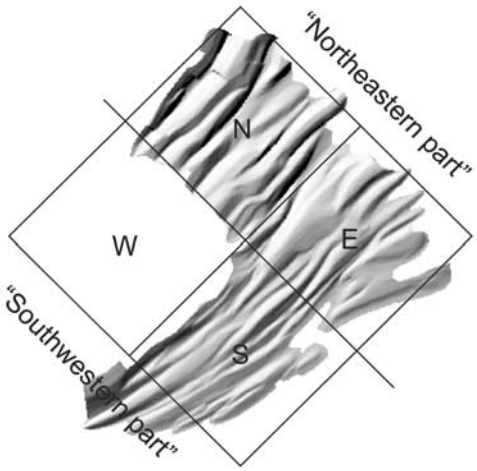

Figure 7. The location of the different areas mentioned in the text: N, northern quadrangle; E, eastern quadrangle; S, southern quadrangle; W, western quadrangle.

The differences of dip of corresponding fold limbs (at the inflexion point) is normally less than 5°. At the map scale there are no overturned limbs and there is no clear fold vergence.

[31] The wavelengths and amplitudes of the folds decrease significantly from north to south. In the northern quadrangle amplitudes of up to 1100 m are attained (northernmost anticline; ''Adrar Tailoukst'' in Figure 6), but decrease toward the eastern quadrangle to typical values of 450 to 550 m. The wavelengths for the northern quadrangle varies between 3.5 km and 4 km. Especially in the northern ''high-amplitude'' quadrangle the limb dips at the inflexion point are up to 60°. Fold limbs are rather straight and the deformation is concentrated to relatively narrow, angular hinge zones. The fold's tops are flat and large. In this quadrangle the folds are very near to the box fold end-member of detachment folds [*Namson*, 1981].

[32] The eastern and southern quadrangles are characterized by a higher variability in wavelength and amplitude. The larger and more continuous folds have amplitudes of 200 to 300 m and wavelengths of 1.5 to 2 km. The amplitudes of the smaller folds vary strongly; their wavelengths are on the order of 500 m or less. Some of these folds are at the transition to outcrop-scale structures. In the southern quadrangle the fold hinges become more rounded. The limb dips vary between 35° and 45° but they rarely exceed 40°. Only the limb dips of folds at the transition to outcrop scale attain high values up to 60°.

[33] A striking feature of the 3-D model of the Ordovician marker bed is the complete absence of thrust faults and/or duplex structures. This absence is real and not just an interpretation. Outcrop quality over large distances is excellent and allows ruling out any hidden, unresolved structures at this level. The low complexity of the structures at the map scale, essentially a continuous surface without thrusts or faults, allows for a straightforward calculation of the shortening. Sections at the borders of the model that contain gaps (because of ''holes'' of missing data) were ignored. The shortening estimates obtained from unfolding the structure contour map in different parts of the model are shown in Figure 9.

[34] The calculated shortenings correspond to the map-scale portion of the total shortening. In the southern quadrangle some structures at the transition to outcrop scale are integrated. The shortening shows considerable variability. It varies between less than 5% and more than 30%. However, if the model is subdivided into a northern ''high-amplitude domain'' (corresponding to the northern quadrangle) and a ''low-amplitude domain'' (eastern and southern quadrangles), the shortening within each of these domains is rather homogeneous. The northern quadrangle displays shortening between 12 and 20% with an average of 16.3% (Figure 9a). The eastern and the southern quadrangle together show shortening between 4% and 14% with an average of 8.7% (Figure 9b). Accordingly, the (long) sections through the whole northeastern part show shortening values between the two mentioned above. They

Figure 8. Tight syncline near the town of Targoumait. The width of the small valley is about 60 m. The or6c horizon forms the limbs of the syncline. This structure is at the transition from outcrop scale to map scale. It is well resolved in the 3-D model.

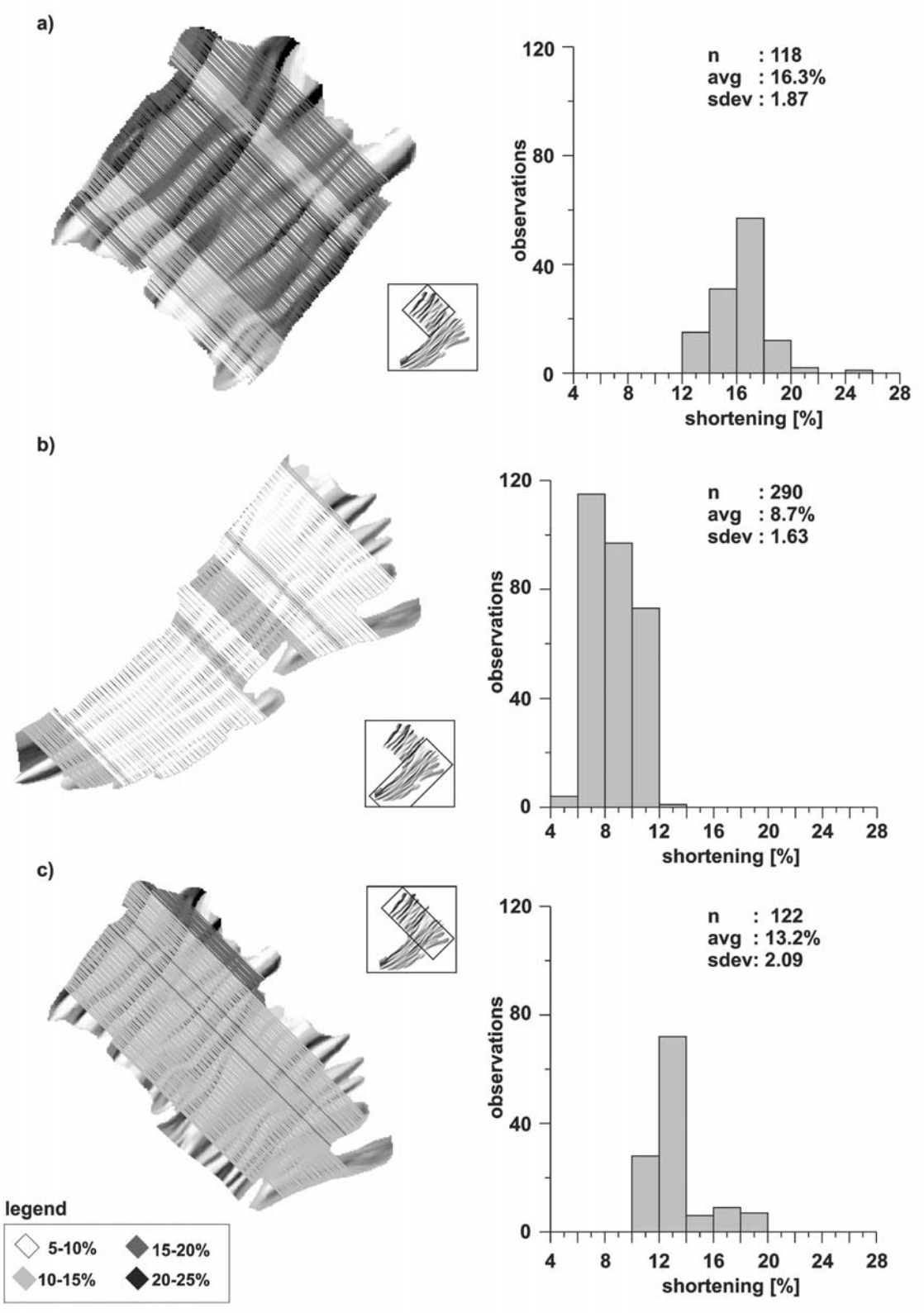

Figure 9. Map-scale shortening calculations for different parts of the top or6c-surface. Abbreviations are; n is number of sections; avg is average shortening; sdev is standard deviation.

vary between 10% and 20% with an average of 13.2% (Figure 9c).

4.2. Outcrop-Scale Shortening

[35] Field observations and the examination of aerial photographs allowed checking different structural positions for outcrop-scale structures. Also, very continuous outcrops, such as the Jbel Oumloulles Anticline west of Assa (Figure 6, southern quadrangle) allowed checking for outcrop-scale structures at several structural positions of the same fold.

[36] The most common outcrop-scale structures are wide flexures of the or6c horizon. Typically, they are characterized by very low amplitude to wavelength ratio. Shortening associated with these structures is minimal, on the order of a few meters in the case of individual, outcrop-scale structures. Their spacing is on the order of hundreds of meters to kilometers. More complex outcrop-scale structures such as tight minor folds and reverse faults are very rare. Such structures could add another few tens of meters of shortening per kilometer of cross section at the map scale. Together, outcrop-scale shortening is estimated to account for less than 5% total shortening at the map scale.

4.3. Microscale Shortening

[37] The or6c horizon exhibits no metamorphic overprint. Illite cristallinity measurement in the Ktaoua clays below and the Silurian shales above indicate that the horizon is located near the transition from diagenetic to anchizone conditions (U. Helg et al., Illite cristallinity patterns on the southeastern flank of the Variscan Anti-Atlas, Morocco, submitted to *Terra Nova*, 2004; hereinafter referred to as Helg et al., submitted manuscript, 2004) estimated at 200°C [*Frey*, 1987]. The or6c quartz arenites lack any cleavage. Rare stylolites are clearly of diagenetic origin, with peaks at high angle to bedding and no tectonic stylolites have been found within the Jbel Bani quartzites despite an intense search for such structures. Synfolding deformation is mostly by brittle fracturing and veining, most prominent in fold hinges, where this deformation is leading to some layer-parallel stretching, rather than shortening [*Guiton et al.*, 2003]. Prefolding LPS fabrics have not been identified. If anything, there might be a hidden component of layer parallel shortening in the rearrangement of the quartz grains on the truly microscopic scale [*Engelder and Marshak*, 1985]. Studies in the Appalachian Tuscarora Sandstone, a framework-supported quartz arenite, have shown that significant amounts of up to 22% horizontal shortening may be accommodated by such subtle microscale deformations [*Onasch*, 1993]. A similar study was conducted in the Tuscaroro Sandstone of the western margin of the Appalachian foreland near Keyser, West Virginia [*Harrison and Onasch*, 2000], where pressure solution together with micro fracturing and crystal plastic strain results in 10% layer parallel shortening, 10% less than the LPS values previously reported by *Onasch* [1993] from a more internal position within the Appalachian chain. Our own preliminary thin section observations made within the or6c quartzite reveal a very similar style of microscale deformations as those observed in the Appalachian Tuscarora Sandstone. In one site near Targoumait (Figure 5), we measured a grain shape preferred orientation of the detrital quartz grains of R_s = 1.15 within the bedding plane. This shortening is oriented NW-SE at a high angle to the local fold axis and it could well be interpreted as due to an early, prefolding shortening of up to 13%, if it was accommodated by pure "volume loss." In any case, LPS shortening in quartz arenites seems to be much more restricted than the highly variable values reported from shales and other clay-rich lithologies [*Kisch*, 1991].

[38] In summary, an absolute minimum horizontal shortening for the studied area, based on the map-scale balancing of folds (13%) with the addition of a conservative estimate of outcrop-scale shortening (2%), is 15%. It is more difficult to give an estimate for the most likely total tectonic shortening. It could be as large 30%, twice the minimum shortening, if microscale deformation was of the same magnitude as reported from comparable Appalachian Tuscaroro Sandstone. A more conservative estimate, based on our preliminary thin section observations, is in the range 15 to 25%.

5. Extent of the Folding

[39] In northwestern parts of the Anti-Atlas belt, Ordovician quartzites have been removed by erosion leaving only small isolated remnants, while southward, they disappear below younger Devonian and Carboniferous strata. The question therefore arises to what extent shortening estimates based on the tightly folded Jbel Bani can be extrapolated to the rest of the Anti-Atlas mountain belt.

[40] In contrast to many previous authors, we assume that similarly folded Ordovician sediments were present above at least the western basement inliers. In our interpretation, the present-day Jbel Bani is but a small erosional remnant of a much larger Ordovician sedimentary basin, preserved only in structural depressions in between basement uplifts. The present-day outline of the folded belt is by no means coincident with the original extent of the folded belt. There is no change in folding style or shortening from the northern quadrangle toward the eroded eastern quadrangle. Similarly, there is no significant decrease in shortening from the eastern toward the southern quadrangle, toward the outline of the Jbel Bani. This is also corroborated by our field observations outside of the study area: most of the mapped fold terminations along the outline of the Jbel Bani are erosional and markedly different, in terms of cylindricity, geometry, fold axis plunge, from real, conical en echelon fold terminations occasionally observed within the fold belt. Remnants of folded Ordovician series are also found outside of the Jbel Bani: The Middle Cambrian Tabanit sandstones, which are structurally coupled to the overlying Ordovician, form an open syncline at the Jbel Tayyert mountain which is the lowermost, not yet eroded part of a large, map-scale fold.

[41] Another indication for a much larger extent of the folding is the Jbel Ouarzemine mountain (JO on Figure 1b), which consists of a map-scale fold in Ordovician rocks. It is

a nearly isoclinal east vergent overturned syncline, located approximately 60 km north of the Jbel Bani. Its axis trends N021°, which is in perfect continuity to the northernmost Bani folds. On its western side it is bounded by a large thrust. Obviously, this structure accommodates more shortening than the open upright folds of the northernmost Jbel Bani, and we conclude that the observed trend of increasing shortening from southeast to northwest continues northwestward outside of our study area [*Belfoul et al.*, 2002].

[42] Folding does not stop at the southeastern border of the Jbel Bani either. A general south-southwestward decrease in deformation intensity is expected, however, and we take this into account in our "conservative" cross section where we let the Bani folds rapidly decrease in amplitude, wavelength, and shortening toward the south. A possible indication for the extent of the folding below the Drâa plain comes from the Adrar Zouggar and Addana mountains [*Desthieux*, 1977] (AZ in Figure 1b). They represent the most external Ordovician outcrops of the Anti-Atlas chain. Both of these Anticlinoria are basement cored domes as documented by drilling in the case of Adrar Zouggar [*Michard and Sougy*, 1977]. Unfortunately, this area is inaccessible for field studies at present. Detailed cross sections of the Addana and Adrar Zouggar mountains [*Desthieux*, 1977] document folding of the same style, wavelength, and "intensity" as our own observations at the southern border of the Jbel Bani.

[43] We conclude that the folded Ordovician strata initially occupied a much larger area than seen today. Folding of the Jbel Bani is not restricted to structural lows where it is preserved from erosion, but covered also large parts above the present day basement inliers. However, as seen in our model and on the basis of additional information from isolated further outcrops, both amplitude and wavelength generally decrease from northwest to southeast. This decrease is most probably related to regional-scale facies changes. The thickness of the Middle Cambrian shales, the décollement horizon, also decreases toward the southeast [*Boudda et al.*, 1979; *Benssaou and Hamoumi*, 2003], thereby progressively losing its ability as an efficient detachment horizon. Toward the southeastern front, the spacing between individual folds becomes more pronounced. This is seen as a consequence of the combined effect of a decrease in layer thickness and an increase in the ratio of competent versus incompetent beds.

[44] Another important unknown in terms of total tectonic shortening at the orogen scale is the southwestern border of the Anti-Atlas, the so-called "Jbel Ouarkziz" (OM in Figure 1b). There is strong geomorphic evidence for this monocline being the surface expression of a major triangle structure. The Ouarkziz mountain chain forms a straight ridge with altitudes of up to 500 m (200–300 m above the valley floors) over more than 300 km length, a landmark feature often photographed from space (images available at http://earthobservatory.nasa.gov/Newsroom/NewImages/images.php3?img_id=7285). This ridge is also used over a large distance as the "natural" boundary between Morocco, Algeria, and the western Sahara, respectively. There is only one road cut (Assa-Zag) at present, where the Ouarkziz chain is accessible for in situ study. In structural terms, it is essentially a large continuous monocline, dipping at ~15° to 30° south-southeastward, forelandward into the Tindouf basin. This monocline stands in stark contrast to the tightly folded Devonian Jbel Rich underneath, from which it is separated by the lowland of the Drâa plain, running along a thick series of Upper Devonian-lower Carboniferous shales and siltstones. The Ouarkziz monocline bears all the key features of a typical triangle structure [*Banks and Warburton*, 1986]. Unfortunately, in the absence of seismic lines, we have no means to determine the additional shortening accommodated by underthrusting below this structure other than minimum estimates based on total structural relief.

6. Tectonic Implications and Discussion

6.1. Crustal-Scale Balancing

[45] Having gained some new information about the shortening in the sedimentary cover of the western Anti-Atlas, some further implications for the basement are now considered. For the illustration of our concepts a section has been chosen where the interaction between basement and sedimentary cover can be best demonstrated. This section runs across the central part the Jbel Bani (see Figure 1b), where our 3-D model has been constructed. We will concentrate first on the tectonic implications, which come from the minimal shortening recorded in the sedimentary cover. A conservative section has been constructed. For the folded Ordovician only map-scale and outcrop-scale shortening were considered. Northwest of the outcropping Jbel Bani folds, now eroded from above the basement high, the structural style is assumed to be the same geometry as within the 3-D model, i.e., open, upright folds with steep limbs. In order to account for an observed increase in thickness of the Ordovician toward the northwest [*Destombes et al.*, 1985], folds were drawn with a slightly increasing amplitude and wavelength in this direction.

[46] Southeast of the model, the Bani folds are depicted as dying out rapidly below the Drâa plain. The Jbel Ouarkziz triangle structure is interpreted as stemming from one single thrust stepping up south-southeastward from the Middle Cambrian shales to Upper Devonian shales before ending blindly somewhere below the Tindouf basin in a tip point, from which a postulated backthrust/décollement horizon must lead back up to the Earth's surface, most likely into the lower Drâa valley. We hold this backthrust responsible for the marked disharmony between the folded Jbel Rich below and the nonfolded Jbel Ouarkziz monocline above.

[47] The top of the lower Cambrian has been reconstructed using down-plunge projections and depth to detachment calculations [*Epard and Groshong*, 1993; *Bulnes and Poblet*, 1999]. In the western Anti-Atlas the Adoudounian (Lower Cambrian) consists mainly of massive platform carbonate series [*Destombes et al.*, 1985; *Benssaou and Hamoumi*, 2003]. Incompetent horizons are scarce and sediments up to the Middle Cambrian are strongly coupled

to the basement (compare Figures 2 and 3). A décollement within these sediments, at least in the western Anti-Atlas, is very unlikely and not corroborated by any structural observations. Therefore the whole pile from the basement up to the top of the Lower Cambrian can be considered as one structural unit, the ''basement-Cambrian'' unit in our rheologic terminology.

[48] As seen on most classical cross sections of the Anti-Atlas and confirmed by our own field observations, the folded Ordovician is clearly decoupled from this basement-Cambrian unit. Folding is not restricted to structural lows between the basement inliers, however, and entire fold trains can be projected sideways above the larger basement domes. This also means that Bani folding at any given location cannot be linked to one specific (assumed) thrust fault in the basement. Shortening in the Ordovician needs to be compared to the overall shortening on a much larger scale, so as to include the entire basement-cover contact. In order to balance the section at the crustal scale, an equal amount of shortening is necessary in the sedimentary cover and the basement. Shortening within the basement is assumed to take place along widely spaced, mostly hidden large-scale reverse faults. Geometric constraints will be discussed below.

6.2. Thin Skin Interpretation

[49] With the Ordovician strongly decoupled from the basement-Cambrian unit and a shortening increasing toward the northwest, the question arises to which degree the observed folding could be the result of a thin skin thrusting-folding phase, predating the formation of the basement uplifts. The westernmost part of the Anti-Atlas, west of the Bas Drâa inlier, is known as a thin skin domain indeed [*Belfoul*, 1991; *Soulaimani*, 1998; *Piqué*, 2001; *Belfoul et al.*, 2002]. It is characterized by map-scale thrusts and reverse faults within Lower Cambrian units. Accordingly, shortening observed in the Ordovician Jbel Bani might be rooted either here or in even more internal positions to the west, currently hidden in the Moroccan offshore. We consider such a distant source for the shortening of the Jbel Bani as very unlikely, however. Such a thin skin interpretation still requires two new postulates, which are not substantiated by any observations. First, a regional-scale basal décollement within Middle Cambrian shales would have to be increasingly important westward, prior to cutting down into the basement-Cambrian unit, in locations where neither direct nor indirect evidence for any major basement ramp is present. Secondly, the basement uplifts of the SW Anti-Atlas would have to be explained by a second deformation phase, in an essentially ''vertical tectonics'' fashion, without any sizeable amount of horizontal shortening. This latter view of the Anti-Atlas basement uplifts does not provide any explanation for the observed crustal-scale thickening.

[50] The fold axis directions within the Adoudounian of the western Anti-Atlas show considerable heterogeneity [*Soulaimani*, 1998]. In many places, they parallel in a conspicuous manner the outlines of the basement domes. This results in places in fold interference patterns with nearly perpendicular fold axes [*Caritg et al.*, 2003]. Most authors agree that the intimate relationship of fold axes directions and basement outlines is due to ''forced'' folding of the sedimentary cover, accommodating differential movements of basement blocks. It is difficult to envisage these complicated fold pattern as the result of an early, thin skin folding phase. Thus, at least in the Adoudounian of the western Anti-Atlas, there exists no evidence for folding independent of the main deformation phase, which is clearly thick skinned, involving basement. The tectonic style of these folds at the lowermost stratigraphic levels is very similar to the Rocky Mountains of Wyoming [*Stone*, 1993, 2002].

[51] Higher up in the stratigraphy, however, within the Ordovician Jbel Bani, fold axes directions are very regular and increasingly independent of the underlying basement structures. Some minor variations in fold axis directions can still be explained as deflections around the basement inliers, albeit strongly attenuated above the Lie de vin detachment level. No polyphase deformation history is required to explain these variations in fold axis trends in the western Anti-Atlas. Note that further east, near Tata, there is evidence for a two-phase history in the form of conspicuous fold interference patterns [*Caritg et al.*, 2003], but even there, both folding phases are best explained in a thick skinned fashion, because of reactivation of former basement faults, in close analogy with Laramide uplifts of the Rockies [*Stone*, 1993; *Marshak et al.*, 2000; *Bump*, 2003].

[52] Paleostress measurements in the western Anti-Atlas fold belt reveal that the local axes of major compressive stress are subperpendicular to the fold axes throughout the Jbel Bani. The paleostress field also shows some heterogeneity and it is characterized by a predominant local component. It seems therefore that the paleostress field is also conditioned by the basement blocks rather than being the result of a distant push. In conclusion, an early thin skin phase is regarded as a very improbable mechanism to explain the folding of the Ordovician Jbel Bani.

6.3. Thick Skin Interpretation

[53] A rapid glance at the tectonic map of the SW Anti-Atlas reveals the existence of ''thick skin'' tectonics, necessary to explain the large domes of Proterozoic-Cambrian [*Rodgers*, 1995]. The central question is not the existence, but the nature and origin of these basement domes, as well as their relationship with the buckle folding observed in the cover series around and above them. Direct evidence for large-scale thrusts within the basement-Cambrian unit is elusive in the western Anti-Atlas. This lack of direct evidence should not be used as an argument against the existence of thrusts or reverse faults at depth, however. There is a series of explanations why such thrusts have not been mapped, nor postulated. The most important reason is the present-day erosion level, revealing only a very small, topmost 2 km of more than 10 km of structural relief of these basement uplifts. This estimate is based on the known depth to basement in the distant foreland of the Tindouf basin, where it is located at approximately −8 km [*Michard*, 1976; *Bertrand-Sarfati et al.*, 1991]. Similarly, the preshortening

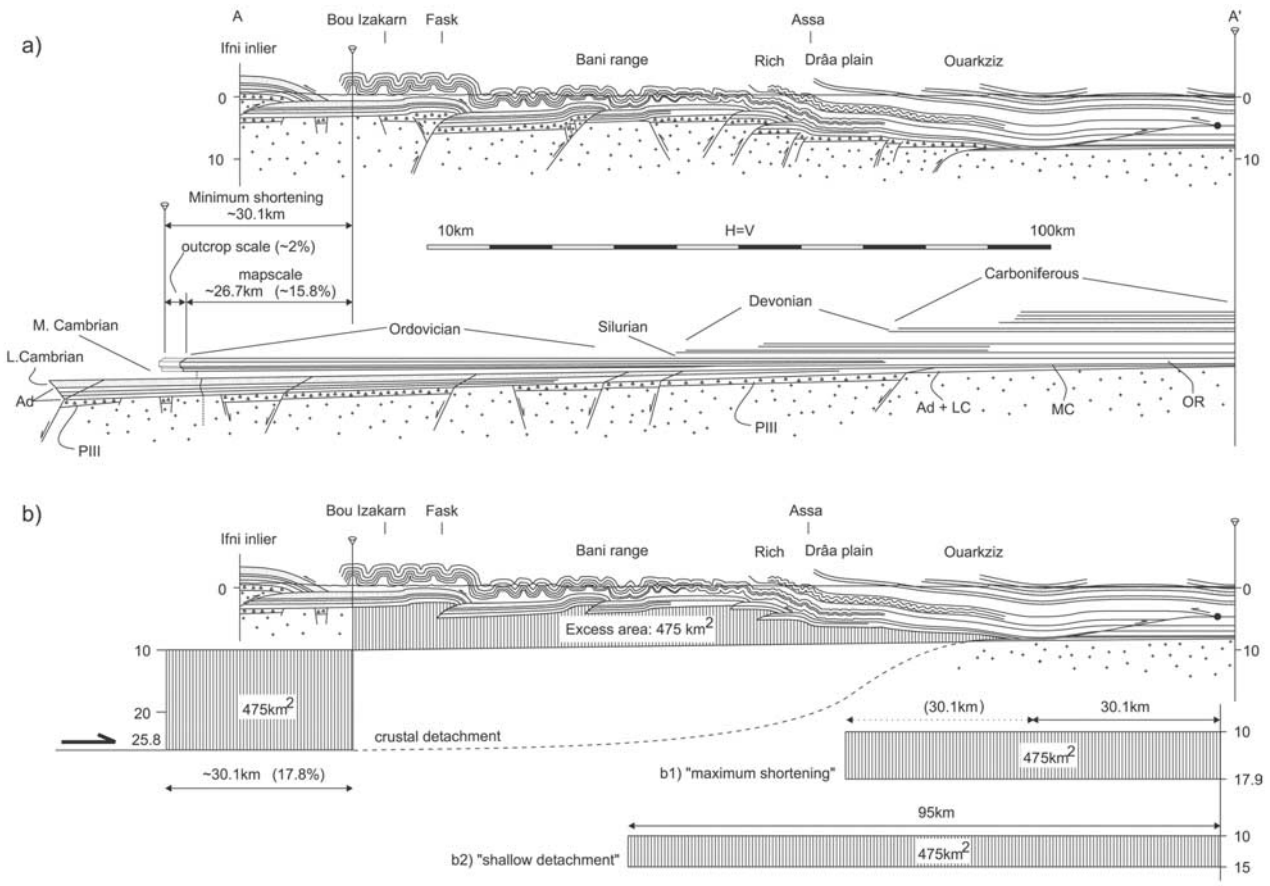

Figure 10. (a) Large-scale cross section through the entire western Anti-Atlas and corresponding unfolded section, with a conservatively estimated minimum horizontal shortening of 30 km. Abbreviations are as follows: Ad, Adoudounian; LC, Lower Cambrian; MC, Middle Cambrian; OR, Ordovician. Stippled area shows the most competent units (mainly quartz arenites, sandstones, and conglomerates). (b) Visualization of the ''excess area'' concept used to estimate the depth to an inferred middle to lower crustal detachment. The cross-sectional area calculations are based on the assumption of an initially 10 km deep sedimentary basin, necessary to accommodate the thickness of the Paleozoic series of the Anti-Atlas chain. A maximum estimate of shortening of the order of 60 km (30 km folding + 15% LPS) requires a midcrustal detachment at about 18 km depth (labeled b1). A shallow detachment at 15 km depth leads to an unreasonably high shortening of 95 km (labeled b2).

top basement level in the southwestern Anti-Atlas region must have been at some −10 km below sea level in order to accommodate the total thickness of Paleozoic sediments, which comprise shallow marine series up to the middle Carboniferous (Visean).

[54] Another reason why no large-scale thrusts were found in the SW Anti-Atlas is the presence of widespread thick Middle Cambrian shales. As depicted in Figure 10, we assume a tectonic style where thrust ramps, breaking through the Lower Cambrian Adoudounian, turn to horizontal ''flats'' within incompetent Middle Cambrian shales. Minor thrusts may level out even deeper in the stratigraphy, within thin evaporitic shales of the Adoudounian unit.

[55] An important reverse fault or thrust has been described in the westernmost Anti-Atlas, at the southern border of the Lower Drâa inlier, where Proterozoic basement is thrust toward the SE onto the sedimentary cover [*Soulaimani*, 1998]. Here, intense deformation under lower greenschist facies lead to the development of a foliation with steeply plunging stretching lineations and a marked internal deformation of rhyolite pebbles of the PIII; all these deformation features are compatible with a south-southeastward thrust.

[56] At the scale of the entire Anti-Atlas, crustal-scale balancing considerations are used to constrain permissible basement geometries at depth. One of the key features of the Anti-Atlas is its high structural relief. A conservative estimate of the total thickness of the Paleozoic cover series of the SW Anti-Atlas yields 10 km thickness. Most of this thickness is preserved today in first-order synclinoria, in between the basement domes. However, there is good evidence for a similar amount of erosion from atop the westernmost basement inliers (Bas Drâa, Ifni, Kerdous), which were invariably at lower greenschist facies metamor-

phic conditions during late Variscan deformation. This metamorphism is obvious from the deformation style at the brittle/ductile transition and from our own illite crystallinity measurements [*Buggisch*, 1988a; *Burkhard et al.*, 2001; Helg et al., submitted manuscript, 2004]. In contrast to previous authors, who mostly considered these basement domes as all-time "horsts," with a reduced thickness of total Paleozoic cover, we assume an essentially continuous thickness of sedimentary series across these basement domes. We therefore assume a similar structural relief to exist at the basement cover contact, where it is documented, and at the Devonian/Carboniferous boundary, where it is mostly based on indirect evidence.

[57] The present-day topography and average elevation of the Anti-Atlas could be at least partly due to Neogene reactivation in relation with High-Atlas inversion tectonics [*Beauchamp et al.*, 1999; *Frizon-de-Lamotte et al.*, 2000]. The Anti-Atlas is also the location of Pliocene volcanic activity, e.g., in the Jbel Siroua, and broad thermal uplift at a regional scale has to be taken into consideration. Accordingly, the removal of more than 10 km of Paleozoic sediments from above the basement inliers may not be solely the result of late Variscan tectonics but the combined effect of late Variscan tectonics, Neogene Atlas inversion, and thermal hot spot related uplifts and concomitant erosion. The total amount of non-Variscan uplift/erosion in the Anti-Atlas is ill constrained. Upper Cretaceous sediments of the "Hamada" clearly seal Variscan folds; their present-day elevation is about 400 m above sea level in the eastern Anti-Atlas but close to sea level near the Atlantic coast. In between, this same marker horizon is completely eroded from above the SW Anti-Atlas, leaving some room for speculation. Thermal uplift, related to the volcanic activity of the Jbel Sirhoua, can only be estimated from general considerations. Surface uplift related to plates moving over hot spots may reach 1 to 3 km, affecting large areas of up to 2000 km across [*Coward*, 1994; *Eisbacher*, 1996].

[58] Nevertheless, even with the assumption of up to 3 km of Neogene surface uplift and High Atlas reactivation, the leveling of more than 7 km of structural relief remains to be explained by late Variscan tectonics with concomitant uplift and erosion. This same amount of structural relief is not only attained at the scale of the orogen but also at the scale of individual basement domes. Between the Jbel Bani and the surrounding basement inliers Kerdous, Lower Drâa, and Ifni (Figure 2), the structural relief is in excess of 7 km. Given the modest amount of cover shortening observed in the Anti-Atlas fold belt, this structural relief is difficult to explain by an antiformal stack of thin basement slabs above a relatively shallow crustal detachment [*Boyer and Elliott*, 1982]. As an example, if we assume 5 km thick basement slabs overlain by a 10 km thick sedimentary series, a horizontal shortening of roughly 95 km would be necessary to create the observed cross sectional excess area of 475 km^2 (Figure 10b, "shallow detachment" diagram labeled b2). This exceeds by far our estimations of the horizontal shortening observed within the sedimentary cover. The discrepancy is too large to be explained by ill evaluated, underestimated outcrop-scale or microscale shortening. Even if we assume a total submap-scale shortening of the same magnitude as map-scale shortening, the calculated depth to detachment remains at about 18 km (Figure 10b, "maximum shortening" diagram labeled b1). Considering only the minimal shortening (the total observed shortening), the detachment depth comes to lie at about 26 km depth.

[59] As an alternative to the antiformal stack of thin basement slabs we postulate basement inversion of thick block-like basement parts with the dimension of the present day boutonnieres, uplifted along steep reverse faults. The depth of the detachment horizon again determines the thickness of such basement blocks.

6.4. Inversion Tectonics

[60] The term inversion is used here in the sense of *Coward* [1994] to describe regions which have experienced a reversal in uplift or subsidence. The Anti-Atlas nicely fits this definition; after an extended period of subsidence during the Paleozoic, the Anti-Atlas basin is the locus of tectonic shortening, uplift, and erosion during the later stages of the Variscan orogeny, possibly with some reactivation in Neogene times [*Frizon-de-Lamotte et al.*, 2000].

[61] Most authors agree that Variscan basements tectonics of the Anti-Atlas is dominated by the reactivation of former weakness zones. In earlier publications these weakness zones are invariably considered to be subvertical [*Michard*, 1976]. Sedimentological evidence for an important post-Panafrican extensional phase has accumulated during the last two decades [*Soulaimani et al.*, 2001; *Benssaou and Hamoumi*, 2003]. Decametric fault-bounded graben structures are documented within the Proterozoic basement in the westernmost Anti-Atlas [*Soulaimani*, 1998]. Regional changes in thickness and facies of Cambrian series have been used to map the location and general orientation of graben structures [*Benssaou and Hamoumi*, 2003] (Figure 11).

[62] In the light of this post Panafrican rifting phase a Variscan inversion of former PIII normal faults seems the most likely explanation for the mostly still hidden reverse faults bounding the present day basement inliers. Rather than all-time horsts [*Michard*, 1976; *Piqué*, 1994; *Benssaou and Hamoumi*, 2003], basement inliers in our interpretation represent the former basin floors. The fault reactivation nicely explains the strong basement involvement and the high basement topography in an otherwise only mildly deformed tectonic setting.

[63] Tectonic inversion is, at least partly, corroborated by the thickness distribution of the rift/early postrift sediments [*Boudda et al.*, 1979]. The thickness of the lowermost Adoudounian unit, also called "Lower Limestones" (Figure 11), is highest in the area of the basement domes of the western Anti-Atlas, decreasing both east and southward, forelandward. In other words, the location of maximum subsidence by rifting corresponds roughly with the area of maximum uplift by late Variscan tectonic inversion.

[64] The widespread occurrence of PIII rift sediments found along the borders of almost all boutonnieres is an additional indication for these to be former grabens, rather

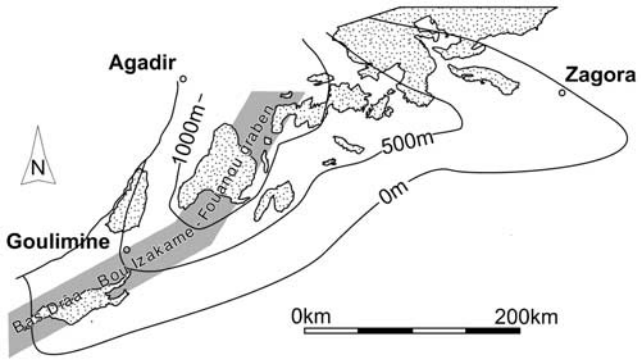

Figure 11. Thickness distribution of the lowermost sedimentary unit of the Paleozoic Anti-Atlas basin according to *Boudda et al.* [1979]. The Bas Drâa-Bou Izakarne-Fouanou graben structure of Middle Cambrian age is shown according to a recent detailed stratigraphic analysis of *Benssaou and Hamoumi* [2003, Figure 2].

than horsts. We have to admit, however, that there is no observational control, nor is there any subsurface data available about the regional-scale variations of PIII series for the large ''synclinal'' areas in between the present day basement domes. According to our inversion hypothesis, there should be only a very limited amount of PIII series in these areas of the former, Late Proterozoic horsts.

7. Conclusions

[65] The Anti-Atlas of Morocco represents a special type of foreland fold belt with a striking absence of observable thrusts. Cover shortening is accommodated by tight detachment folding of competent quartzite and carbonate layers, but no ramping or duplexing has ever been observed. This tectonic style is dictated by the mechanical stratigraphy of the Paleozoic cover series, dominated by thick intervals of shale and siltstones. Four competent units are distinguished (Figure 3), from bottom to top: (1) basement-Lower Cambrian, (2) Jbel Bani (Ordovician), (3) Jbel Rich (Devonian), and (4) Jbel Ouarkziz (lower Carboniferous). The basement-Lower Cambrian unit (1) is involved in massive inversion of Late Proterozoic normal faults, leading to Laramide style basement domes of several tens of kilometers wavelength, with ''amplitudes'' or structural relief on the order of 7 to 10 km: the ''first-order'' basement folds or so-called ''plis de fond'' [*Argand*, 1924]. A more than 1 km thick series of Middle Cambrian shales allows for a complete decoupling and disharmony between this basement unit (1) and the overlying Paleozoic cover series (2 and 3), which react essentially by polyharmonic multilayer folding [*Ramsay and Huber*, 1987]. Larger wavelengths (1 km) and amplitudes (500 m) are observed within folds of the thicker Ordovician sandstones of the Jebel Bani than within the Devonian Jbel Rich folds (500 m, 200 m). Carboniferous series (4) are only preserved at the very mountain front, where they are involved in a triangle structure. The total width of the SW Anti-Atlas foreland belt is about 150 km and basement domes occur at less than 30 km behind the mountain front. A minimum total amount of 30 km (17%) of cover shortening is obtained from restoration of the Jbel Bani fold train. Balancing considerations require a middle to lower crustal detachment at 18 to 25 km depth for the basement inversion.

[66] **Acknowledgments.** We wish to thank A. Soulaimani for introducing us to the geology of the Anti-Atlas, his hospitality, and for many inspiring discussions. Ongoing support by the Moroccan ''Ministère de l'Energie et des Mines, Direction de la Géologie'' and the state petroleum agency ONAREP is gratefully acknowledged. We wish to thank personally M. Dahmani, A. M. Morabet, and M. Zizi for their help. We are grateful to Bert Bally, André Michard, Alain Piqué, Jean-Paul Schaer, and Dieter Schroeder for encouragement and for sharing their ideas and data about the Anti-Atlas of Morocco. Financial support by the Swiss National Science Foundation, grants 21-52516.7 and 20-63790.00 is gratefully acknowledged.

References

Argand, E. (1924), La tectonique de l'Asie, *Proc. Int. Geol. Congr.*, *13th*, 171–372.

Azizi-Samir, M. R., J. Ferrandini, and J. L. Tane (1990), Late Pan-African (580–560 M.A.) tectonic activity and volcanism in the Anti-Atlas Mountains of Morocco: Geodynamic interpretation on the scale of north-west Africa, *J. Afr. Earth Sci.*, *10*, 549–563.

Banks, C. J., and J. Warburton (1986), ''Passive-roof'' duplex geometry in the frontal structures of the Kirthar and Sulaiman mountain belts, Pakistan, *J. Struct. Geol.*, *8*, 229–237.

Beauchamp, W., R. W. Allmendinger, M. Barazangi, A. Demnati, M. Alji, and M. Dahmani (1999), Inversion tectonics and the evolution of the High Atlas Mountains, Morocco, based on a geological-geophysical transect, *Tectonics*, *18*, 163–184.

Belfoul, M. (1991), La structuration hercynienne de la région de Labiar-Oued Boussafene (Guelmim, Anti-Atlas sud-occidental), thèse 3ème cycle thesis, 162 pp., Univ. de Rabat, Rabat, Morocco.

Belfoul, M. A., F. Faik, and B. Hassenforder (2002), Evidence of a tangential tectonic event prior to the major folding in the Variscan belt of the western Anti-Atlas, Morocco, *J. Afr. Earth Sci.*, *32*, 723–739.

Benssaou, M., and N. Hamoumi (2003), The Lower-Cambrian western Anti-Atlasic graben: Tectonic control of paleogeography and sequential organisation, *C. R. Geosci.*, *335*, 297–305.

Bertrand-Sarfati, J. (1981), Problème de la limite Précambrien-Cambrien: La section de Tiout (Maroc): Les stromatolithes et leur biostratigraphie, *Newsl. Stratigr.*, *10*, 20–26.

Bertrand-Sarfati, J., A. Moussine-Pouchkine, P. Affaton, R. Trompette, and Y. Bellion (1991), Cover sequences of the West African Craton, in *The West African Orogens and Circum Atlantic Correlatives*, edited by R. D. Dallmeyer and J. P. Lecorche, pp. 65–82, Springer-Verlag, New York.

Bonhomme, M., and B. Hassenforder (1985), Le métamorphisme hercynien dans les formations tardi-et post-panafricaines de l'Anti-Atlas occidental (Maroc): Données isotopiques Rb/Sr et K/Ar des fractions fines, *Sci. Geol. Bull.*, *38*, 175–183.

Boudda, A., G. Choubert, and A. Faure-Muret (1979), Essai de stratigraphie de la couverture sédimentaire de l'Anti-Atlas: Adoudounien - Cambrien Inférieur, *Notes Mem. Serv. Geol. Maroc*, *271*, 96.

Boyer, S. E., and D. Elliott (1982), Thrust systems, *AAPG Bull*, *66*, 1196–1230.

Buggisch, W. (1988a), Diagenesis and very low-grade metamorphism of the Lower Cambrian rocks in the Anti-Atlas, Morocco, in *The Atlas System of Morocco: Studies on Its Geodynamic Evolution*, *Lecture Notes in Earth Sci.*, vol. 15, edited by Volker H. Jacobshagen, pp. 123–128, Springer-Verlag, New York.

Buggisch, W. (1988b), The Precambrian-Cambrian boundary in the Anti-Atlas (Morocco), in *The Atlas System of Morocco: Studies on Its Geodynamic Evolution*, *Lecture Notes in Earth Sci.*, vol. 15, edited by Volker H. Jacobshagen, pp. 81–90, Springer Verlag, New York.

Bulnes, M., and J. Poblet (1999), Estimating the detachment depth in cross sections involving detachment folds, *Geol. Mag.*, *136*, 395–412.

Bump, A. P. (2003), Reactivation, trishear modeling, and folded basement in Laramide uplifts: Implications for the origins of intra-continental faults, *GSA Today*, *13*(3), 4–10.

Burkhard, M., S. Caritg, U. Helg, and C. Robert-Charrue (2001), Forced, disharmonic multilayer buckle folding in the late Variscan Antiatlas of Morocco, paper presented at American Association

of Petroleum Geologists 2001 Annual Meeting, Tulsa, Okla.

Caritg, S., M. Burkhard, R. Ducommmun, U. Helg, L. Kopp, and C. Sue (2003), Fold interference patterns in the late Paleozoic Anti-Atlas of Morocco, *Terra Nova*, *16*, 27–37.

Choubert, G. (1963), Histoire géologique du précambrien de l'Anti-Atlas, *Notes Mem. Serv. Geol. Maroc*, *162*, 352.

Choubert, G., and A. Faure Muret (1971), Anti-Atlas (Maroc), in *Tectonique de l'Afrique* (*Tectonics of Africa*), *Earth Sci. Ser.*, vol. 6, pp. 163–175, UNESCO, Paris.

Coward, M. (1994), Inversion Tectonics, in *Continental Deformation*, edited by P. L. Hancock, pp. 289–304, Pergamon, New York.

Desthieux, F. (1977), Etude tectonique et métallogénique du Jbel Addana, Ordovicien des plaines du Dra. Maroc présaharien, *Notes Serv. Geol. Maroc*, *268*, 209–236.

Destombes, J., H. Hollard, and S. Willefert (1985), Lower Paleozoic rocks of Morocco, in *Lower Palaeozoic of North-Western and West-Central Africa*, vol. 4, edited by C. H. Holland, pp. 91–336, Trinity Coll., Dep. of Geol., Dublin, Ireland.

Donzeau, M. (1974), L'Arc Anti-Atlas-Ougarta (Sahara nord-occidental, Algérie-Maroc), *C. R. Acad. Sci., Ser. II*, *278*, 417–420.

Eisbacher, G. H. (1996), *Einführung in die Tektonik*, 374 pp., F. Enke, Stuttgart, Germany.

Engelder, T., and S. Marshak (1985), Disjunctive cleavage formed at shallow depths in sedimentary rocks, *J. Struct. Geol.*, *7*, 327–343.

Epard, J. L., and R. H. J. Groshong (1993), Excess area and depth to detachment, *AAPG Bull.*, *77*, 1291–1302.

Faik, F., M. A. Belfoul, M. Bouabdelli, and B. Hassenforder (2002), The structures of the Late Neoproterozoic and Early Palaeozoic cover of the Tata area, western Anti-Atlas, Morocco: Polyphased deformation or basement/cover interactions during the Variscan orogeny?, *J. Afr. Earth Sci.*, *32*, 765–776.

Frey, M. (1987), *Low Temperature Metamorphism*, Chapman and Hall, New York.

Frizon-de-Lamotte, D., B. Saint-Bezar, R. Bracene, and E. Mercier (2000), The two main steps of the Atlas building and geodynamics of the western Mediterranean, *Tectonics*, *19*, 740–761.

Geyer, G., and E. Landing (1995), *MOROCCO '95—The Lower-Middle Cambrian Standard of Western Gondwana*, 269 pp., Inst. für Paläontol., Univ. Würzburg, Würzburg, Germany.

Guerraoui, A., M. Bensaid, and M. Dahmani (1997), Carte géologique du Maroc 1:100'000, Fask, *Notes Serv. Geol. Maroc*.

Guiton, M. L. E., W. Sassi, Y. M. Leroy, and B. D. M. Gauthier (2003), Mechanical constraints on the chronology of fracture activation in folded Devonian sandstone of the western Moroccan Anti-Atlas, *J. Struct. Geol.*, *25*, 1317–1330.

Harrison, M. J., and C. M. Onasch (2000), Quantitative assessment of low-temperature deformation mechanisms in a folded quartz arenite, Valley and Ridge Province, West Virginia, *Tectonophysics*, *317*, 73–91.

Hassenforder, B. (1987), La tectonique panafricaine et varisque de l'Anti Atlas dans le Massif du Kerdous (Maroc), Thèse Sci. thesis, 249 pp., Univ. L. Pasteur Strasbourg, Strasbourg, France.

Hogan, J. P., and W. M. Dunne (2001), Calculation of shortening due to outcrop-scale deformation and its relation to regional deformation patterns, *J. Struct. Geol.*, *23*, 1507–1529.

Homberg, C. (1996), Analyse des déformations cassantes dans le Jura et modélisation numérique des perturbations des contraintes tectoniques autour d'accidents majeurs, Ph.D. thesis, 282 pp., Univ. Pierre et Marie Curie, Paris.

Huon, S. (1985), Clivage ardoisier et réhomogénisation isotopique K-Ar dans des schistes paléozoiques du Maroc: Etude microstructurale et isotopique: Conséquences régionales, Ph.D. thesis, 124 pp., Univ. Louis Pasteur, Strasbourg.

Jeannette, D. (1981), Influence de structures panafricaines sur des déformations hercyniennes (Bordure septentrionale de la boutonnière d'Igherm, Anti-Atlas occidental), *Notes Serv. Geol. Maroc*, *42*, 25–32.

Kisch, H. J. (1991), Development of slaty cleavage and degree of very-low-grade metamorphism: A review, *J. Metamorph. Geol.*, *9*, 735–750.

Kogbe, C. A. (1998), Sedimentary Basins of Morocco, *Afr. Geosci. Rev.*, *5*, 232.

Latham, A. (1988), The Precambrian-Cambrian transition in Morocco: Problems and perspectives, in *Trace Fossils, Small Shelly Fossils, and the Precambrian-Cambrian Boundary*, edited by E. Landon, G. M. Narbonne, and P. M. Myrow, *Bull. N. Y. State Mus.*, *1076*, 14 pp.

Leblanc, M. (1972), Sur le style disharmonique des plis hercyniens, à la base de la couverture, dans l'Anti-Atlas central (Maroc), *C. R. Acad. Sci., Ser. D*, *275*, 803–806.

Leblanc, M., and J. R. Lancelot (1980), Interpretation geodynamique du domaine pan-africain (Precambrien terminal) de l'Anti-Atlas (Maroc) a partir de donnees geologiques et geochronologiques, *Can. J. Earth Sci.*, *17*, 142–155.

Marshak, S., K. Karlstrom, and J. M. Timmons (2000), Inversion of Proterozoic extensional faults: An explanation for the pattern of Laramide and Ancestral Rockies intracratonic deformation, United States, *Geology*, *28*, 735–738.

Mattauer, M., F. Proust, and P. Tapponnier (1972), Major strike-slip fault of late Hercynian age in Morocco, *Nature*, *237*, 160–162.

Michard, A. (1976), Eléments de géologie Marocaine, *Notes Mem. Serv. Geol. Maroc*, *252*, 408.

Michard, A., and J. Sougy (1977), L'orogenèse hercynienne à la lisière nord-ouest de l'Afrique (Structure des chaînes primaires du Maroc au Sénégal), in *La Chaîne varisque d'Europe moyenne et occidentale*, *Colloq. Int. Cent. Natl. Rech. Sci.*, vol. 243, pp. 605–640, Cent. Natl. de la Rech. Sci., Paris.

Mitra, G. (1994), Strain variation in thrust sheets and across the Sevier fold-and-thrust belt (Idaho-Utah-Wyoming): Implications for section restoration and wedge taper evolution, *J. Struct. Geol.*, *16*, 585–602.

Mitra, S. (1992), Balanced structural interpretations in fold and thrust belts, in *Structural Geology of Fold and Thrust Belts*, edited by S. Mitra and G. W. Fisher, pp. 53–77, Johns Hopkins Univ. Press, Baltimore, Md.

Namson, J. (1981), Structure of the western Foothills Belt, Miaoli-Hsinchu area Taiwan: (1) Southern Part, *Pet. Geol. Taiwan*, *18*, 31–51.

Onasch, C. M. (1993), Determination of pressure solution shortening in sandstones, *Tectonophysics*, *227*, 145–159.

Piqué, A. (1994), *Géologie du Maroc: Les Domaines Structuraux et Leur Évolution Structurale*, 283 pp., Ed. PUMAG, Marrakech, Morocco.

Piqué, A. (2001), *Geology of Northwest Africa*, 310 pp., Gebrüder Bornträger, Stuttgart, Germany.

Piqué, A., and A. Michard (1989), Moroccan hercynides: A synopsis: The paleozoic sedimentary and tectonic evolution at the northern margin of West Africa, *Am. J. Sci.*, *289*, 286–330.

Piqué, A., J. J. Cornée, J. Müller, and J. Roussel (1991), The Moroccan Hercynides, in *The West African Orogens and Circum Atlantic Correlatives*, edited by R. D. Dallmeyer and J. P. Lecorche, pp. 229–263, Springer-Verlag, New York.

Piqué, A., M. Bouabdelli, and J.-R. Darboux (1995), Le rift cambrien du Maroc occidental, *C. R. Acad. Sci., Ser. II*, *320*, 1017–1024.

Piqué, A., M. Bouabdelli, A. Soulaimani, N. Youbi, and M. Iliani (1999), Upper Neoproterozoic PIII conglomerates in the Anti-Atlas, southern Morocco: Pan-African molasses, or indicators of upper Proterozoic rifting?, *C. R. Acad. Sci., Ser. II*, *328*, 409–414.

Plessmann, W. (1972), Horizontal-Stylolithen im französisch-schweizerischen Tafel-und faltenjura und ihre Einpassung in den regionalen Rahmen, *Geol. Rundsch.*, *61*, 332–347.

Ramsay, J. G., and I. M. Huber (1983), *The Techniques of Modern Structural Geology*, 307 pp., Academic, San Diego, Calif.

Ramsay, J. G., and I. M. Huber (1987), *The Techniques of Modern Structural Geology*, 697 pp., Academic, San Diego, Calif.

Rodgers, J. (1990), Fold-and-thrust belts in sedimentary rocks, part 1: Typical examples, *Am. J. Sci.*, *290*, 321–359.

Rodgers, J. (1995), Lines of basement uplifts within the external parts of orogenic belts, *Am. J. Sci.*, *295*, 455–487.

Schenk, P. E. (1971), Southeastern Atlantic Canada, northwestern Africa, and continental drift, *Can. J. Earth Sci.*, *8*, 1218–1251.

Sebai, A., G. Feraud, H. Bertrand, and J. Hanes (1991), AR-40/AR-39 dating and geochemistry of tholeiitic magmatism related to the early opening of the central Atlantic rift, *Earth Planet. Sci. Lett.*, *104*, 455–472.

Smart, K. J., W. M. Dunne, and R. D. Krieg (1997), Roof sequence response to emplacement of the Wills Mountain duplex: The roles of forethrusting and scales of deformation, *J. Struct. Geol.*, *19*, 1443–1459.

Soulaimani, A. (1998), Dynamique et interactions Socle/Couverture dans l'Anti-Atlas occidental (Maroc): Rifting fini-protérozoïque et orogenèse hercynienne, Thèse d'état, Univ. Cadi Ayyad, Marrakech, Morocco.

Soulaimani, A., C. Le Corre, and R. Farazdaq (1997), Deformation hercynienne et relation socle/couverture dans le domaine du Bas-Draa (Anti-Atlas occidental, Maroc), *J. Afr. Earth Sci.*, *24*, 271–284.

Soulaimani, A., A. Piqué, and M. Bouabdelli (2001), La série du PII–PIII de l'Anti-Atlas occidental (Sud marocain): Un olistostrome à la base de la couverture post-panafricaine (PIII) du Protérozoic supérieur, *Earth Planet. Sci. Lett.*, *332*, 121–127.

Soulaimani, A., M. Bouabdelli, and A. Piqué (2003), L'extension continentale au Néo-Protérozoïque supérieur-Cambrien inférieur dans l'Anti-Atlas (Maroc), *Bull. Soc. Geol. Fr.*, *174*, 83–92.

Stone, D. (1993), Basement-involved thrust-generated folds as seismically imaged in the subsurface of the central Rocky Mountain foreland, in *Laramide Basement Deformation in the Rocky Mountain Foreland of the Western United States*, edited by R. Chase, E. Erlsev, and C. Schmidt, *Spec. Pap. Geol. Soc. Am.*, *280*, 271–318.

Stone, D. (2002), Morphology of the Casper Mountain uplift and related subsidiary structures, central Wyoming: Implications for Laramide kinematics, dynamics, and crustal inheritance, *AAPG Bull.*, *86*, 1417–1440.

Villa, I. (1998), Isotopic closure, *Terra Nova*, *10*, 42–47.

Villeneuve, M., and J. J. Cornee (1994), Structure, evolution and palaeogeography of the West African Craton and bordering belts during the Neoproterozoic, *Precambrian Res.*, *69*, 307–326.

Weijermars, R. (1993), Estimation of paleostress orientation within deformation zones between two mobile plates, *Geol. Soc. Am. Bull.*, *105*, 1491–1510.

M. Burkhard, S. Caritg, U. Helg, and C. Robert-Charrue, Institut de Géologie, Université de Neuchâtel, Case Postale, Rue E. Argand 11, CH-2007, Neuchâtel, Switzerland. (martin.burkhard@unine.ch)

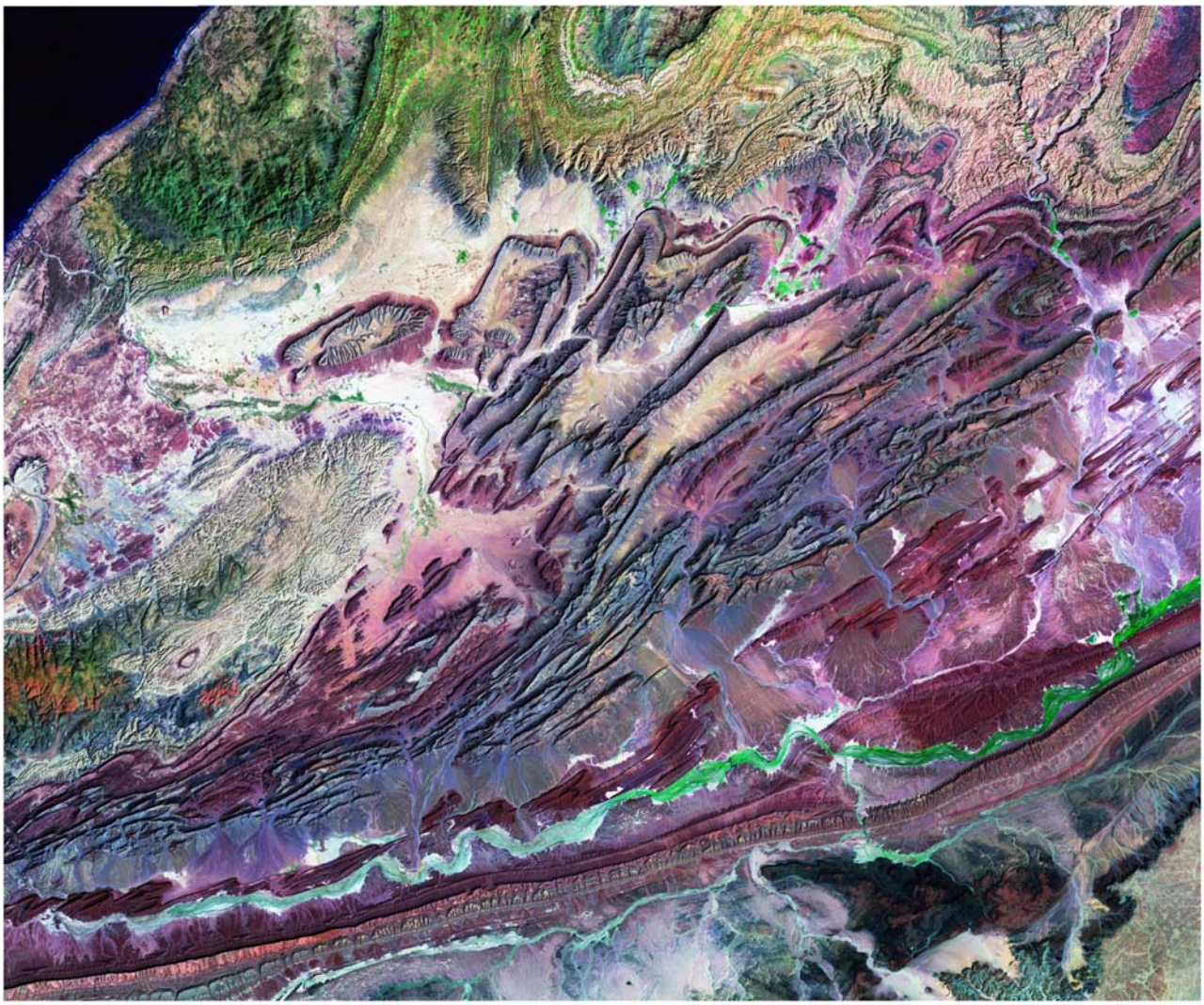

Figure 2. Landsat image of the westernmost Anti-Atlas chain. Compare with Figure 1 for major landmark features such as the basement inliers (dark green) with their "autochthonous" Cambrian cover in light green and tan colors. Quartz-rich lithologies of the Jbel Bani, the Jbel Rich, and Jbel Ouarkziz appear in dark purple. Image courtesy of NASA and Earth Satellite Corporation (available at http://zulu.ssc.nasa.gov/mrsid/mrsid.pl).

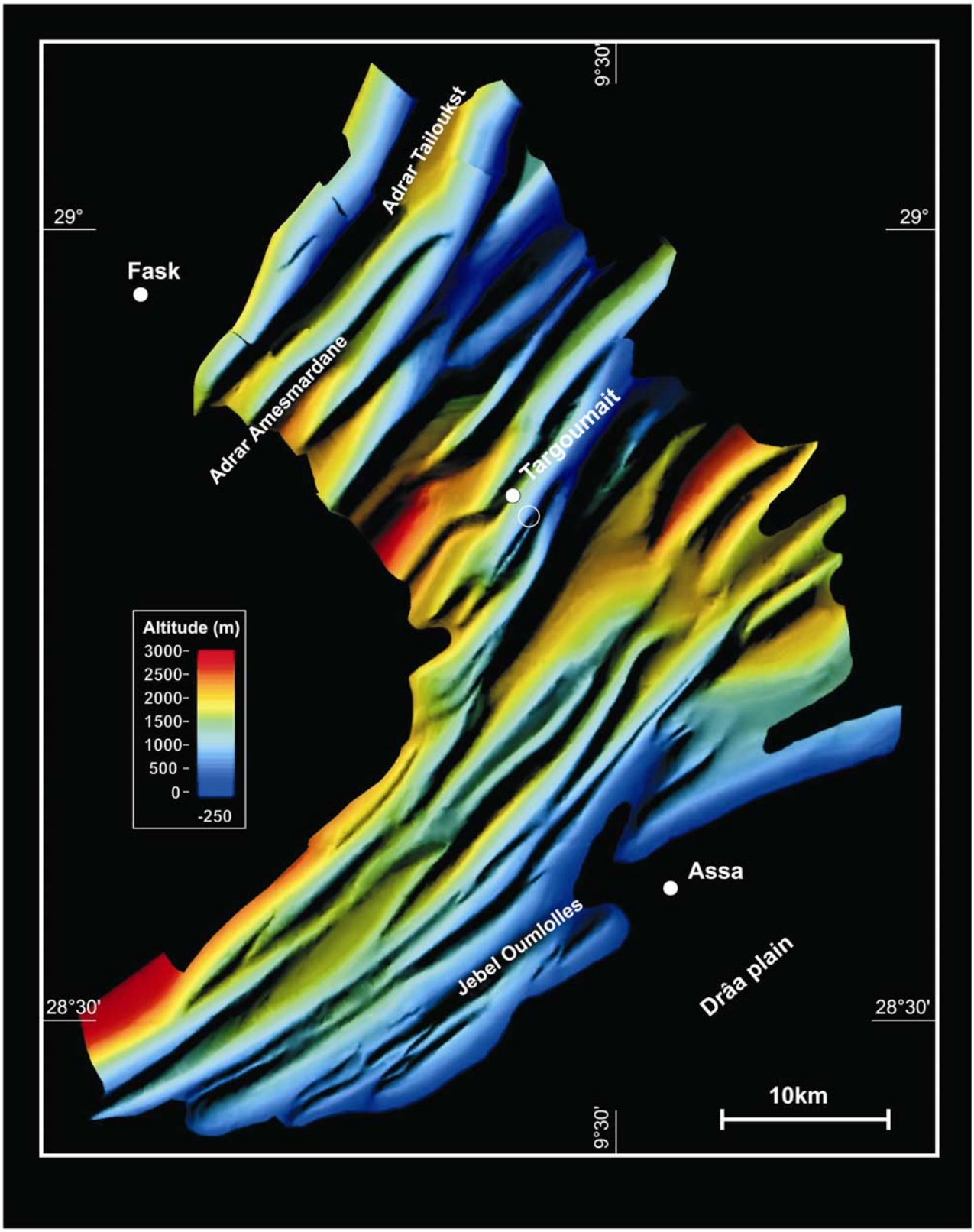

Figure 6. Three-dimensional rendering of a structure contour map constructed for the top of the or6c marker horizon in the western part of the Jbel Bani. The small white circle shows the location of the photograph of Figure 8. Note the decreasing amplitude and wavelength toward the south.

PROJET D'ARTICLE

Un troisième article est prévu abordant les thèmes suivants :

- Interférence Anti-Atlas – Ougarta (Figures 34 et 40), avec l'élaboration d'un modèle tridimensionnel représentant l'ipsographie du sommet de l'Ordovicien supérieur au paroxysme varisque.
- Mise en évidence de la déformation d'orientation ougartienne par la construction d'une coupe ENE-WSW au sud des boutonnières.
- Analyse des relations géométriques entre l'Anti-Atlas et les sédiments post-varisques (Figure 36).

C

RESUMES ET POSTERS

- Late Variscan Inversion Tectonics in the Paleozoic Tafilalt basin of South-Eastern Morocco. Abstract. MIOG 2002.

- Inversion tectonics in the hercynian Anti-Atlas of Morocco. Abstract. SGM 2003.

- The Anti-Atlas fold-belt of Morocco : Thick skin inversion tectonics in the hinterland of the alleghenian orogeny. Abstract. RST 2004.

- Tectonique d'inversion dans l'Anti-Atlas oriental. Abstract. 3Ma 2005.

- The Anti-Atlas fold belt of Morocco : variscan inversion tectonics and interference pattern of an "intracratonic" basin. Abstract. SGM 2005.

- The Anti-Atlas fold-belt of Morocco. Poster. RST 2004.

- Structural study of the eastern Anti-Atlas, the variscan belt of Morocco. Poster. SGM 2005.

ABSTRACTS

Abstract présenté au Marrakech International Oil & Gas 2002, session poster.

Late Variscan Inversion Tectonics in the Paleozoic Tafilalt basin of South-Eastern Morocco

The Paleozoic Tafilalt basin in south eastern Morocco is located in the "hinterland" of the late Variscan Appalachian-Antiatlas chain. A post-panafrican sedimentary cycle starts with rifting in Late Proterozoic (PIII), followed by thermal subsidence during most of the Paleozoic. An increase in subsidence rates in Late Devonian, with an associated change from marl/carbonates to shale/siliciclastics is interpreted in terms of a change to a foreland basin setting – in response to closure of the Japetos ocean and tectonic activity within an early Appalachian/ Variscan chain forming in the far distance to the NW. We could not find any evidence for syn-sedimentary tectonics within this Late Paleozoic clastic wedge. NE-SW oriented compressional deformation is entirely post- Late Carboniferous and lead to spectactular inversion structures – seen on geologic maps and satellite images. This compression is due to a late phase of Variscan collision tectonics expressed here as mostly thick skin – intracratonic shortening in Wind river style. Seemingly thin skin folding takes place above thick incompetent shale horizons – particularly in the southern Tafilalt. Structural trends of the large scale broad folds and associated faults are inherited from the Panafrican and or Late Proterozoic (PIII). This compression is followed by marked event of extension in a NNW-SSE direction of uncertain age (Late Variscan – Permian? or early Alpine - Liassic?). The interference between the forced folding (inversion) and renewed extension in an oblique direction lead to a complex map pattern of folds and faults, further complicated by a third reactivation in a dextral strike slip regime.

Abstract présenté au Swiss Geoscience Meeting 2003 à Bâle, conférence dans la session du Swiss Tectonic Studies Group.

Inversion tectonics in the hercynian Anti-Atlas of Morocco

Charles Robert-Charrue, Martin Burkhard

Geological Institute, Neuchâtel University, CP 2 , CH-2007 Neuchâtel, charles.robert-charrue@unine.ch

The Anti-Atlas of Morocco is a foreland belt, limited to the south by the west african craton and to the north by the alpine High Atlas. This chain is included in the Appalachian orogeny. The Anti-Atlas appears as a huge NE-SW anticlinorium. Locally, the basement is cropping out as " Boutonnières", but the main part is made of an important Paleozoïc cover, wich is gently folded and of low grade metamorphism.

An entire Wilson cycle of mountain building left its imprint in these rocks. Sedimentation started with a Late Proterozoic rifting phase, leading to the opening of the Japetos ocean to the west. Post-rift sediments of Lower Cambrian to Middle Carboniferous age are dominated by detrial input from the cratonic hinterland of Africa, leading to the accumulation of a thick pile of alterning quartzites, siltstones, shales and occasional carbonates. During the last stages of closure of the Japetos ocean, this passive margin is squeezed in the collision between Euramerica and North Africa. This collision leads to a massive inversion of former normal faults, enormous uplifts of the Precambrian basement and a simultaneous folding of the overlying cover series. Syn- to post-tectonic erosion and isostatic re-equilibration lead to the removal of beetween 2 and 15 km of material, bringing lower green-schist facies rocks back to the earth's surface. Minor phases of reactivation include far field effects of a new cycle of High Atlas / Atlantic rifting during Mesozoic, Late Miocene compression in relation with the Alpine collision and High Atlas inversion, and possibly some recent hot spot related thermal uplift responsible for the high present day topography and relief.

In the studied central and eastern part of Anti-Atlas, the paleozoic serie is thinning gradually to about 6 to 8 km, while more then 12 km are found in the south-west. This thinning affects the behaviour of the cover. Important rheologic contrasts determine the strutural style. The total shortening of the cover also decreases gradually, from some 30 km in the SW to a maximum of 10 km in the eastern part. Excess areas in sections pass from 500 to 250 km^2. These two changes (thinning and decreasing shortening) go along with a gradual change in structural style. The whole of the Anti-Atlas is affected by inversion tectonics in a thick skin mode. Paleozoic cover series of the southwestern Anti-Atlas are tightly folded into upright detachement folds in a disharmonic multilayer buckling fashion. Further east, cover folding is more closely related to the underlying basement inversion in a typical Windriver - Rocky Mountain style [ERSLEV]. An additional post-folding phase of extension, interpreted as related to the opening of the High Atlas Rift basin, is more developped in the central and eastern part of the belt, where the High Atlas is immediately adjacent to the North. The dip of these normal faults varies according to the lithology and produces Rollover structures, which have often been mistaken as "folds".

Structural sections across the central and eastern parts of the Anti-Atlas are constructed from field observations, existing geological maps and litterature (regarding the stratigraphy). Field observations include detailed dip measurements in order to constrain the fold geometry, systematic measurement of faults and their striation, meso- and micro- structural observations and a detailed mapping of the basement-cover contact.

ERSLEV, E. A.,1991, Geology, v. 19, p. 617-620.

Abstract présenté à la Réunion des Sciences de la Terre 2004 à Strasbourg, session poster.

THE ANTI-ATLAS FOLD-BELT OF MOROCCO : THICK SKIN INVERSION TECTONICS IN THE HINTERLAND OF THE ALLEGHENIAN OROGENY

Ch. Robert-Charrue (1), M. Burkhard (2)
Geological Institute, Neuchâtel University, C.P., CH-2007 Neuchâtel, Switzerland, (1) charles.robert-charrue@unine.ch, (2) martin.burkhard@unine.ch

The Anti-Atlas of Morocco formed in the hinterland of the larger Appalachian Orogen, time equivalent with the Alleghenian front to the West. It is limited to the south by the north-west african craton and to the north by the Alpine High Atlas. The Anti-Atlas appears as a huge NE-SW anticlinorium. Locally, the basement is cropping out as inliers, but the main part is made of an important Paleozoïc cover, which is gently folded and of low grade metamorphism.
An entire Wilson cycle of mountain building left its imprint in this belt. Sedimentation started with a Late Proterozoïc rifting phase, leading to the opening of first the Rheic and second the Paleotethys oceans to the west. Post-rift sediments of lower Cambrian to middle Carboniferous age are dominated by detrial input from the cratonic hinterland of Africa, leading to the accumulation of a thick pile of alternating quartzites, siltstones, shales and occasional carbonates. During the last stages of closure of the Paleotethys ocean, this passive margin is squeezed in the collision between Laurussia and Gondwana. This variscan collision lead to a massive inversion of former normal faults, substantial uplift of the Precambrian basement and a concommittant folding of the overlying cover series. A post-folding phase of extension, interpreted as a new cycle of High Atlas / Atlantic rifting during Mesozoïc times, is more developed in the central and eastern part of the belt, where the High Atlas is immediately adjacent to the North. The dip of these normal faults varies according to the lithology and produces Rollover structures, which have often been mistaken as variscan folds. Late Miocene compression in relation with the Alpine collision and High Atlas inversion, and possibly some Neogene hot spot related thermal uplift are responsible for the high present day rejuvenated topography. Syn- and post-tectonic erosion and isostatic re-equilibration lead to the removal up to 10 km of overburden, bringing lower green-schist facies rocks back to the earth's surface - allowing for deep insight into this otherwise mildly deformed fold belt. The Anti-Atlas is a thick skinned inversion belt, not a thin skinned foreland fold-thrust-belt.

Abstract présenté au Congrès 3Ma 2005 à Agadir, Conférence.

TECTONIQUE D'INVERSION DANS L'ANTI-ATLAS ORIENTAL

Robert-Charrue Ch., Burkhard M

Institut de Géologie, Université de Neuchâtel, CP 2, CH-2007 Neuchâtel, Suisse
charles.robert-charrue@unine.ch, martin.burkhard@unine.ch

L' Anti-Atlas du Maroc s'inscrit dans l'orogène Appalachien. Limité au sud par le craton ouest africain (WAC) et au nord par le Haut-Atlas alpin, l'Anti-Atlas apparaît comme un vaste anticlinal d'orientation NE-SW. Localement, le socle affleure en boutonnières, mais la majeure partie de son édifice est faite d'une importante couverture paléozoïque légèrement plissée et de métamorphisme faible.

Cette chaîne montre un cycle de Wilson entier. La sédimentation débute avec une phase de rifting au Protérozoïque tardif qui mène à l'ouverture de l'océan Rhéic plus à l'ouest, mais dont les nombreuses structures de rifting locales sont avortées. Les sédiments post-rift, du Cambrien au Carbonifère, sont dominés par l'apport détritique du craton. Il en résulte une épaisse série d'alternances de quartzites, argilites, schistes et de quelques carbonates. L'environnement des dépôts paléozoïques ainsi que la courbe de subsidence semblent d'avantage correspondre à un bassin intracratonique qu'à une marge passive, dont aucun élément profond n'est présent dans l'Anti-Atlas. Durant les derniers stades de la fermeture de l'océan Paléotéthys, la collision entre les continents Laurussia et Gondwana entraîne la déformation de ce bassin. Cet événement varisque provoque une sur-inversion des failles normales, une remontée du socle précambrien et un plissement polyharmonique de la couverture.

Une nouvelle phase d'extension affecte principalement l'Anti-Atlas central et oriental, à proximité du Haut-Atlas. Elle est interprétée comme un nouveau cycle : l'ouverture de l'Atlantique au mésozoïque. Au sein des séries paléozoïques, le plongement de ces nouvelles failles normales varie selon les lithologies ce qui provoque des structures en « Rollover » souvent confondues avec des plis varisques.

La topographie actuelle a certainement été rajeunie par la compression miocène (collision alpine et inversion du Haut-Atlas) et peut-être par un uplift thermique néogène (hot spot). L'érosion syn- et post-tectonique et la rééquilibration isostatique ont engendré par endroit une ablation de plus de 10 km de roche, permettant l'accès à des roches de faciès schistes verts, ce dans une chaîne que moyennement déformée. L'Anti-Atlas est une chaîne d'inversion de type « thick skinned » et non une chaîne d'avant-pays plissée.

Abstract présenté au Swiss Geoscience Meeting 2005 à Zürich, session poster.

The Anti-Atlas fold belt of Morocco : variscan inversion tectonics and interference pattern of an "intracratonic" basin.

Robert-Charrue, Ch. & Burkhard, M.

Institut de Géologie et d'Hydrogéologie, University of Neuchâtel,

CP 2, 2007 Neuchâtel, Switzerland, charles.robert-charrue@unine.ch

The Anti-Atlas fold belt is formed in the larger Appalachian Orogen system, time equivalent with the Alleghenian front to the West. Anti-Atlas appears as a huge anticlinorium oriented NE-SW. Locally, the basement is cropping out as inliers. The important palaeozoic cover is gently folded and of low grade metamorphism. The lack of major "décollement", deformation front or thrust fault makes the Anti-Atlas an unusual type of belt, which does not fit with classic schemes.

The Anti-Atlas is located (Fig.1) on the northern border of the West African Craton (WAC), limited to the South by the Tindouf basin, tectonically not affected, and to the North by the High-Atlas (Cenozoic to lower Quaternary deformation of Meso-Cenozoic sediments). The studied area is the eastern part of the Anti-Atlas which structurally differs strongly from the rest of the chain further west (Helg et al. 2004).

For this study, the basement is defined in terms of rheological "basement/cover" relationships. The basement is an assemblage of crystalline, metamorphic and sedimentary rocks with complex history (Ennih & Liégeois 2001). Note that the Anti-Atlas correspond to the northern limit of the Eburnian WAC (c. 2 Ga), which replayed in the Neoproterozoic continental breakup and was last consolidated during the Pan-African orogeny. Late Proterozoic extension produces normal faults and halfgraben structures filled with coarse clastics which are linked to the basement from a rheological (variscan) point of view. These normal faults and the WAC limits are important structures for the comprehension of the variscan phase deformation, since they preconfigure the later inverted blocks.

The whole palaeozoic cover is dominated by shallow marine mostly fine-grained clastic sediments. The departure of terranes from the WAC margin, brought the Anti-Atlas basin closer to the open sea. Detrital input from the WAC dominates sedimentation from Cambrian to Silurian times. Carbonate sedimentation takes place from the end of Silurian to the end of Devonian. The late Devonian is marked by a return to detrital sediments that will dominate during all the Carboniferous. This strong subsidence leads to the accumulation of 12 km in the SW Anti-Atlas, 6 km at the most eastern part. Note that the total thickness and the incompetent/competent ratio are the two key parameters which will dictate the structural style in the cover.

In Late Carboniferous, the last stages of closure of the Paleotethys ocean (Stampfli & Borel 2002),cause the collision between Laurussia and Gondwana. This compression leads to a massive inversion of the former normal faults, substantial uplift of the Precambrian basement and a concommittant folding of the overlying cover series, by the intervention of thick detachment horizons, in a trishear mode (Erslev 1991). The major variscan trend of the Anti-Atlas is given by the outcropping inliers as a huge anticlinorium with NE-SW axis. Well developed in the eastern Anti-Atlas, a regional gradient in deformation style, intensity and orientation is observed from north (thick skinned inversion style with ENE-WSW fold axis) to south (thin skinned detachment folding with NW-SE fold axis). This egg-box interference pattern is to be linked to the shape of the WAC.

Some folded folds show that the NE-SW Anti-Atlas global trend has developed before the NW-SE Ougartian trend. However, these two trends are interpreted as the product of the underlying shape of the WAC and not as two distinct deformation phases.

The next Wilson cycle begins at the end of Triassic. The new "Mesozoic High-Atlas basin" opens just north of the Anti-Atlas. It affects the whole belt by dolerites dykes and sills intrusions. Normal faulting is specially developed in the eastern Anti-Atlas to produce extensional fault-related folding (hanging-wall synclines) in the palaeozoic cover. The next sedimentary layers which really seal the variscan deformation are cretaceous conglomerates, no permian to jurassic sediments are found in the Anti-Atlas.

The actual high topography of the Anti-Atlas (up to 2500 m) does not result only from the variscan orogeny. Cretaceous to neogene sediments around the eastern Anti-Atlas show some unconformities and tilts which correspond with the inversion of High-Atlas at Eocene-Oligocene and Pliocene-Pleistocene epochs (Frizon de Lamotte et al., 2000). A neogene thermal uplift may also rejuvenate the topography. Except a light doming, no significant deformation affects the variscan belt.

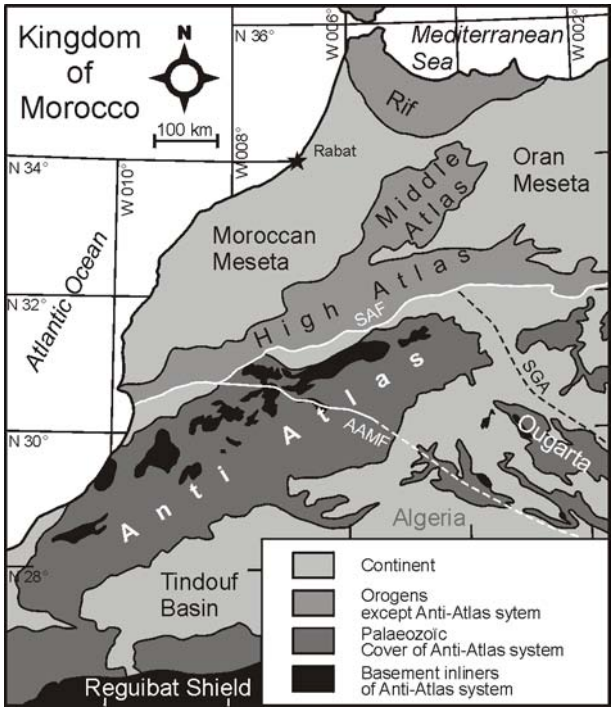

Figure 1. Geographic situation and geological context of the Anti-Atlas. The northern limit of the WAC is newly defined by the SAF and the SGA (Ennih & Liégeois 2001). AAMF: Anti-Atlas Major Fault (older WAC limit); SAF: South Atlas Fault ; SGA: Saoura gravimetric anomaly.

REFERENCES

Ennih, N. & Liégeois, J.-P. (2001): The Moroccan Anti-Atlas: the West African craton passive margin with limited Pan-African activity. Implications for the northern limit of the craton. Precambrian Research 112: 289-302.

Erslev E.A. (1991): Trishear fault-propagation folding. Geology 19: 617-620.

Frizon de Lamotte D., Saint Bezar B., Bracène R. (2000): The two main steps of the Atlas building and geodynamics of western Mediterranean. Tectonics 19 (4): 740-761.

Helg U., Burkhard M., Caritg S., Robert-Charrue C. (2004): Folding and inversion tectonics in the Anti-Atlas of Morocco. Tectonics, 23, TC4006, doi:10.1029/2003TC001576.

Stampfli, G.M. & Borel, G.D. (2002): A plate tectonic model for the Paleozoic and Mesozoic constrained by dynamic plate boundaries and restored synthetic oceanic isochrones. Earth Planet. Sci. Lett. 196: 17-33.

POSTERS

- Poster présenté à la RST 2004 à Strasbourg

- Poster présenté au SGM 2005 à Zürich

The Anti Atlas fold-belt of Morocco

Thick skin inversion tectonics in the hinterland of the Alleghanian Orogeny

Swiss National Science Foundation, grant n° 22-52516.97 / 20-63790.00

Charles ROBERT-CHARRUE
&
Martin BURKHARD

University of Neuchâtel
Switzerland

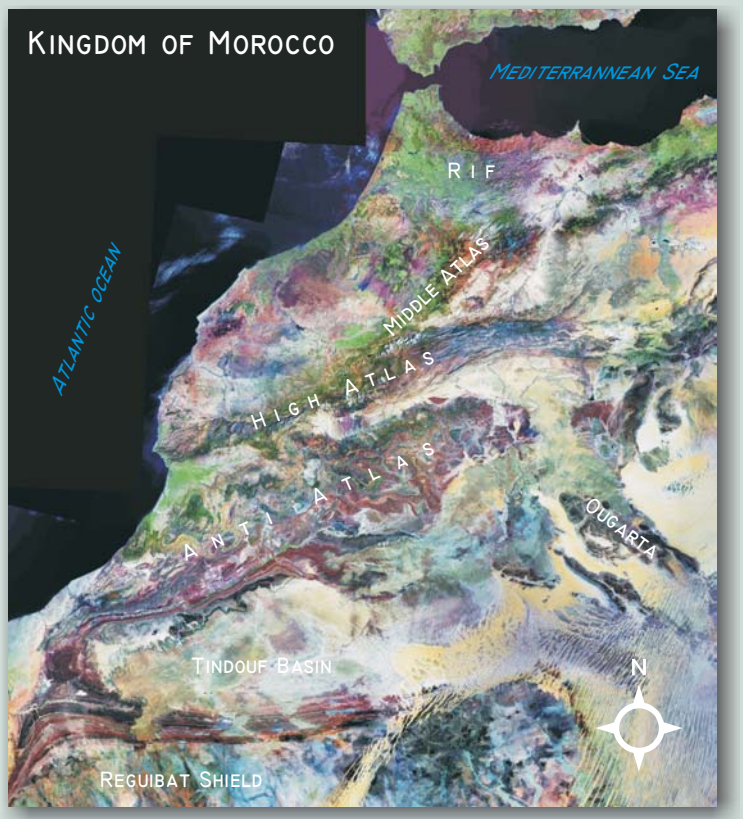

Geological setting

The Anti-Atlas of Morocco is formed in the hinterland of the larger Appalachian Orogen, time equivalent with the Alleghanian front to the West. It is limited to the South by the Tindouf Basin and the north-west african craton (Reguibat Shield and to the north by the Alpine High-Atlas). The Anti-Atlas appears as a huge NE-SW anticlinorium. Locally, the basement is cropping out as inliners, but the main part is made of an important Paleozoïc cover, wich is gently folded and of low grade metamorphism. The Anti-Atlas system clearly includes the Algerian Ougarta chain. Syn- and post-tectonic erosion and isostatic re-equilibration lead to the removal up to 10 km of overburden, bringing lower green-schist facies rocks back to the Earth's surface - allowing for deep insight into this otherwise mildly deformed fold belt. The high present day topography of Anti-Atlas has been rejuvenated by late Miocene compression in relation with the Alpine collision and High Atlas inversion, and possibly by some Neogene hot spot related thermal uplift.

Paleozoïc sediments are dominated by detrial input from the cratonic hinterland of Africa, leading to the accumulation of a thick pile of alternating quartzites, siltstones, shales and occasional carbonates. Triassic dolerites testify the extension phase of the opening of Atlantic ocean. The Hammada seals the deformed folds of Anti-Atlas, but is itself tilted a few degress to the south.

The rheology of the paleozoïc cover dictates the geometry of the final fold chain. This structural style depends on two key parameters namely the total thickness of the cover (decreasing from 12 km thick in the west to 6 km eastward) and the ratio of competent and incompetent layers

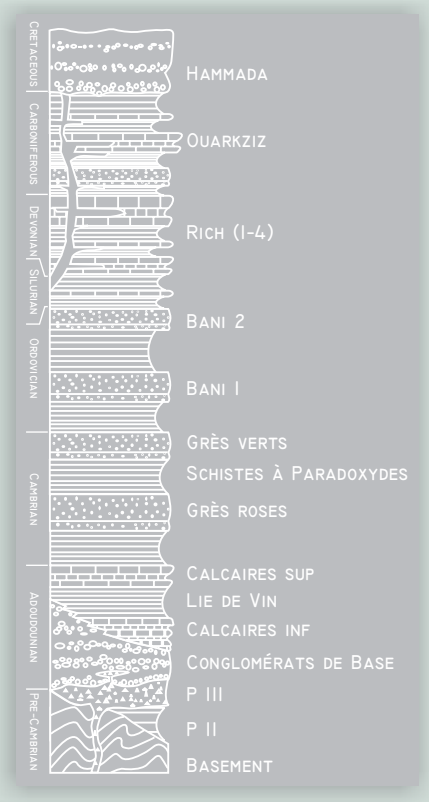

Landsat view

This image shows the excellent outcrop condition. Note (from NW to SE) : The Alpine High Atlas, The Ouarzazate Basin, The Saghro Anti-Atlas Inliner (dark-green), the "folded"Paleozoïc cover appearing as cuestas, here and there chopped by normal faults or graben and finally the sealing light-green Hammada.

Landsat 4/5 1990. Bands : 7 / 4 / 2.
Original pixel is at 28.5 meters.
Source of Landsat images :
https://zulu.ssc.nasa.gov/mrsid/

- Cross section
- Cretaceous-Neogene "Hammada"
- Carboniferous "Ouarkziz"
- Devonian "Rich"
- Upper Ordovician "Bani 2"
- Lower Ordovician "Bani I"
- Upper Cambrian
- Middle Cambrian
- Adoudounian
- P III / Basement

Cross section

Cross section shown on the landsat view. Stratigraphy from Cambrian to Devonian. The super-structure is a huge antiform. It appears to be chopped by normal faults. The dip of these normal faults varies according to the lithology and produce Rollover structures. No major detachement is observed at the basement-cover contact, wich indicates a Thick Skin structural style.

Reconstructed cross section of the Cambrian and Ordovician series at different stages : (1) after deposition ,(2) after compression and (3) actual configuration (after normal faulting). Stage 2 is the configuration at the end of the variscan orogeny. The horizontal shortening between stage 1 and 2 reaches 7.5 km (~12 %).

By measuring the differential surface between stages 1 and 2 (225 km^2) and the shortening (7.5 km), the depth of detachment must be of 33 km. But if the LPS (Layer Parallel Shortening) observed in the field, reaches 50 %, the detachment will be localised at 15 km depth.

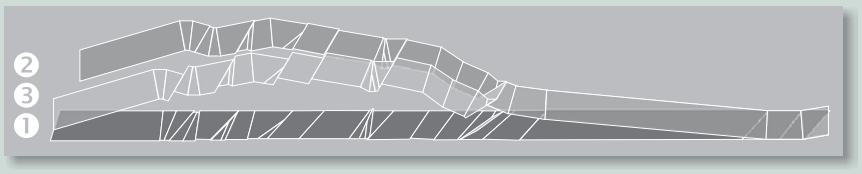

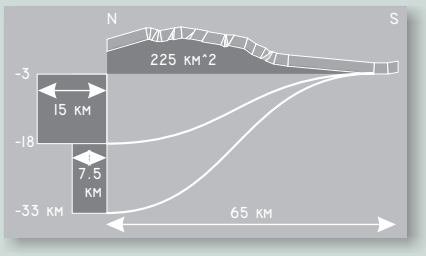

Conclusions

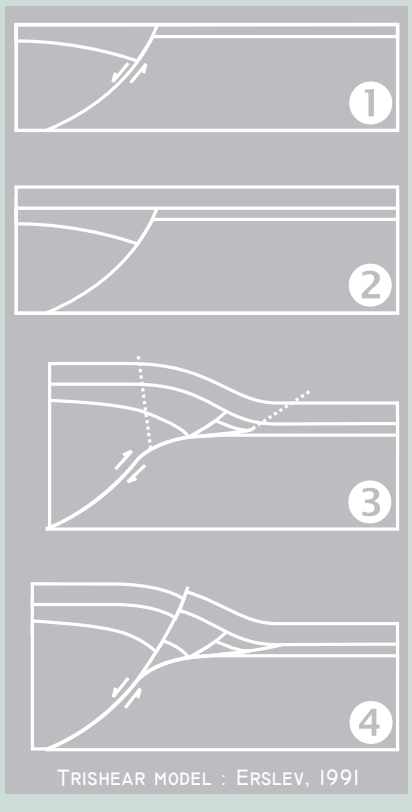

Trishear model : Erslev, 1991

An entire Wilson cycle of mountain building left its imprint in this belt.
1. Sedimentation started with a Late Proterozoïc rifting phase (opening of Rheic and Paleotethys oceans to the west).
2. Post-rift sediments of lower Cambrian to middle Carboniferous age are dominated by detrial input, leading to the accumulation of a thick pile of sediments.
3. During the last stages of closure of the Paleotethys ocean, this passive margin is squeezed in the collision between Laurussia and Gondwana. This variscan collision lead to a massive inversion of former normal faults, substantial uplift of the Precambrian basement and a concomittant folding of the overlying cover series.
4. A post-folding phase of extension is interpreted as a new cycle of High-Atlas / Atlantic rifting.

The Anti-Atlas is a thick skinned inversion belt, not a thin skinned foreland fold-thrust-belt.

Charles ROBERT-CHARRUE / Institut de géologie / Université de Neuchâtel / CP 2 / CH-2007 Neuchâtel / ++41 32 718 27 39 / charles.robert-charrue@unine.ch

STRUCTURAL STUDY OF THE EASTERN ANTI-ATLAS THE VARISCAN BELT OF MOROCCO

IGH

CENOZOIC: NEOG., PALEOGENE
MESOZOIC: CRETACEOUS, JURASSIC, TRIASSIC
PALEOZOIC: PERMIAN, CARBONIF., DEVONIAN, SILUR., ORDOVIC., CAMBRIAN
NEOPROTEROZOIC: EDIACARA

High-Atlas Inversion

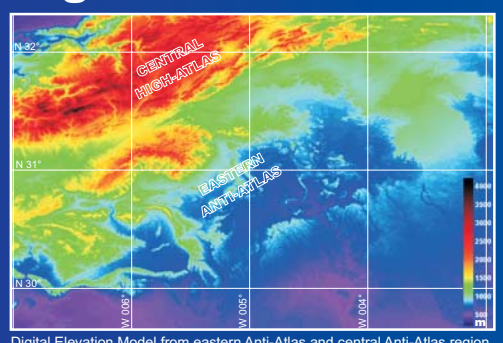

Digital Elevation Model from eastern Anti-Atlas and central Anti-Atlas region. (Data from GTopo30 @ http://edcdaac.usgs.gov/gtopo30/gtopo30.asp).

The present day high topography of the Anti-Atlas (up to 2500 m) does not result from the variscan orogeny alone. Cretaceous to Neogene sediments around the eastern Anti-Atlas show some unconformities and tilts which correspond to the inversion of the High-Atlas in Eocene-Oligocene and Pliocene-Pleistocene times (Frizon de Lamotte et al., 2000). A Neogene thermal uplift may also rejuvenate the topography. But except doming, no significant deformation re-affects the variscan belt.

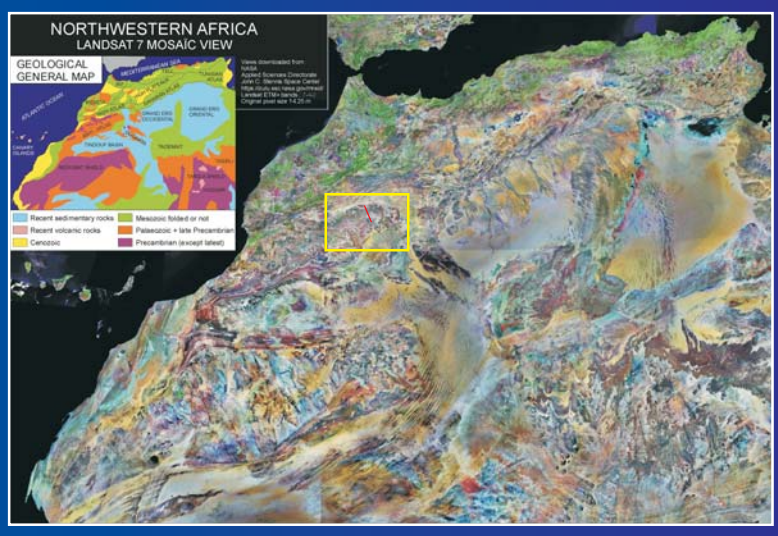

A New Cycle Starts

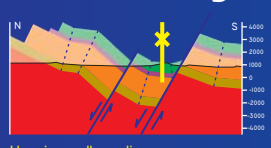

Hanging-wall syncline

The next Wilson cycle begins at the end of Triassic. The new "Mesozoic High-Atlas basin" opens just north of the Anti-Atlas. It affects the whole belt by dolerites dykes and sills intrusions. Normal faulting is especially developed in the eastern Anti-Atlas to produce extensional fault-related folding (hanging-wall synclines) in the Palaeozoic cover. The next sedimentary layers which really seal the variscan deformation are Cretaceous conglomerates, no Permian to Jurassic sediments are found in the Anti-Atlas.

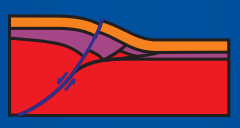

Ultraweak Cover

"Blind" thrusts in the shales.

The particular rheology of the cover dictates the deformation style. There is no major "décollement". The deformation is absorbed in pureshear style by an anabundance of incompetent layers. Competent layers are gently buckle-folded in a trishear mode (Erslev 1991). The Layer Parallel Shortening must be very significant but it remains difficult to determine.

Unsuccessful Rift Intracratonic Basin

The entire Palaeozoic cover is dominated by shallow marine mostly fine-grained clastic sediments. The departure of terranes from the WAC margin, brought the Anti-Atlas basin closer to the open ocean. Detrital input from the WAC dominates sedimentation from Cambrian to Silurian times. Carbonate sedimentation takes place from the end of Silurian to the end of Devonian. The late Devonian is marked by a return to detrital sediments that will dominate during all the Carboniferous. This strong subsidence leads to the accumulation of 12 km in the SW Anti-Atlas, 6 km at the most in eastern parts. Note that the total thickness and the incompetent/competent ratio are the two key parameters which will dictate the structural style in the cover.

LITHOLOGICAL SYMBOLS
- Conglomerate
- Sandstone / Quartzite
- Sandstone and shale
- Carbonate and sandstone
- Carbonate
- Shale and carbonate
- Black shale
- Shale
- Volcaniclastics
- Volcanics

WAC Limits

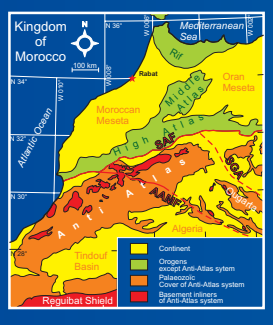

Exposed further west in the Bou Azzer inlier, the Major Anti-Atlas Suture or Anti-Atlas Major Fault (AAMF) was interpreted as the old front of the african shield but is newly seen as integrated in a metacratonic evolution. The northern boundary of the WAC is now defined by the South Atlas Fault (SAF) bording the High-Atlas to the south and by the Saoura gravimetric anomaly (SGA) to the east.

SW Anti-Atlas | Eastern Anti-Atlas

Neoproterozoic Rifting

The basement is an assemblage of crystalline, metamorphic and sedimentary rocks with a complex history (Ennih & Liégeois 2001). The Anti-Atlas corresponds to the northern limit of the Eburnian West African Craton (c. 2 Ga), reactivated in the Neoproterozoic continental breakup and last consolidated during the Pan-African orogeny. Late Proterozoic extension produces normal faults and halfgraben structures filled with coarse volcaniclastics which are linked to the basement from a rheological (variscan) point of view. These normal faults and the WAC limits are important structures for the comprehension of the variscan phase deformation, since they preconfigure the later inverted blocks.

Detachment Depth

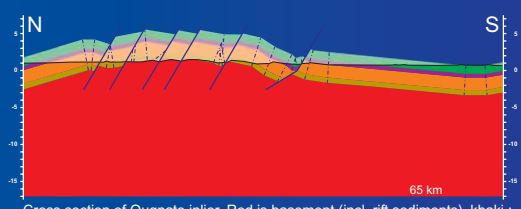

Cross section of Ougnate inlier. Red is basement (incl. rift sediments), khaki : Cambrian, orange : Ordovician, purple : Silurian, green Devonian. Note the hanging-wall syncline in the Devonian, produced by normal faulting.

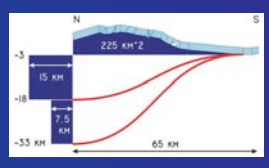

Reconstructed profile at the end of Variscan deformation (without normal faults). Detachment depth at -33 km with mesured 7.5 km shortening and at -18 km with 15 km shortening including a 50 % of layer parallel shortening.

The first calculation of detachment depth gives -33 km : Lower crustal scale detachment. In fact, this calculation does not take the Layer Parallel Shortening (LPS) into account. An assumed 50 % of LPS is not over estimated and yields a detachment depth at -18 km which corresponds to a more reasonable midcrustal detachment.

Egg-Box Interference Patterns from Variscan Inversion

In Late Carboniferous, the last stages of closure of the Paleotethys ocean (Stampfli & Borel 2002),cause the collision between Laurussia and Gondwana. This compression leads to a massive inversion of the former normal faults, substantial uplift of the Precambrian basement and a concommittant folding of the overlying cover series, by the intervention of thick detachment horizons. The major variscan trend of the Anti-Atlas is given by the outcropping inliers as a huge anticlinorium with a NE-SW axis. Well developed in the eastern Anti-Atlas, a regional gradient in deformation style, intensity and orientation is observed from north (thick skinned inversion style with ENE-WSW fold axis) to south (thin skinned detachment folding with NW-SE fold axis). Some folded folds show that the NE-SW Anti-Atlas global trend has developed before the NW-SE Ougartian trend. However, these two trends are interpreted as the product of the underlying shape of the WAC and not as two distinct deformation phases.

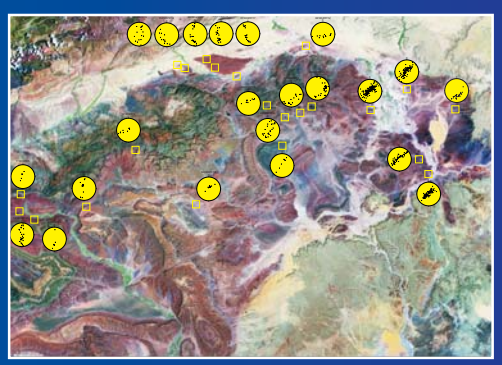

View of the eastern Anti-Atlas with stereograms of the bedding plane poles of small scale folds.
Landsat 7 downloaded @ https://zulu.ssc.nasa.gov/mrsid/

Small scale fold. Stick is one meter.

Except north of the inliers, the small scale folds axis have the orientation of the Ougartian trend (NW-SE in the eastern area, E-W in central Anti-Atlas).

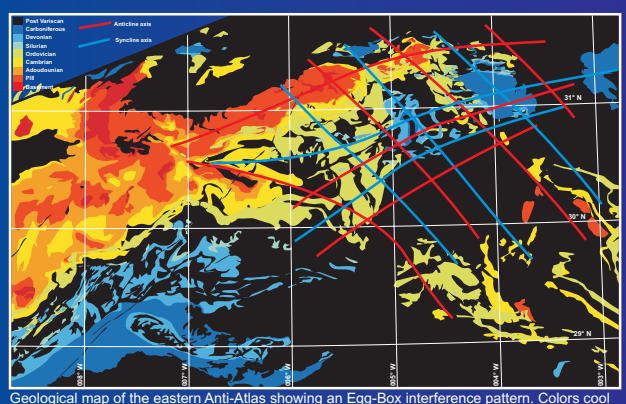

Geological map of the eastern Anti-Atlas showing an Egg-Box interference pattern. Colors cool down up the stratigraphy, from red Precambrian to blue Carboniferous. Post variscan in black. Anticlines (red) and synclines (blue) indicate fold axis of the superstructure folds.

References

Ennih N., J.-P. Liégeois (2001), The Moroccan Anti-Atlas: the West African craton passive margin with limited Pan-African activity. Implications for the northern limit of the craton, *Precambrian Research*, 112, pp. 289-302.

Erslev E.A. (1991), Trishear fault-propagation folding, *Geology*, v. 19, pp. 617-620.

Frizon de Lamotte D., B. Saint Bezar, R. Bracène (2000), The two main steps of the Atlas building and geodynamics of western Mediterranean, *Tectonics*, Vol. 19, N° 4, pp. 740-761.

Stampfli , G.M., G.D. Borel (2002), A plate tectonic model for the Paleozoic and Mesozoic constrained by dynamic plate boundaries and restored synthetic oceanic isochrones, *Earth Planet. Sci. Lett.* , 196, pp 17-33.

Charles ROBERT-CHARRUE & Martin BURKHARD
Institut de Géologie et d'Hydrogéologie
Université de Neuchâtel - 2007 Neuchâtel
charles.robert-charrue@unine.ch

Université de Neuchâtel unine

D

FIGURES

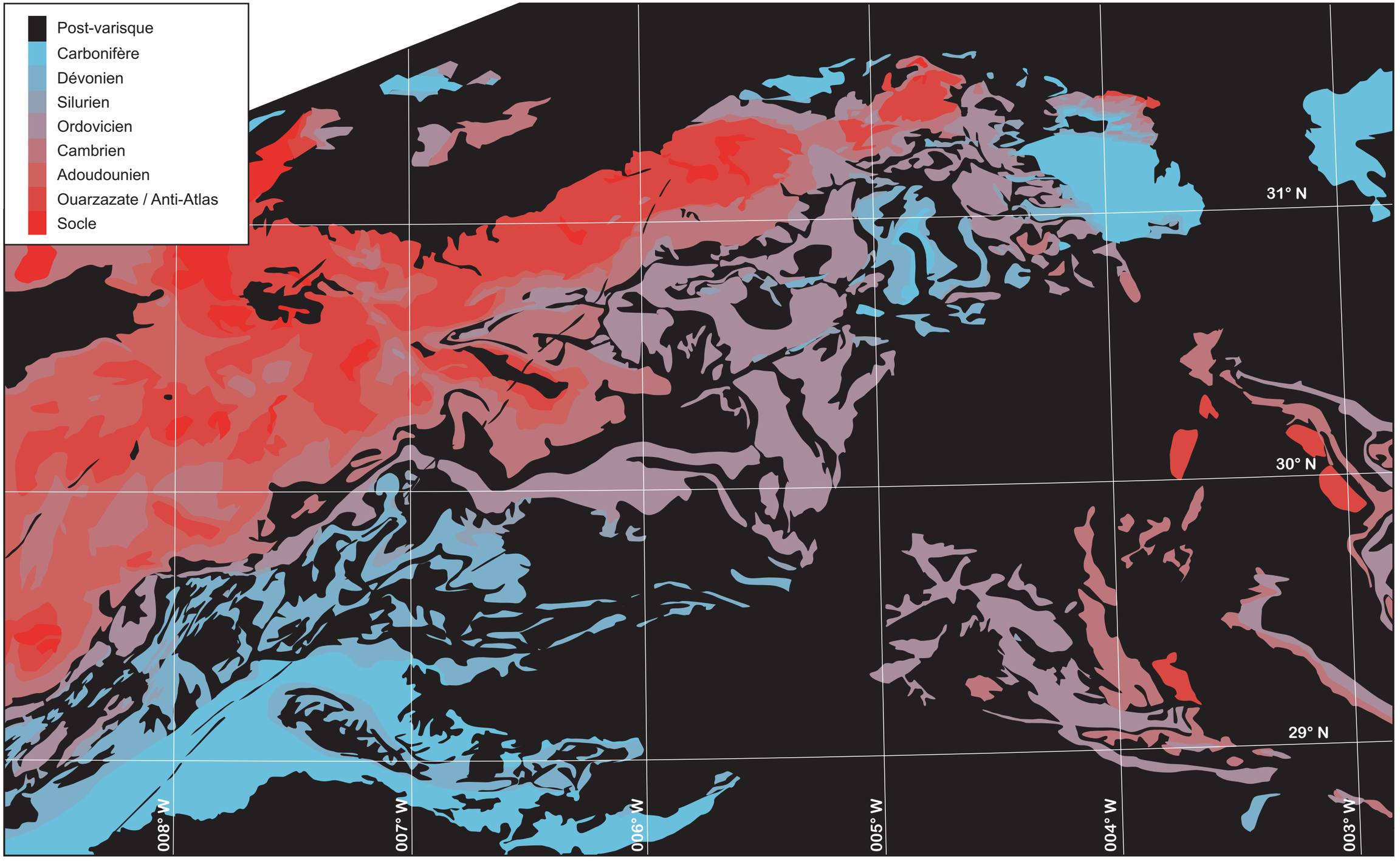
Post-varisque
Carbonifère
Dévonien
Silurien
Ordovicien
Cambrien
Adoudounien
Ouarzazate / Anti-Atlas
Socle
31° N
30° N
29° N
008° W
007° W
006° W
005° W
004° W
003° W

CROSS SECTIONS OF EASTERN ANTI-ATLAS OF MOROCCO

1: 200’000
no vertical exageration

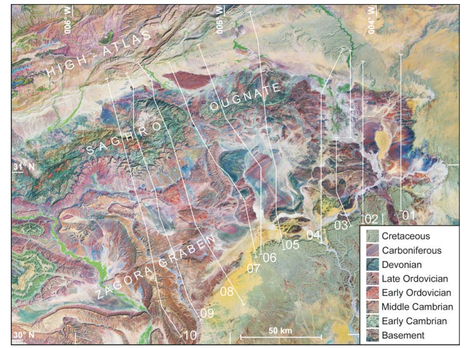

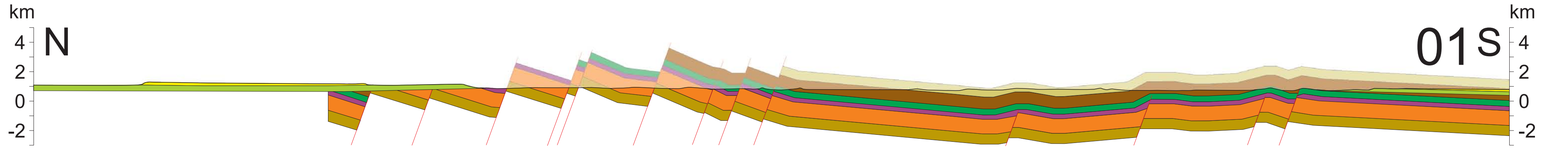

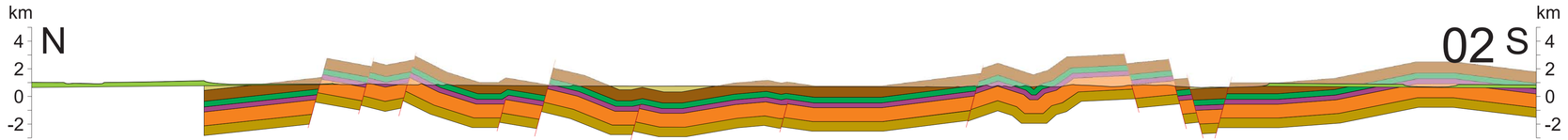

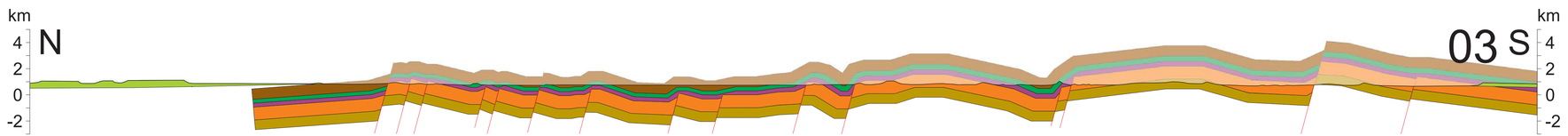

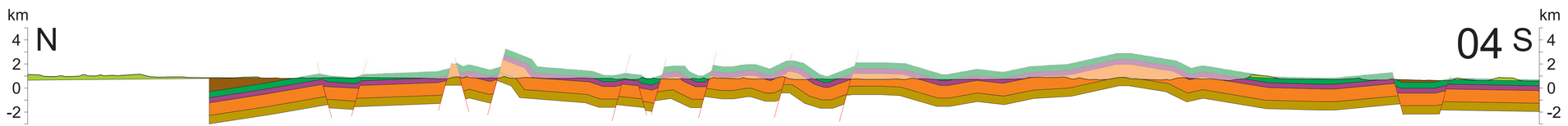

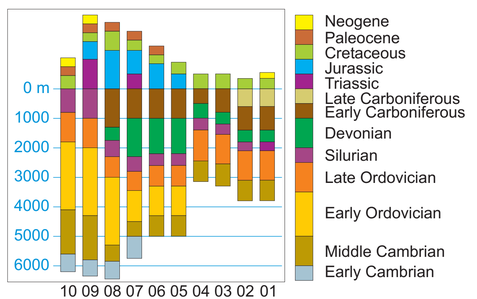

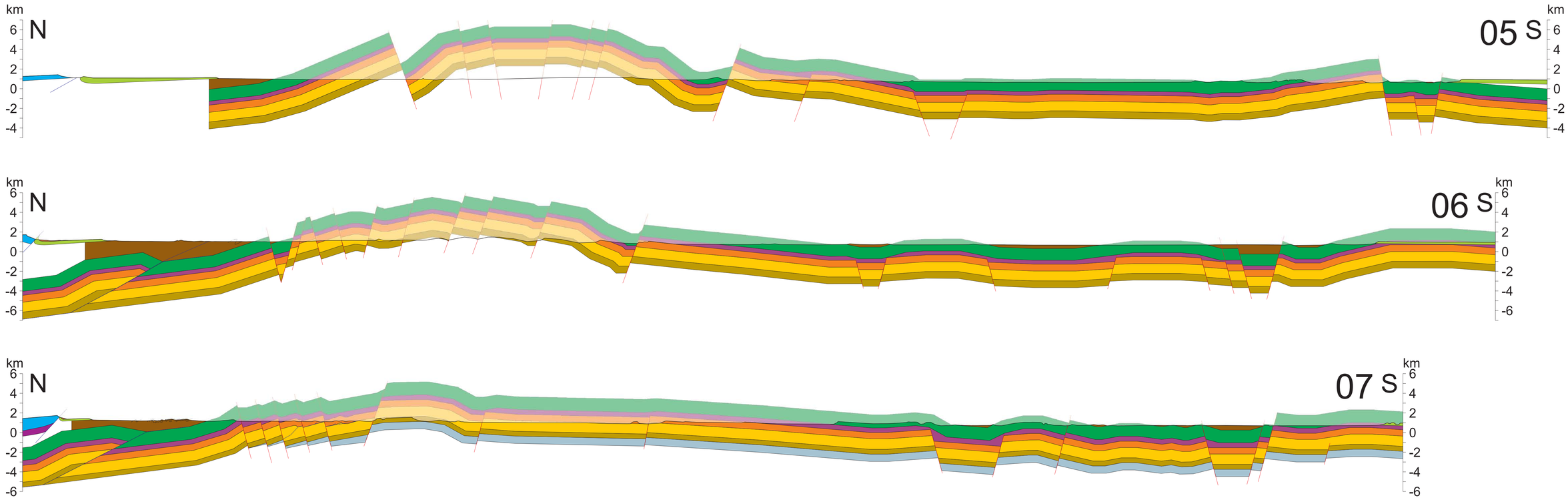
km
N
6
4
2
0
-2
-4
05
S
km
6
4
2
0
-2
-4
km
N
6
4
2
0
-2
-4
-6
06
S
km
6
4
2
0
-2
-4
-6
km
N
6
4
2
0
-2
-4
-6
07
S
km
6
4
2
0
-2
-4
-6

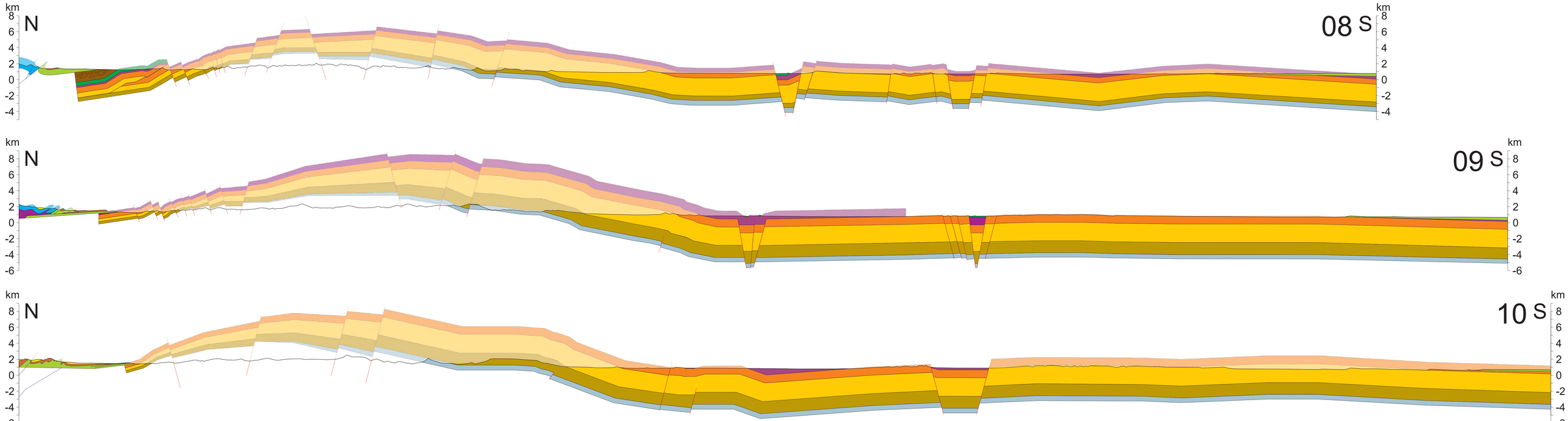
km
N
8
6
4
2
0
-2
-4
08
S
km
8
6
4
2
0
-2
-4
km
N
8
6
4
2
0
-2
-4
-6
09
S
km
8
6
4
2
0
-2
-4
-6
km
N
8
6
4
2
0
-2
-4
-6
10
S
km
8
6
4
2
0
-2
-4
-6

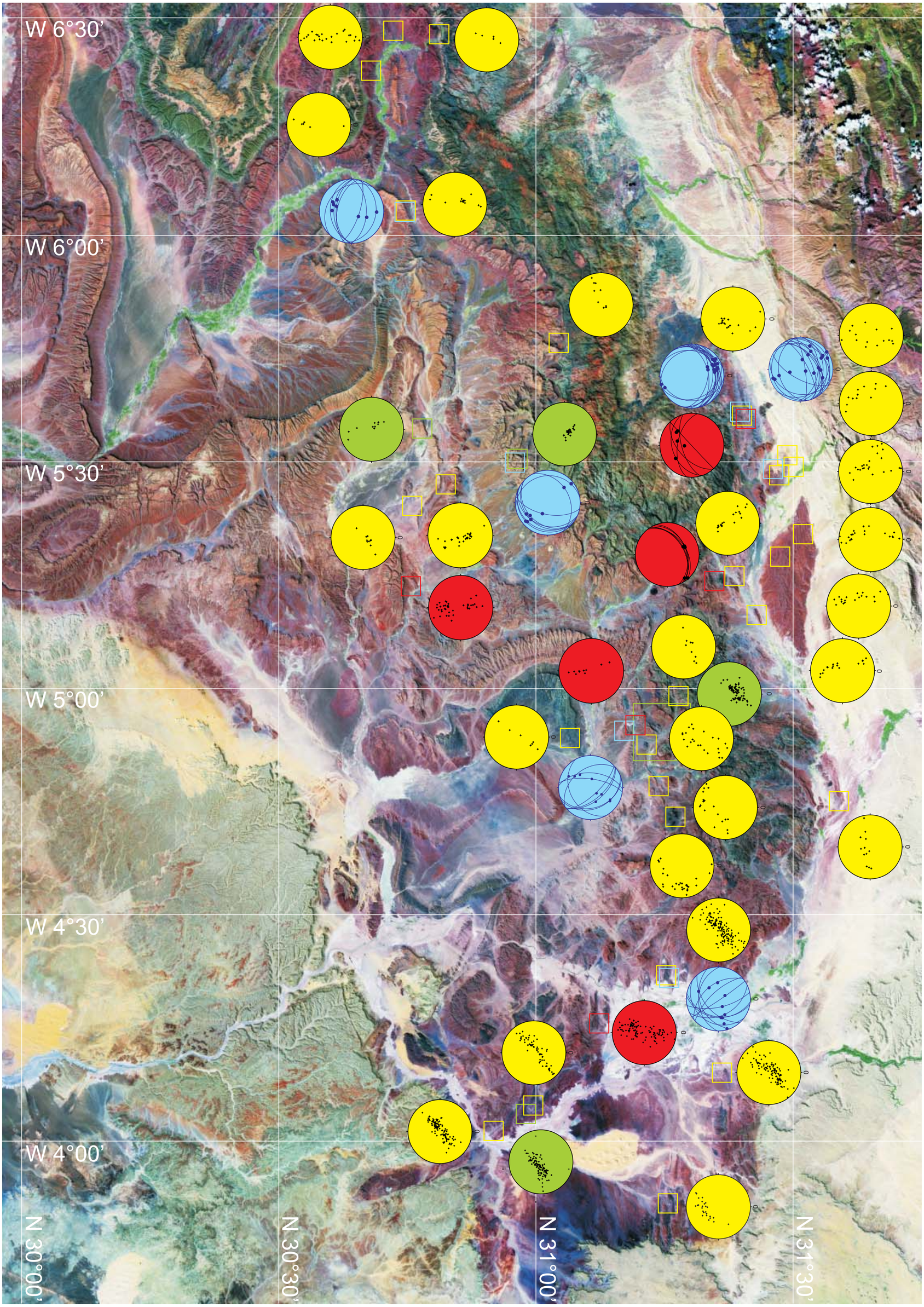
W 6°30’
W 6°00’
W 5°30’
W 5°00’
W 4°30’
W 4°00’
N 30°00’
N 30°30’
N 31°00’
N 31°30’

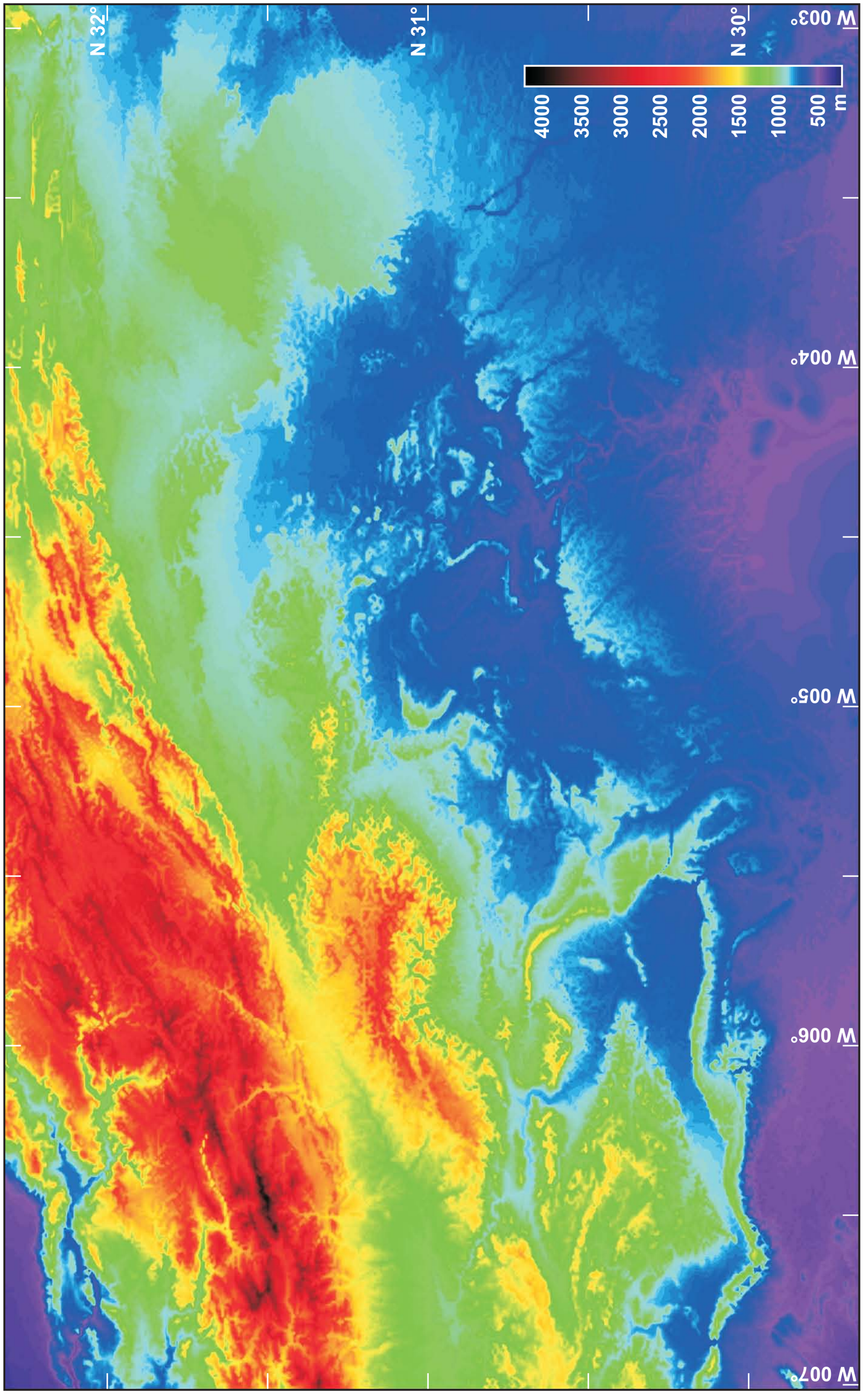
N 32°
N 31°
N 30°
W 003°
W 004°
W 005°
W 006°
W 007°
4000
3500
3000
2500
2000
1500
1000
500
m

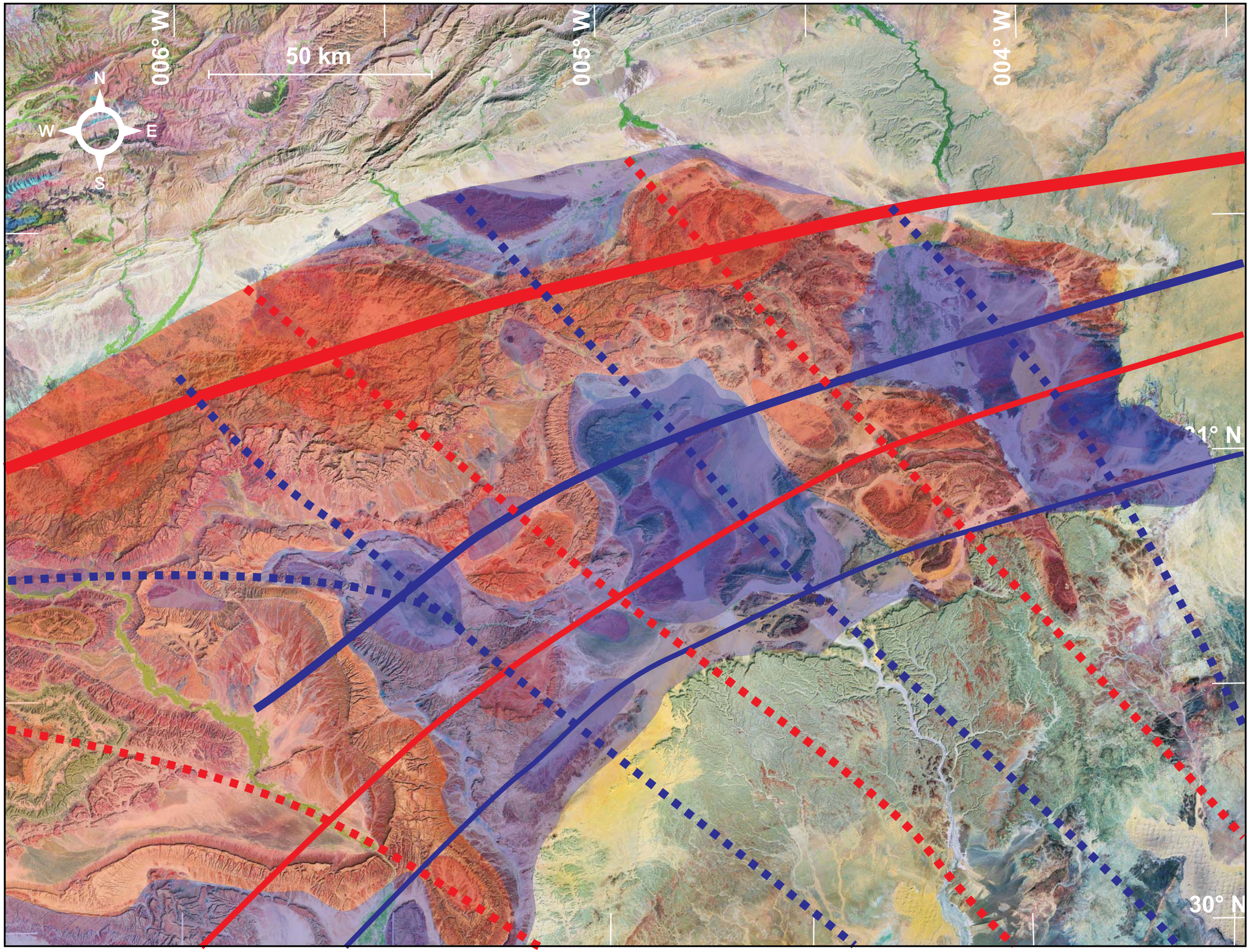
006° W
50 km
005° W
004° W
N
W
E
S
31° N
30° N

TOPOGRAPHIE ET GEOLOGIE

DE SURFACE ET SUBSURFACE DE L'ANTI-ATLAS ORIENTAL

Echelle verticale 1 : 55'000
Echelle horizontale 1 : 550'000
Exagération verticale 10 x

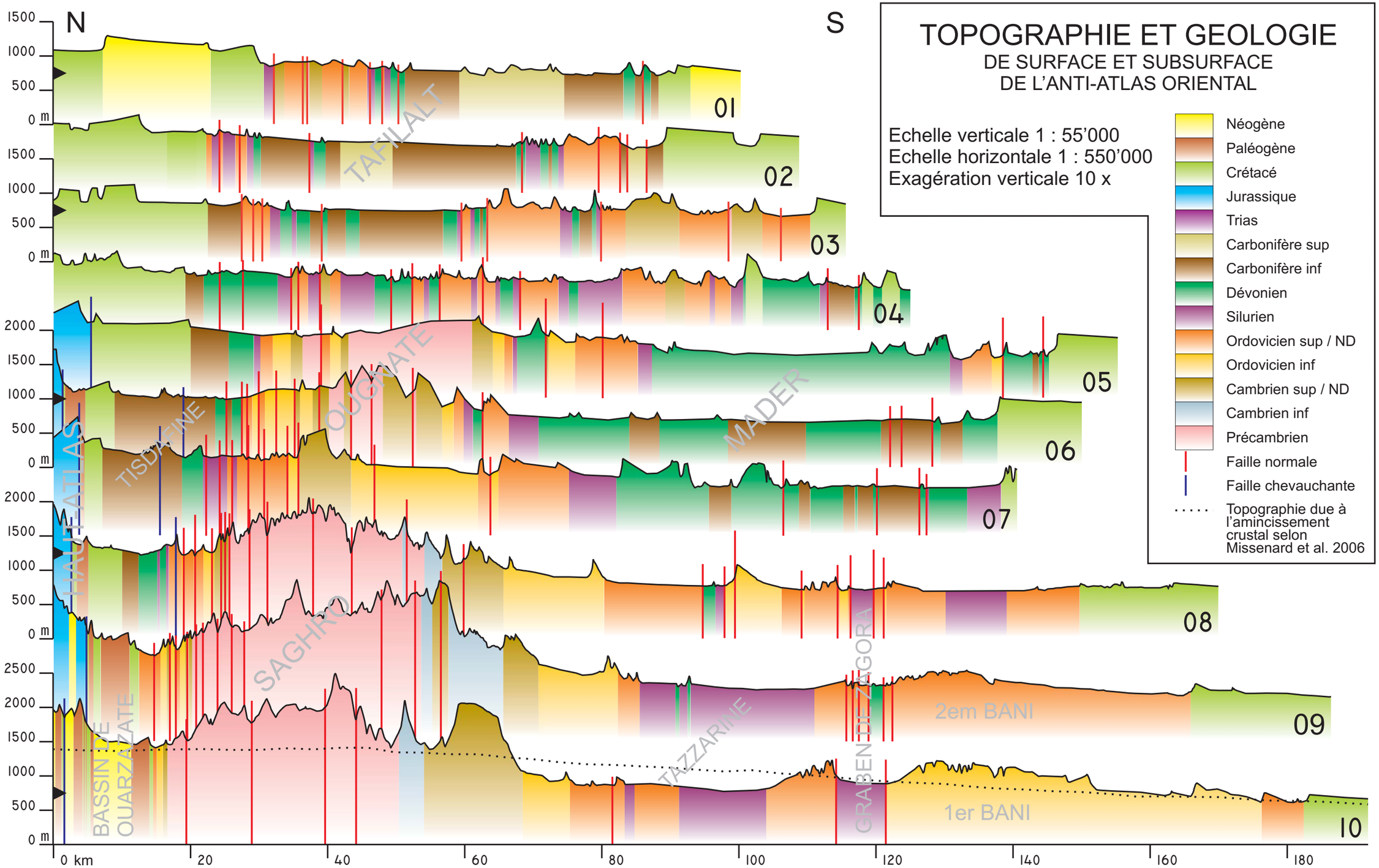

- Néogène
- Paléogène
- Crétacé
- Jurassique
- Trias
- Carbonifère sup
- Carbonifère inf
- Dévonien
- Silurien
- Ordovicien sup / ND
- Ordovicien inf
- Cambrien sup / ND
- Cambrien inf
- Précambrien
- Faille normale
- Faille chevauchante
- Topographie due à l'amincissement crustal selon Missenard et al. 2006

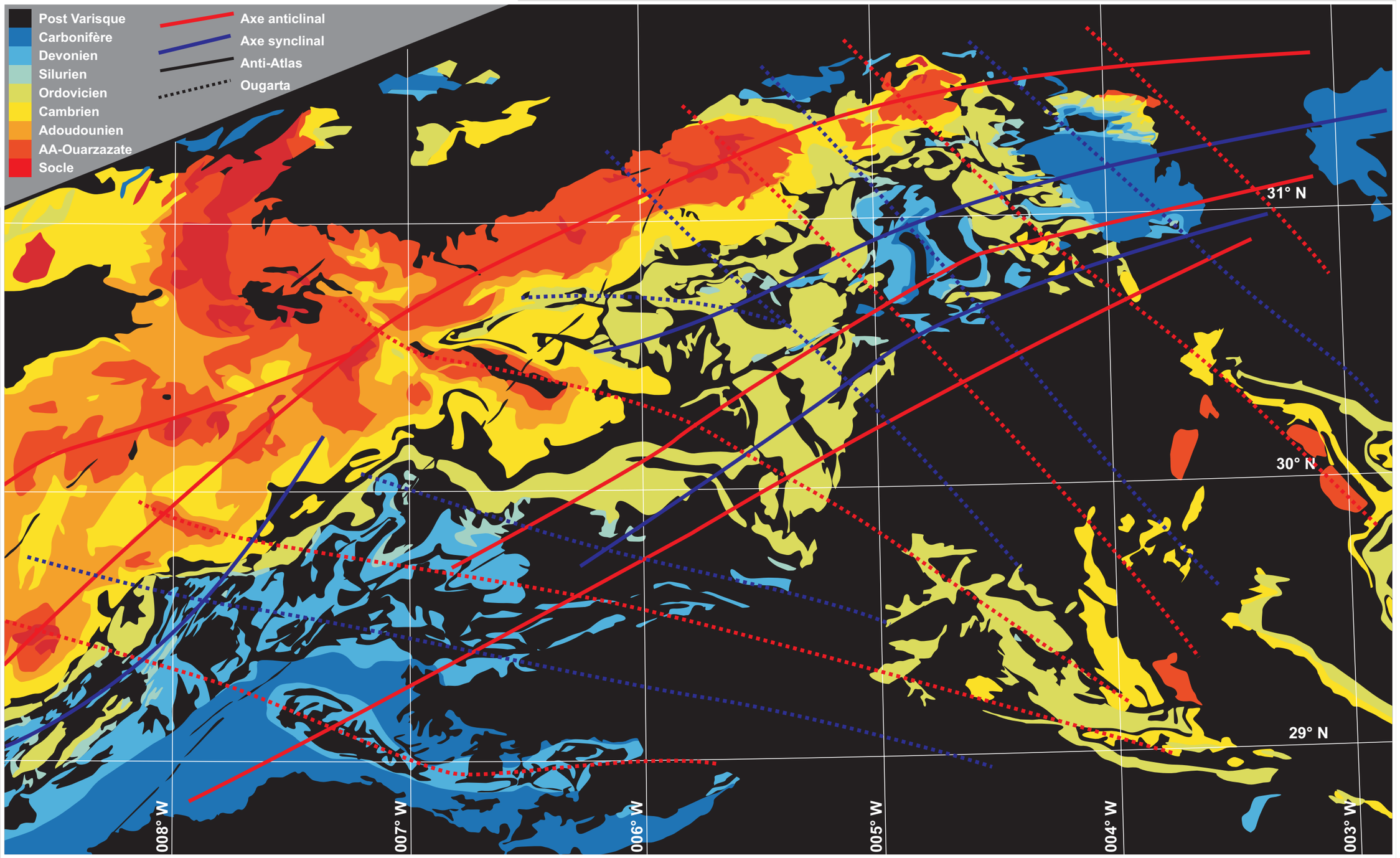
Post Varisque
Carbonifère
Devonien
Silurien
Ordovicien
Cambrien
Adoudounien
AA-Ouarzazate
Socle
Axe anticlinal
Axe synclinal
Anti-Atlas
Ougarta
31° N
30° N
29° N
008° W
007° W
006° W
005° W
004° W
003° W

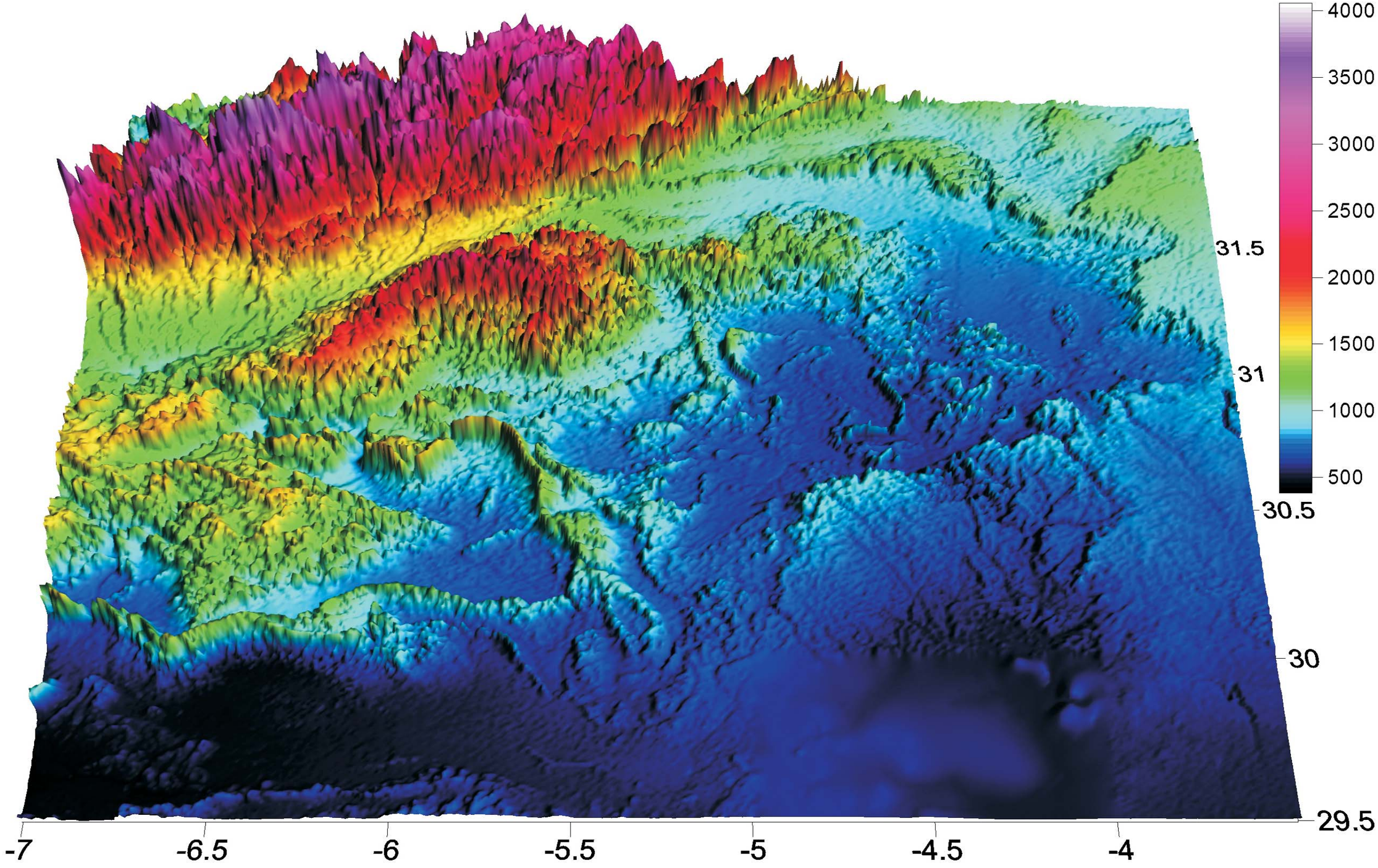
4000
3500
3000
2500
2000
1500
1000
500
31.5
31
30.5
30
29.5
-7
-6.5
-6
-5.5
-5
-4.5
-4

E

ATLAS LANDSAT 7

NW Africa

Anti-Atlas

AA oriental : découpage et légendes de la mosaïque

Mosaïque de l'Anti-Atlas oriental

NORTHWESTERN AFRICA
LANDSAT 7 MOSAÏC VIEW

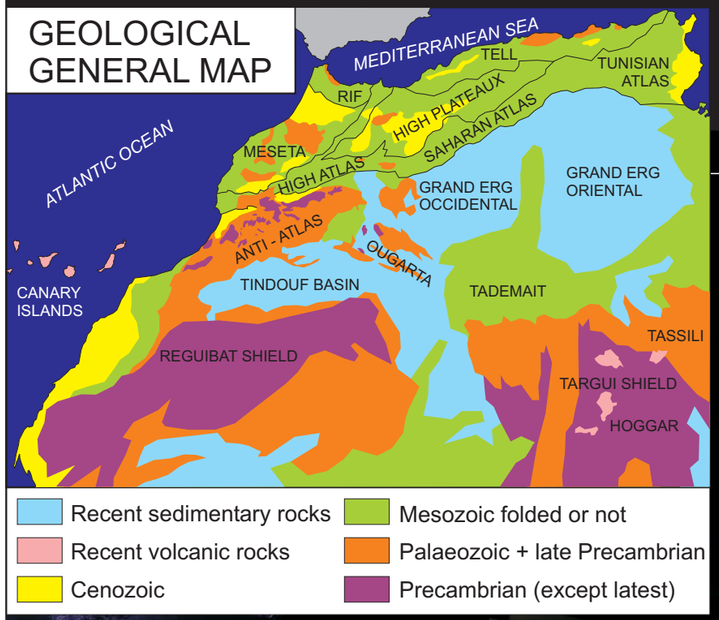

Views downloaded from :
NASA
Applied Sciences Directorate
John C. Stennis Space Center
https://zulu.ssc.nasa.gov/mrsid/
Landsat ETM+ bands : 7-4-2
Original pixel size 14.25 m


ANTI-ATLAS
OF
MOROCCO
100 km

Répartition des vues

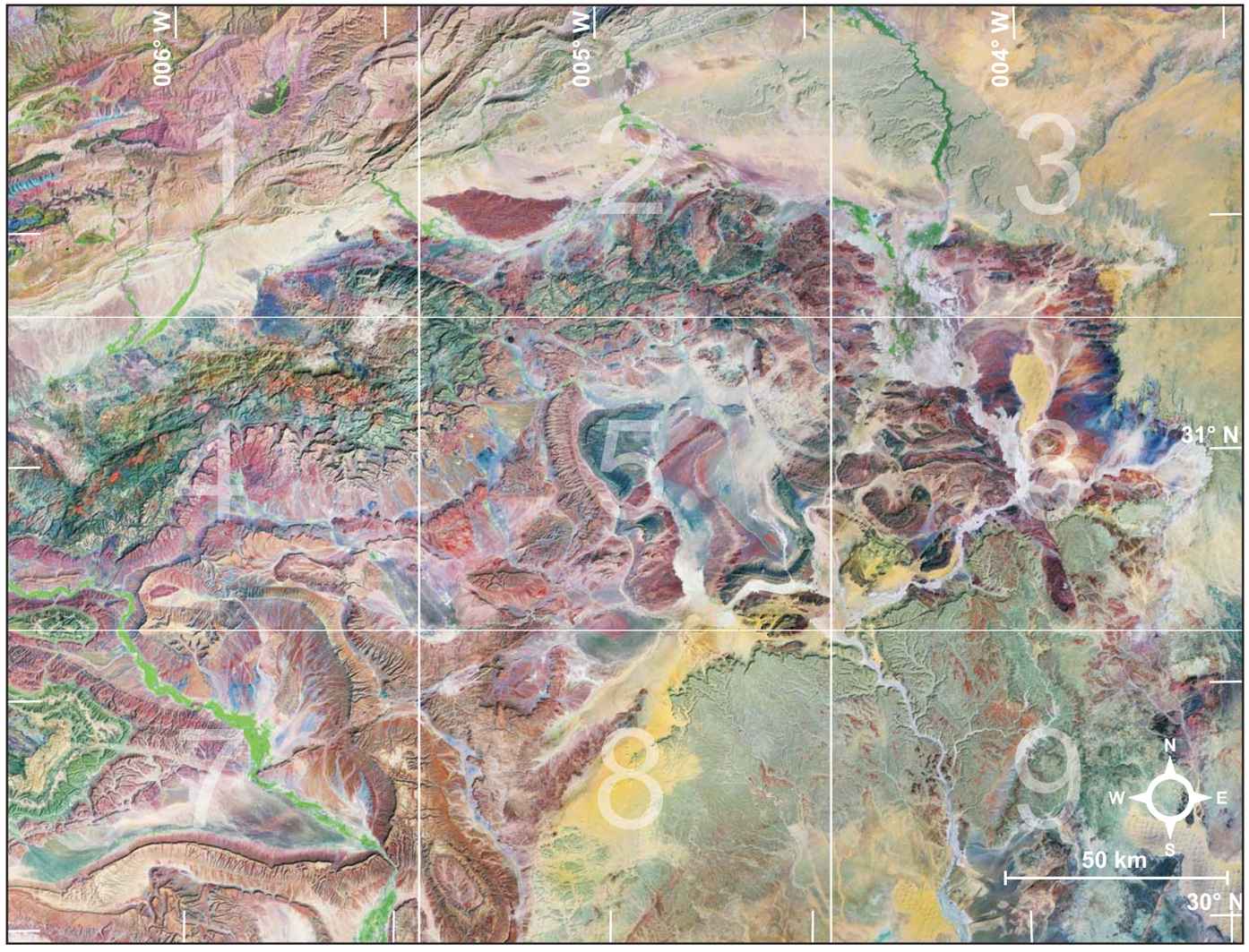

Légendes

- Palmeraie / Dune
- Cénozoïque
- Crétacé
- Jurassique
- Carbonifère *Ouarkziz*
- Dévonien *Rich*
- Ordovicien sup *2ème Bani*
- Ordovicien inf *1er Bani*
- Cambrien moyen
- Cambrien inférieur
- *Adoudounien*
- *Socle*